SELF PRESERVING, TWO-DIMENSIONAL TURBULENT JETS AND WALL JETS IN A MOVING STREAM

by

R.P. Patel

A thesis submitted to the Faculty of Graduate Studies and Research in partial fulfilment of the requirements for the degree of Master of Engineering.

Department of Mechanical Engineering,
McGill University,
Montreal.

April 1962.

SUMMARY

The self preserving free jet in streaming flow has been investigated by studying the equations of mean motion for two-dimensional turbulent flow. It is found that at high Reynolds number the jet may be self preserving if the free stream velocity varies as the downstream co-ordinate to a power which in turn depends on the non-dimensional velocity of the jet. The growth of the jet is then linear. The effect of an upstream boundary-layer on the outside of the slot is also considered. This analysis is then applied to the outer part of a wall jet in a similar pressure gradient. The effect of the inner boundary-layer on the outer part of the flow is considered and formulae for the growth of the inner boundary-layer and the variation of skin friction are given. Also a form for the non-dimensional mean velocity profile including the inner boundary-layer is suggested.

The predictions of the theory are found to be in substantial agreement with measurements of the mean velocity, the static pressure and the skin friction in wall jets with an equilibrium pressure gradient. Experimental measurements have also been made for wall jets in streaming flow with zero pressure gradient and wall jets in still air. The results of these experiments compare well with those of previous investigators.

The law-of-wall and the velocity defect law for wall jets are investigated and the former is found to be limited in application. A simple power law appears to be useful for representing the whole boundary-layer velocity profile and forms the basis for the analysis of the inner boundary-layer.

ACKNOWLEDGEMENTS

The author is very much indebted to Dr. B.G. Newman for his guidance, advice and help throughout the investigation of this project.

The wind tunnel and the experimental apparatus were mainly constructed by Mr. A.A. Gustavsen and Mr. E. Hansen and their help is gratefully acknowledged.

The author wishes to extend his gratitude to Miss J. Archer for the typing of the manuscript and to Mrs. A.J. Patten and her staff for reproducing this thesis.

Thanks are due to the Royal College, Nairobi, for granting the author leave of absence during the course of this work.

The author is currently supported financially by a Canadian Commonwealth Scholarship.

The work was undertaken with the financial assistance of the Defence Research Board of Canada under DRB Grant, No. 9551-12.

CONTENTS

NOTATION

A - constant in the law-of-wall.

$\bar{A}$ - Function of n as defined in equation (28).

B - constant in the law-of-wall.

$\bar{B}$ - function of n as defined in equation (28).

b - slot width for a wall jet or half the slot width for a free jet.

C - constant of proportionality defining the rate of growth of the outer part of the wall jet. Equation (46)

C_1 - constant of proportionality defining variation of U_1. Equation (16).

C_2 - constant of proportionality defining variation of U_M. Equation (16).

C_f - skin friction coefficient.

D - diameter of sphere.

d - nominal height of Stanton tube or outside diameter of Preston tube.

F_1 - function of jet velocity ratio $(\frac{U_j}{U_{is}})$ and $(\frac{\delta^*_s}{b})$. Equation (14).

F_2 - function of $(\frac{U_M}{U_1})$, equation (15).

f - function of non-dimensional cross stream co-ordinate η for the variation of mean velocity, equation (2).

g_1, g_2, g_{12} - functions of non-dimensional cross stream co-ordinate η for the turbulent Reynolds stresses, equation (2).

H - free jet form parameter as defined in equation (6).

K - a constant = 0.833.

l_o - length scale.

m - exponent for the downstream variation of velocity scale. Equation (5).

n - exponent for the inner boundary-layer mean velocity profile.

N - $= (\frac{n+1}{2})$, equation (27).

P - stagnation pressure measured with pitot tube

p_b - pressure at the base of sphere.

p_s - wall static pressure.

p_T - total pressure in tunnel main stream.

R_e - Reynolds number $= (\frac{U_j b}{\nu})$.

Re_s - Reynolds number $= (\frac{U_{M_s} b}{\nu})$.

U - mean velocity in the x-direction.

u - turbulent fluctuating component of velocity in the x-direction.

u_o - velocity scale $= (U_M - U_1)$.

U_1 - free stream velocity.

U_j - jet exit velocity.

U_M - maximum velocity in the x-direction.

U_{M_s} - hypothetical maximum velocity in the x-direction at the slot exit. Equation (11).

U_{is} - free stream velocity at slot exit.

U_τ - skin friction velocity $= \sqrt{\frac{\tau_o}{\rho}}$.

V - mean velocity in the y-direction.

v - turbulent fluctuating component of velocity in the y-direction.

X - downstream distance from hypothetical origin $= (x + x_o)$.

x - downstream distance from slot exit.

x_o - distance of hypothetical origin from slot exit.

y - distance perpendicular to the flat plate.

y_M - value of y where $U = U_M$.

$y_{M/2}$ - larger value of y where $(\frac{U-U_1}{U_M-U_1}) = \frac{1}{2}$

α - experimental constant.

δ^*_s - displacement thickness of the free stream boundary-layer on one side of the slot exit.

δ_f - length based on the slope of the mean velocity profile at the inflexion $= \frac{U_M}{(\frac{\partial U}{\partial y})_{y_{M/2}}}$

η - non-dimensional cross stream co-ordinate $= (\frac{y}{l_o})$.

η_1 - non-dimensional cross stream co-ordinate $= K(\frac{y - y_M}{y_{M/2}-y_M})$.

ν - kinematic viscosity.

ρ - density.

Ⓗ - free jet momentum thickness $= \int_{-\infty}^{+\infty} \frac{U(U - U_1)}{U_1^2} dy$.

θ_s - momentum thickness of the free stream boundary-layer on one side of the slot exit.

τ - turbulent shear stress.

τ_o - shear stress at the surface.

Subscript s refers to conditions at the slot exit.

1. INTRODUCTION

Useful solutions of the boundary layer equations have been obtained by examining those particular flows for which the profiles of mean velocity are similar or self-preserving as the flow proceeds downstream. For such flows the partial differential equation of motion is replaced by a total differential equation which can be solved either analytically or numerically. Such solutions have been obtained in the past for both laminar and turbulent flow although in the latter case some phenomenonological theory for the shear stress has been assumed in order to determine the velocity distribution.

The purpose of the present investigation is to examine the conditions for which the flow of a two-dimensional turbulent jet surrounded by a moving stream is similar and self-preserving. The application of the theory to a two-dimensional wall jet is also considered.

For a jet surrounded by similar fluid at rest it can be shown by dimensional analysis [1] or by a detailed examination of the equation of motion[2] that, if the static pressure is uniform everywhere, the velocity profiles become similar once the potential core emerging from the slot has disappeared. When the jet is surrounded by a moving stream of constant velocity aligned with the jet, the flow is not strictly similar, although

similarity has been assumed in the analysis of Abramovich[3] and Craven[4]. This procedure is to some extent justified on the grounds that the flow is closely similar for the two extreme cases:

(i) when the jet speed exceeds the free stream speed by a small amount and the flow resembles a negative wake of small perturbation.

(ii) when the jet speed exceeds the free stream speed by a large amount and the flow approximates to that with surrounding fluid at rest.

A jet surrounded by a parallel stream in which the speed varies in the downstream direction has not yet been examined, although the flow is closely related to that of a two-dimensional wall jet in a streaming flow for which tentative theories have been given by Carriere, Eichelbrenner and Poisson Quinton[5] and by George[6]. In both these theories a form of downstream similarity is assumed. In general the flow in the outer part of the wall jet is similar to that of a free jet as long as the jet momentum is very much greater than the wall friction, although the wall constraint appears to modify the rate of spreading of the jet.

In the present investigation the conditions for similarity of a two-dimensional turbulent jet in a parallel streaming flow with variable pressure gradient are examined. The analysis

closely follows the work of Townsend[7] on equilibrium turbulent boundary layers, which layers have similar profiles in velocity defect in the downstream direction. The analysis is applied to a wall jet in a similar pressure gradient, and as a first approximation the effect of the newly growing boundary layer on the wall is neglected. The analysis of the newly growing boundary layer is then considered. Finally as a second approximation the effect of the inner boundary layer on the outer part of the wall jet is also investigated and an emperical formula for the total mean velocity profile is given.

The present solution is of interest in the application of blowing for boundary layer control to prevent separation in that it gives, subject to the requirement that the jet momentum is sufficiently large, a class of solutions for which the velocity profile may be predicted.

The predictions of the theory are compared with measurements of a wall jet in a pressure gradient tailored to produce mean velocity profiles with downstream similarity. Results for six ratios of jet velocity to free stream velocity at the slot exit and four slot widths are presented. In addition the skin friction was measured with Stanton tubes for three ratios of jet velocity to free stream velocity and with one slot width. For comparison, measurements were also made on wall jets in still air and wall jets in streaming flow with zero pressure gradient. A few measurements of the longitudinal turbulence are also presented.

2. THEORETICAL ANALYSIS

2.1 Free Turbulent Jet in Streaming Flow:

For two-dimensional incompressible flow in the x-y plane, the steady boundary-layer equation of motion in the downstream direction x is

$$U \frac{\partial U}{\partial x} + V \frac{\partial U}{\partial y} + \frac{\partial(\overline{u^2} - \overline{v^2})}{\partial x} + \frac{\partial \overline{uv}}{\partial y} = U_1 \frac{dU_1}{dx} + \nu \frac{\partial^2 U}{\partial y^2} \quad \ldots(1)$$

where U and V are the mean velocities in the directions x and y,

u and v are the turbulent fluctuations about the mean,

U_1 is the free stream velocity external to the shear flow.

Following Townsend[7] self preserving flow is assumed in the downstream direction with a length scale l_o and a velocity scale u_o, which are both functions of x.

$$\left.\begin{aligned} &\text{Thus the mean velocity } U = U_1 + u_o \; f\left(\frac{y}{l_o}\right) \\ &\text{and the turbulence stresses } \overline{u^2} = u_o^2 \, g_1 \left(\frac{y}{l_o}\right) \\ &\qquad\qquad \overline{v^2} = u_o^2 \, g_2 \left(\frac{y}{l_o}\right) \\ &\qquad\qquad \overline{uv} = u_o^2 \; g_{12} \left(\frac{y}{l_o}\right) \end{aligned}\right\} \ldots(2)$$

where f, g_1, g_2 and g_{12} are functions of the non-dimensional cross stream coordinate $\eta = \frac{y}{l_o}$

Invoking the equation of continuity for the mean flow

$$\frac{\partial U}{\partial x} + \frac{\partial V}{\partial y} = 0 \qquad \ldots(3)$$

and substituting equations (2) in (1) gives

$$\frac{d(u_o U_1)}{dx} f + u_o \frac{du_o}{dx}\left[2(g_1 - g_2) + f^2\right] - \frac{u_o}{l_o}\frac{d(l_o U_1)}{dx}\eta f' - \frac{u_o}{l_o}\frac{d}{dx}(l_o u_o) f' \int_o^\eta f d\eta - \frac{u_o^2}{l_o}\eta(g_1' - g_2')\frac{dl_o}{dx} + \frac{u_o^2}{l_o} g'_{12} = \nu \frac{u_o}{l_o^2} f'' \qquad \ldots(4)$$

where primes denote differentiation with respect to η

If the Reynolds number $\frac{u_o l_o}{\nu}$ is sufficiently large, the direct viscous term on the right hand side of equation (4) is relatively small and may be neglected. Equation (4) is then independent of x if the various coefficients in the equation are proportional to one another. Thus if equation (4) is to be valid for all values of x the following parameters, obtained by dividing through the equation by $(\frac{u_o^2}{l_o})$ must be independent of x:

$$\frac{l_o}{u_o^2}\frac{d(u_o U_1)}{dx} \; ; \; \frac{l_o}{u_o}\frac{du_o}{dx} \; ; \; \frac{1}{u_o}\frac{d(l_o U_1)}{dx} \; ; \; \frac{1}{u_o}\frac{d(l_o u_o)}{dx} \; ; \; \frac{dl_o}{dx}$$

These requirements are satisfied if $\frac{dl_o}{dx}$; $\frac{l_o}{u_o}\frac{du_o}{dx}$ and $\frac{u_o}{U_1}$ are independent of x.

It follows that

$$\begin{aligned} l_o &\propto (x + x_o) \\ u_o &\propto (x + x_o)^m \\ U_1 &\propto (x + x_o)^m \end{aligned} \qquad \ldots(5)$$

where x_o and m are constants.

A second solution is l_o = constant, u_o and U_1 both proportional to e raised to a power which is proportional to $(x + x_o)$.

These results as applied to the outer part of the turbulent boundary layer were first derived on the basis of more restrictive assumptions by Rotta [8], and later discussed more rigorously by Townsend [2],[7], for flows with small velocity defect.

These equations may be applied to a two-dimensional turbulent jet in a streaming flow, if $U_1(x)$ is the main stream velocity surrounding the jet, and $u_o(x) + U_1(x)$ is chosen to be the velocity at the center of the jet.

The component m can be related to the non-dimensional jet velocity $(\frac{u_o}{U_1})$ as follows:

The integral momentum equation may be written

$$\frac{d\,\textcircled{H}}{dx} + \frac{\textcircled{H}}{U_1}\,(H + 2)\,\frac{dU_1}{dx} = 0 \qquad \ldots(6)$$

where $\textcircled{H} = \int_{-\infty}^{+\infty} \frac{U(U-U_1)}{U_1^2}\,dy = \frac{l_o u_o}{U_1}\int_{-\infty}^{+\infty} (f + \frac{u_o}{U_1} f^2)\,d\eta$

and $H\,\textcircled{H} = \int_{-\infty}^{+\infty} \frac{U - U_1}{U_1}\,dy = \frac{l_o u_o}{U_1}\int_{-\infty}^{+\infty} f\,d\eta$

using conventional boundary-layer notation.

For similar profiles (5) in (6) gives

$$1 + m(H + 2) = 0 \qquad \ldots(7)$$

$$\text{and thus } \frac{1}{m} = -\left[2 + \frac{\int_{-\infty}^{+\infty} f d\eta}{\int_{-\infty}^{+\infty} (f + \frac{u_o}{U_1} f^2)\, d\eta} \right] \qquad \ldots(8)$$

The form of the function f may be determined from equation (4) by invoking one of the phenomenonological theories for the functions g_1, g_2, and in particular g_{12}. However the available experimental data on wall jets and free jets in streaming flow suggests that f is given with reasonable accuracy by

$$f = e^{-\eta^2} \qquad \ldots(9)$$

a form which correctly satisfies the boundary conditions

$$f(o) = 1$$

$$f(\pm\infty) = 0$$

Substituting (9) in (8) gives a relationship between m and the jet strength ratio $(\frac{u_o}{U_1})$.

$$m = -\left[2 + \frac{1}{1 + \frac{u_o}{\sqrt{2}U_1}} \right]^{-1} \qquad \ldots(10)$$

It is noted that for jet flow, $(\frac{u_o}{U_1}) > 0$, the pressure gradient is adverse and m lies between $-\frac{1}{3}$ for a weak jet and $-\frac{1}{2}$ for strong jet, the latter being equivalent to a free jet in still air. If $-1 < \frac{u_o}{U_1} < 0$, the solution represents a self preserving wake in an adverse pressure gradient with m between $-\frac{1}{3}$ and -0.185.

For larger values of m, backflow occurs.

The flow constants may also be related to the flow emerging from a slot of width 2b. Suppose that the slot is situated at x = 0, the jet velocity profile is uniform there and equal to U_j, and that the boundary layer passing over each side of the slot has a displacement thickness δ_s^* and a momentum thickness θ_s. The hypothetical "similar-flow" profile at x = 0 is

$$U = U_{is} + u_{os}\, f\left(\frac{y}{l_{os}}\right)$$

where suffix s refers to conditions at the slot.

The two flows may be related approximately by matching both the mass flow and the momentum flux from the centre line y = 0, to the plane, y = h, where h is large and is so chosen that the flow is effectively irrotational there.

Mass:
$$U_j b + \int_{b_{B.L.}}^{h} U\, dy = \int_0^h \left[U_{is} + u_{os}\, e^{-\eta^2}\right] dy$$

$$U_j b - U_{is}\,(\delta_s^* + b) = u_{os}\, l_{os}\, \frac{\sqrt{\pi}}{2}$$

Momentum:
$$U_j^2 b + \int_{b_{B.L.}}^{h} U^2\, dy = \int_0^h \left[U_{is} + u_{os}\, e^{-\eta^2}\right]^2 dy$$

$$U_j^2 b - U_{is}^2(\theta_s + \delta_s^* + b) = u_{os}\, l_{os}\, \frac{\sqrt{\pi}}{2}\,(2U_{is} + \frac{u_{os}}{\sqrt{2}}).$$

whence, by eliminating l_{os},

$$\frac{u_{os}}{U_{is}} = \frac{\sqrt{2}\left[\left(\frac{U_j}{U_{is}}\right)^2 b - \theta_s + \delta_s^* + b - \frac{2U_j}{U_{is}}\, b\right]}{\left(\frac{U_j}{U_{is}}\right) b - \delta_s^* - b} \qquad \ldots(11)$$

Combining equations (10) and (11)

$$m = -\left[2 + \frac{(\frac{U_j}{U_{is}})b - \delta_s^* - b}{(\frac{U_j}{U_{is}})^2 b - (\frac{U_j}{U_{is}})b - \theta_s}\right]^{-1} \qquad \ldots(12)$$

which reduces to the simple form

$$m = -\left[2 + (\frac{U_{is}}{U_j})\right]^{-1} \qquad \ldots(13)$$

when the upstream boundary-layer is very thin compared with the slot width b.

The values of m computed from equation (12) are shown in Fig. (1) as a function of the jet velocity ratio at the slot, $(\frac{U_j}{U_{is}})$, for various values of $(\frac{\delta_s^*}{b})$ assuming that the form factor of the upstream boundary-layer $\frac{\delta_s^*}{\theta_s} = 1.4$, which is the conventional flat plate value at moderate Reynolds number. It is noted that in the vicinity of $(\frac{U_j}{U_{is}}) = 1.5$, self preserving forward flow is impossible unless the upstream boundary-layer is very thin. A strong departure from similarity is therefore anticipated in this region and such a behaviour may be seen in the results of George[6]. For larger values of $\frac{U_j}{U_{is}}$ it is clear that a self preserving jet flow is possible even if the initial boundary layer is quite thick. Furthermore for values of $\frac{U_j}{U_{is}}$ less than unity a self preserving wake flow is possible.

If the slot position is chosen as the zero for x, the value of x_o will depend on the jet velocity ratio $\frac{U_j}{U_{is}}$, the slot width b and the upstream boundary-layer parameters, since

scale effects are usually very small at sufficiently high Reynolds numbers. The dependence on the form parameter of the upstream boundary-layer may be neglected if the upstream pressure gradient is sufficiently small.

$$\text{Thus } \left(\frac{x_o}{b}\right) = F_1 \left(\frac{U_j}{U_{is}}, \frac{\delta^*_s}{b}\right) \qquad \ldots(14)$$

The only experimental information on the value of this function applies to the particular case of a free jet. From the measurements of Förthmann,

$$F_1 (\infty, 0) = - 1.5$$

By dimensional considerations it is also concluded that at sufficiently high Reynolds numbers, the rate of growth of the length scale,

$$\frac{dl_o}{dx} = F_2\left(\frac{U_M}{U_1}\right) \qquad \ldots(15)$$

where $F_2(1) = 0$ and the function increases with increasing $\frac{U_M}{U_1}$.

2.2. Turbulent Wall Jet in Streaming Flow:

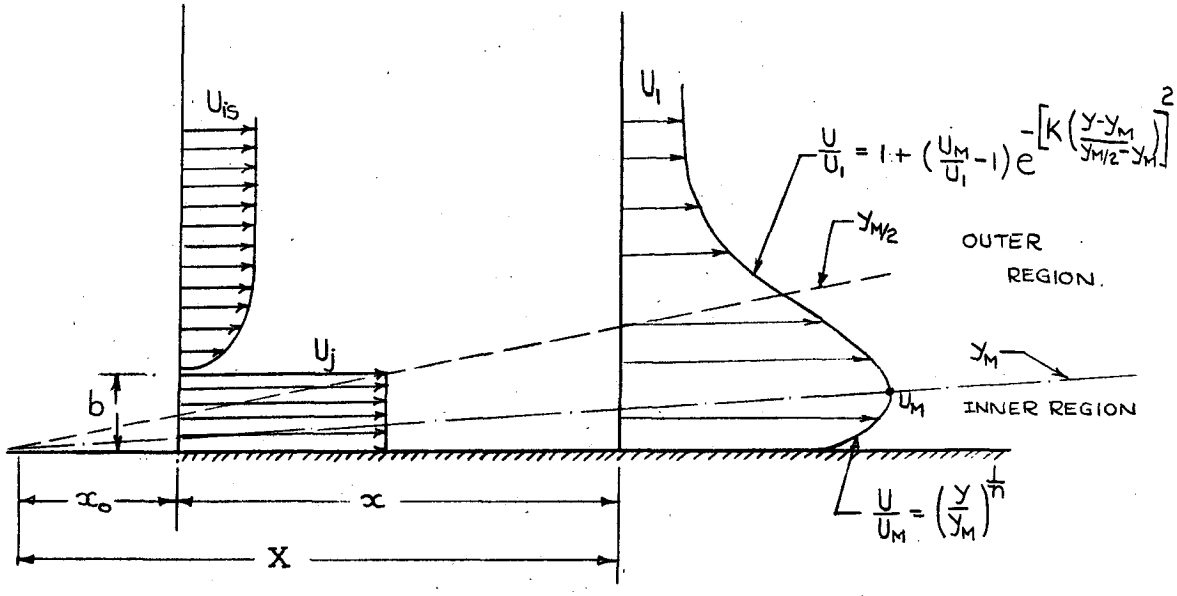

In the case of a fully developed turbulent wall jet it is possible to devide the velocity profile at any section sufficiently far downstream of the slot exit into mainly two regions as shown above. The inner region includes that part of velocity profile which resembles an ordinary turbulent boundary-layer with U_M as the velocity at the edge of boundary-layer and y_M the boundary-layer thickness. The outer region includes the part of velocity profile which resembles half a free jet in streaming flow. The analysis of this outer region is given in the next section.

Outer Region of Turbulent Wall Jet in Streaming Flow.

The flow in a two-dimensional wall jet in streaming flow is similar to half the previous flow at sufficiently high Reynolds number, for then the boundary-layer represents only a small proportion of the total velocity profile.

Since the similarity should now strictly extend into the wall law region further restrictions are necessary to ensure self preservation. The skin friction velocity U_τ as well as u_o and U_1, must be proportional to $(x + x_o)^m$. Further the Reynolds number formed by the scaling parameters $\frac{u_o l_o}{\nu}$ must be constant[2].

Thus $m = -1$ and $\frac{u_o}{U_1} = -2\sqrt{2}$.

Hence a strictly self preserving forward flow is not possible.

Approximate self preservation may be attained for small $\frac{u_o}{U_1}$ when the length scale and the velocity scale are related by the logarithmic form of the wall law. For such a case l_o is no longer proportional to $(x + x_o)$. (Refs. (2) and (7)).

For large $\frac{u_o}{U_1}$ approximate self preservation may be possible on the grounds that the coupling between the outer flow and the inner boundary-layer is weak so that the outer half jet conforms to the analysis of the previous section. Such an assumption has been fruitful in the analysis of wall jets in quiescent fluid[1],[9]. In such a case the analysis of the previous section may be carried over without change:

b then represents the slot width and δ_s^*, θ_s the thicknesses of the boundary-layer flowing over the top of the slot. The exponent m governing the variation of main stream velocity is given by equations (10) or (12). However the rate of linear growth of the outer half jet and the exact form of the functional relationship for x_o (equation (14)) may be expected to differ from that for free jet flow.

2.3 Inner Boundary-Layer Development

In the following analysis of the inner region it is assumed that,

(i) all the conventional boundary-layer approximations apply including that the Reynolds normal stresses are negligibly small and

(ii) the shear stress at the edge of the inner layer ($y = y_M$) is zero.

The last assumption is at variance with the measurements of Bradshaw and Gee[10] using slanting hot wires, but such measurements are notoriously difficult to make and further measurements are clearly necessary. The above assumption No. (ii) is also in disagreement with Schwarz and Cosart.[11] However, the present theory gives useful results. Furthermore, longitudinal turbulence measurements show a minimum at $y = y_M$ thus indicating zero turbulence production at $y = y_M$, (Mixing length theory) and seems to contrast with the measurements of Bradshaw and Gee[10], and Schwarz and Cosart[11].

They investigated wall jet in still air for which it is expected that the turbulence is greater than in wall jets in streaming flow at the velocity peak. However, in the case of wall jet in equilibrium pressure gradient turbulence will be small at the velocity peak. On these grounds it is possible to make the assumption No.(ii). No attempt has yet

been made to measure the shear stress at the velocity peak, however, the experimental results agree very well with the theory given below.

From previous analysis it is shown that:

$$\left.\begin{aligned} U_1 &= C_1 (x + x_o)^m \\ \text{and} \quad U_M &= C_2 (x + x_o)^m \end{aligned}\right\} \quad \ldots(16)$$

where m is a known constant and a function of $\frac{U_M}{U_1} = \frac{C_2}{C_1}$.

For the inner region U_M represents the streaming flow and y_M the boundary-layer thickness of a flow which resembles a conventional turbulent boundary-layer but with a relatively high main stream turbulence.

Thus momentum and continuity equations can be written as:

$$\text{Momentum: } U\frac{\partial U}{\partial x} + V\frac{\partial U}{\partial y} = -\frac{1}{\rho}\frac{dP}{dx} + \frac{1}{\rho}\frac{\partial \tau}{\partial y} \quad \ldots(17)$$

$$\text{where: } \tau = (\mu \frac{\partial U}{\partial y} - \rho\overline{uv})$$

$$\text{Continuity: } \frac{\partial U}{\partial x} + \frac{\partial V}{\partial y} = 0 \quad \ldots(18)$$

With boundary layer approximations the momentum equation can be written as:

$$U\frac{\partial U}{\partial x} + V\frac{\partial U}{\partial y} = U_1\frac{dU_1}{dx} + \frac{1}{\rho}\frac{\partial \tau}{\partial y} \quad \ldots(19)$$

Integrating equations (18) and (19) from $y = 0$ to $y = y_M$ with boundary conditions:

$$\left.\begin{aligned} &\text{at } y = 0 \quad \tau = \tau_o \text{ and } U = V = 0 \\ &\text{and} \quad \text{at } y = y_M \; \tau = 0 \text{ and } U = U_M \end{aligned}\right\} \quad \ldots(20)$$

$$- \frac{\tau_o}{\rho} + U_M \cdot \frac{dU_M}{dx} \cdot y_M \cdot \left(\frac{c_1}{c_2}\right)^2 = \int_o^{y_M} \left(U\frac{\partial U}{\partial x} + V\frac{\partial U}{\partial y}\right) .dy$$

$$= \frac{d}{dx}\left(U_M^2 \cdot y_M\right) \left[\int_o^1 (\eta)^{\frac{2}{n}} d\eta - \int_o^1 (\eta)^{\frac{1}{n}} .d\eta\right]$$

$$+ U_M \cdot y_M \cdot \frac{dU_M}{dx} \cdot \int_o^1 (\eta)^{\frac{1}{n}} .d\eta$$

where $\frac{U}{U_M} = (\eta)^{\frac{1}{n}}$ and $\eta = \frac{y}{y_M}$

$$\therefore \quad \frac{\tau_o}{\rho} = \frac{d}{dx}\left(U_M^2\, y_M\right) \left[\int_o^1 (\eta)^{\frac{1}{n}}\, d\eta - \int_o^1 (\eta)^{\frac{2}{n}}\, d\eta\right]$$

$$- U_M\, y_M \frac{dU_M}{dx} \left[\int_o^1 (\eta)^{\frac{1}{n}} .d\eta - \left(\frac{c_1}{c_2}\right)^2\right] \qquad \ldots(21)$$

If $\tau \neq o$ at $y = y_M$ the above equation is modified to

$$\left(\frac{\tau_o}{\rho} - \frac{\tau}{\rho}\right) = \frac{d}{dx}\left(U_M^2\, y_M\right) \left[\int_o^1 (\eta)^{\frac{1}{n}} .d\eta - \int_o^1 (\eta)^{\frac{2}{n}} .d\eta\right]$$

$$- U_M\, y_M \frac{dU_M}{dx} \left[\int_o^1 (\eta)^{\frac{1}{n}} .d\eta - \left(\frac{c_1}{c_2}\right)^2\right] \qquad \ldots(22)$$

Assume a power law form for skin friction

$$\frac{\tau_o}{\rho} = \frac{\alpha U_M^2}{\left(\frac{U_M\, y_M}{\nu}\right)^{\frac{1}{N}}} \qquad \ldots(23)$$

where α is a constant and $N = \frac{n+1}{2}$ from the law of the wall and is consistant with the assumption of a power profile for $\left(\frac{U}{U_M}\right) = \eta^{\frac{1}{n}}$, and can be easily derived as follows:

From equation (23)

$$\frac{\tau_o}{\rho U_M^2} \propto \frac{1}{(U_M)^{\frac{1}{N}}}$$

$$\therefore \left(\frac{U_\tau}{U_M}\right)^2 \propto \left(\frac{1}{(U_M)^{\frac{1}{N}}}\right) \qquad \ldots(24)$$

If the law-of-wall applies then

$$\left(\frac{U}{U_\tau}\right) = f\left(\frac{yU_\tau}{\nu}\right)$$

i.e. with the assumption of $\left(\frac{1}{n}\right)^{th}$ power law velocity profile near the wall the law-of-wall would be

$$\frac{U}{U_\tau} = \text{constant.} \left(\frac{yU_\tau}{\nu}\right)^{\frac{1}{n}} \qquad \ldots(25)$$

at $y = y_M \quad U = U_M$

$$\therefore \frac{U_M}{U_\tau} \propto \left(\frac{y_M U_\tau}{\nu}\right)^{\frac{1}{n}}$$

i.e. $$U_M \propto U_\tau^{\frac{n+1}{n}} \qquad \ldots(26)$$

Substituting equation (26) in equation (24) gives:

$$\left(\frac{U_\tau}{U_M}\right)^2 \propto (U_M)^{-\frac{2}{n+1}} \propto (U_M)^{-\frac{1}{N}}$$

$$\therefore N = \left(\frac{n+1}{2}\right) \qquad \ldots(27)$$

It should be noted that equation (27) is generally true and does not depend on the existence of the universal, logarithmic, law-of-wall with A = 5.6 and B = 4.9.

However, due to the high level of turbulence in wall jets it is expected that the exponent n will be greater than that in an ordinary turbulent boundary-layers at a comparable R_e (i.e. n = 7). It should be noted that similar assumption of a power law form for skin friction was also made by Myers et al[12] when analysing wall jet in still air.

Substituting equation (23) in equation (21) gives:

$$\frac{\alpha U_M^2}{\left(\frac{U_M Y_M}{\nu}\right)^{\frac{1}{N}}} = \bar{A}\frac{d}{dx}\left(U_M^2 Y_M\right) - \bar{B}\, U_M Y_M \frac{dU_M}{dx} \qquad \ldots(28)$$

where $$\bar{A} = \int_0^1 (\eta)^{\frac{1}{n}}.d\eta - \int_0^1 (\eta)^{\frac{2}{n}}.d\eta = \frac{n}{(n+1)(n+2)}$$

and $$\bar{B} = \int_0^1 (\eta)^{\frac{1}{n}}.d\eta - \left(\frac{C_1}{C_2}\right)^2 = \frac{n}{(n+1)} - \left(\frac{C_1}{C_2}\right)^2$$

Now writing $X = (x + x_o)$ and substituting for $U_M = C_2 X^m$ equation (28) reduces to:

$$\frac{\alpha \nu^{\frac{1}{N}}}{\left(C_2 X^m Y_M\right)^{\frac{1}{N}}} = \frac{m y_M}{X}\left(2\bar{A} - \bar{B}\right) + \bar{A}\frac{dy_M}{dX} \qquad \ldots(29$$

The proper selection of velocity profile in the inner layer defines the quantities $\bar{A}$ and $\bar{B}$, which are determined by the exponent n describing the velocity profile.

The solution of equation (29) can be easily obtained as:

$$y_M = \left[\frac{(N+1)\alpha\nu^{\frac{1}{N}}}{\bar{A}\, C_2^{\frac{1}{N}} \left\{ m\left[\left(\frac{2\bar{A} - \bar{B}}{\bar{A}} \right)(N+1) - 1 \right] + N \right\}} \right]^{\frac{N}{N+1}} \cdot x^{\frac{N-m}{N+1}} \quad \ldots(30)$$

The equation (30) can be written in non-dimensional form as follows:

$$\left(\frac{y_M}{b}\right) = \left[\frac{(N+1)\,\alpha}{\bar{A}\left\{ m\left[\left(\frac{2\bar{A} - \bar{B}}{\bar{A}} \right)(N+1) - 1 \right] + N \right\}} \right]^{\frac{N}{N+1}} \cdot \left(\frac{\nu}{bU_{M_s}}\right)^{\frac{1}{N+1}} \cdot \left(\frac{x_o}{b}\right)^{\frac{m}{N+1}} \cdot \left(\frac{x + x_o}{b}\right)^{\frac{N-m}{N+1}} \quad \ldots(31)$$

where $$\left(\frac{U_{M_s} - U_{is}}{U_{is}}\right) = \frac{\sqrt{2}\left[\left(\frac{U_j}{U_{is}}\right)^2 - \frac{\theta_s}{b} + \frac{\delta_s^*}{b} + 1 - 2\left(\frac{U_j}{U_{is}}\right) \right]}{\left[\left(\frac{U_j}{U_{is}}\right) - \frac{\delta_s^*}{b} - 1 \right]} \quad \ldots(32)$$

$$\frac{U_M}{U_{M_s}} = \left(\frac{x + x_o}{x_o}\right)^m \quad \ldots(33)$$

and $$Re_s = \left(\frac{U_{M_s} b}{\nu}\right) \quad \ldots(34)$$

Hence $$\left(\frac{y_M}{b}\right) \propto \left(\frac{x + x_o}{b}\right)^{\frac{N-m}{N+1}} \quad \ldots(35)$$

Skin friction variation:-

Define skin friction as $C_f = \dfrac{\tau_o}{\frac{1}{2}\rho U_M^2}$

$$\therefore C_f = \frac{2\alpha}{\left(\frac{U_M y_M}{\nu}\right)^{\frac{1}{N}}} \qquad \ldots(36)$$

Substituting the values of U_M and y_M from above analysis into equation (36), gives:

$$(R_{e_s})^{\frac{1}{N+1}} \cdot C_f = \frac{2\alpha \left(\frac{x_o}{b}\right)^{\frac{m}{N+1}}}{\left[\frac{(N+1)\alpha}{\bar{A}\left\{m\left[\left(\frac{2\bar{A}-\bar{B}}{\bar{A}}\right)(N+1)-1\right]+N\right\}}\right]^{\frac{1}{N+1}} \cdot \left(\frac{x+x_o}{b}\right)^{\frac{m+1}{N+1}}} \qquad \ldots(37)$$

It is clear from equation (37) that

$$C_f (R_{e_s})^{\frac{1}{N+1}} \propto \frac{1}{\left(\frac{x+x_o}{b}\right)^{\frac{m+1}{N+1}}} \qquad \ldots(38)$$

Equation (38) is similar in form to Myers et al[12].

Considering the limiting values of m for weak and strong jets in equilibrium pressure gradient, namely $m = -\frac{1}{3}$ and $-\frac{1}{2}$ and exponent $n = 11$, $C_f R_{e_s}^{\frac{1}{7}}$ varies proportionately to $\frac{1}{\left(\frac{x+x_o}{b}\right)^{0.0952}}$ and $\frac{1}{\left(\frac{x+x_o}{b}\right)^{0.0715}}$ respectively. This indicates that C_f is not very sensitive to changes in either R_{e_s} or $\left(\frac{x+x_o}{b}\right)$. Schwarz and Cosart[11] found experimentally that C_f does not vary much with x for a wall jet in still air. As a strong

wall jet in equilibrium pressure gradient tends to a wall jet in the still air case, their observation is in agreement with equation (38).

2.4 Effect of Inner Boundary Layer on Outer Flow.

As a second approximation to the analysis of section 2.2, the effect of the inner boundary-layer is now considered.

From the previous analysis it is clear that the outer part of the wall jet (i.e. $y > y_M$) can be represented by $\frac{U}{U_1} = 1 + (\frac{U_M}{U_1} - 1)e^{-\eta_1^2}$ and the inner boundary-layer region (i.e. $y < y_M$) can be represented by $(\frac{U}{U_1}) = (\frac{U_M}{U_1})\eta^{\frac{1}{n}}$

The integral momentum equation for the whole flow can be written as:

$$\frac{\tau_o}{\rho U_1^2} = \frac{d\theta}{dx} + \frac{\theta}{U_1}\frac{dU_1}{dx}(H + 2) \qquad \ldots(39)$$

where $\theta = \int_o^\delta \frac{U}{U_1}\cdot(1 - \frac{U}{U_1})\cdot dy$

and $H\,\theta = \int_o^\delta (1 - \frac{U}{U_1}).dy$

Now $\theta = \int_o^\delta \frac{U}{U_1}\cdot(1 - \frac{U}{U_1}).dy$

$$= \underbrace{\int_o^{y_M} \frac{U}{U_1}(1 - \frac{U}{U_1})\,dy}_{\text{B/L.}} + \underbrace{\int_{y_M}^{\delta\to\infty} \frac{U}{U_1}(1 - \frac{U}{U_1}).dy}_{\text{outer part}}$$

$$= y_M \int_o^1 \left[\frac{U_M}{U_1}\cdot\eta^{\frac{1}{n}} - (\frac{U_M}{U_1})\cdot\eta^{2\frac{2}{n}}\right] d\eta + \int_o^\infty \left[1 + \frac{u_o}{U_1}\, e^{-\eta_1^2}\right]\cdot$$

$$\left[-\frac{u_o}{U_1}\, e^{-\eta_1^2}\right]\cdot\left[\frac{y_{M/2} - y_M}{K}\right]\cdot d\eta_1$$

where $u_o = (U_M - U_1)$: $\eta = (\frac{y}{y_M})$

and using $l_o = (y_{M/2} - y_M) \propto (x + x_o)$: $\eta_1 = K(\frac{y - y_M}{\frac{y_M}{2} - y_M})$;

K = arbitrary constant = 0.833.

(see sections 4.1:3 and 4.1:4).

$$\therefore \theta = y_M \left[\frac{U_M}{U_1}\left(\frac{n}{n+1}\right) - \left(\frac{U_M}{U_1}\right)^2\left(\frac{n}{n+2}\right)\right] - \left[\left(\frac{y_{M/2}-y_M}{K}\right)\left(\frac{u_o}{U_1}\cdot\frac{\sqrt{\pi}}{2}\right)\left(1+\frac{u_o}{\sqrt{2}U_1}\right)\right] \quad \ldots(40)$$

$$\text{Similarly } H\theta = y_M\left[1 - \frac{U_M}{U_1}\left(\frac{n}{n+1}\right)\right] - \left[\left(\frac{y_{M/2}-y_M}{K}\right)\left(\frac{u_o}{U_1}\right)\left(\frac{\sqrt{\pi}}{2}\right)\right] \quad \ldots(41)$$

Substituting equations (40) and (41) in equation (39) gives

$$\frac{\tau_o}{\rho U_1^2} = \left(\frac{U_M}{U_1}\right)\cdot\left[\left(\frac{n}{n+1}\right) - \left(\frac{U_M}{U_1}\right)\left(\frac{n}{n+2}\right)\right]\cdot\frac{dy_M}{dx} - \left[\frac{c}{K}\cdot\frac{u_o}{U_1}\cdot\frac{\sqrt{\pi}}{2}\left(1+\frac{u_o}{\sqrt{2}U_1}\right)\right]$$

$$+ \quad m\left[2 + \frac{y_M\left[1 - \frac{U_M}{U_1}\cdot\left(\frac{n}{n+1}\right)\right] - \left(\frac{y_{M/2}-y_M}{K}\right)\cdot\frac{u_o}{U_1}\cdot\frac{\sqrt{\pi}}{2}}{\frac{U_M y_M}{U_1}\left[\frac{n}{n+1} - \left(\frac{U_M}{U_1}\right)\cdot\left(\frac{n}{n+2}\right)\right] - \left(\frac{y_{M/2}-y_M}{K}\right)\frac{u_o}{U_1}\frac{\sqrt{\pi}}{2}\cdot\left(1+\frac{u_o}{\sqrt{2}U_1}\right)}\right]\cdot\left[\frac{U_M y_M}{U_1(x+x_o)}\left\{\left(\frac{n}{n+1}\right) - \left(\frac{U_M}{U_1}\right)\cdot\left(\frac{n}{n+2}\right)\right\} - \frac{1}{K}\left(\frac{y_{M/2}-y_M}{x+x_o}\right)\left(\frac{u_o}{U_1}\frac{\sqrt{\pi}}{2}\right)\left(1+\frac{u_o}{\sqrt{2}U_1}\right)\right] \quad \ldots(42)$$

As previously observed (equation (35) and also see section 4.1:9) y_M is very nearly proportional to $(x+x_o)$. Also $(y_{M/2}-y_M) = C(x+x_o)$. Hence substituting these in equation (42), it becomes:

$$\frac{\tau_o}{\rho U_M^2} = \left(\frac{U_1}{U_M}\right)\left[\left\{\left(\frac{n}{n+1}\right) - \left(\frac{U_M}{U_1}\right)\left(\frac{n}{n+2}\right)\right\}\cdot\frac{dy_M}{dx} - \left(\frac{C}{K}\cdot\frac{u_o\sqrt{\pi}}{U_M}\,2\right)\left(1+\frac{u_o}{2U_1}\right)\right]\cdot\left[1 + m\left\{2 + \frac{\left[1 - \frac{U_M}{U_1}\left(\frac{n}{n+1}\right)\right] - \left[\left(\frac{y_{M/2}-y_M}{Ky_M}\right)\left(\frac{u_o}{U_1}\cdot\frac{\sqrt{\pi}}{2}\right)\right]}{\left(\frac{U_M}{U_1}\right)\cdot\left[\left(\frac{n}{n+1}\right) - \left(\frac{U_M}{U_1}\right)\left(\frac{n}{n+2}\right)\right] - \left[\left(\frac{y_{M/2}-y_M}{Ky_M}\right)\frac{u_o}{U_1}\,\frac{\pi}{2}\left(1+\frac{u_o}{2U_1}\right)\right]}\right\}\right] \quad \ldots(43)$$

When the boundary layer is neglected this equation reduces to:

$$1 + m\left[2 + \frac{1}{1 + \frac{u_o}{\sqrt{2}U_1}}\right] = 0.$$

in agreement with equation (10) of section 2.1.

To assess the effect of the inner boundary-layer on the outer part, the value of m is obtained from equation (43) and compared with that obtained from equation (10).

Rearranging equation (43),

$$m = \left[\frac{\left\{\frac{\left(\frac{\tau_o}{\rho U_M}2\right)\cdot\left(\frac{U_M}{U_1}\right)}{\left[\left(\frac{n}{n+1}\right)-\left(\frac{U_M}{U_1}\right)\left(\frac{n}{n+2}\right)\right]\cdot\frac{dy_M}{dx} - \frac{C}{K}\cdot\frac{u_o}{U1}\frac{\sqrt{\pi}}{2}\left(1+\frac{u_o}{\sqrt{2}U_1}\right)}\right\} - 1}{2 + \frac{\left[1-\left(\frac{U_M}{U_1}\right)\left(\frac{n}{n+1}\right)\right] - \left(\frac{y_{M/2}-y_M}{y_M}\right)\cdot\frac{1}{K}\cdot\frac{u_o}{U_1}\cdot\frac{\sqrt{\pi}}{2}}{\left(\frac{U_M}{U_1}\right)\left[\left(\frac{n}{n+1}\right)-\left(\frac{U_M}{U_1}\right)\left(\frac{n}{n+2}\right)\right] - \left(\frac{y_{M/2}-y_M}{y_M}\right)\cdot\frac{1}{K}\cdot\frac{u_o}{U_1}\cdot\frac{\sqrt{\pi}}{2}\left(1+\frac{u_o}{\sqrt{2}U_1}\right)}}\right] \quad \ldots(44)$$

which when the boundary-layer is neglected once more reduces to:

$$m = - \left[2 + \frac{1}{1 + \frac{u_o}{\sqrt{2} u_1}} \right]^{-1} \qquad \ldots(10)$$

The following table gives a comparison of the m values obtained from equations (10) and (44), using measured results which are described later and n = 11.

$\frac{U_j}{U_{is}}$	$b_{ins.}$	$\frac{dy_M}{dx}$	$\frac{y_{M/2}}{y_M}$	m From equa. (10)	m From equa. (44)
3.00	0.2	0.0072	3.84	-0.407	-0.4175
6.00	0.2	0.00955	5.465	-0.448	-0.451

It is seen that the values of m obtained from equation (44) are sufficiently in close agreement, for most practical purposes, with those obtained from equation (10).

Thus the inner boundary-layer indeed has little effect on the outer part of the wall jet in equilibrium pressure gradient.

2.5 Non-dimensional Mean Velocity Profile Including the Inner Boundary-Layer in an Equilibrium Pressure Gradient:

From the analysis of the previous section (2.4) it is seen that the complete velocity profile for a wall jet in an equilibrium pressure gradient can be given by adding two regions together. However, it is worth noting that due to the selection of a power profile for the inner region, the gradient of mean velocity profile will not be zero at the velocity peak. On the other hand the outer region profile has a zero slope there. However, the condition that $U = U_m$ at the matching point is fulfilled by both the inner and the outer profiles. Furthermore, consistent with the assumption the shear stress at the matching point is also zero.

Thus the complete non-dimensional mean velocity profile is given by:

$$\left(\frac{U-U_1}{U_M-U_1}\right) = \underbrace{\left[\frac{\left(\frac{U_M}{U_1}\right)\left(\frac{Y}{Y_M}\right)^{\frac{1}{n}} - 1}{\left(\frac{U_M}{U_1} - 1\right)}\right]}_{0 < Y < Y_M} + \underbrace{e^{-\left[K\cdot\left(\frac{Y - Y_M}{Y_{M/2}-Y_M}\right)\right]^2}}_{Y_M < Y < \infty} \qquad \ldots(45)$$

It should be noted that each part on the right hand side of equation (45) only applies within the respective limits and is assumed to be zero elsewhere. Also note that $Y_{M/2} \propto (x + x_o)$ and $Y_M \propto (x + x_o)$ thus $\left(\frac{Y_{M/2}}{Y_M}\right)$ is a constant which in turn is a function of $\left(\frac{U_M}{U_1}\right)$.

3. GENERAL DETAILS OF THE EXPERIMENTAL INVESTIGATION:

Detail of the experimental apparatus is described in the Appendix I. The aim was to produce a wall jet in streaming flow for which the longitudinal pressure gradient could be readily adjusted and in which the mean flow was effectively two-dimensional. This was achieved by using a blower tunnel and a test section with adjustable louvres similar to the test section of Clauser[13].

Due to the flexibility of the apparatus it was possible to investigate for comparison wall jets in still air and also wall jets in streaming flow with zero pressure gradient. The wall jet in still air was investigated for jet velocity U_j equal to 239 ft./sec. and 317.5 ft./sec. and with a slot of width 0.20ins. The wall jet in streaming flow with zero pressure gradient was investigated for $(\frac{U_j}{U_{is}})$ equal to 2.66, 3.0 and 5.95 and with a slot of width 0.20in. and 0.375in.

The wall jet in an equilibrium pressure gradient was investigated thoroughly to support the theoretical analysis given before. The measurements were made for the jet velocity ratios, $(\frac{U_j}{U_{is}})$, of 1.07, 1.501, 3.0, 4.05, 6.0 and 6.01, and slot widths of 0.20in., 0.375in., 0.40in., and 0.402in.

Pitot traverses on the centre line of the plate were made by a round pitot tube with sharpened lips and also by a flat pitot tube. The details of these pitot tubes are given in Appendix I. Extreme care was taken in traversing the flow and in particular for obtaining distance of pitot tube centre from the plate surface. The pitot tube was lowered down to touch the plate and then moved up with an increment of 0.001in. The pitot tube readings were plotted simultaneously. When the pitot tube had just left the wall a change in reading was observed and was found to be linear with y for about 0.003in. However, when the pitot tube was in contact with the plate it gave a constant reading. Thus knowing the size of the pitot tube the two intersecting straight lines gave the distance of pitot tube centre line from the plate. This procedure was adopted as a preliminary for all the velocity measurements. This method was extremely successful and the repeatability was very good. The correction for the displacement of the pitot tube centre line was not made. The velocities were calculated on the assumption that the static pressure at a particular section was constant across the boundary-layer.

Two-dimensionality checks for wall jet in streaming flow were made at x = 0.5in. and 15.5in. downstream of the slot exit. The results are described in Appendix II. Within 6ins. of the centre line the profiles were almost identical

across the flow. Thus with the main measurements being made on the centre line the flow was considered to be effectively two-dimensional.

The adverse pressure gradient on the plate was set as follows:

For a particular value of $\frac{U_j}{U_{is}}$, b and δ_s^* the value of m was calculated from equation (12). A suitable free stream velocity at the slot, U_{is}, was then chosen. Using equation (5) $(\frac{U_1}{U_{is}}) = (1 + \frac{x}{x_o})^m$, it was then possible to calculate the free stream velocity U_1 at various $\frac{x}{x_o}$. The value of x_o was then determined approximately by extrapolating George's[6] results. Using these approximate values of U_1 and assuming that the flow at any section was one dimensional the mass flow at each section was calculated to establish the amount of excess air to be bled from the top louvers. Assuming that the louver profiles were sufficiently streamlined to ensure that the flow left smoothly and without a vena contracta it was possible to determine the louver settings to give the required pressure gradient.

The skin friction measurements were made by using Stanton tubes. These were fixed at x = 6.5in., 12.5in., and 18.5in. from the slot exit. A Preston tube was also used at x = 18.5in. The details of these tubes and the calibrations are described in Appendix II. The skin friction

measurements were also made for wall jets in still air and wall jets in streaming flow with zero pressure gradient.

A brief investigation was made to determine the longitudinal turbulence by using the DISA constant temperature anemometer 55 A 01.[14] Two separate hot wire probes were used to check the repeatability. Platinum plated Tungsten wire of 0.005mm. diameter and approximately 1mm. length was used. The results of the longitudinal turbulence at x = 19.2in. are presented for the two cases of wall jet in equilibrium pressure gradient ($\frac{U_j}{U_{is}}$ = 3.0 and 6.0 and b = 0.20in.), and for a wall jet in still air (U_j = 317.5 ft./sec., b = 0.20in.)

4. DISCUSSION OF THE EXPERIMENTAL RESULTS AND COMPARISON WITH THE THEORY.

Experimental results are divided into three parts as follows:

(i) Wall Jet in Equilibrium Pressure Gradient.

(ii) Wall Jet in Streaming Flow With Zero Pressure Gradient.

(iii) Wall Jet in Still Air.

4.1 Wall Jet in Equilibrium Pressure Gradient:

4.1.1 General

Pitot traverses on the centre line of the plate were made at 6.5in., 9.5in., 12.5in., 15.5in., 18.5in., and 21.5in. downstream from the slot exit. The Stanton tubes were fixed 1in. on either side of the centre line at 6.5in., 12.5in., and 18.5in. from the slot exit. The hot wire anemometer traverses were made at 19.2in., from the slot exit.

The experimental results are for jet velocity ratios, $(\frac{U_j}{U_{is}})$ of 1.07, 1.501, 3.0, 4.05, 6.0 and 6.01 and slot widths of 0.2in., 0.375in., 0.40in., and 0.402in. The test conditions together with the upstream boundary-layer Reynolds number $(\frac{U_{is}\theta_s}{\nu})$ are shown in Table 1. Also shown in this table are the associated values of $(\frac{U_M}{U_1})$, the exponent m, x_o, the rate of growth C and the wall jet Reynolds number $(\frac{U_M y_M/2}{\nu})$.

4.1.2 Variation of $(\frac{U_M}{U_1})$.

It is seen from Figures (3.1, 3.2, 3.3, 3.4, 3.5, and 3.6), that the ratio $(\frac{U_M}{U_1})$ is practically independent of x as required for similarity. The average value of $(\frac{U_M}{U_1})$ for each test is used to compute the exponent m in equation (10). The values of m obtained from equations (10) and (12) are given in Table 1 and are in fair agreement with one another. The values of m obtained from equation (10) are presumably more reliable because the analytical formulation of this equation does not depend on a simplified allowance for the upstream boundary-layer involving an overall matching of continuity and momentum.

4.1.3 Velocity Profiles.

Figures (4) show the velocity profiles plotted as $(\frac{U}{U_{is}})$ vs y at various downstream distances, x, from the slot for the seven test conditions. These plots show that the maximum velocity U_M decays as the downstream distance from the slot increases and that the free stream velocity U_1 has been decreased in proportion by the imposed pressure gradient.

Furthermore it is seen that the measurements were made sufficiently far downstream of the slot for the flow to be fully developed in the sense that the detailed structures

of the flow emerging from the slot and the flow within the boundary-layer outside the slot, are no longer apparent except for the cases of $(\frac{U_j}{U_{is}})$ = 1.501 and 1.07. In the case of $(\frac{U_j}{U_{is}})$ = 1.501 and b = 0.20in., the velocity profiles distinctly exhibit the influence of the upstream boundary-layer. Farther downstream however, the velocity profiles more clearly resemble an ordinary turbulent boundary-layer. For this particular test it was observed that the flow separated at approximately $(\frac{x}{b})$ = 122.5 and confirmed by visual observation made by using tufts on the surface of the plate. In the case of $(\frac{U_j}{U_{is}})$ = 1.07 and b = 0.20in. the influence of the boundary-layer outside the slot is even more prominent and velocity profiles retain this influence over the entire length of the plate. A distinct negative Stanton tube reading was observed at $(\frac{x}{b})$ = 92.5 indicating the separation of flow from the surface of the plate. This was furthermore confirmed by the visual observation of the tufts. The above two cases were investigated to confirm the predictions made in the theoretical analysis.

For $(\frac{U_j}{U_{is}})$ = 1.07 case, it can be seen that the velocity profiles are definitely not similar. For the case $(\frac{U_j}{U_{is}})$ = 1.501 it is difficult to conclude from these plots that the velocity profiles are not similar, however, further investigation shows that the achievement of similarity for such low values of $\frac{U_j}{U_{is}}$

is clearly always difficult (Fig.1).

Another interesting point to note is that the distance from the slot exit where the core of a jet disappears may be a function of $(\frac{U_j}{U_{is}})$ and slot width. This effect although not obvious in the velocity profiles for slot widths b = 0.375in. 0.40in., and 0.402in. is clearly indicated in the non-dimensional mean velocity profiles.

Figs. (5) show the velocity profiles plotted non-dimensionally in accordance with equation (2), except that the non-dimensional cross stream co-ordinate is transferred to exclude the effect of the inner boundary-layer of the wall jet. Thus the parameters $(\frac{U-U_1}{U_M-U_1})$ and $(\frac{Y-Y_M}{Y_{M/2}-Y_M})$ are chosen to represent the similar velocity profile for the outer region. The length scale $Y_{M/2}$ is the larger value of y where $(\frac{U-U_1}{U_M-U_1}) = \frac{1}{2}$ and Y_M is the value of y where $U = U_M$. In these figures an empirical form of the function $f(\eta) = (\frac{U-U_1}{U_M-U_1})$ is provided for comparison.

$$f(\eta) = (\frac{U-U_1}{U_M-U_1}) = e^{-\left[0.833\cdot(\frac{Y-Y_M}{Y_{M/2}-Y_M})\right]^2}$$

The Sech.^{2} function is also plotted for comparison i.e. $f(\eta) = (\frac{U-U_1}{U_M-U_1}) = \text{Sech.}^2\left[0.88\left(\frac{Y-Y_M}{Y_{M/2}-Y_M}\right)\right]$. It will be recalled that this latter function is used by Eichelbrenner

et al[15] in their method for calculating the development of wall jets in streaming flow.

It is noted that despite the existence of the inner boundary layer region a satisfactory degree of similarity has been achieved in the outer region of the flow and also that the exponential function is in better agreement with the results. It should be noted that the experimental results are slightly lower than the values of the exponential function in the region between y_M and $y_{M/2}$.

Figs. (5.1, 5.3, and 5.4) show clearly that the velocity profiles at a distance of 6.5in. from the slot exit deviate slightly from the similarity profile. This may be accounted due to the core of the jet not having completely vanished at this distance. Recent investigation by R. Knystautas[16] of a free two-dimensional jet indicated that the core of a jet disappears at approximately $(\frac{x}{b}) = 8$. Myers et al[12] have found that for wall jet in still air the distance where the jet core disappears lies between $\frac{x}{b} = 4$ and $\frac{x}{b} = 14$. However, for wall jet in streaming flow the rate of growth of the jet being smaller than that of a wall jet in still air; it is expected that the jet core will exist for a longer distance. As mentioned before this distance may be a function of $\frac{U_j}{U_{is}}$ and slot width.

Fig. (5.6) is of interest in the sense that it confirms the prediction of difficulty in obtaining similar velocity profiles for $(\frac{U_j}{U_{is}}) = 1.501$.

Figs.(6) show the velocity profiles plotted using the non-dimensional cross stream co-ordinate as suggested in the theory. (Section 2.5, equation (45)). Also on these figures a full velocity profile obtained from theory is drawn for comparison.

The inner boundary layer is represented by an $\frac{1}{11}^{th}$ power profile and the outer part of the jet is represented by an exponential function. The values of $(\frac{U_M}{U_1})$ and $(\frac{y_M}{y_{M/2}})$ were obtained from the measurements. It is clear from these figures that, apart from the discontinuity in slope at $y = y_M$, the experimental results are fairly well represented by matching the two profiles. As observed in Figs.(5), the experimental results are slightly lower than the theoretical values obtained from exponential function in the region $y_M < y < y_{M/2}$.

4.1.4 Growth of Wall Jet:

The growth of wall jet in terms of $(\frac{y_{M/2}}{b})$ and $(\frac{y_M}{b})$ is shown in Figs.(7). Both curves are seen to be linear for the range of $(\frac{x}{b})$ which was investigated. Thus the curves define the values of x_o and C in the growth equation for the outer flow:

$$(y_{M/2} - y_M) = C(x + x_o) \qquad \ldots(46)$$

In agreement with equation (14)

$$(\frac{x_o}{b}) = F_1 (\frac{U_j}{U_{is}}, \frac{\delta^*_s}{b})$$

and the available values for this function for wall jets are given in Table II. The values of C are also tabulated in Table I and seen to vary consistently with $(\frac{U_1}{U_M})$ as expected for self preserving flows, (equation (15)). Fig.(7a) shows the variation of $(\frac{dy_{M/2}}{dx})$ and $(\frac{dy_M}{dx})$ with $(\frac{U_1}{U_M})$. The latter parameter is chosen to enable still air wall jet results to be plotted on the same figure. The growth parameters $\frac{dy_M}{dx}$ and $\frac{dy_{M/2}}{dx}$ may be expected to vary with $(\frac{U_1}{U_M})$ and in Fig.(7a) it appears that the relation is approximately linear.

The present experimental results are in fair agreement with this prediction. Further, experimental results are however required before a specific law is given.

4.1.5 Variation of $(\frac{U_M}{U_j})$ with $(\frac{x}{b})$.

The theory indicates that $U_M \propto (x + x_o)^m$. Hence, when $(\frac{U_M}{U_j})^{\frac{1}{m}}$ is plotted against x a linear curve is expected. The measured values have been plotted this way in

Figs. (8). It is seen from these figures that $(\frac{U_M}{U_j})^{\frac{1}{m}}$ is proportional to $(\frac{x}{b})$ over the range of $(\frac{x}{b})$ for which the pitot traverses were taken. Note that the curves are not extrapolated in the region of the slot exit. In this region it was impossible to correct for the inadequacies of the one dimensional theory used in setting the position of the louvers since similarity is not possible in the mixing region near the slot. In passing it should be noted that high wall pressures are usually found near the slot exit in wall jet experiments (e.g. Ref.6), and are attributed to the high rate of entrainment there. These wall static pressures may be also plotted to obtain additional but less accurate values of $(\frac{x_o}{b})$ [Patel and Newman[17]] and these are shown in Table I.

4.1.6 Mean Velocity Profiles - Inner Law Plot:

In all unseparated flows it is expected that sufficiently near a smooth wall, the velocity profile is of the universal form

$$\frac{U}{U_\tau} = f(\frac{y\ U_\tau}{\nu}) \qquad \ldots(47)$$

where $U_\tau = \sqrt{\frac{\tau_o}{\rho}}$

Very near the wall i.e. in the laminar sublayer, the above expression takes the form of $\frac{U}{U_\tau} = \frac{yU_\tau}{\nu}$ on the assumption that the shear stress is constant across the sublayer.

In the outer part of the wall region $\frac{y}{U_\tau}\frac{\partial U}{\partial y}$ = constant which is usually independent of conditions in the outer part of the flow.

Thus $\frac{U}{U_\tau} = A \log \left(\frac{yU_\tau}{\nu}\right) + B$ ...(48)

It is expected that these laws will hold sufficiently close to the wall but the values of A and B may depend on the outer conditions and in particular $\left(\frac{U_M}{U_1}\right)$: (see section 4.1.12) Similar observation was also made by Schwarz and Cosart[11].

Figs. (9) show a pronounced semi-logarithmic region when mean velocity profiles are plotted with $\left(\frac{U}{U_\tau}\right)$ against $\left(\frac{yU_\tau}{\nu}\right)$. The skin friction velocity U_τ was obtained by using Stanton tubes and the details of their calibrations are given in Appendix II. Fig.(9.5) shows that the logarithmic form of law-of-wall approximately applies to the wall jet in an equilibrium pressure gradient. The values of A and B are, however, different than those used for conventional turbulent boundary layers. The available values of A and B for wall jets are tabulated in Table III.

As one would expect from the velocity profiles which resemble turbulent boundary-layers, the values of A and B tend to those of the conventional turbulent boundary layer. Fig.(9.6) shows clearly that the universal logarithmic law-of-wall does not exist for the case of $\frac{U_j}{U_{is}} = 1.501$. This is expected because the velocity profiles for this case are not similar. From the

measurements of Bradshaw and Gee[10] who investigated a wall jet in a pressure gradient it was found that the values of A and B also tend to those of the boundary-layer (Table III).

The deviations of experimental points very near the wall may be attributed to the error (approximately 0.0005in.) in locating the exact distance from the wall.

4.1.7 Mean Velocity Profiles - Outer Defect Law for Inner Boundary-Layer:

For an equilibrium layer at high R_e and farther out from the wall $(\frac{y}{U_\tau} \cdot \frac{\partial U}{\partial y})$ is a function of $\frac{y}{y_M}$, $\frac{y_{M/2}}{y_M}$ and $\frac{U_M}{U_1}$.

However, for wall jets in an equilibrium pressure gradient it is shown in the theory that $\frac{y_{M/2}}{y_M} = f(\frac{U_M}{U_1})$ which in turn is a constant for a particular wall jet.

Hence, the outer defect law can be written as:

$$\frac{U_M - U}{U_\tau} = f(\frac{y}{y_M}, \frac{U_M}{U_1}) \qquad \ldots(49)$$

This is compared with the experiments, and the results are shown in Figs.(10). It is seen from Figs.(10.2 and 10.5) that the velocity defect law extends down to a value of $(\frac{y}{y_M})$ approximately equal to 0.30. Also it is interesting to note that the velocity defect law for $\frac{U_j}{U_{is}} = 6$, (Fig. 10.5), tends to that of wall jet in still air as expected (Figs. 41 and 42). The velocity defect law does clearly and satisfactorily describe the results

for $\frac{U_j}{U_{is}} = 1.501$ Fig.(10.6), but the outer part profiles are also not exactly similar.

4.1.8 Boundary-Layer Mean Velocity Profiles Using Power Law:

In the theoretical analysis for the development of the inner boundary-layer of a wall jet in equilibrium pressure gradient, it was anticipated that the mean velocity distribution in this region may be given by a power profile. Hence, with U_M as the velocity at the edge of inner boundary-layer and y_M as inner boundary-layer thickness the mean velocity profile is represented by:

$$\frac{U}{U_M} = \left(\frac{y}{y_M}\right)^{\frac{1}{n}}$$

Due to the high level of turbulence in wall jets, it was expected that the exponent n will be greater than that in an ordinary turbulent boundary layer at a comparable R_e (i.e. n = 7).

Figs.(11) show the inner boundary-layer velocity profiles plotted on log-log paper. Fig.(11) shows the investigation at $\left(\frac{x}{b}\right) = 92.5$ for different jet velocity ratios. On the figure are also plotted conventional $\frac{1}{7}^{th}$ power boundary-layer profile and $\frac{1}{14}^{th}$ power profile suggested by Myers et al[12] for wall jets in still air. It is seen from Figs. (11 and 11.5) that an $\frac{1}{11}^{th}$ power profile is in best agreement with the experimental results generally for $\frac{U_M}{U_1}$ greater than about 1.8.

It is noted later in the description of the experimental investigation of wall jets in still air and wall jets in zero pressure gradient that the inner boundary-layers are also in agreement with an $\frac{1}{11}^{th}$ power profile. It is interesting to observe from Figs. (11 and 11.6) that for $\frac{U_M}{U_1} < 1.8$ the inner boundary-layer profiles tend to the $\frac{1}{7}^{th}$ power profile and the complete velocity profiles of wall jets tend to ordinary turbulent boundary-layer profile. In other words n varies with $(\frac{U_M}{U_1})$ as well as Reynolds number.

4.1.9 Variation of $(\frac{y_M}{b})$.

The theoretical analysis of the inner boundary-layer indicated that $(\frac{y_M}{b})$ is proportional to $(\frac{x + x_o}{b})^{\frac{N-m}{N+1}}$. Considering the two extreme cases namely a strong wall jet and a weak wall jet, the values of m are $-\frac{1}{2}$ and $-\frac{1}{3}$ respectively. Furthermore, it was found experimentally that the inner boundary-layer velocity profiles for wall jets with $\frac{U_M}{U_1} > 1.8$, can be represented by an $\frac{1}{11}^{th}$ power profile, thus giving N = 6. With these values of m and N, for a strong wall jet $(\frac{y_M}{b}) \propto (\frac{x + x_o}{b})^{0.929}$ The exponent 0.929 compares satisfactorily with the exponent 0.90 given by Myers et al[12] for wall jet in still air. The difference between the two exponents however, is entirely due to the different power profiles used. For a weak jet $(\frac{y_M}{b}) \propto (\frac{x + x_o}{b})^{0.905}$.

The results of the experimental investigation are shown in Fig. (12) where $R_{e_s}^{\frac{1}{7}} \cdot (\frac{y_M}{b})$ is plotted against $(\frac{x + x_o}{b})$ on logarithmic paper. The values of $(\frac{x_o}{b})$ were obtained from the growth law and values m from equation (10). On the figure are also plotted the lines with respective theoretical values of the exponent $(\frac{N - m}{N + 1})$. It is seen that the experimental points agree satisfactorily with the theoretical predictions. For the slot widths of approximately 0.40in. it is found that the experimental points deviate considerably from the theory. This is not surprising as mentioned before that the distance where the jet core disappears depends on $(\frac{U_j}{U_{is}})$ and the slot width. In previous figures of growth law-of-wall jets in an equilibrium pressure gradient the $(\frac{y_M}{b})$ variation was assumed linear, i.e. $(\frac{y_M}{b}) \propto (\frac{x}{b})$; (see Figs.(7)). In Fig. (12) a line with slope equal to one is drawn so as to compare the slopes of the experimental lines. From this figure it can be concluded that for all practical purposes $(\frac{y_M}{b})$ is directly proportional to $(\frac{x}{b})$.

4.1.10 Variation of Skin Friction:

From the theoretical analysis of the inner boundary-layer of a wall jet in equilibrium pressure gradient it was found that $C_f \cdot (R_e)_s^{\frac{1}{N+1}}$ is proportional to $\frac{1}{\left[\frac{x+x_o}{b}\right]^{\frac{m+1}{N+1}}}$.

To confirm this the skin friction was measured by using Stanton

tubes. The calibration and use of Stanton tubes are given in the Appendix II. In Fig.(13), $C_f.(R_e)_s^{\frac{1}{5}}$ is plotted against $(\frac{x + x_o}{b})$ on logarithmic paper. The experimental results in this figure are compared with the theoretical curves obtained from equation (37) by using Sigalla's[18] and Blasius values of α and $\frac{1}{7}^{th}$ power profile and the extreme values of m for a weak and a strong jet ($-\frac{1}{3}$ and $-\frac{1}{2}$). It is seen that the Blasius skin friction law for strong jet agrees reasonably well with the experimental results for $\frac{U_j}{U_{is}} = 6.0$. It should be noted that the theoretical results are fairly insensitive to the choice of m and that for $\frac{U_j}{U_{is}} = 3.0$ and 6.0, the value of $m = -\frac{1}{2}$ for a strong jet is sufficiently accurate. Blasius skin friction law gives values of the skin friction which are smaller than those computed using Sigalla's constants.

It is also interesting to note that for $\frac{U_j}{U_{is}} = 1.501$ the measured skin friction values fall quickly as $(\frac{x + x_o}{b})$ increases. This is expected from an examination of the complete velocity profiles which are similar to ordinary turbulent boundary-layer profiles near separation.

Fig. (14) shows the skin friction coefficient plotted as predicted by equation (38). However, $\frac{1}{11}^{th}$ power profile is used because it represents the inner boundary-layer profiles more accurately. Thus $C_f\ (R_{e_s})^{\frac{1}{7}}$ vs. $(\frac{x + x_o}{b})$ is plotted logarithmically in this figure. As mentioned above the value

of $m = -\frac{1}{2}$ was used to compute the exponent $(\frac{m+1}{N+1})$. Thus the present experimental results for $\frac{U_j}{U_{is}} = 3.0$ and 6.0 agree very well with the skin friction variation law given by $C_f (Re_s)^{\frac{1}{7}}$

$$= \frac{\text{constant}}{(\frac{x + x_o}{b})^{0.0715}}.$$ The constant was found to be 0.03284. (11)

At this stage it is worth noting that Schwarz and Cosart found very litte variation in skin friction with downstream distance in their experiments on wall jets in still air. This is not surprising in view of the present theory for strong wall jets in an equilibrium pressure gradient are similar to wall jets in still air. For comparison the values of C_f are tabulated in the Table III.

4.1.11. Turbulence Intensity:

Fig.(15) shows the r.m.s. longitudinal turbulence as a proportion of the local mean velocity for a wall jet in still air (U_j = 317.5 ft./sec.) and two cases of wall jets in an equilibrium pressure gradient ($\frac{U_j}{U_{is}} = 3.0$ and 6.0). The wall jets were traversed at a distance of x = 19.2in. from the slot exit using two separate hot wire probes to check repeatability. The probes and the constant current hot wire anemometer used in this investigation are described in the Appendix I. It is seen from this figure that wall jet in still air has the highest turbulence intensity and as the jet velocity ratio decreases the turbulence intensity also decreases. This

is expected on physical grounds for the local values of $\frac{\partial U}{\partial y}$ in the outer part of the flow are reduced in general as the velocity of the external stream U_1 approaches the maximum jet velocity U_M. Associated with the increased intensity it is found that the rate of growth of wall jets in still air is higher than that of wall jets with external stream; (see Fig. (7a) . It is also apparent (through Mixing length theory) that the values of A in the semilogarithmic law-of-wall will decrease as the turbulence intensity increases. Thus for wall jets in still air it is expected that the values of A will be smaller than those of wall jets in streaming flow.

Figs. (16.2 and 16.5) show the variation of the longitudinal turbulence as a proportion of the external streaming velocity and the corresponding mean velocity profile for the two equilibrium cases. It is interesting to note that the longitudinal turbulence plotted in this way is greater near the wall surface than at $y = y_M$. In the outer region turbulence intensity once more increases and finally it decreases again to the value in the free stream. The shape of the turbulence intensity profiles is similar to the measurements of Bradshaw and Gee[10] on a wall jet with small $\frac{U_M}{U_1}$ in a pressure gradient slightly more adverse than the relevant equilibrium value. It should be noted that the hot-wire anemometer was not linearized hence the readings in high turbulence zone may be in doubt.

4.1.12 Variation In The Value of A For The Logarithmic Law-of-Wall;

For equilibrium flows it is reasonable to assume that A will depend on U_1, U_M, Y_M, $Y_{M/2}$, μ and ρ

Thus $$A = f\left(\frac{U_1}{U_M}, \frac{U_M Y_M}{\nu}, \frac{Y_M}{Y_{M/2}}\right) \quad \ldots(50)$$

But $Y_{M/2} \propto x+x_o$ and $Y_M \propto x+x_o$

$\therefore \frac{Y_M}{Y_{M/2}}$ is a constant and depends on $\left(\frac{U_1}{U_M}\right)$

Hence $$A = f\left(\frac{U_M Y_M}{\nu}, \frac{U_1}{U_M}\right) \quad \ldots(51)$$

Fig. (17) shows the variation of A with $\frac{U_M Y_M}{\nu}$ for various ratios of $\left(\frac{U_1}{U_M}\right)$. Despite considerable scatter in the results it is clear that A does not depend too much on $\frac{U_M Y_M}{\nu}$ but varies considerably with $\frac{U_1}{U_M}$. From Fig. (17) mean values of A were obtained and this is plotted in Fig. (18). Note that as expected A tends to the value for a conventional boundary-layer as $\left(\frac{U_1}{U_M}\right)$ increases. In Fig. (18) are also shown the values of A obtained from wall jets in streaming flow with zero pressure gradient (see Figs. 29 and 30) and it is interesting to note that the points agree reasonably well with the equilibrium cases. Thus it is apparent that A tends to depend more on local conditions than on the previous history of the flow. The values of A and B are tabulated in Table III.

4.2 Wall Jet in Streaming Flow With Zero Pressure Gradient:

4.2.1 General

The wall jet in zero pressure gradient was investigated for comparison with some of the results of George.[6] To achieve this experimentally the perforated plate was removed from the exit of the test section and the louvers were closed. Pitot traverses on the centre line of the plate were made at 6.5in., 12.5in., and 18.5in., downstream of the slot. The experimental results are for jet velocity ratios $(\frac{U_j}{U_{is}})$ of 2.66, 3.0, and 5.95 and slot widths of 0.375in. and 0.20in.

4.2.2 Variation of $(\frac{U_M}{U_1})$.

Fig. (19) shows the variation of $(\frac{U_M}{U_1})$ with $(\frac{x}{b})$. It is seen that the decay of maximum velocity near the slot exit is greater than that farther downstream and generally the rate of decay increases with the jet velocity ratio. Also the high decay rate near the slot exit can be explained with the momentum transfer. The slower moving region of the outside boundary-layer is being supplied with the momentum from the jet. Thus due to the vigourous momentum transfer taking place near the slot exit it is expected that the maximum velocity will decay faster. However, farther downstream when the mixing of the two flows is well settled the variation in U_M will be smaller.

The results of George[6] are shown in this figure for comparison. It is clear that the results of George lie below the present experimental results and this is no doubt due to the difference in jet momentum for the two investigations.

4.2.3 Velocity Profiles.

Figs. (20, 21, and 22) show the velocity profiles plotted as $(\frac{U_j}{U_{is}})$ vs. y in. As mentioned before the flow was traversed at three stations only and it should be noted that the effect of the jet core has disappeared at least before $\frac{x}{b} = 17.34$.

The velocity profiles in Figs. (23, 24, 25 and 26), are plotted non-dimensionally for direct comparison with the results in an equilibrium pressure gradient. It will be seen that the scatter of points, particularly farther away from the wall, is noticeably greater. All the figures therefore indicate that the velocity profiles are only approximately similar in a zero pressure gradient, a conclusion which George[6] also reached. It is interesting to note however that the departure from similarity is not large and thus an approximate method, incorporating a similarity hypothesis, for predicting the growth of wall jets in arbitrary pressure gradient (i.e. one in which U_1 is not proportional to $(x + x_o)^m$) is not likely to be seriously in error. Once again it appears that the

exponential function is in better agreement with the experimental results than the Sech. function.

4.2.4 Growth of Wall Jet.

Figs. (27 and 28) show the downstream variation of $(\frac{y_{M/2}}{b})$ and $(\frac{y_M}{b})$ with $(\frac{x}{b})$. For comparison the results of George[6] are also plotted in Fig. (28). It can be seen that the $(\frac{y_M}{b})$ variation is approximately linear, however the $(\frac{y_{M/2}}{b})$ variation is definitely not linear. It is expected that $(\frac{y_{M/2}}{b})$ may be proportional to $(\frac{x}{b})$ near the slot and sufficiently farther downstream it may be proportional to $(\frac{x}{b})^{\frac{1}{2}}$. If $(\frac{U_j}{U_{is}})$ is large the wall jet growth tends to that of a plane wall jet i.e. $y_{M/2} \propto x$. From Fig. (28) it is clear that for $(\frac{U_j}{U_{is}}) = 5.95$, the variation of $(\frac{y_{M/2}}{b})$ is approximately linear. Also it is clear that with larger jet momentum the growth of wall jet is smaller. It appears therefore that in formulating the growth law for wall jets in zero pressure gradient, jet momentum will be the main influencing parameter.

4.2.5 Mean Velocity Profiles - Inner Law Plot.

Figs. (29 and 30) show mean velocity profiles plotted as $(\frac{U}{U_\tau})$ against $(\frac{yU_\tau}{\nu})$. The skin friction velocity (U_τ) was obtained by using Stanton tubes which were calibrated in turbulent boundary-layer with zero pressure gradient using Clauser's[13] universal curves; (see Appendix II). It can be

seen that there is no evidence of universal law of the wall, however, there is a semi-logarithmic region in each velocity profile. The semi-logarithmic law for individual profile is given and it can be seen that the values of A and B are different from the conventional values for turbulent boundary-layers. The values of A and B are tabulated in Table III and are consistent with values of other wall jets.

4.2.6 Mean Velocity Profiles - Outer Defect Law For Inner Boundary-Layer.

With $(\frac{U_M-U}{U_\tau})$ and $(\frac{Y}{Y_M})$ as parameters the velocity prifiles are plotted in Figs. (31 and 32). For the case of jet velocity ratio of 3.0 it is clear that the velocity defect law does not exist, Fig.(31). However, for the case of jet velocity ratio of 5.95 it appears from Fig. (32) that the defect law extends up to a value of $(\frac{Y}{YM}) = 0.15$. This can be expected on the grounds that the strong jet in effect tends to a plain wall jet in still air and the experimental results of plain wall jets indicated the existence of a velocity defect law; (see Figs. 41 and 42).

4.2.7 Boundary-Layer Mean Velocity Profiles Using a Power Law.

It is of interest to see whether the inner boundary-layer velocity profiles of wall jets in zero pressure gradient

can be represented by a simple power profile. With this view in mind the velocity profiles in Fig. (33) are plotted with $(\frac{U}{U_M})$ against $(\frac{y}{y_M})$. For comparison $\frac{1}{7}^{th}$, $\frac{1}{11}^{th}$, and $\frac{1}{14}^{th}$ power profiles are also plotted. It is clear from the figure that the inner boundary-layer profiles are in best agreement with the $\frac{1}{11}^{th}$ power profile.

4.3 Wall Jet In Still Air.

4.3.1 General:

For comparison and completeness wall jets in still air were investigated. The same apparatus was used with tunnel speed set at zero. The results represent two jet Reynolds numbers $R_e = (\frac{U_j b}{\nu}) = 22900$ and 30400. The slot width b was set at 0.20ins. The results are compared with the theories suggested by Myers et al[12] and thus the parameters used in the figures are the same for direct comparison with their results. Skin friction variation was measured by using Stanton tubes located at three downstream distances from the slot exit. Pitot traverses on the centre line of the plate were made at 6.5in., 12.5in., and 18.5in. downstream of the slot exit. Turbulence intensity and the corresponding mean velocity profile were measured at one station only. The turbulence intensity was measured by using DISA hot wire anemometer[14] and the results are compared with those of Bradshaw and Gee[10].

4.3.2 Variation of $(\frac{U_M}{U_j})$.

Fig. (34) shows the variation of maximum velocity with downstream distance. A theoretical curve and a best experimental line as given by Myers et al[12] are also plotted. The best line suggested by them is $(\frac{U_M}{U_j}) = 3.45\ (\frac{x}{b})^{-0.49}$. The present experimental results are in better agreement with

their theoretical curve. Thus confidence was established in the investigation of wall jets with the present experimental technique.

4.3.3 Velocity Profiles.

Pitot traverses were taken at x = 6.5ins., 12.5ins., and 18.5ins. downstream of the jet exit. The jet velocities investigated are U_j = 239 ft./sec. and 317.5 ft./sec. Figs. (35 and 36) show the velocity profiles. It is worth noting that the effect of the jet core is not existing in these velocity profiles as the measurements were taken sufficiently far downstream of the slot exit.

Fig. (37) shows the non-dimensional mean velocity profile. In this figure the results of Bradshaw and Gee[10] and the theoretical mean velocity profile given by Glauert[9] with α = 1.2 are also plotted. The experimental results are in very good agreement with both these profiles. However, at the outer edge $(\frac{Y}{y_{M/2}}) > 1.2$ the velocity profile of Bradshaw and Gee deviates from Glauert's profile and the present experimental results are in better agreement with Glauert's profile.

4.3.4 Growth of Wall Jets.

To compare the experimental results for the growth of the wall jets with the theory of Myers et al[12], Fig. (38) is drawn on log-log paper with parameters $(\frac{y_{M/2}}{b})$ and $(\frac{x}{b})$. Two theoretical curves as given by them are shown in this figure. The results of the present investigation agree extremely well with their theoretical prediction. It is clear that the growth law is not very sensitive to the variation in Reynolds number $(\frac{U_j b}{\nu})$ and sufficiently far downstream of the slot exit, the growth of the wall jet is approximately linear. From this figure confidence was further established in the present wall jet investigations.

4.3.5 Mean Velocity Profiles - Inner Law Plot.

With dimensional analysis it can be shown that:

$$\frac{U}{U_\tau} \cdot \frac{\partial U}{\partial y} = f\left(\frac{y}{y_M}, \frac{U_M y_M}{\nu}, \frac{U_M y_{M/2}}{\nu}\right) \qquad \ldots(52)$$

Sufficiently near the surface

$$\frac{U}{U_\tau} \cdot \frac{\partial U}{\partial y} = f\left(\frac{U_M y_M}{\nu}\right) \qquad \ldots(53)$$

Thus $\frac{U}{U_\tau} = A \log \left(\frac{y U_\tau}{\nu}\right) + B$ where A and B depend on $(\frac{U_M y_M}{\nu})$. Furthermore, it is shown that A is not very sensitive to changes in the value of $(\frac{U_M y_M}{\nu})$ (see section. 4.1.12). Hence if B is also insensitive to the values of $(\frac{U_M y_M}{\nu})$, then, one would expect a universal, semi-logarithmic, law-of-wall, in wall jets in still air.

In Figs. (39 and 40) $\frac{U}{U_\tau}$ is plotted against $\frac{yU_\tau}{\nu}$ on semi-logarithmic paper. From these figures it is seen that there is a semi-logarithmic region in the velocity profiles but the values of A and B are different than the conventional turbulent boundary-layer. Similar observation was also made by Schwarz and Cosart[11]. From these figures it is apparent that A and B slightly depend on the values of $(\frac{U_M y_M}{\nu})$ and thus the universal law-of-wall was not found. The results of Bradshaw and Gee[10] also indicate that the law-of-wall is not universal. Contrary to this Myers et al[12] concluded that within a small range $(\frac{yU_\tau}{\nu} < 30)$ the universal law-of-wall for the flat plate (i.e. $\frac{U}{U_\tau} = 5.6 \log \frac{yU_\tau}{\nu} + 4.9$) holds for wall jet as well. However, their experimental results show considerable scatter in this region and such a conclusion seems to be unjustified.

The values of A and B are tabulated in Table III.

4.3.6 Mean Velocity Profiles - Outer Defect Law For Inner Boundary-Layer.

From dimensional analysis it can be shown that for the outer part of the boundary-layer

$$\frac{U}{U_\tau} \frac{\partial U}{\partial y} = f(\frac{y}{y_M}) \qquad \ldots(54)$$

Hence the outer defect law becomes:

$$\frac{U_M - U}{U_\tau} = f(\frac{y}{y_M}) \qquad \ldots(55)$$

Figs. (41 and 42) show the outer defect law plotted with $\frac{U_M - U}{U_\tau}$ against $\frac{y}{y_M}$ for jet velocity U_j = 239 ft./sec. and 317.5ft/sec. Both figures exhibit a universal defect law in agreement with the above prediction. The outer defect law extends down to a value of $\frac{y}{y_M}$ approximately equal to 0.10.

4.3.7 Boundary-Layer Mean Velocity Profiles Using a Power Law.

For comparison the inner boundary-layer mean velocity profiles were plotted as shown in Fig.(43). In this figure are also plotted the conventional $\frac{1}{7}^{th}$ power boundary-layer profile, $\frac{1}{14}^{th}$ power profile given by Myers et al[12] and $\frac{1}{11}^{th}$ power profile obtained from the investigation of wall jets in equilibrium pressure gradient. It is seen from Fig.(43) that the $\frac{1}{11}^{th}$ power profile is in best agreement with the experimental results.

4.3.8 Skin Friction Variation.

To obtain confidence in the Stanton tube measurements, the skin friction was plotted for direct comparison with the results of Myers et al[12]. Fig.(44) shows the variation of skin friction against downstream distance from the slot exit. The skin friction coefficient C_f' is defined as $C_f' = \frac{\tau_o}{\frac{1}{2}\rho U_j^2}$ and the Reynolds number as $R_e = \frac{U_j b}{\nu}$. Thus Fig.(44) is directly replotted from Myers et al. The results of the present investigation show extremely good agreement with the results of Myers et al.

Their results were obtained by using hot-film technique. Thus it was concluded that the skin friction values obtained from Stanton tubes for the wall jets were very satisfactory. The values of skin friction coefficient $C_f = \frac{\tau_o}{\frac{1}{2}\rho U_M^2}$ are tabulated in Table III.

4.3.9 Turbulence Intensity.

As mentioned in section (4.1.11) the turbulence intensity was measured at x = 19.2in. for the wall jet in still air. (U_j = 317.5 ft./sec.) Fig.(45) shows the r.m.s. longitudinal turbulence as a proportion of the local mean velocity. The turbulence intensity is plotted against $(\frac{y - y_{M/2}}{\delta_f})$, where $\delta_f = \frac{U_M}{(\frac{\partial U}{\partial y})_{y_{M/2}}}$, for direct comparison with similar results of Bradshaw and Gee[10]. On the figure the corresponding mean velocity profiles are also plotted. It is seen that the experimental mean velocity profile is in good agreement except near the wall with the mean velocity profile of Bradshaw and Gee. The turbulence intensity profiles deviate considerably near the jet peak and at the edge of the wall jet. It should be noted that the hot-wire anemometer was not linearized for high turbulence measurements hence the readings near the edge of the wall jet may be in error.

5. CONCLUSIONS

1. The analysis of a self preserving free jet in streaming flow can be applied to the outer part of a wall jet in a similar streaming flow and that the effect of the inner boundary-layer is small. The growth of the jet is linear and the flow is easy to establish experimentally when the jet velocity ratio is high. At low jet velocity ratios (i.e. $\frac{U_j}{U_{is}} \leq 1.5$) similarity of the flow is difficult to obtain experimentally. Approximate similarity is also obtained for wall jets in streaming flow with zero pressure gradient. In the cases where $\frac{U_j}{U_{is}} \geq 6$ the wall jets in streaming flow are similar to a wall jet in still air.

2. The inner boundary-layer velocity profile of the wall jets can be represented by an $\frac{1}{11}^{th}$ power profile and the boundary-layer thickness y_M increases almost linearly with downstream distance.

3. The skin friction coefficient measured with Stanton tubes for wall jets in an equilibrium pressure gradient is not very sensitive to the variation in downstream distance and is in agreement with the prediction of the theory based on the power profile.

4. The law of the wall and the velocity defect law exist for wall jets in an equilibrium pressure gradient

and for the wall jets in still air. However, the values of A and B in the semi-logarithmic law-of-wall are different than those of a conventional turbulent boundary-layer in zero pressure gradient. The values of A and B depend mainly on the velocity ratio $\frac{U_M}{U_1}$ and slightly on the Reynolds number. Thus they may probably be related to the turbulence intensity in the outer part of the wall jet for this is found to increase in general with the velocity ratio.

5. The experimental measurements on the wall jets in still air are in very good agreement with those of previous investigators.

6. The present work could usefully be extended in the following areas:

   (a) A detailed study of the flow near the slot exit.

   (b) Further investigation of the values of A and B in the semi-logarithmic law-of-wall.

   (c) Turbulence measurements and in particular the shear stress distribution across the flow.

   (d) A study of wall jets on rough surfaces.

APPENDIX I

APPARATUS AND INSTRUMENTATION

The McGill blower tunnel which was used for the experiment has an exit section 30" wide and 17" high. It is driven by a 25 H.P., fixed r.p.m., centrifugal fan and has variable inlet vanes for speed control. Downstream of the fan is a 5° diffuser, a settling chamber with deep cell honey-comb and three removable screens, followed by a 6:1 two-dimensional contraction. The test section for the present investigation is attached to the tunnel exit as shown in Figs.(2).

The bottom of the test section consisted of a flat Plexiglas plate and a slot. The jet was emitted tangential to the flat plate and below the oncoming flow from the tunnel. The jet air supply was provided by an auxiliary 20 H.P. centrifugal compressor. An 8" diameter flexible pipe followed by a 6° diffuser connected the compressor supply to the slot. The mass flow to the jet was controlled by a bleed valve far upstream of the slot. The slot exit was designed so that the jet width could be varied from zero to approximately 0.425in. The contraction ratio at the maximum slot opening was approximately 10.

Static pressure taps were provided on both sides of the centre line of the Plexiglas plate. To prevent separation from the side walls of the test section these were provided with bleed slots. The exit of the test section was fitted with a

perforated plate of 23 per cent open area. The top of the test section was fitted with adjustable louvers so shaped that the flow emerged smoothly between them at an angle of approximately 30^{o} with the axis of the tunnel.

Stagnation pressure was measured using pitot tubes with outside diameter 0.031in., inside diameter 0.0195in., and 20^{o} sharpened lips. Also a flattened pitot tube was used to traverse the flow. The overall height of the flattened end was approximately 0.0097in. and the height of opening was 0.00485in. A traversing gear incorporating a double ended dial gauge was used to traverse the flow at each downstream station. The static pressure was determined from surface taps of 0.015in. diameter. The pressures were measured with conventional single tube and multitube manometers filled with alcohol.

The skin friction measurements were made using Stanton tubes. These consisted of half ground razor blades glued on to the surface of the plate as shown in Fig.(49). The Preston tube was made from brass tube with outside diameter 0.030in. and inside diameter 0.0195in. It was mounted as shown in Fig.(50).

A Statham differential pressure transducer (Model PM 5TC) was used to measure the Stanton tube readings. The range of pressure difference for this transducer was $\pm$ 0.15 p.s.i.

The turbulence intensity was measured by using a DISA

constant temperature anemometer, 55 A 01. The details of the instrument can be found in Reference (14). The hot wire probes were made of thin tungsten wire connected to nickel supports. The wire was 0.005 mm. in diameter and approximately 1 mm. long.

APPENDIX II

TWO-DIMENSIONALITY CHECK - WALL JET IN EQUILIBRIUM PRESSURE GRADIENT

Figs. (46 and 47) show the velocity traverses for a jet velocity ratio $(\frac{U_j}{U_{is}})$ = 4.05 and b = 0.375in. The wall jet was surveyed with a pitot tube at two stations 0.5in. and 15.5in. downstream of the slot exit. Within 6in. of the centre line the profiles were almost identical across the flow and indicated only $\pm$ 0.90 per cent variation in maximum velocity at 0.5in. downstream of the slot and $\pm$ 0.80 per cent variation at 15.5in. downstream. Observation of surface tufts also indicated that the flow remained effectively two-dimensional even for values of $(\frac{U_j}{U_{is}})$ less than 1.5., for which the flow tended to separate. Thus the flow was considered to be effectively two-dimensional for the range of measurements which are presented here.

STANTON AND PRESTON TUBE CALIBRATION.

Stanton tubes were staggered one inch on either side of the centre line of the wall at 6.5in., 12.5in., and 18.5in. downstream of the slot exit. These were mounted on the wall as shown in the sketch, (see Fig.(49)). It was important to check the two-dimensionality of the boundary-layer flow before calibrating the Stanton tubes in turbulent boundary-layer with zero pressure gradient. Fig.(48) shows typical boundary-layer velocity profiles at x = 15.5in. The velocity profiles within

6in. on either side of the centre line of the wall were almost identical and thus the flow in boundary-layer was considered satisfactory for calibration.

An extensive investigation was carried out on the Stanton tube at x = 18.5 in. to find out the effect of dust and dirt. The dust and dirt did have effect on the Stanton tube readings. The flow was filtered and the dust and dirt was blown out of the Stanton tube using an ordinary bicycle pump. The tube was then recalibrated. It is seen from the calibration curve of this tube (Fig. 49) that the change in calibration is hardly noticeable. Once sufficient confidence was obtained from this tube, two other tubes were mounted at 6.5in. and 12.5in. All the Stanton tubes were calibrated in turbulent boundary-layers with zero pressure gradient using Clauser's[13] universal curves with A = 5.6 and B = 4.9.

Fig.(49) shows the calibration curves for these tubes. The Stanton tubes readings were extremely small and it was not possible to use an alcohol manometer. A sensitive pressure transducer was used to measure the Stanton tube pressure differences, and the transducer output was fed to a vacuum tube millivoltmeter. Thus the Stanton tubes readings are presented in terms of mV using Preston's[19] non-dimensional parameters. In plotting these results a nominal height of 0.001in. was

assumed for the Stanton tubes. It was not possible to calibrate the tubes beyond $\log_{10} \left(\frac{U_\tau^2 d^2}{\nu}\right) = + 0.24$, with the existing range of boundary-layer thickness, however the calibration curves are extrapolated linearly beyond this value, a procedure which is justified by the calibrations of the Stanton tubes by Bradshaw and Gregory[20]. It should be noted that only the Stanton tubes were finally used in the present experimental investigation although a Preston tube at x = 18.5in. was used initially before it was confirmed that the law of wall was not universal for wall jets.

Fig.(50) shows the Preston tube calibration curve. The tube was calibrated in the same fashion as the Stanton tubes, but the pressure difference being large was measured on an alcohol manometer. In this figure, Preston's pipe calibration[19], Smith and Walker's[21] calibration and Relf's[22] calibration are also plotted. It is interesting to note that the experimental results are in best agreement with Relf's boundary-layer calibration, but these in turn are not very different from the calibration of Smith and Walker who used a moving element technique.

TUNNEL TURBULENCE LEVEL.

As a preliminary to the investigations (and before the availability of the hot-wire equipment) the turbulence in the free stream of the tunnel flow was determined by measuring the

base pressure coefficient behind two smooth spheres of different sizes. The results are shown in Fig.(51). The measurements on the larger sphere indicate a slight tunnel blockage but the smaller gives a critical Reynolds number (corresponding to a base pressure coefficient of - 0.22) of 3.65×10^5. This is indistinguishable from the value in free air and corresponds to a longitudinal turbulence which is certainly less than 0.5 per cent. (Goldstein[23]).

REFERENCES

1. Newman, B.G. — The Deflection of Two-Dimensional Jets. U.T.I.A., Decennial Symposium, Paper 2, Oct. 1959.

   See also: Boundary-Layer Control - Principles and Applications, edited by G.V. Lachmann. Pergamon Press, 1961.

2. Townsend, A.A. — The Structure of Turbulent Shear Flow. Cambridge University Press, 1956.

3. Abramovich, G.N. — The Turbulent Jet in a Moving Fluid. RAE Trans. 778, Oct. 1958.

4. Craven, A.H. — The Effect of Density on Jet Flow at Subsonic Speeds. College of Aeronautics, Cranfield, Report 120.

5. Carriere, E. Eichelbrenner, E. Poisson-Quinton, Ph. — Étude du Control de la Couche Limite. Advances in Aeronautical Sciences, Vol.2, Pergaman Press, 1959, P.620.

6. George, A.R. — An Investigation of a Wall Jet in a Free Stream. Department of Aeronautical Engineering, Princeton University, Report 479, Sept. 1959.

7. Townsend, A.A. — The Properties of Equilibrium Boundary-Layers. Journal of Fluid Mechanics, Vol.1, 1956, P. 561.

8. Rotta, J. — On the Theory of the Turbulent Boundary-Layers. NACA. TM 1344, Feb. 1953.

9. Glauert, M.B. — The Wall Jet. Journal of Fluid Mechanics, Vol.1, 1956, P.625.

10. Bradshaw, P. Gee, M.T. — Turbulent Wall Jets With and Without an External Stream. A.R.C. 22,008, F.M.2971, June 1960.

11. Schwarz, W.H.
Cosart, W.P.
The Two-Dimensional Turbulent Wall Jet. Journal of Fluid Mechanics, Vol.10, Part 4, June 1961. P.481.

12. Myers, G.E.
Schauer, J.J.
Eustis, R.H.
The Plane Turbulent Wall Jet. Part 1. Jet Development and Friction Factor. Department of Mechanical Engineering, Stanford University, Technical Report No.1, June 1961.

13. Clauser, F.H.
Turbulent Boundary-Layer in Adverse Pressure Gradient. Journal of Aeronautical Sciences. Vol.21. 1954.

14.
Flowmeter, DISA Constant Temperature Anemometer 55 A 01. Instruction Manual, DISA ELEKTRONIK, A/s. Herlev, Denmark.

15. Eichelbrenner, E.
Remarks on Tangential Blowing. Private Communications.

16. Knystautas, R.
The Turbulent Jet From a Series of Holes In Line. McGill University, Mechanical Engineering Research Laboratory, Report 62-1, January 1962.

17. Patel R.P.
Newman, B.G.
Self-Preserving, Two-Dimensional Turbulent Jets and Wall Jets In a Moving Stream. McGill University, Aerodynamics Section, Report No. Ae 5, September 1961.

18. Sigalla, A.
Measurements of Skin Friction In a Plane Turbulent Wall Jet. J.R. Ae. S. Vol. 62, P.873, 1958.

19. Preston, J.H.
The Determination of Turbulent Skin Friction by Means of Pitot Tubes. J.R.Ae.S. Vol.58, P.109, 1954.

20. Bradshaw, P.
Gregory, M.A.
The Determination of Local Turbulent Skin Friction From Observations In The Viscous Sub-Layer. A.R.C. 20,895, F.M.2802, March 1959.

21. Smith, D.W.
Walker, J.H.
Skin Friction Measurements In Incompressible Flow. NACA TN. 4231, March 1958.

22. Relf, E.F.
Pankhurst, R.C.
Walker, W.S.
The Use of Pitot Tubes to Measure Skin Friction on a Flat Plate. A.R.C. 17,025, F.M. 2121, August 1954.

23. Goldstein, S.
Modern Developments In Fluid Dynamics. Vol.II, P.500-501. Oxford 1938.

TABLE I

TABULATED RESULTS OF THE PRESENT EXPERIMENTS

WALL JET IN EQUILIBRIUM PRESSURE GRADIENT

TEST	$\frac{U_j}{U_{is}}$	$b_{ins.}$	$\delta^*_{s\,ins}$	$\theta_{s\,ins.}$	$\frac{U_{is}\theta_s}{\nu}$	$\frac{U_M}{U_1}$	(m) FROM EQU^N (10)	(m) FROM EQU^N (12)	$\left(\frac{x_o}{b}\right)$ FROM GROWTH OF $(y_{M/2}-y_M)$	$\left(\frac{x_o}{b}\right)$ FROM STATIC PRESSURE DISTRIBUTION	C	RANGE OF $Re=\frac{U_M y_{M/2}}{\nu}$
1	4·05	0·375	0·0375	0·030	1535	2·92	−0·413	−0·446	−7·75	−8·0	0·0457	$7·02\times10^4$ $10·0\times10^4$
2	3·0	0·20	0·0288	0·025	1000	2·65	−0·407	−0·432	−7·0	−8·0	0·0355	$3·48\times10^4$ $5·95\times10^4$
3	3·0	0·402	0·0313	0·025	1000	3·0	−0·414	−0·43	−10·0	−10·2	0·0458	$6·0\times10^4$ $9·1\times10^4$
4	6·01	0·40	0·011	0·010	226·5	5·75	−0·449	−0·462	−5·0	−5·0	0·0637	$7·13\times10^4$ $11·15\times10^4$
5	6·0	0·20	0·025	0·0138	282·0	5·65	−0·448	−0·462	−3·0	−2·5	0·0515	$4·12\times10^4$ $6·79\times10^4$
6	1·501	0·20	0·0388	0·030	1385	1·325	−0·356	−0·398	−11·5	−11·5	0·0167	$1·625\times10^4$ $2·82\times10^4$
7	1·07	0·20	NON SIMILAR PROFILES									

TABLE II

AVAILABLE DATA FOR EQUATION (14): AS APPLIED TO THE OUTER PART OF A WALL JET.

CASE	SOURCE	b ins.	$\frac{U_j}{U_{is}}$	$\frac{\delta_s^*}{b}$	$\frac{x_o}{b}$
WALL JET IN STILL AIR	SIGALLA	0·313	∞	–	−8·33
	SCHWARZ & COSART	1·00	∞	–	−11·2
	FÖRTHMANN	1·18	∞	–	−6·7
	PRESENT INVESTIGATION	0·20	∞	–	−10·0
WALL JET IN ZERO PRESSURE GRADIENT	GEORGE	0·051	2·96	0·9025	−23·0
		0·055	3·001	0·837	−23·0
		0·0525	5·89	0·876	−18·0
	PRESENT INVESTIGATION	0·20	3·0	–	−20·0
		0·20	5·95	–	−16·0
WALL JET IN EQUILIBRIUM PRESSURE GRADIENT.	PRESENT INVESTIGATION	0·20	3·0	0·144	−7·0
		0·375	4·05	0·10	−7·75
		0·402	3·0	0·0782	−10·0
		0·40	6·01	0·0275	−5·0
		0·20	6·0	0·125	−3·0
		0·20	1·501	0·197	−11·5

TABLE III

COLLECTED VALUES OF A AND B IN THE LOG LAW-OF-WALL AND COEFFICIENT OF SKIN FRICTION.

CASE	SOURCE	$\frac{U_j}{U_{is}}$	b ins.	$C_f = 2\left(\frac{U_\tau}{U_M}\right)^2$	$\frac{U_1}{U_M}$	$\frac{U_M y_M}{\nu}$	A	B
WALL JET IN STILL AIR	MYERS et al.	–	0·50	–	0·0	$8·61\times10^3$ $6·52\times10^3$ $4·46\times10^3$	3·9 3·95 3·75	9·6 7·45 8·5
	PRESENT INVESTIGATION.	–	0·20	0·00673 0·00554 0·00531	0·0	$6·83\times10^3$ $8·44\times10^3$ $9·1\times10^3$	4·45 4·35 4·75	6·55 8·05 7·7
		–	0·20	0·00568 0·00512 0·00524	0·0	$9·92\times10^3$ $11·56\times10^3$ $12·43\times10^3$	4·3 3·9 4·4	7·95 9·7 8·0
	BRADSHAW & GEE.	–	0·018	–	0·0	$2·51\times10^3$ $12·59\times10^3$	4·7	6·8
WALL JET IN ZERO PRESSURE GRADIENT	PRESENT INVESTIGATION.	3·0	0·20	0·00573 0·00482 0·00494	0·428 0·510 0·570	$8·65\times10^3$ $10·50\times10^3$ $13·35\times10^3$	4·3 4·1 4·15	7·8 8·55 9·1
		5·95	0·20	0·00591 0·00518 0·00522	0·2322 0·294 0·353	$8·88\times10^3$ $10·3\times10^3$ $10·53\times10^3$	4·4 4·15 4·95	7·3 8·6 7·35
	BRADSHAW & GEE	–	0·018	–	≈0·858	–	4·81	6·25
WALL JET IN EQUILIBRIUM PRESSURE GRADIENT	PRESENT INVESTIGATION	1·501	0·20	0·00612 0·00457 0·00374	0·755	$6·34\times10^3$ $8·85\times10^3$ $11·50\times10^3$	4·65 5·5 5·6	6·45 6·2 7·1
		3·0	0·20	0·0056 0·00498 0·00515	0·378	$9·15\times10^3$ $10·87\times10^3$ $12·3\times10^3$	3·45 3·8 3·8	10·2 10·2 10·2
		6·0	0·20	0·006 0·00529 0·00542	0·177	$8·55\times10^3$ $9·20\times10^3$ $10·38\times10^3$	4·2 3·3 4·8	7·6 9·9 6·9
	BRADSHAW & GEE.	–	0·040	–	≈0·80	–	5·4	5·2

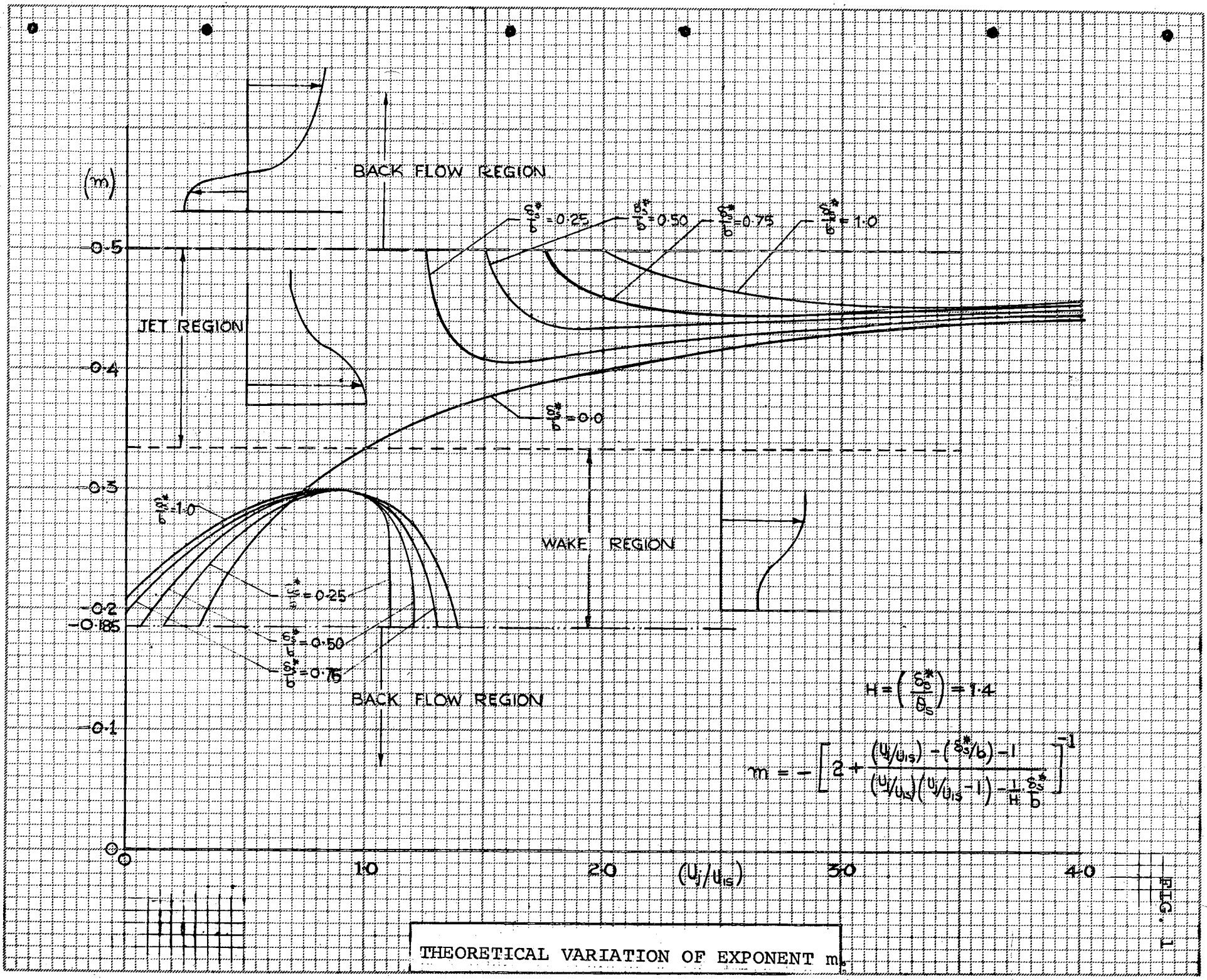

FIG. 1

THEORETICAL VARIATION OF EXPONENT m_s

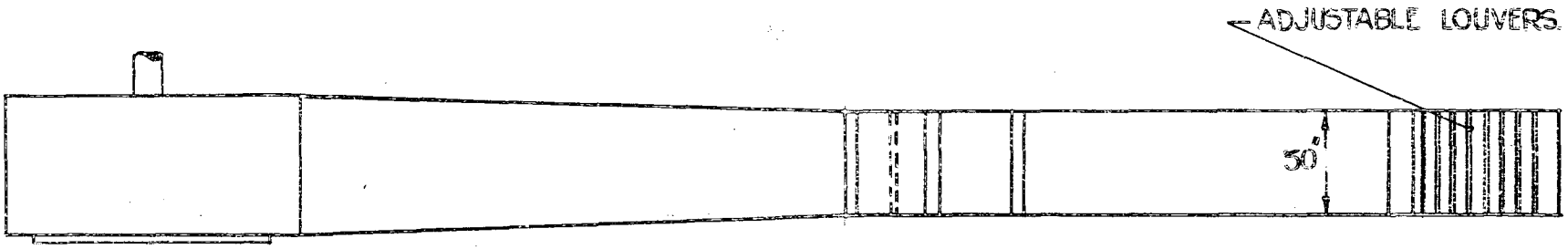

PLAN VIEW

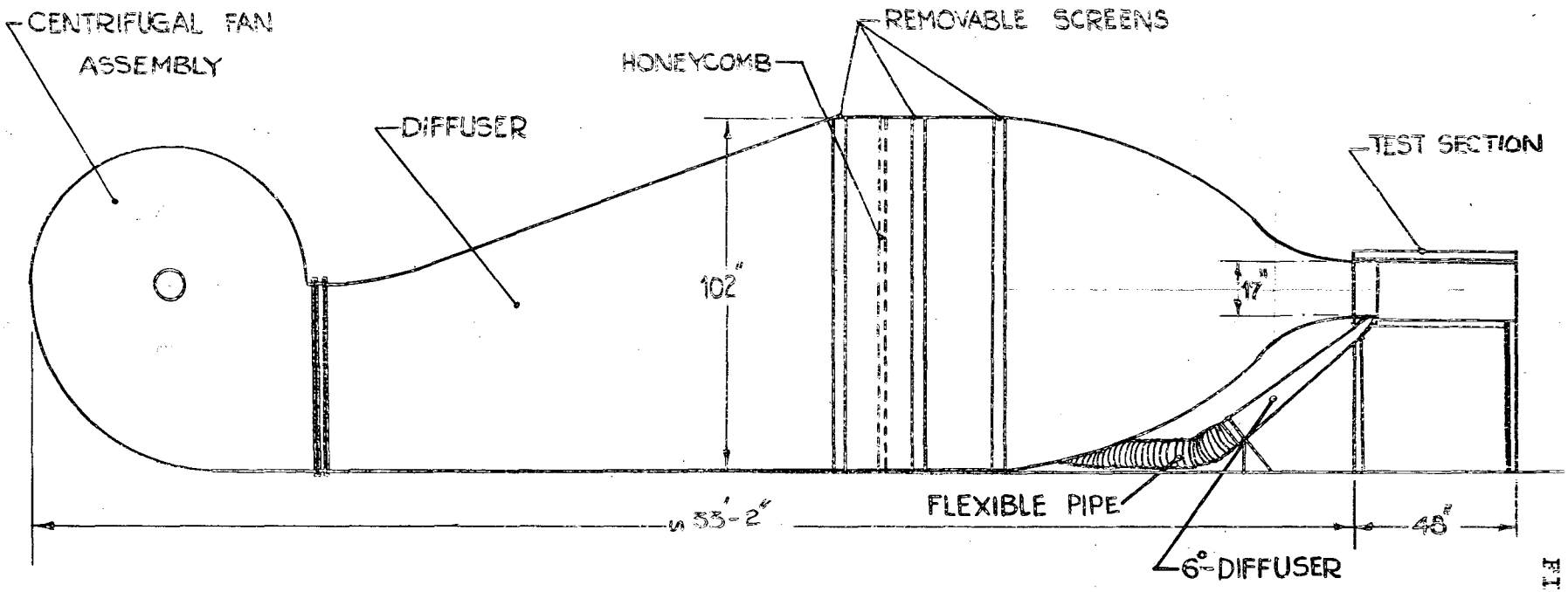

SKETCH OF TUNNEL

FIG. 2.1

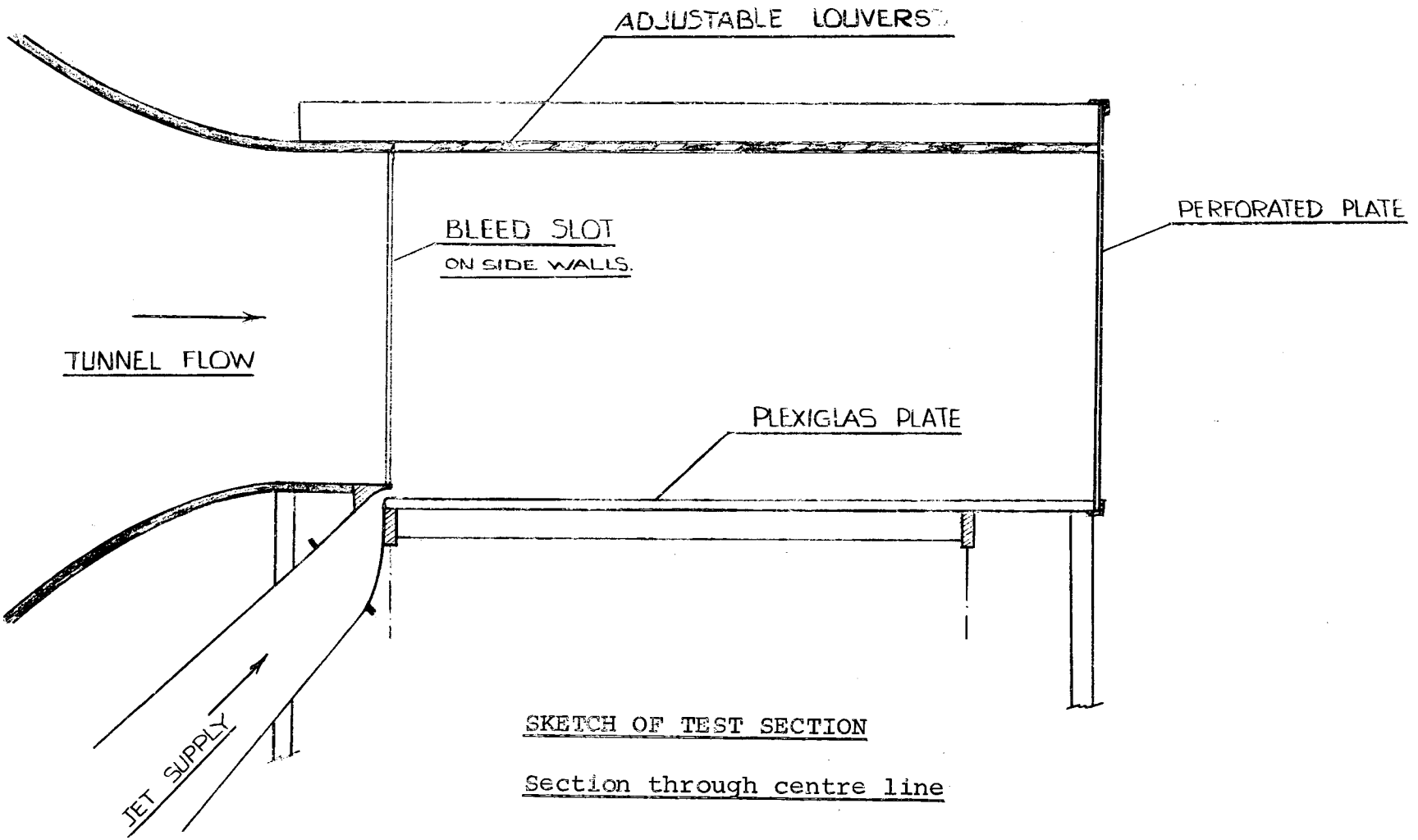

SKETCH OF TEST SECTION

Section through centre line

FIG. 2.2

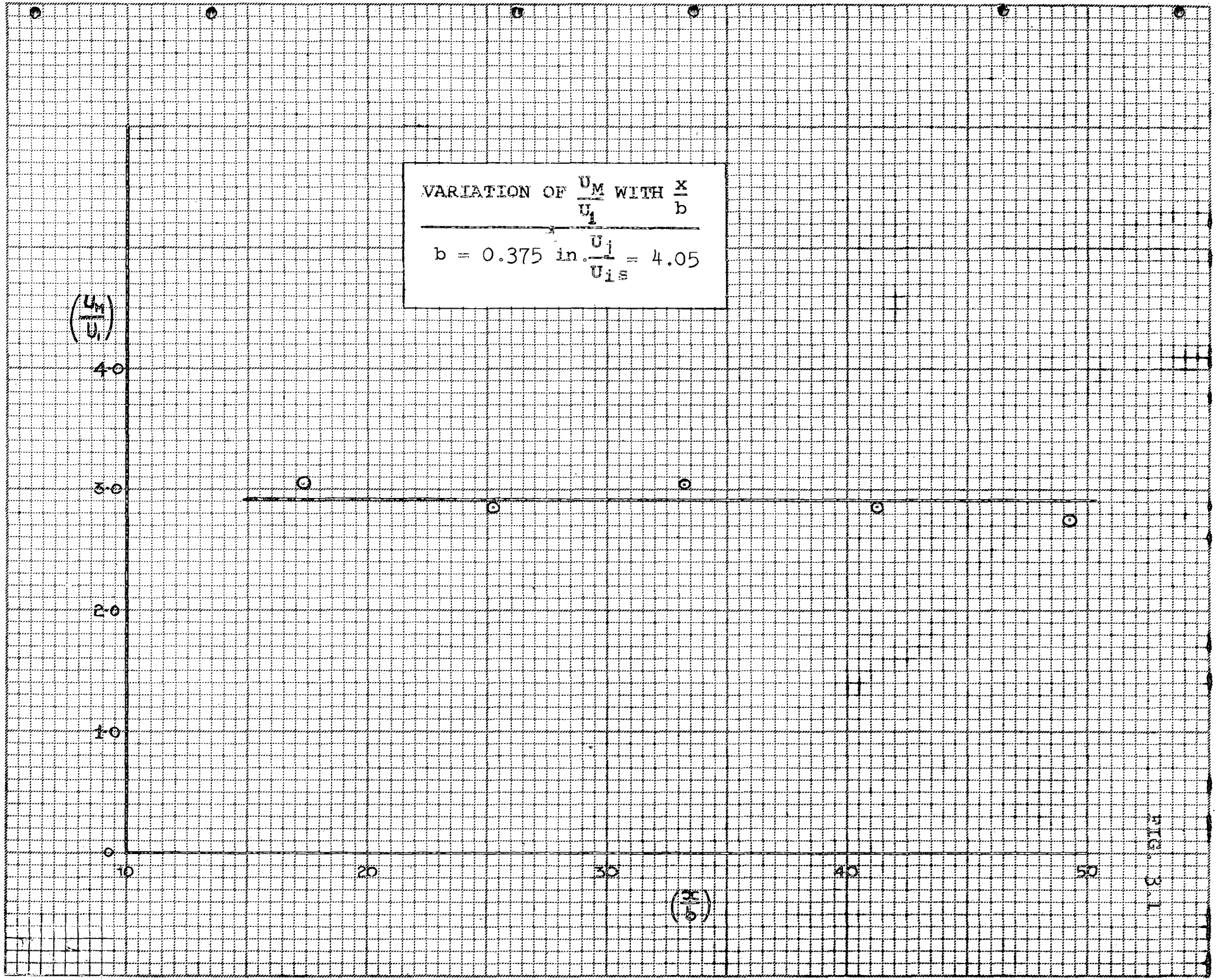
VARIATION OF $\frac{U_M}{U_1}$ WITH $\frac{x}{b}$
b = 0.375 in. $\frac{U_j}{U_{is}}$ = 4.05
$\left(\frac{U_M}{U_1}\right)$
4·0
3·0
2·0
1·0
0
10
20
30
40
50
$\left(\frac{x}{b}\right)$

FIG. 3.1

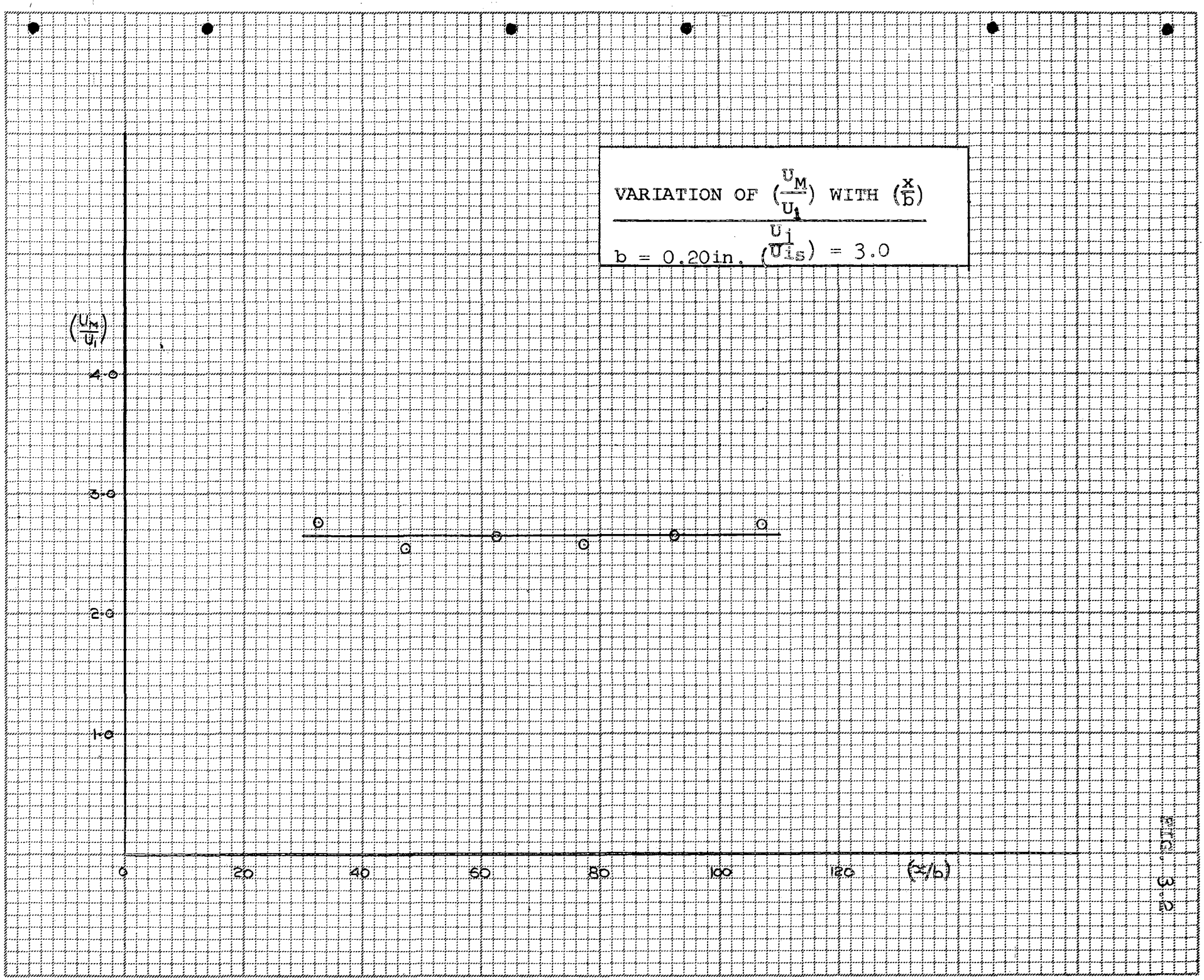
VARIATION OF $(\frac{U_M}{U_1})$ WITH $(\frac{x}{b})$
b = 0.20in. $(\frac{U_j}{U_{is}})$ = 3.0
$(\frac{U_M}{U_1})$
4.0
3.0
2.0
1.0
0
20
40
60
80
100
120
$(\frac{x}{b})$

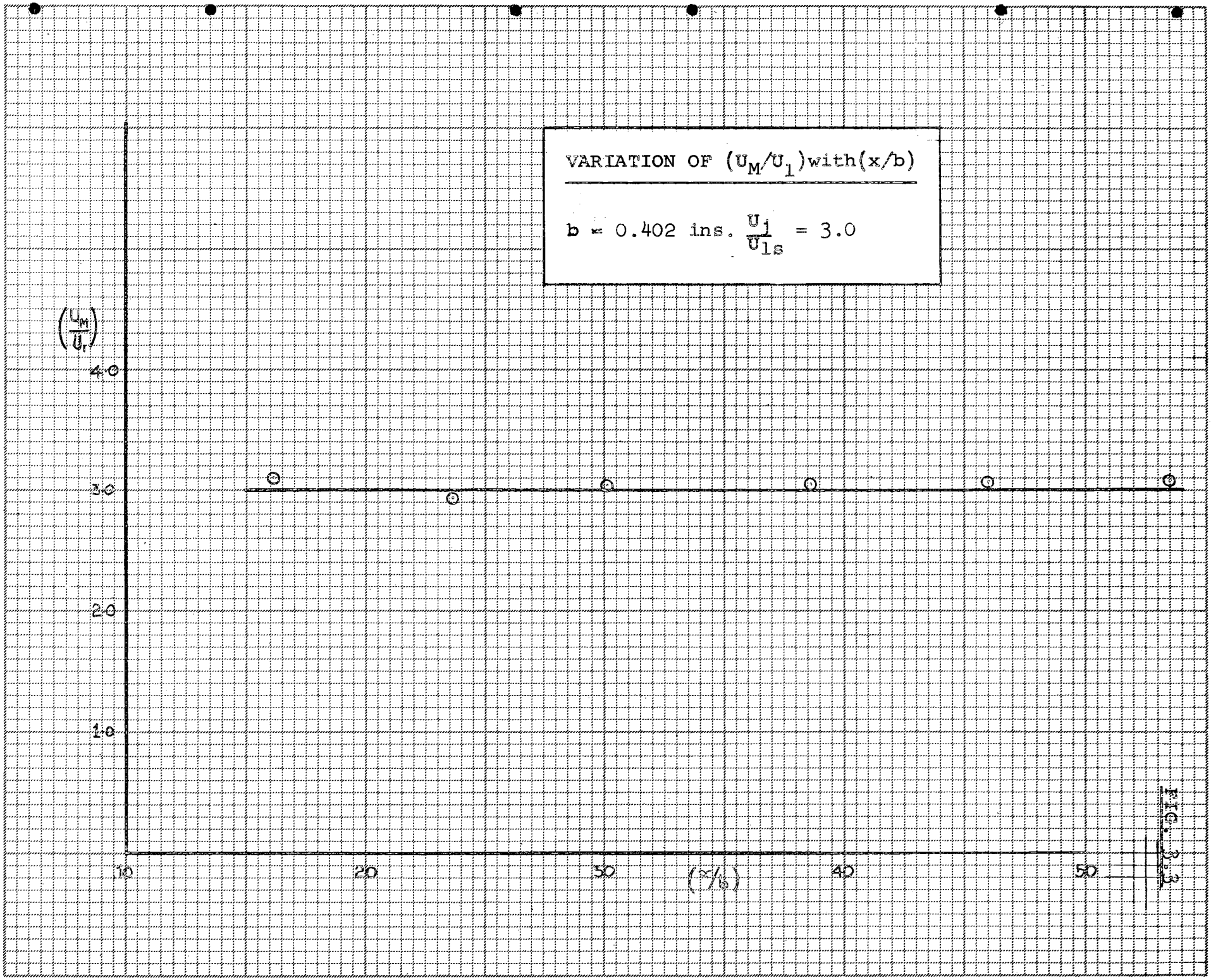
VARIATION OF (U_M/U_1) with (x/b)
b = 0.402 ins. $\frac{U_1}{U_{1s}} = 3.0$
$\left(\frac{U_M}{U_1}\right)$
4.0
3.0
2.0
1.0
10
20
30
40
50
(x/b)
FIG. 13

FIG. 3.4

VARIATION OF (U_M/U_1) with (x/b)

$b = 0.40$ ins. $\frac{U_1}{U_{is}} = 6.01$

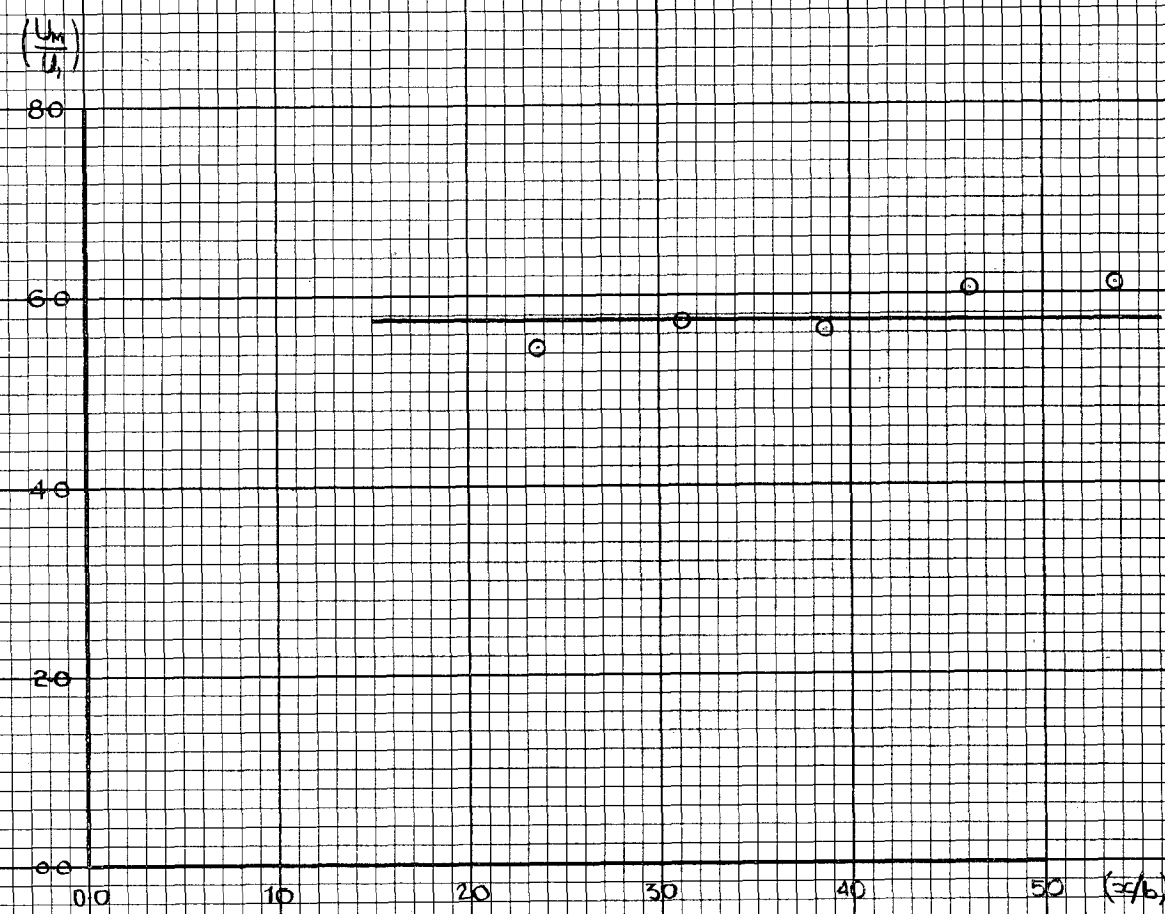

FIG. 3.5

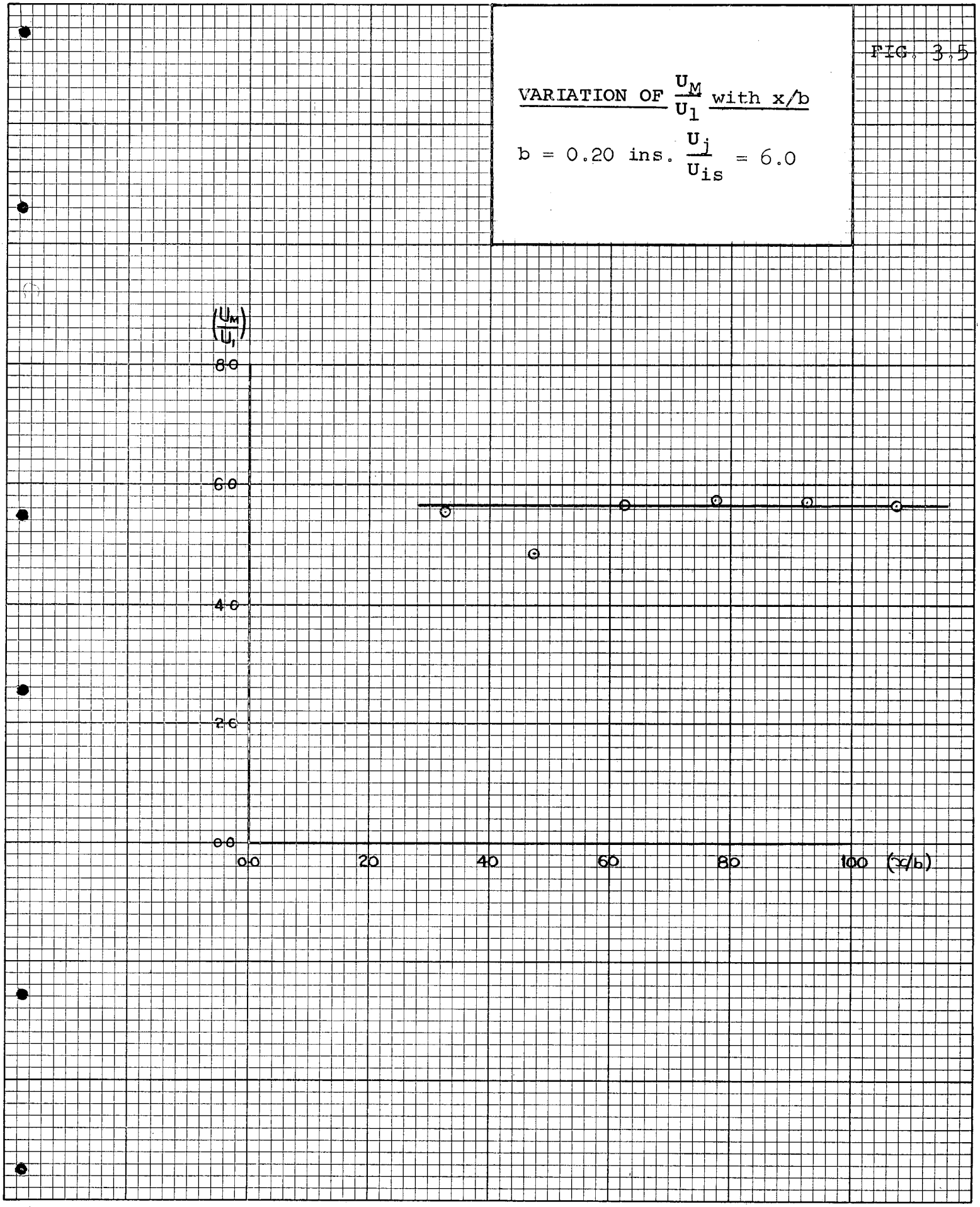
VARIATION OF $\frac{U_M}{U_1}$ with x/b
b = 0.20 ins. $\frac{U_j}{U_{is}}$ = 6.0
$\left(\frac{U_M}{U_1}\right)$
.80
.60
.40
.20
.00
.00
20
40
60
80
100
(x/b)

FIG. 3.6

VARIATION OF $\frac{U_M}{U_1}$ with x/b

b = 0.20 ins. $\frac{U_1}{U_{is}}$ = 1.501

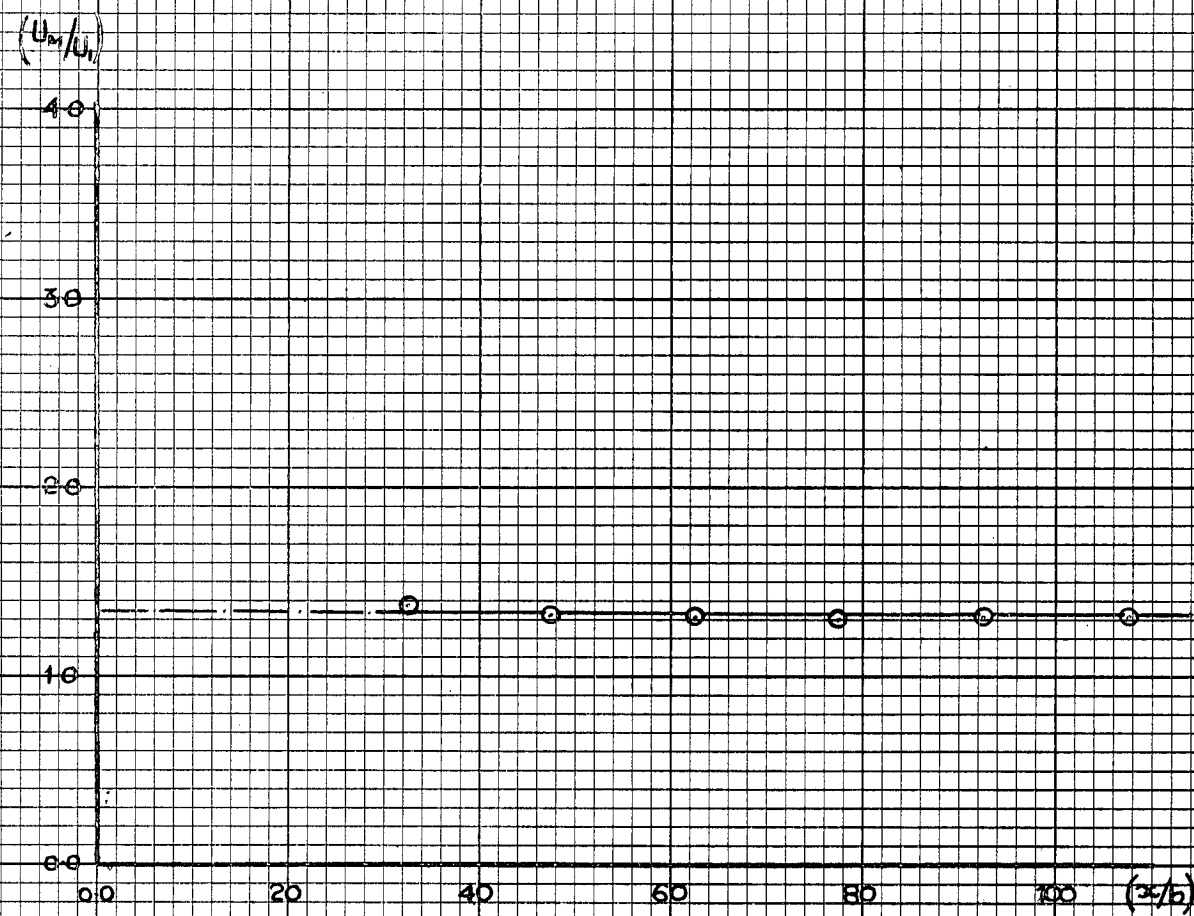

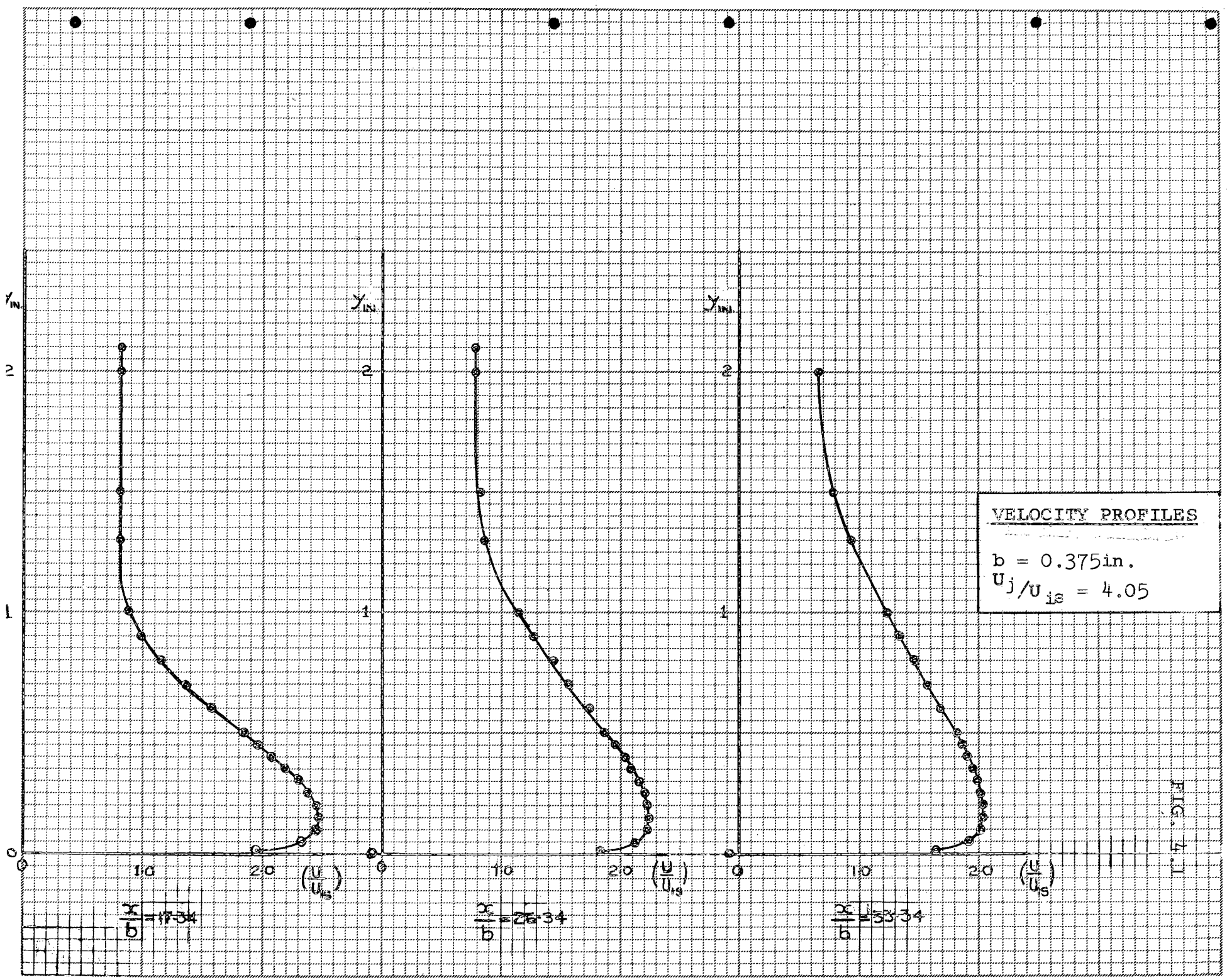
VELOCITY PROFILES
b = 0.375in.
U_j/U_{is} = 4.05
$y_{IN.}$
2
1
0
1.0
2.0
$\left(\frac{U}{U_{is}}\right)$
$\frac{x}{b}$ = 17.34
$\frac{x}{b}$ = 26.34
$\frac{x}{b}$ = 33.34

FIG. 7.11

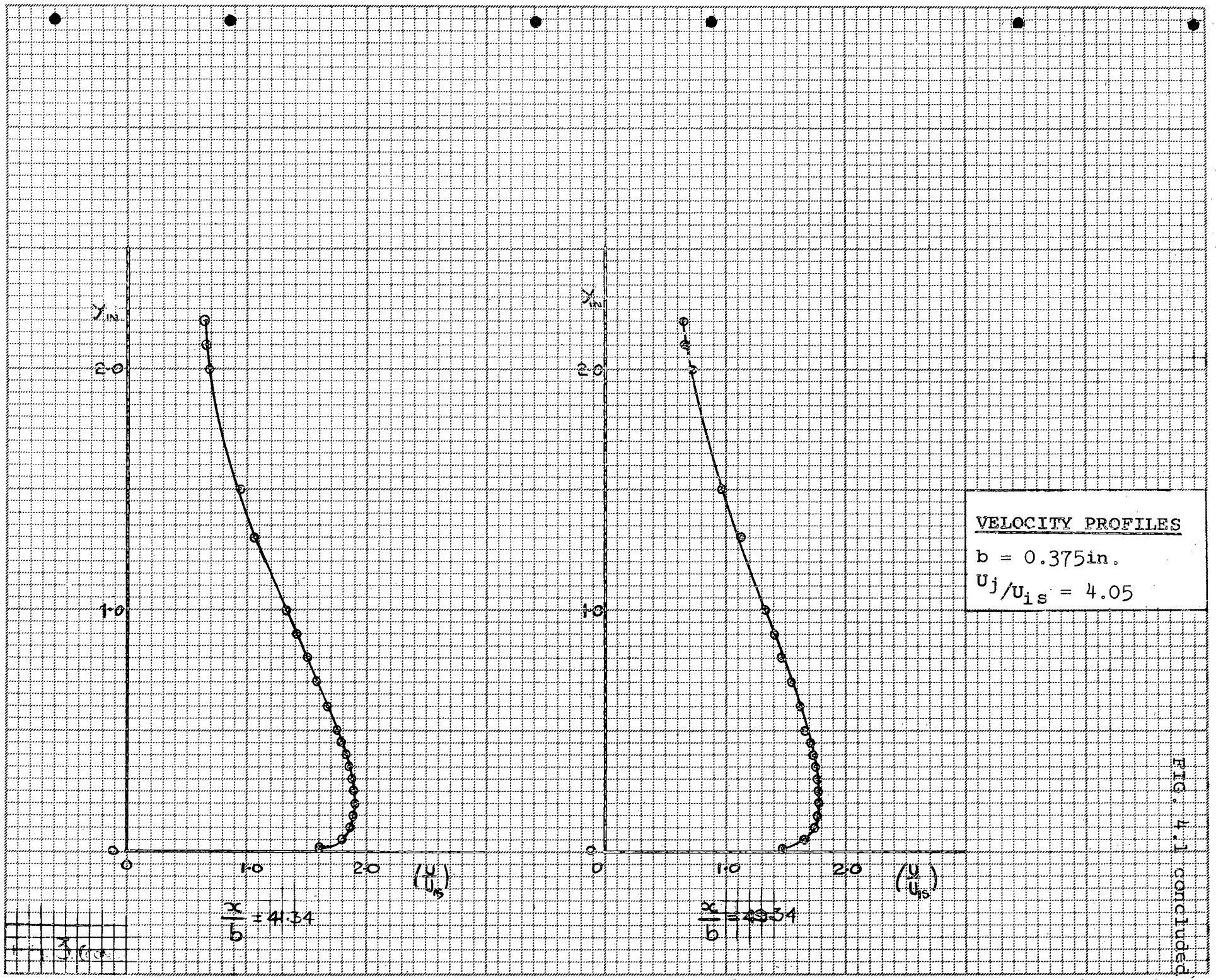

FIG. 4.1 concluded

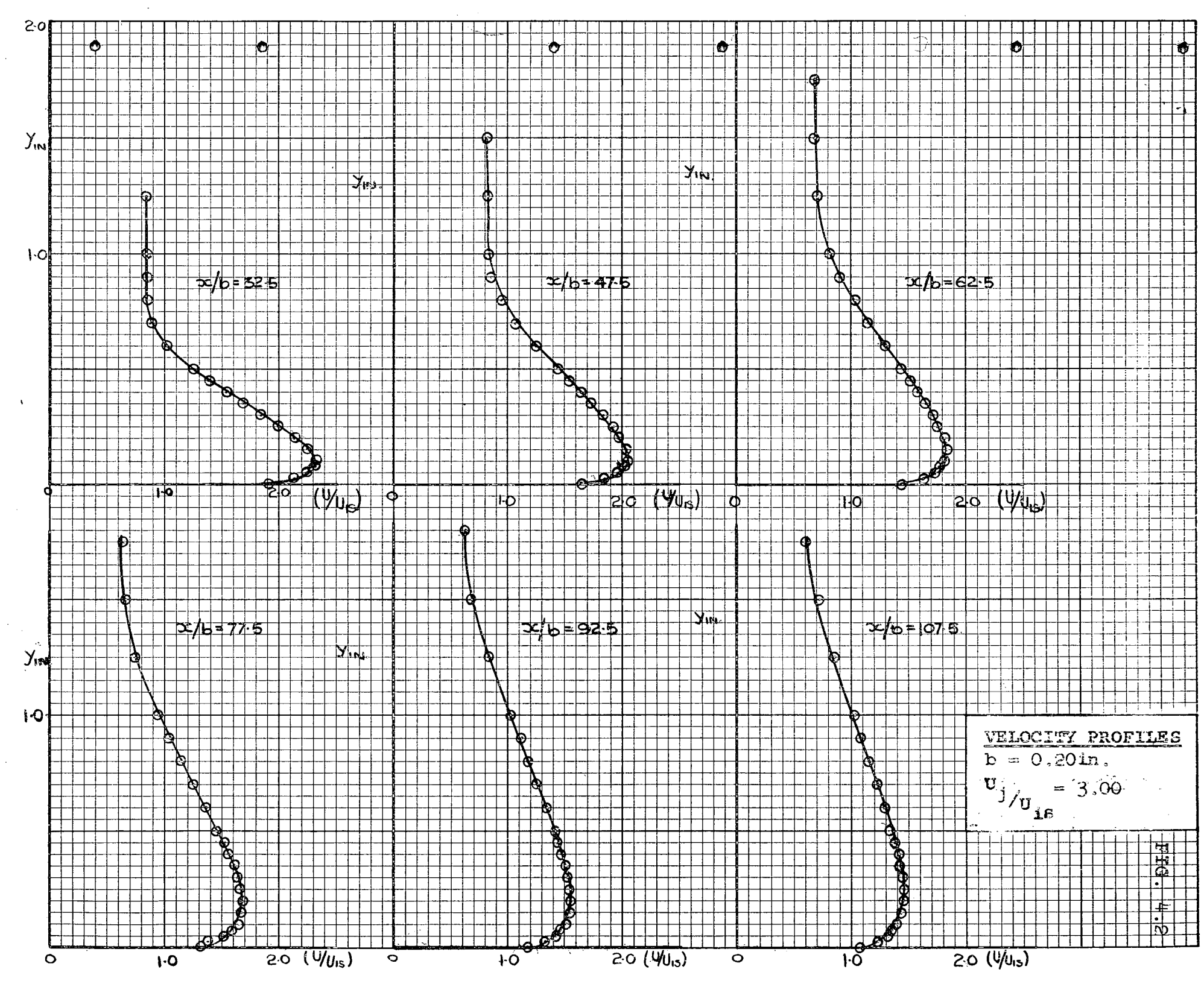
2·0
1·0
0
y_{IN}
$x/b = 32.5$
$x/b = 47.5$
$x/b = 62.5$
$x/b = 77.5$
$x/b = 92.5$
$x/b = 107.5$
1·0
2·0
(U/U_{IS})
VELOCITY PROFILES
b = 0.20in.
U_j/U_{IS} = 3.00
2·# GE#

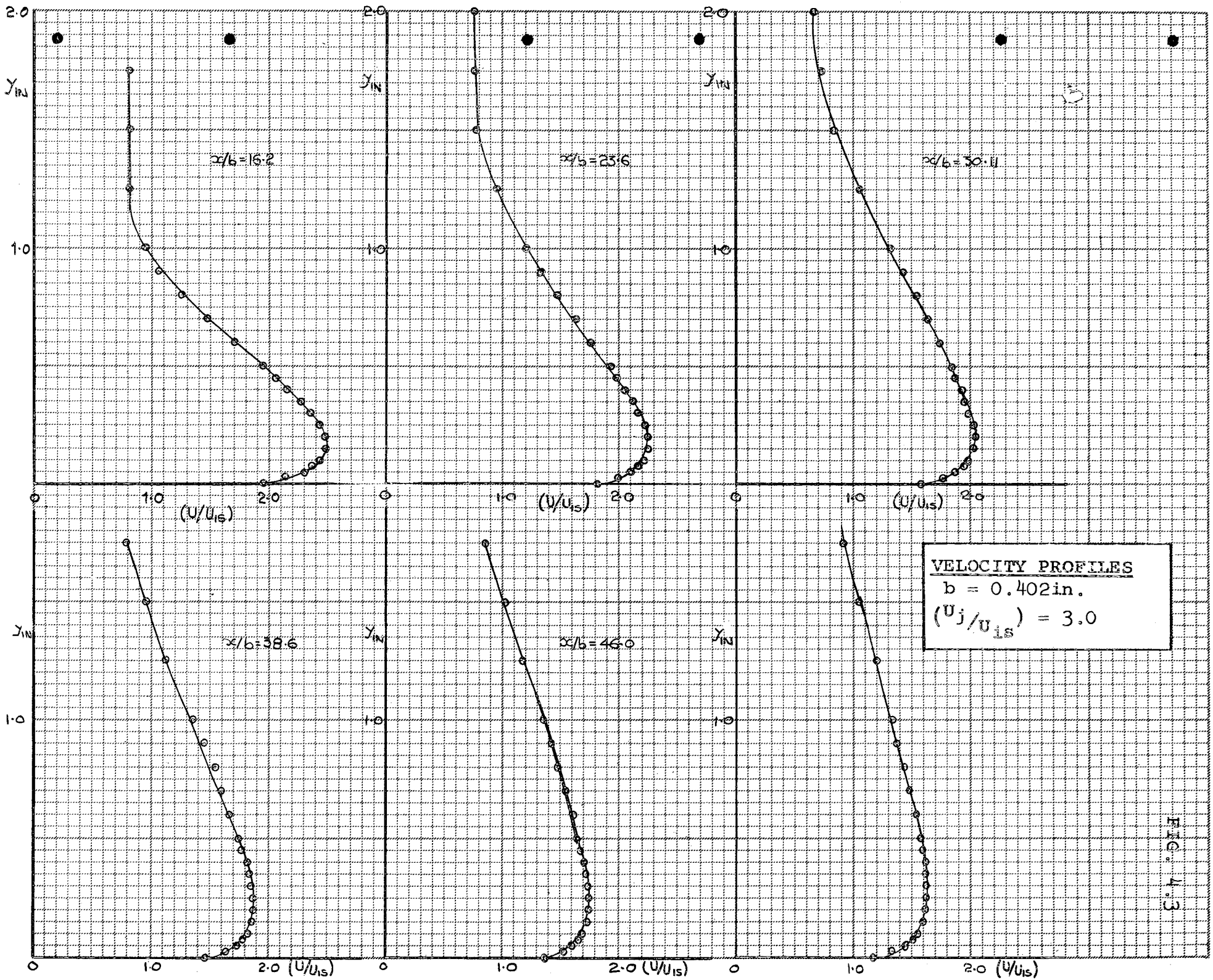
2·0
1·0
0
y_{IN}
x/b = 16·2
x/b = 23·6
x/b = 30·11
x/b = 38·6
x/b = 46·0
1·0
2·0
(U/U_{IS})
VELOCITY PROFILES
b = 0.402in.
$(U_j/U_{IS}) = 3.0$

Fig. 4.3

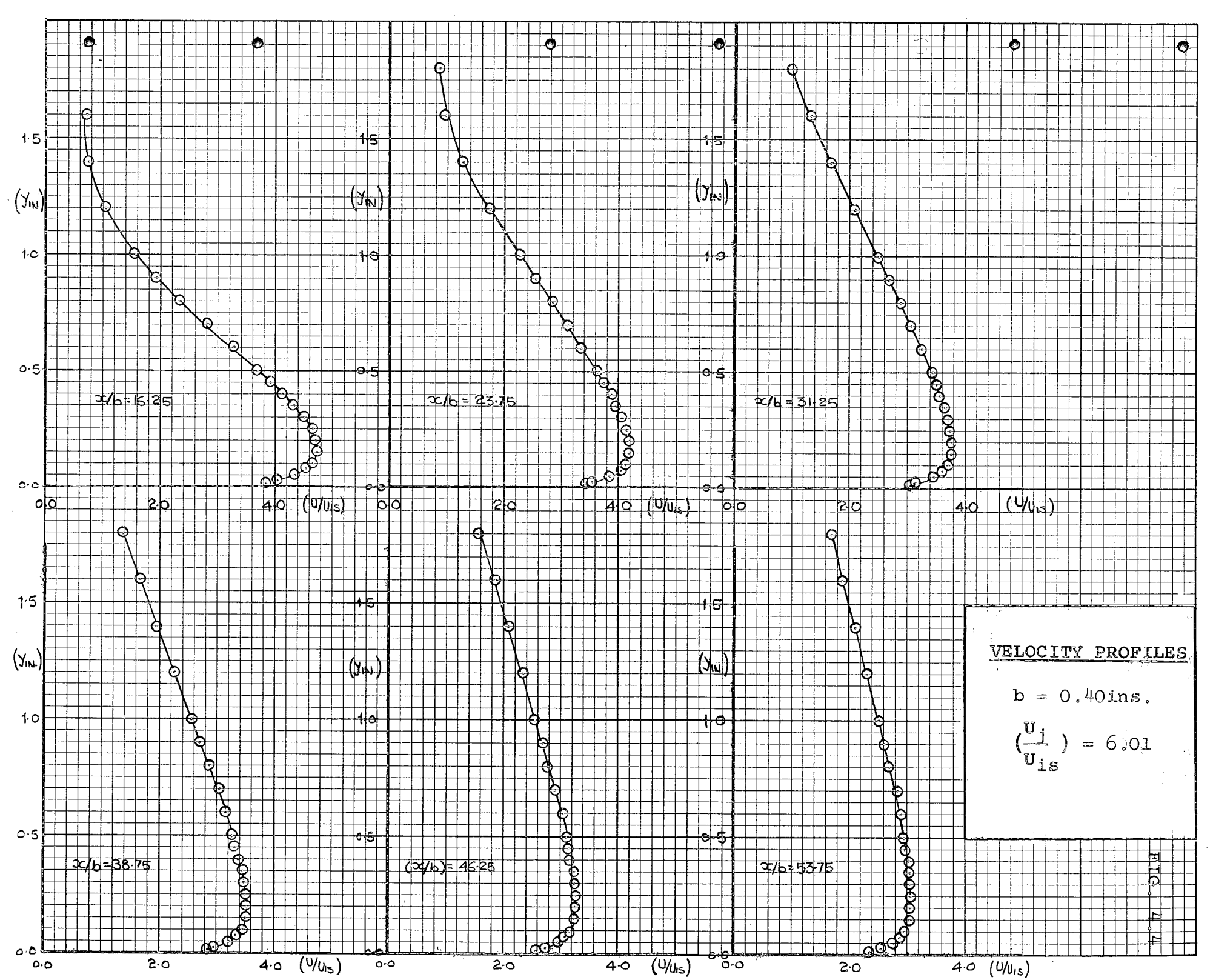
(Y/N)
1·5
1·0
0·5
0·0
0·0
2·0
4·0
(U/Uis)
x/b = 16·25
x/b = 23·75
x/b = 31·25
x/b = 38·75
(x/b) = 46·25
x/b = 53·75
VELOCITY PROFILES
b = 0.40ins.
(Ui/Uis) = 6.01
FIG. 4.4

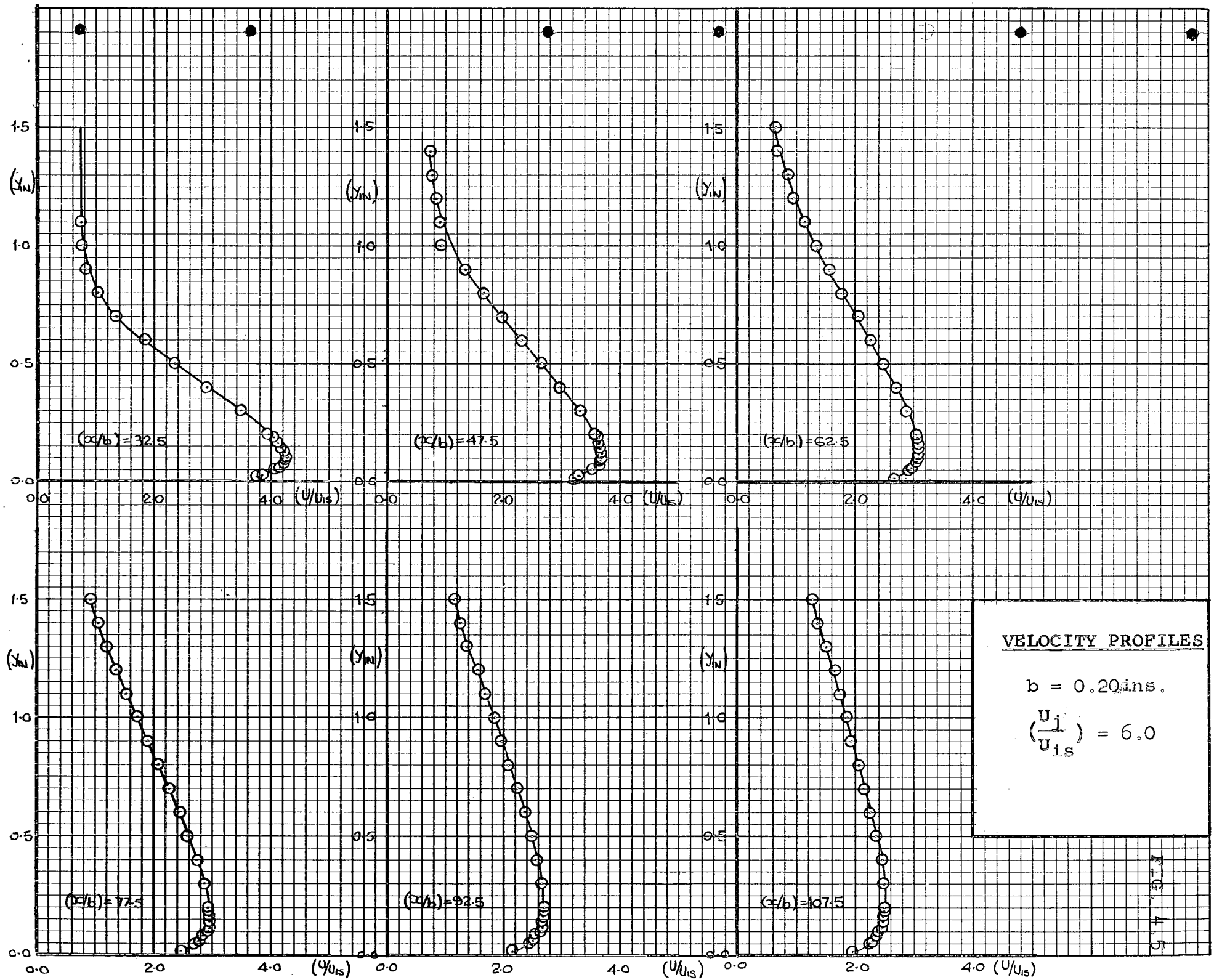
1·5
(Y/N)
1·0
0·5
0·0
0·0
2·0
4·0
(U/Uis)
(x/b) = 32·5
(x/b) = 47·5
(x/b) = 62·5
(x/b) = 77·5
(x/b) = 92·5
(x/b) = 107·5
VELOCITY PROFILES
b = 0.20 ins.
(Ui/Uis) = 6.0

Fig. 4.5

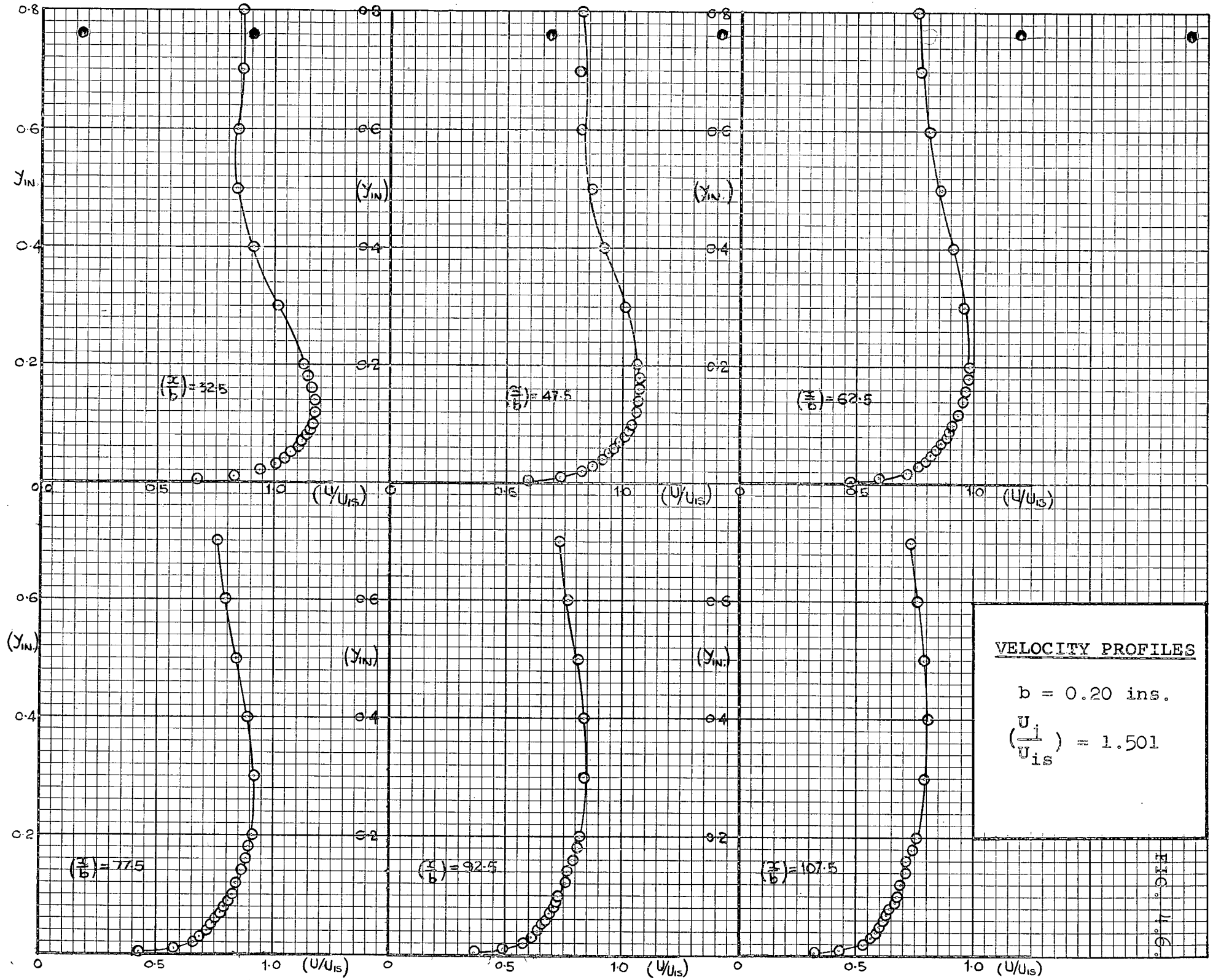
$y_{IN.}$
$(y_{IN.})$
$(\frac{x}{b}) = 32.5$
$(\frac{x}{b}) = 47.5$
$(\frac{x}{b}) = 62.5$
$(\frac{x}{b}) = 77.5$
$(\frac{x}{b}) = 92.5$
$(\frac{x}{b}) = 107.5$
(U/U_{IS})
0
0.2
0.4
0.6
0.8
0.5
1.0
VELOCITY PROFILES
b = 0.20 ins.
$(\frac{U_i}{U_{is}}) = 1.501$
FIG. 4.6.

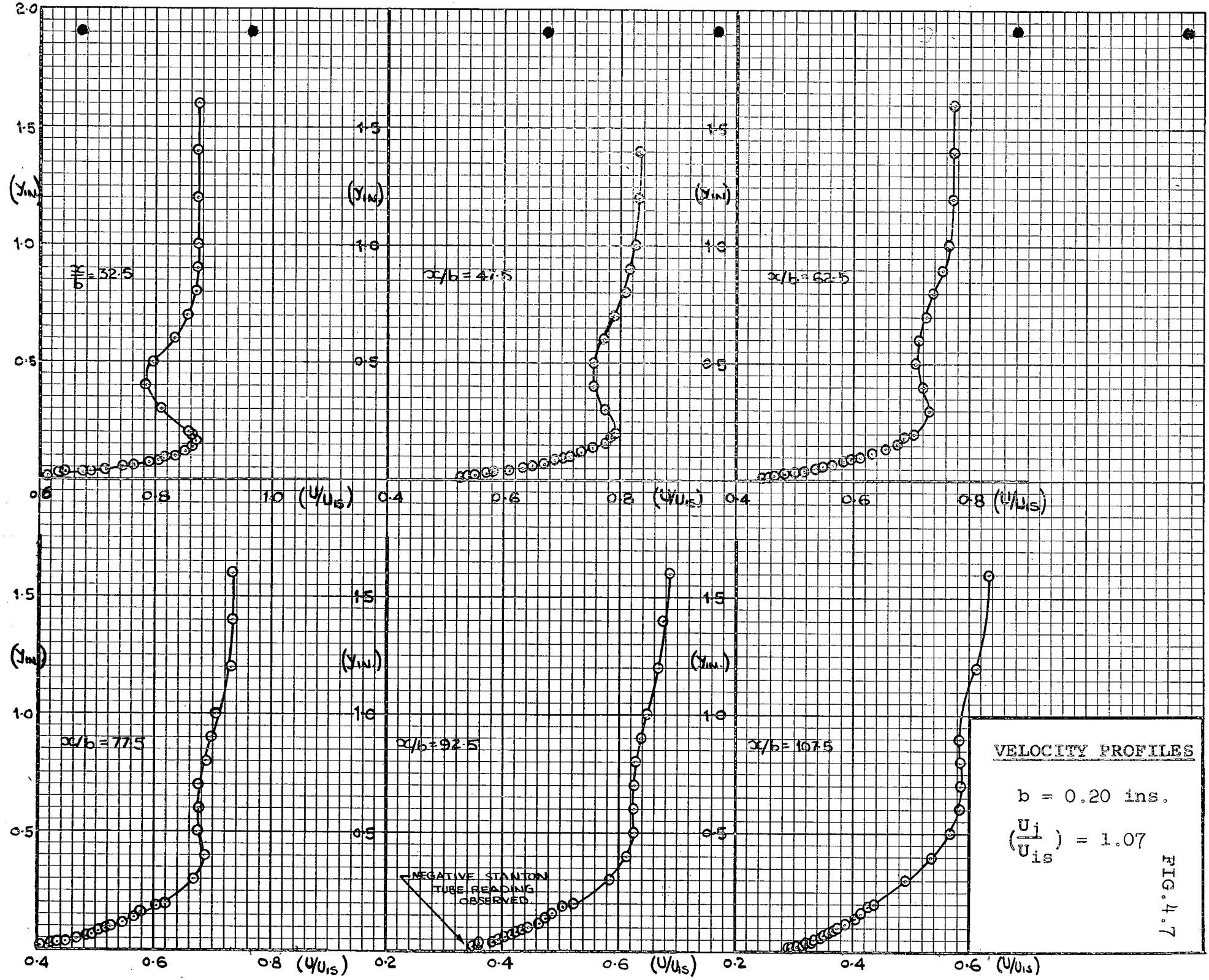
x/b = 32.5
x/b = 47.5
x/b = 62.5
x/b = 77.5
x/b = 92.5
x/b = 107.5
(y/N)
(U/Uis)
NEGATIVE STANTON TUBE READING OBSERVED
VELOCITY PROFILES
b = 0.20 ins.
(Uj/Uis) = 1.07

FIG. 4.7

FIG. 5.1

NON-DIMENSIONAL MEAN VELOCITY PROFILES EXCLUDING INNER BOUNDARY LAYER IN A TAILORED PRESSURE GRADIENT.

$b = 0.375$in. $\left(\frac{U_j}{U_{is}}\right) = 4.05$

	$\left(\frac{U_M Y_M/2}{\nu}\right)$
• x/b = 17.34	7.02×10^4
⊡ x/b = 25.34	7.96×10^4
× x/b = 33.34	8.93×10^4
⊙ x/b = 41.34	9.66×10^4
△ x/b = 49.34	10.00×10^4

$$\left[\frac{U-U_1}{U_M-U_1}\right] = \text{SECH}^2\left[0.88\left\{\frac{y-y_M}{y_{M_2}-y_M}\right\}\right]$$

$$\left[\frac{U-U_1}{U_M-U_1}\right] = e^{-0.693\left(\frac{y-y_M}{y_{M_2}-y_M}\right)^2}$$

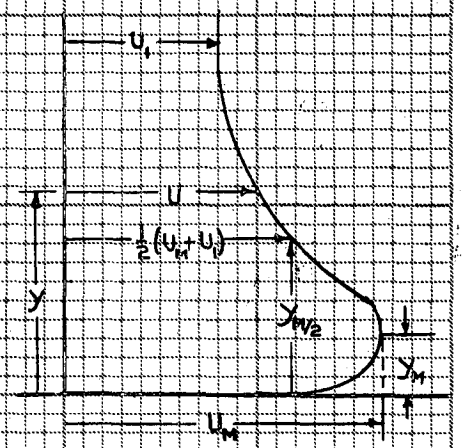

$\frac{(y-y_M)}{(y_{M_2}-y_M)}$

3·0
2·5
2·0
1·5
1·0
0·5
0
−0·5

0·2
0·4
0·6
0·8
1·0

$\frac{(U-U_1)}{(U_M-U_1)}$

FIG. 5.2

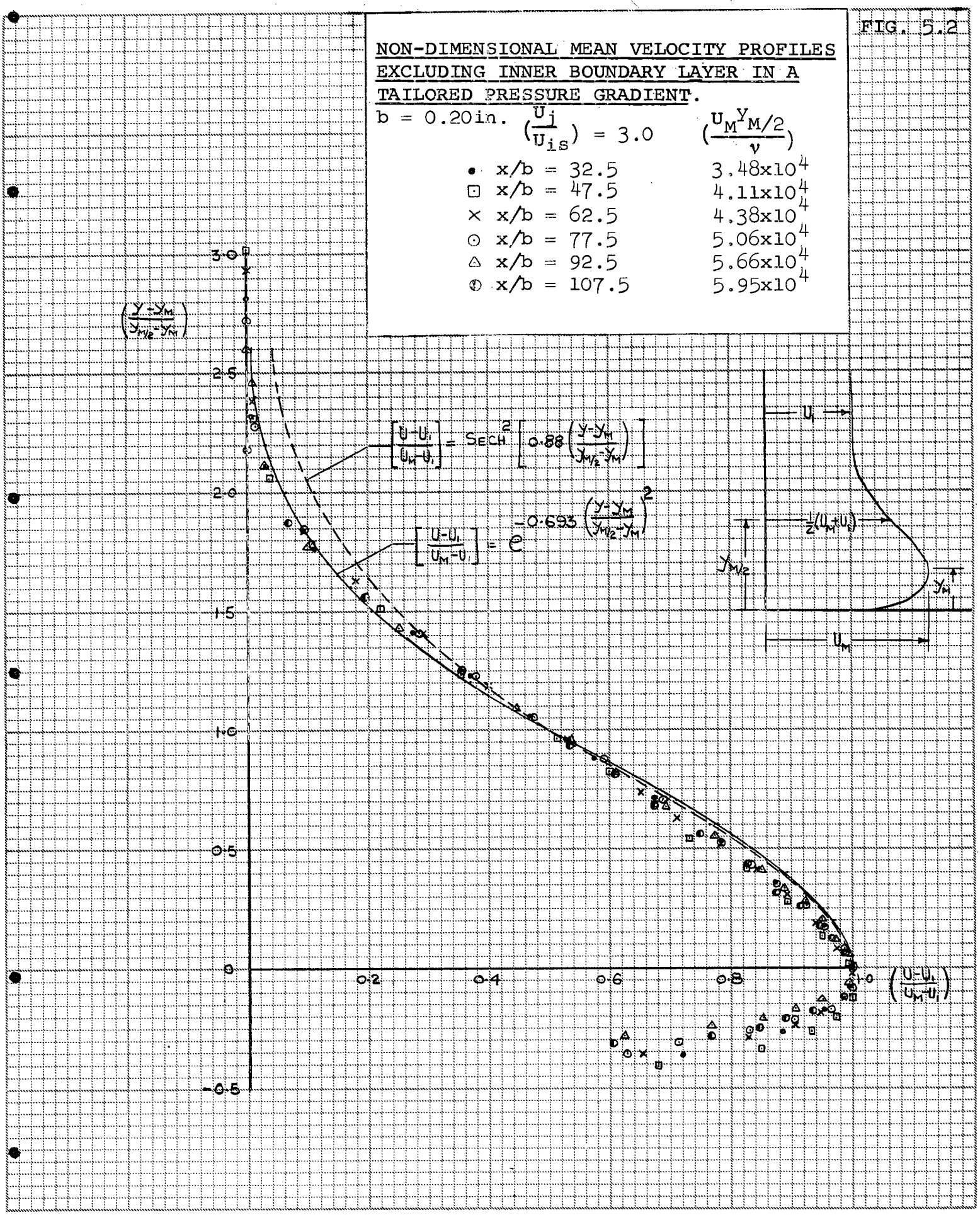
NON-DIMENSIONAL MEAN VELOCITY PROFILES EXCLUDING INNER BOUNDARY LAYER IN A TAILORED PRESSURE GRADIENT.
b = 0.20in. $(\frac{U_j}{U_{is}}) = 3.0$ $(\frac{U_M Y_{M/2}}{\nu})$
• x/b = 32.5 3.48x10^4
⊡ x/b = 47.5 4.11x10^4
× x/b = 62.5 4.38x10^4
⊙ x/b = 77.5 5.06x10^4
△ x/b = 92.5 5.66x10^4
◐ x/b = 107.5 5.95x10^4
$\left(\frac{Y-Y_M}{Y_{M/2}-Y_M}\right)$
$\left[\frac{U-U_i}{U_M-U_i}\right] = SECH^2\left[0.88\left(\frac{y-y_M}{y_{M/2}-y_M}\right)\right]$
$\left[\frac{U-U_i}{U_M-U_i}\right] = e^{-0.693\left(\frac{y-y_M}{y_{M/2}-y_M}\right)^2}$
U_i
$\frac{1}{2}(U_M+U_i)$
$Y_{M/2}$
Y_M
U_M
3.0
2.5
2.0
1.5
1.0
0.5
0
-0.5
0.2
0.4
0.6
0.8
1.0
$\left(\frac{U-U_i}{U_M-U_i}\right)$

NON-DIMENSIONAL MEAN VELOCITY PROFILES FIG. 5.3
EXCLUDING INNER BOUNDARY LAYER IN A
TAILORED PRESSURE GRADIENT.

$b = 0.402\text{in.}$ $\left(\frac{U_j}{U_{is}}\right) = 3.00$ $\left(\frac{U_M y_{M/2}}{\nu}\right)$

•	x/b = 16.2	6.00×10^4
⊡	x/b = 23.6	6.97×10^4
×	x/b = 30.11	7.71×10^4
⊙	x/b = 38.6	8.21×10^4
△	x/b = 46.0	8.84×10^4
◐	x/b = 53.5	9.10×10^4

$\left(\frac{y-y_M}{y_{M/2}-y_M}\right)$

3.0
2.5
2.0
1.5
1.0
0.5
0
-0.5

$\left[\frac{U-U_i}{U_M-U_i}\right] = \text{SECH}^2\left[0.88\left(\frac{y-y_M}{y_{M/2}-y_M}\right)\right]$

$\left[\frac{U-U_i}{U_M-U_i}\right] = e^{-0.693\left(\frac{y-y_M}{y_{M/2}-y_M}\right)^2}$

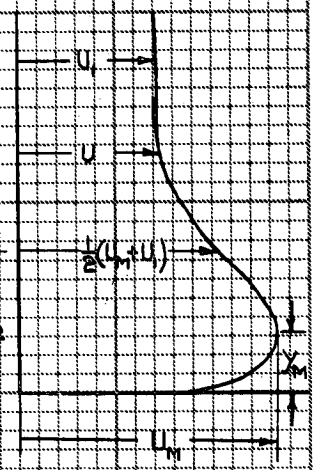

0.2 0.4 0.6 0.8 1.0 $\left(\frac{U-U_i}{U_M-U_i}\right)$

NON-DIMENSIONAL MEAN VELOCITY PROFILES EXCLUDING INNER BOUNDARY LAYER IN A TAILORED PRESSURE GRADIENT

FIG. 5.4

$b = 0.40$ ins. $\left(\frac{U_j}{U_{is}}\right) = 6.01$

⊙	x/b = 16.25	7.13×10^4
⊡	x/b = 23.75	8.26×10^4
△	x/b = 31.25	9.11×10^4
⊙	x/b = 38.75	10.03×10^4
▽	x/b = 46.25	10.73×10^4
⊗	x/b = 53.75	11.15×10^4

$\left(\frac{U_M Y_M/2}{\nu}\right) =$

$\left(\frac{Y-Y_M}{Y_{M_2}-Y_M}\right)$

$\left[\frac{U-U_i}{U_M-U_i}\right] = \text{SECH}^2\left[0.88\left(\frac{Y-Y_M}{Y_{M_2}-Y_M}\right)\right]$

$\left[\frac{U-U_i}{U_M-U_i}\right] = e^{-0.693\left(\frac{Y-Y_M}{Y_{M_2}-Y_M}\right)^2}$

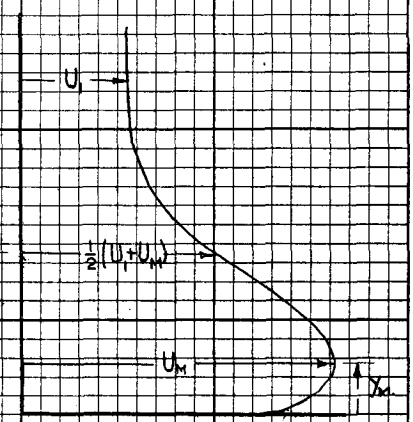

2.5
2.0
1.5
1.0
0.5
0.0
-0.5
0.2
0.4
0.6
0.8
1.0 $\left(\frac{U-U_i}{U_M-U_i}\right)$

FIG. 5.5

NON-DIMENSIONAL MEAN VELOCITY PROFILES EXCLUDING INNER BOUNDARY LAYER IN A TAILORED PRESSURE GRADIENT

$b = 0.20$ ins. $\left(\frac{U_j}{U_{is}}\right) = 6.0$

⊙	x/b = 32.5	4.12×10^4
⊡	x/b = 47.5	4.71×10^4
△	x/b = 62.5	5.22×10^4
⊙	x/b = 77.5	5.99×10^4
▽	x/b = 92.5	6.46×10^4
⊗	x/b = 107.5	6.79×10^4

$\left(\frac{U_M Y_{M/2}}{\nu}\right) =$

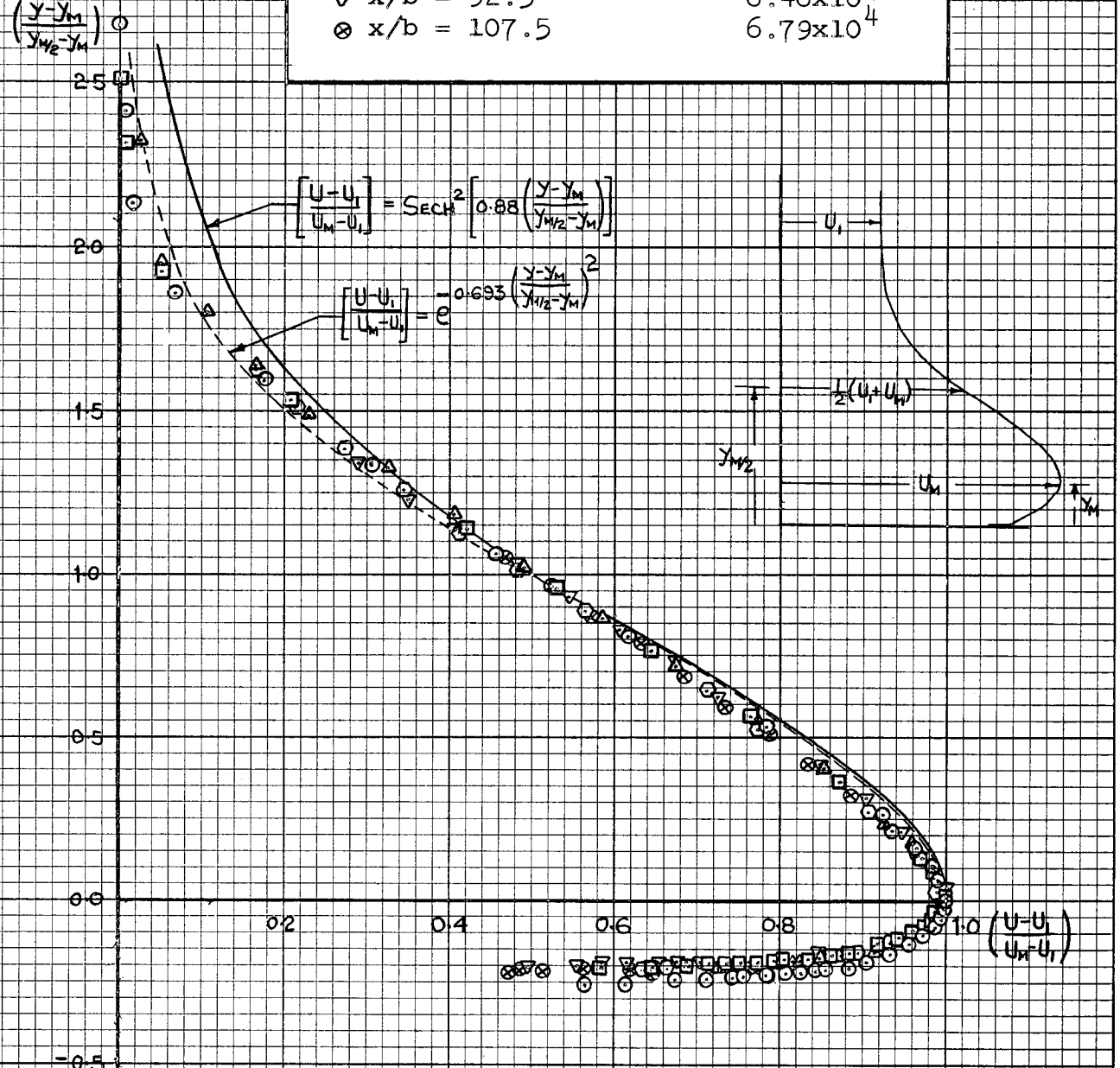

NON-DIMENSIONAL MEAN VELOCITY PROFILES EXCLUDING INNER BOUNDARY LAYER IN A TAILORED PRESSURE GRADIENT

FIG. 5.6

$b = 0.20$ ins. $\left(\frac{U_j}{U_{is}}\right) = 1.501$

⊙	x/b = 32.5	1.625×10^4
⊡	x/b = 47.5	1.85×10^4
△	x/b = 62.5	2.12×10^4
⊙	x/b = 77.5	2.35×10^4
▽	x/b = 92.5	2.52×10^4
⊗	x/b = 107.5	2.82×10^4

$\left(\frac{U_M Y_{M/2}}{\nu}\right) =$ as listed above

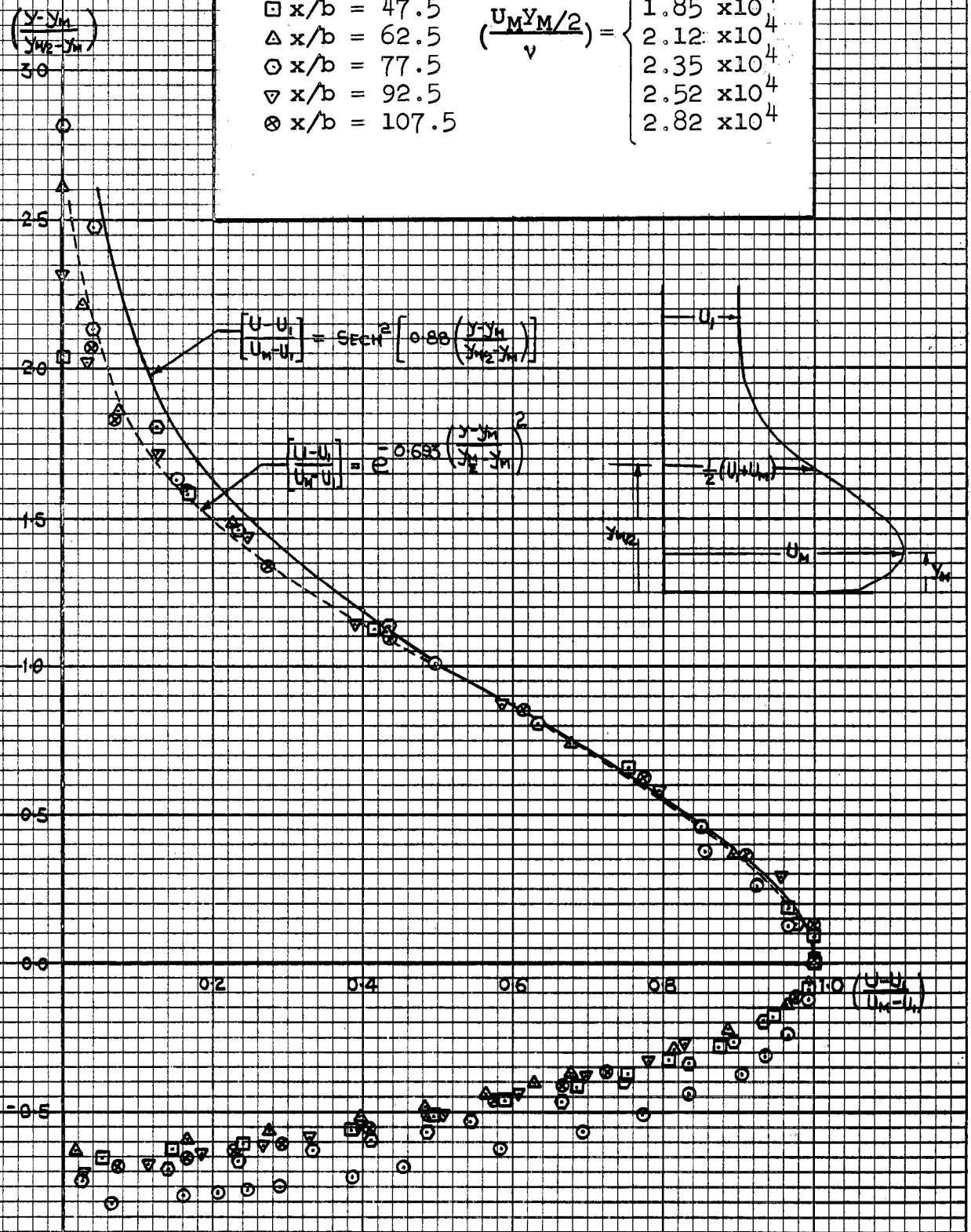

NON-DIMENSIONAL MEAN VELOCITY PROFILES INCLUDING INNER BOUNDARY LAYER IN A TAILORED PRESSURE GRADIENT.

FIG. 6.1

$b = 0.375$ in. $\left(\frac{U_j}{U_{is}}\right) = 4.05$

- • $x/b = 17.34$
- ⊡ $x/b = 25.34$
- × $x/b = 33.34$
- ⊙ $x/b = 41.34$
- △ $x/b = 49.34$

$\left(\frac{U_M Y_M/2}{\nu}\right) = \begin{cases} 7.02\times10^4 \\ 7.96\times10^4 \\ 8.93\times10^4 \\ 9.66\times10^4 \\ 10.00\times10^4 \end{cases}$

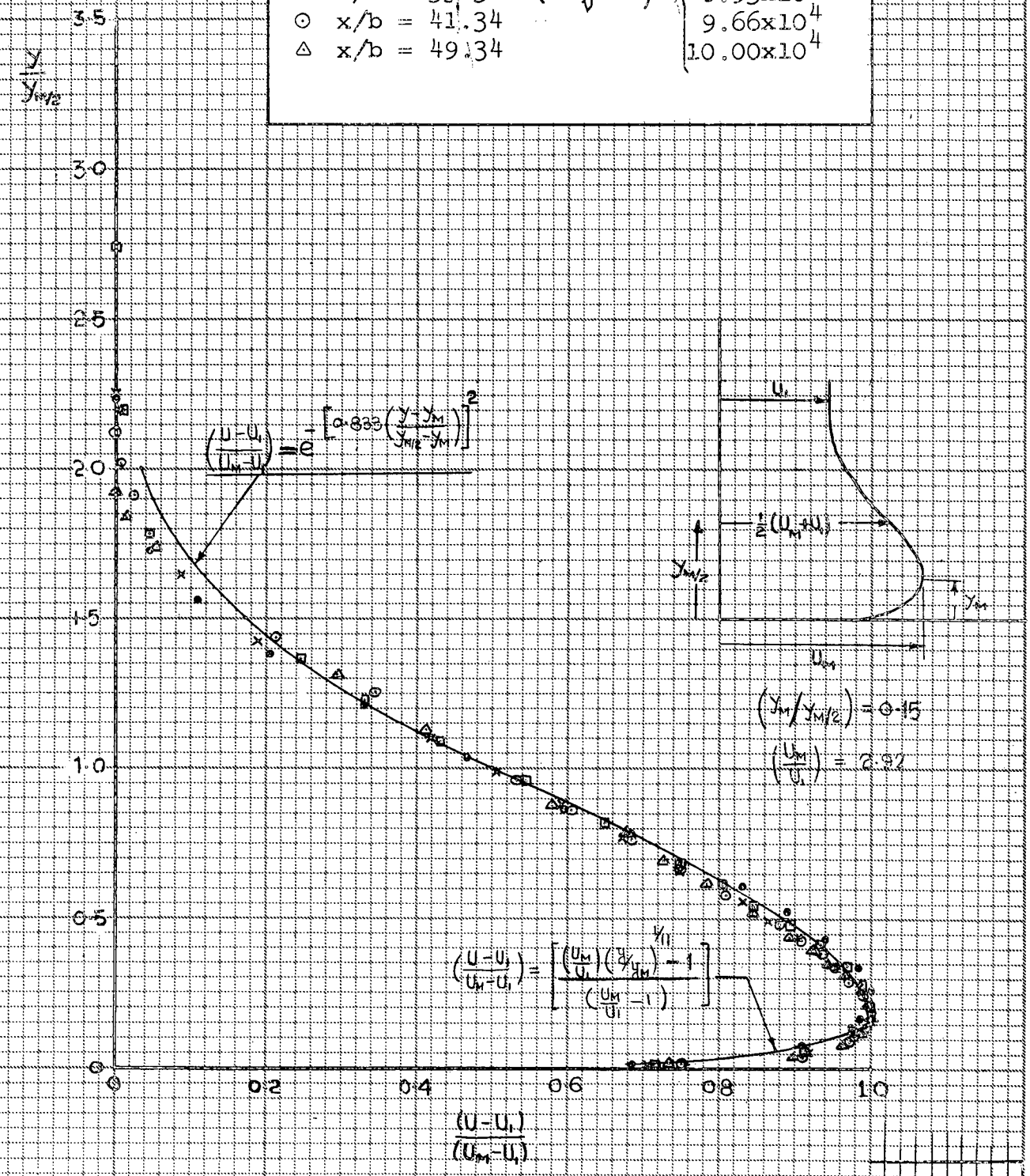

FIG. 6.2

NON-DIMENSIONAL MEAN VELOCITY PROFILES INCLUDING INNER BOUNDARY LAYER IN A TAILORED PRESSURE GRADIENT.

$b = 0.20\text{in.}$ $\left(\frac{U_j}{U_{is}}\right) = 3.0$

•	x/b = 32.5	3.48×10^4
⊡	x/b = 47.5	4.11×10^4
×	x/b = 62.5	4.38×10^4
⊙	x/b = 77.5	5.06×10^4
△	x/b = 92.5	5.66×10^4
◐	x/b = 107.5	5.95×10^4

$\left(\frac{U_M Y_{M/2}}{\nu}\right) =$

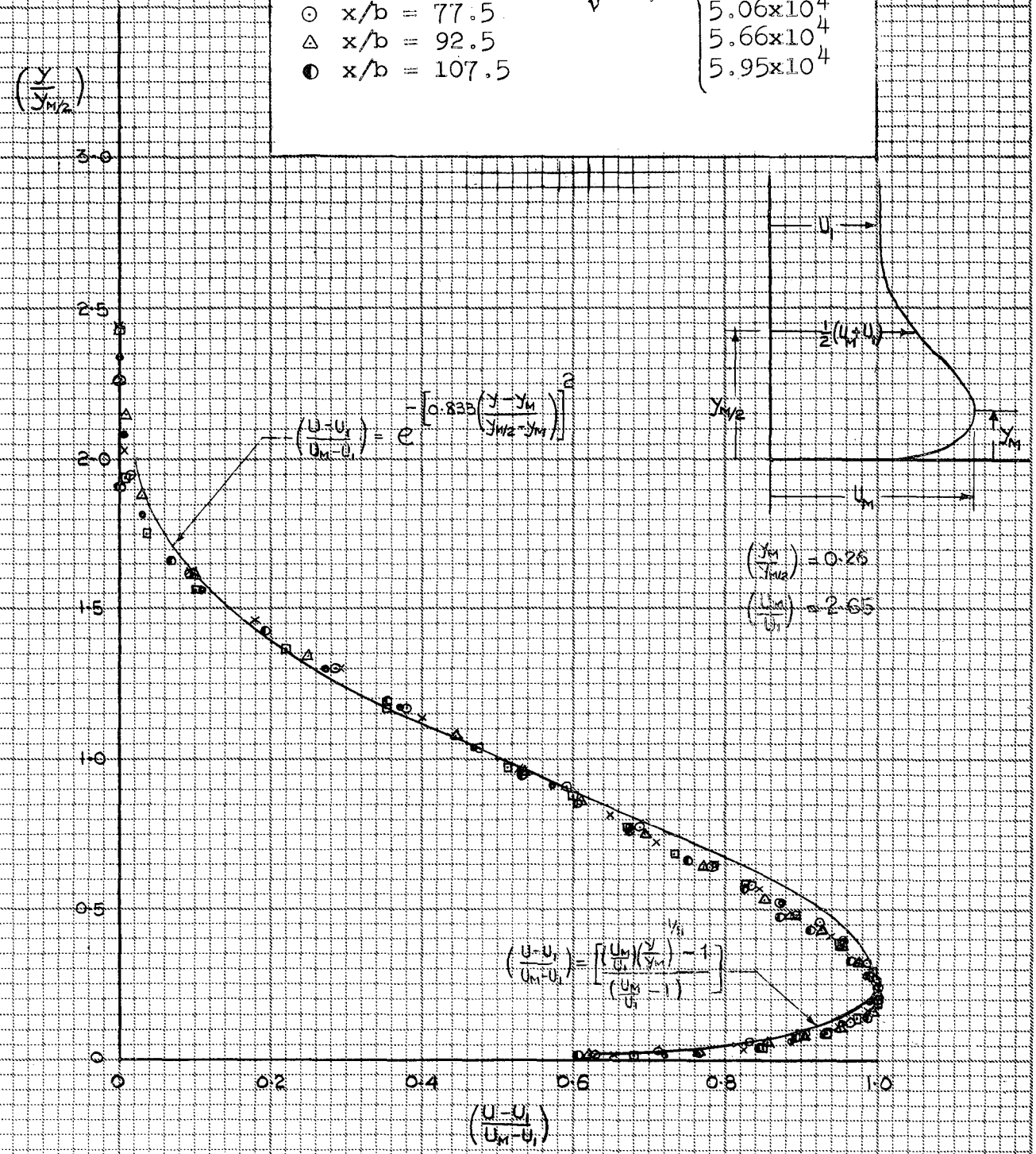

FIG. 6.3

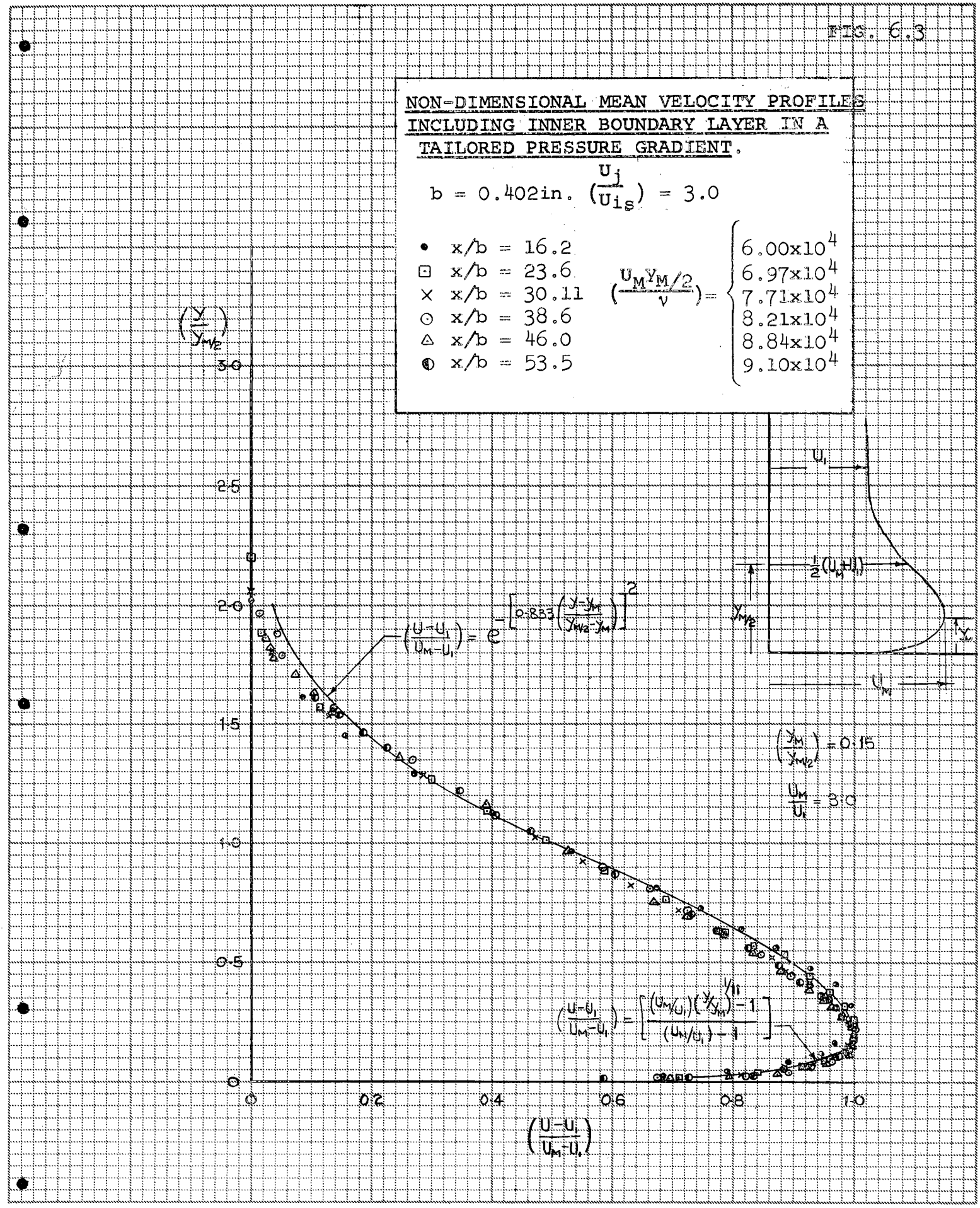
NON-DIMENSIONAL MEAN VELOCITY PROFILES INCLUDING INNER BOUNDARY LAYER IN A TAILORED PRESSURE GRADIENT.
b = 0.402in. (Uj/Uis) = 3.0
• x/b = 16.2
⊡ x/b = 23.6
× x/b = 30.11
⊙ x/b = 38.6
△ x/b = 46.0
◐ x/b = 53.5
(UM yM/2/ν) = 6.00x10^4, 6.97x10^4, 7.71x10^4, 8.21x10^4, 8.84x10^4, 9.10x10^4
(y/yM/2)
(U-Ui)/(UM-Ui) = e^-[0.883((y-yM)/(yM/2-yM))^2]
(U-Ui)/(UM-Ui) = [((UM/Ui)(y/yM)^1/11 - 1)/((UM/Ui) - 1)]
(yM/yM/2) = 0.15
UM/Ui = 3.0
Ui
1/2(UM+Ui)
UM
yM/2
yM
3.0
2.5
2.0
1.5
1.0
0.5
0
0.2
0.4
0.6
0.8
1.0
(U-Ui)/(UM-Ui)

NON-DIMENSIONAL MEAN VELOCITY PROFILES INCLUDING INNER BOUNDARY LAYER IN A TAILORED PRESSURE GRADIENT

FIG. 6.4

$b = 0.40\text{ins.}$ $\left(\frac{U_j}{U_{is}}\right) = 6.01$

⊙	x/b = 16.25	7.13×10^4
⊡	x/b = 23.75	8.26×10^4
△	x/b = 31.25	9.11×10^4
⊙	x/b = 38.75	10.03×10^4
▽	x/b = 46.25	10.73×10^4
⊗	x/b = 53.75	11.15×10^4

$\left(\frac{U_M Y_{M/2}}{\nu}\right) =$

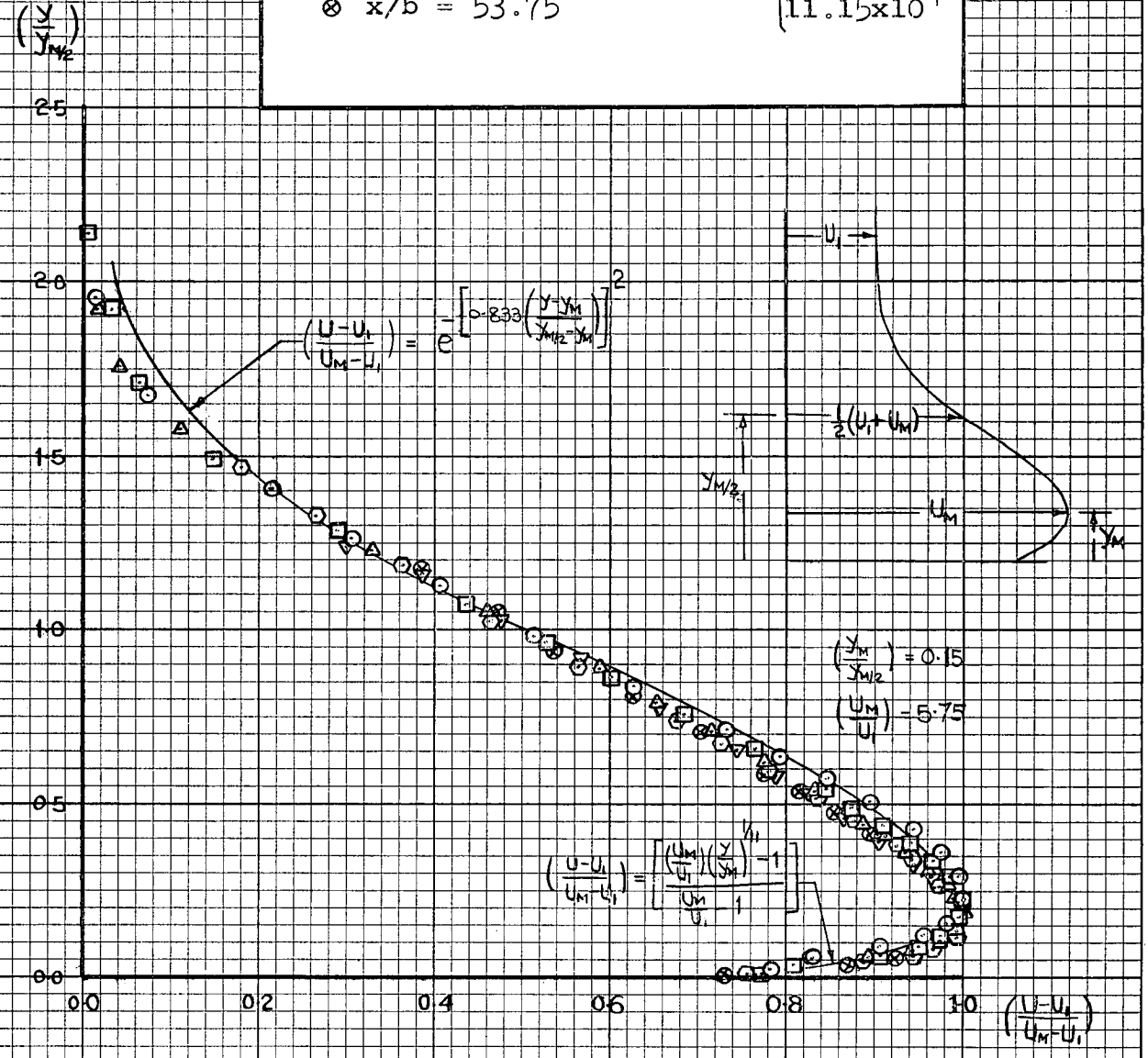

NON-DIMENSIONAL MEAN VELOCITY PROFILES INCLUDING INNER BOUNDARY LAYER IN A TAILORED PRESSURE GRADIENT

FIG. 6.5

$b = 0.20$ ins. $\left(\frac{U_j}{U_{is}}\right) = 6.00$

⊙ x/b = 32.5	$\left(\frac{U_M y_{M/2}}{\nu}\right) =$	4.12×10^4
⊡ x/b = 47.5		4.71×10^4
△ x/b = 62.5		5.22×10^4
⊙ x/b = 77.5		5.99×10^4
▽ x/b = 92.5		6.46×10^4
⊗ x/b = 107.5		6.79×10^4

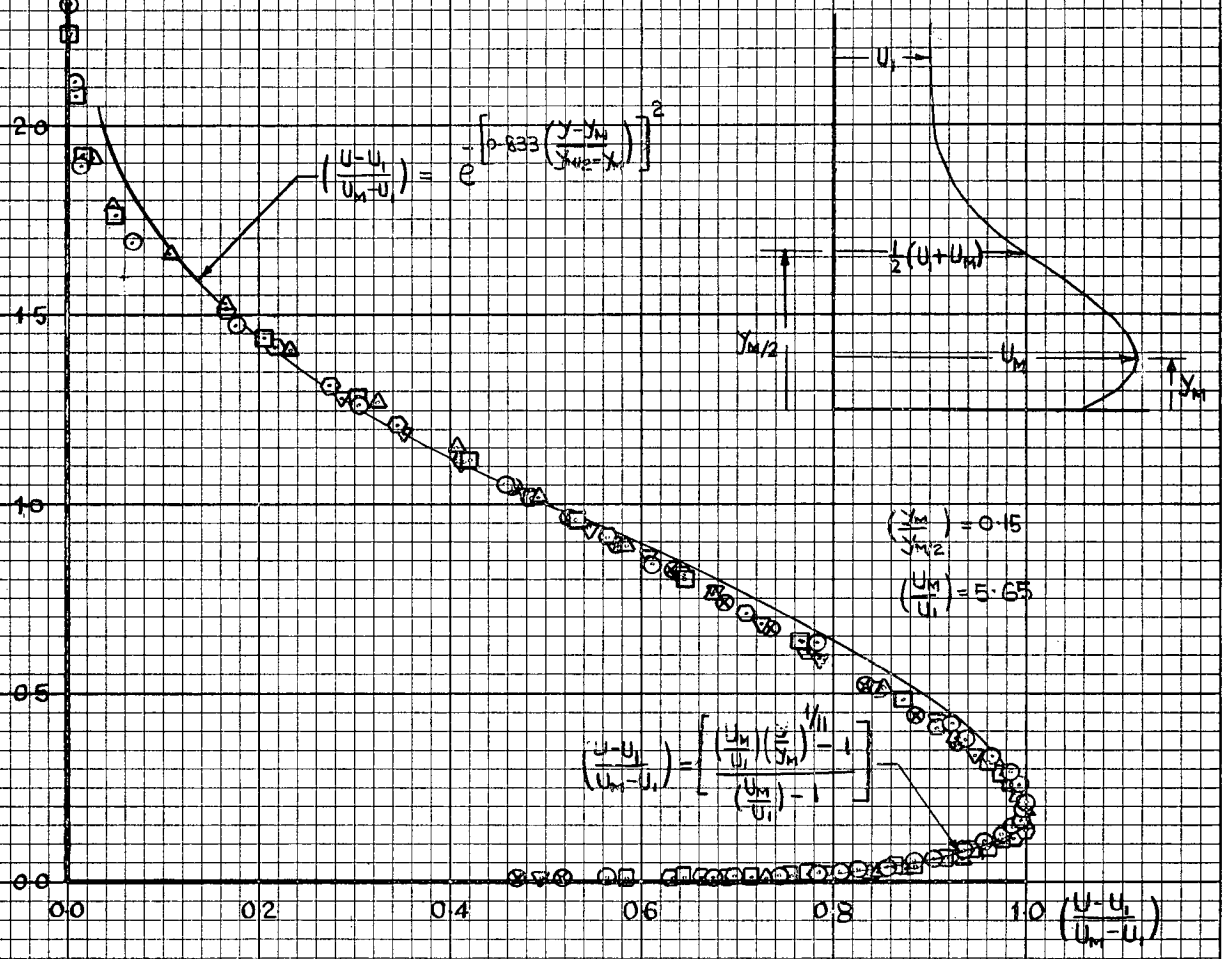

FIG. 6.6

NON-DIMENSIONAL MEAN VELOCITY PROFILES INCLUDING INNER BOUNDARY LAYER IN A TAILORED PRESSURE GRADIENT

$b = 0.201\text{ins.}$ $\left(\frac{U_j}{U_{is}}\right) = 1.501$

		$\left(\frac{U_M Y_{M/2}}{\nu}\right) =$
⊙	x/b = 32.5	1.625×10^4
□	x/b = 47.5	1.85×10^4
△	x/b = 62.5	2.12×10^4
⊙	x/b = 77.5	2.35×10^4
▽	x/b = 92.5	2.52×10^4
⊙	x/b = 107.5	2.82×10^4

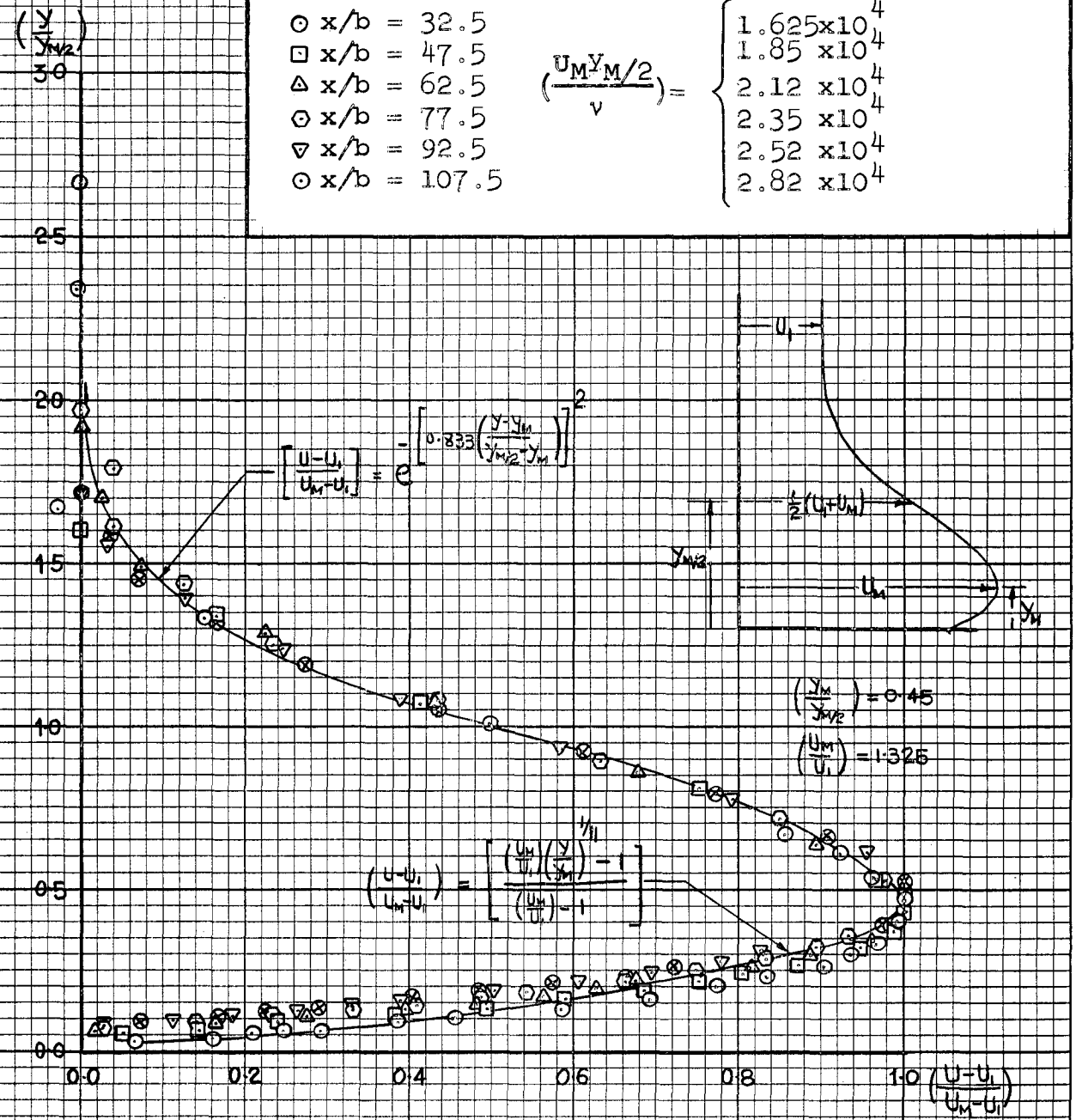

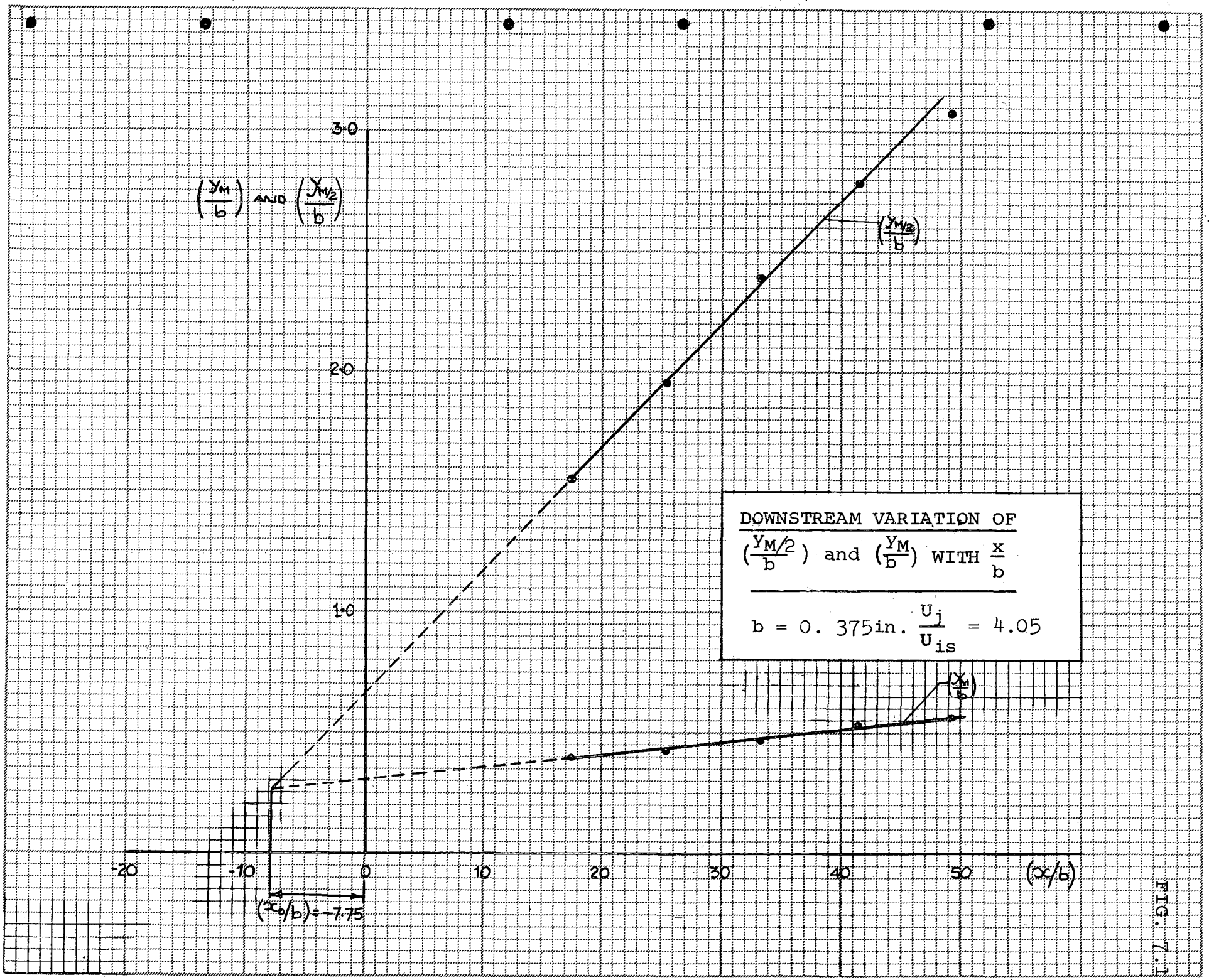
$\left(\frac{y_M}{b}\right)$ AND $\left(\frac{y_{M/2}}{b}\right)$
3·0
2·0
1·0
$\left(\frac{y_{M/2}}{b}\right)$
$\left(\frac{y_M}{b}\right)$
-20
-10
0
10
20
30
40
50
(x/b)
$(x_0/b) = -7.75$
DOWNSTREAM VARIATION OF
$\left(\frac{y_{M/2}}{b}\right)$ and $\left(\frac{y_M}{b}\right)$ WITH $\frac{x}{b}$
b = 0.375in. $\frac{U_j}{U_{is}}$ = 4.05

Fig. 7.1

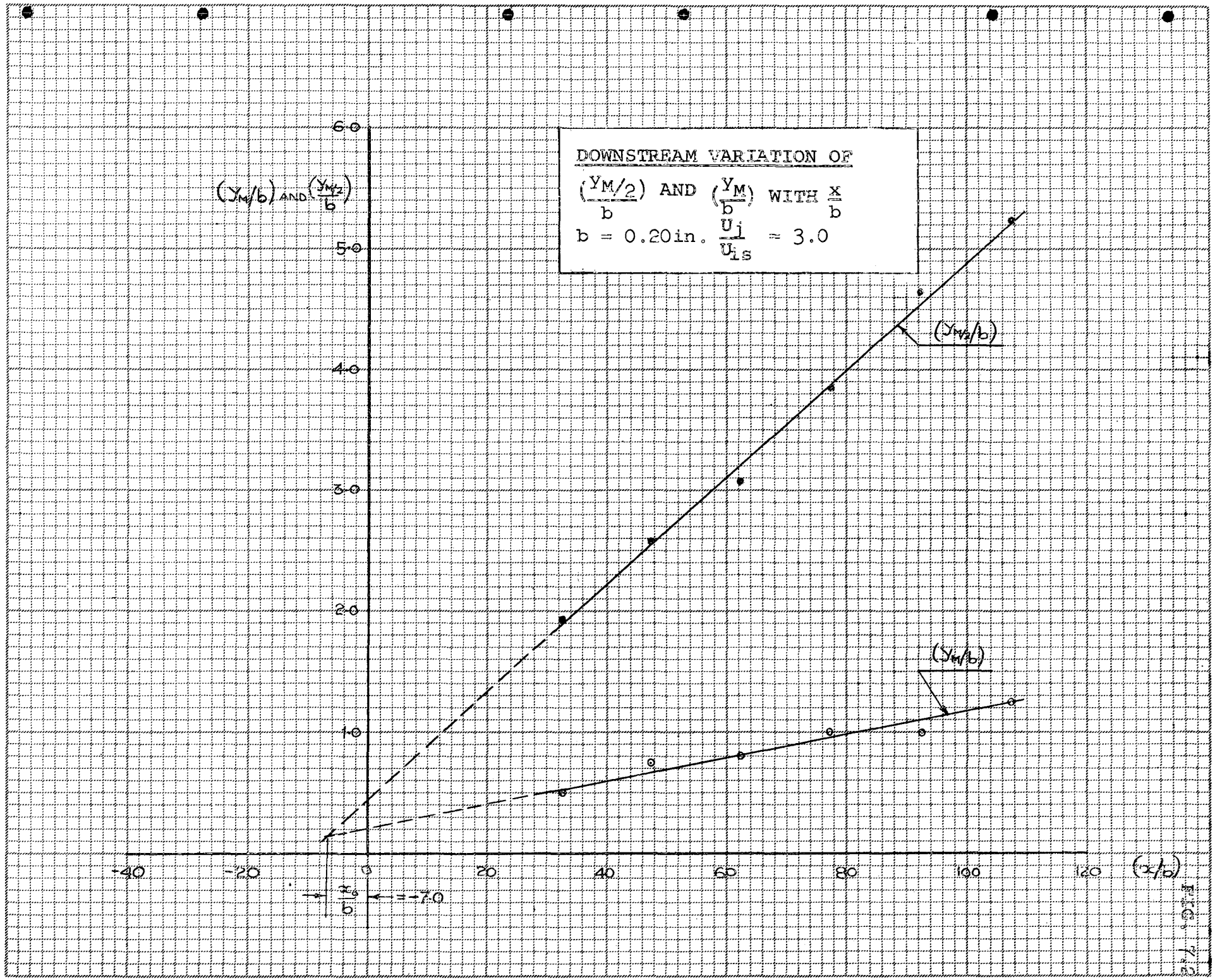
DOWNSTREAM VARIATION OF
$(\frac{y_{M/2}}{b})$ AND $(\frac{y_M}{b})$ WITH $\frac{x}{b}$
b = 0.20in. $\frac{U_j}{U_{is}} \approx 3.0$
(y_M/b) AND $(\frac{y_{M_2}}{b})$
6.0
5.0
4.0
3.0
2.0
1.0
(y_{M_2}/b)
(y_M/b)
-40
-20
0
20
40
60
80
100
120
(x/b)
$\frac{x_o}{b} = -7.0$

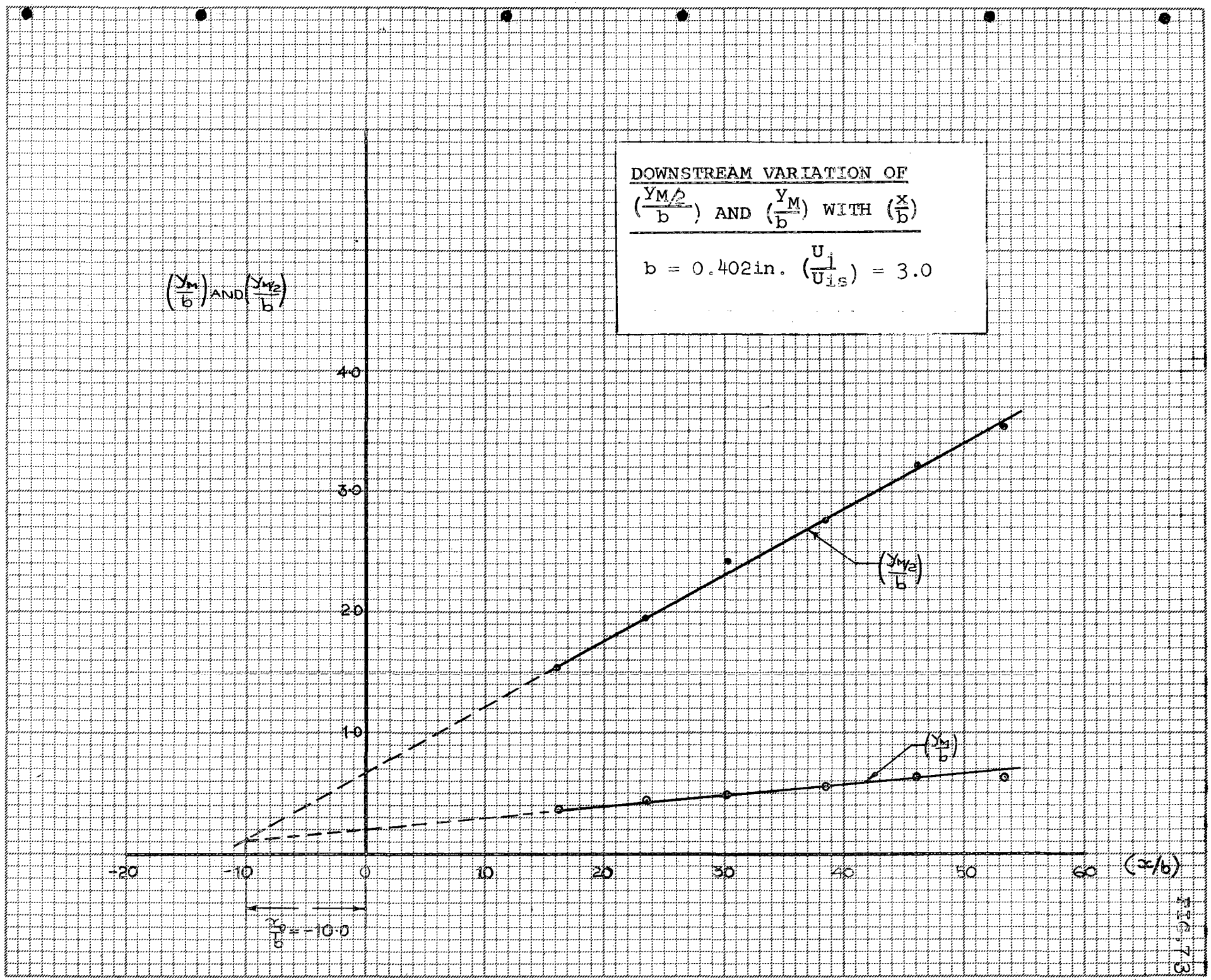
DOWNSTREAM VARIATION OF $(\frac{y_{M/2}}{b})$ AND $(\frac{y_M}{b})$ WITH $(\frac{x}{b})$
b = 0.402in. $(\frac{U_j}{U_{is}})$ = 3.0
$(\frac{y_M}{b})$ AND $(\frac{y_{M/2}}{b})$
4·0
3·0
2·0
1·0
$(\frac{y_{M/2}}{b})$
$(\frac{y_M}{b})$
-20
-10
0
10
20
30
40
50
60
(x/b)
$\frac{x_0}{b}$ = -10·0

FIG. 7.4

DOWNSTREAM VARIATION OF $(\frac{Y_{M/2}}{b})$ AND $(\frac{Y_M}{b})$ WITH $(\frac{x}{b})$

b = 0.40ins. $(\frac{U_j}{U_{is}})$ = 6.01

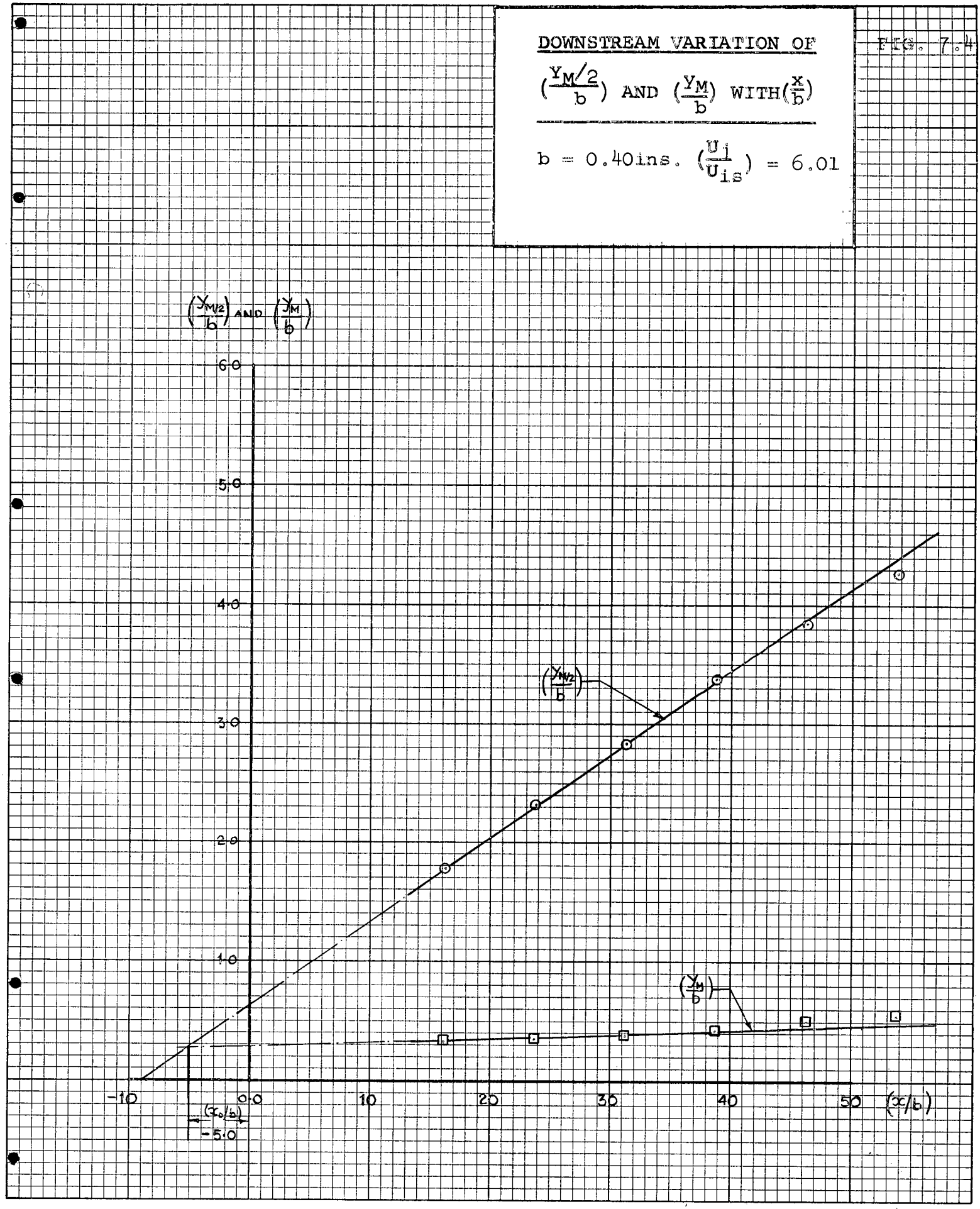

FIG. 7.5

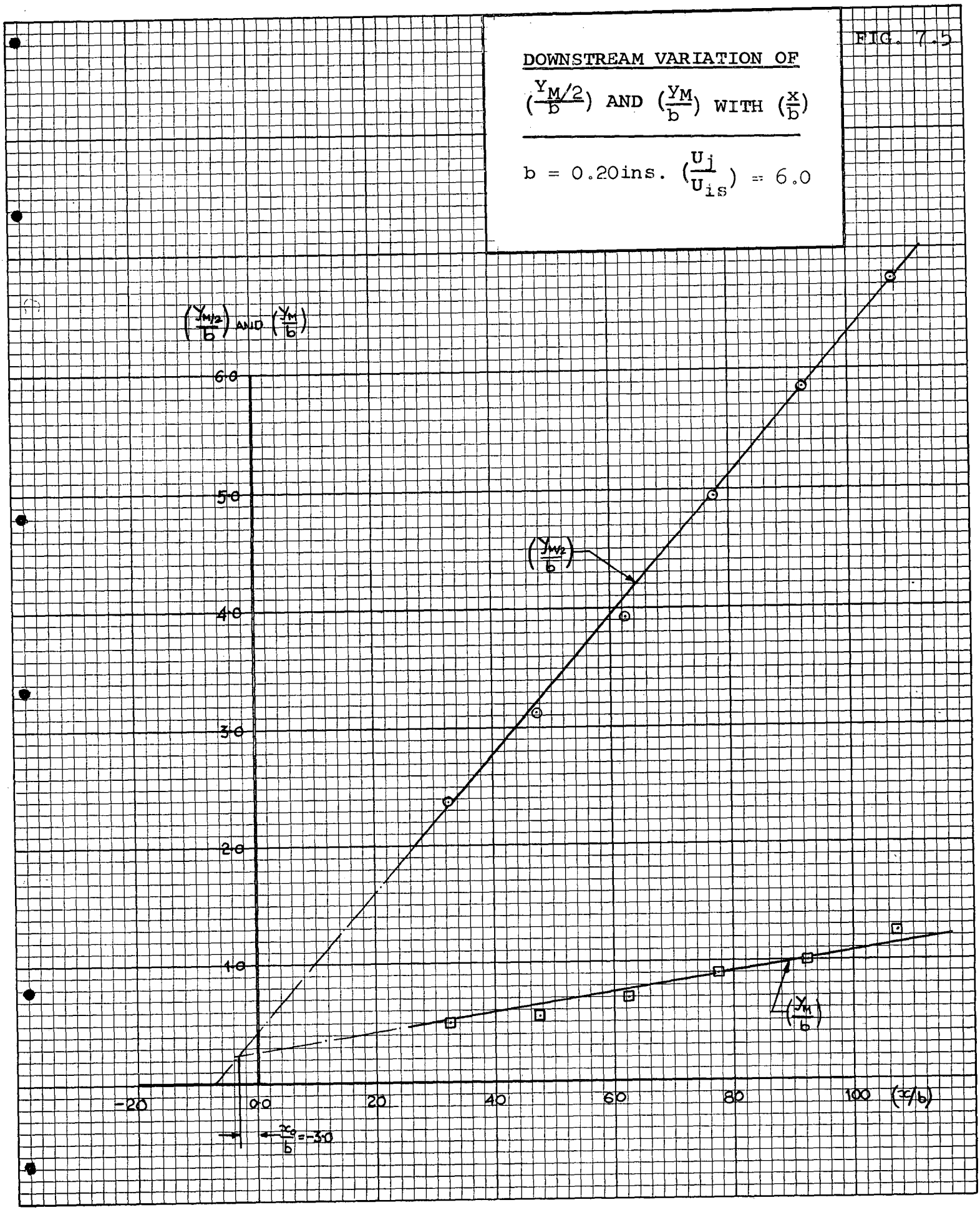
DOWNSTREAM VARIATION OF
$(\frac{Y_{M/2}}{b})$ AND $(\frac{Y_M}{b})$ WITH $(\frac{x}{b})$
b = 0.20ins. $(\frac{U_j}{U_{is}})$ = 6.0
$(\frac{Y_{M/2}}{b})$ AND $(\frac{Y_M}{b})$
6.0
5.0
4.0
3.0
2.0
1.0
$(\frac{Y_{M/2}}{b})$
$(\frac{Y_M}{b})$
-20
0.0
20
40
60
80
100
$(\frac{x}{b})$
$\frac{x_o}{b}$=-3.0

FIG. 7.6

DOWNSTREAM VARIATION OF $(\frac{Y_{M/2}}{b})$ AND $(\frac{Y_M}{b})$ WITH $(\frac{x}{b})$

$b = 0.20$ ins. $(\frac{U_i}{U_{is}}) = 1.501$

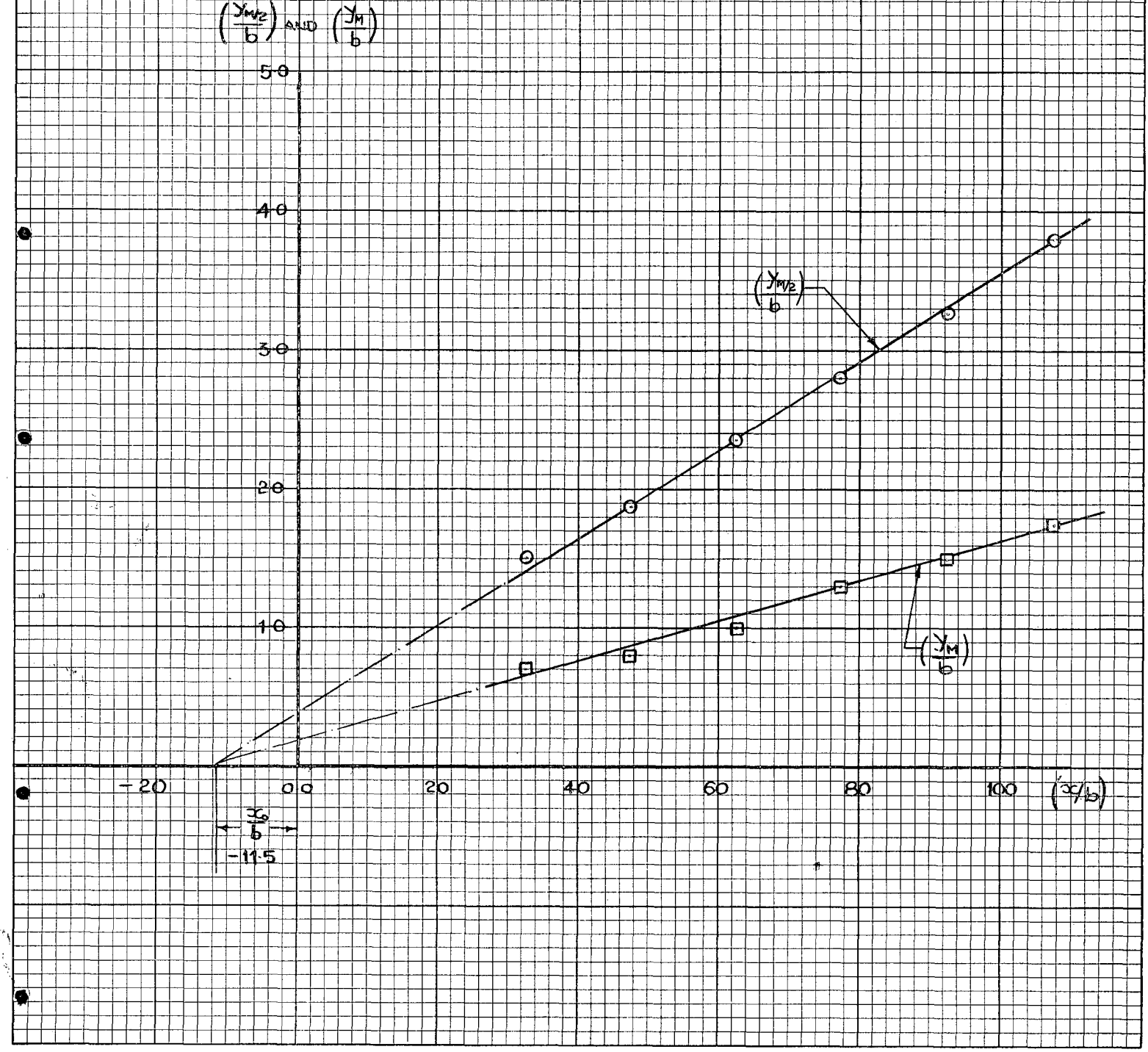

FIG. 7a

VARIATION OF $\left(\frac{dy_{M/2}}{dx}\right)$ AND $\left(\frac{dy_M}{dx}\right)$ WITH $\left(\frac{U_1}{U_M}\right)$

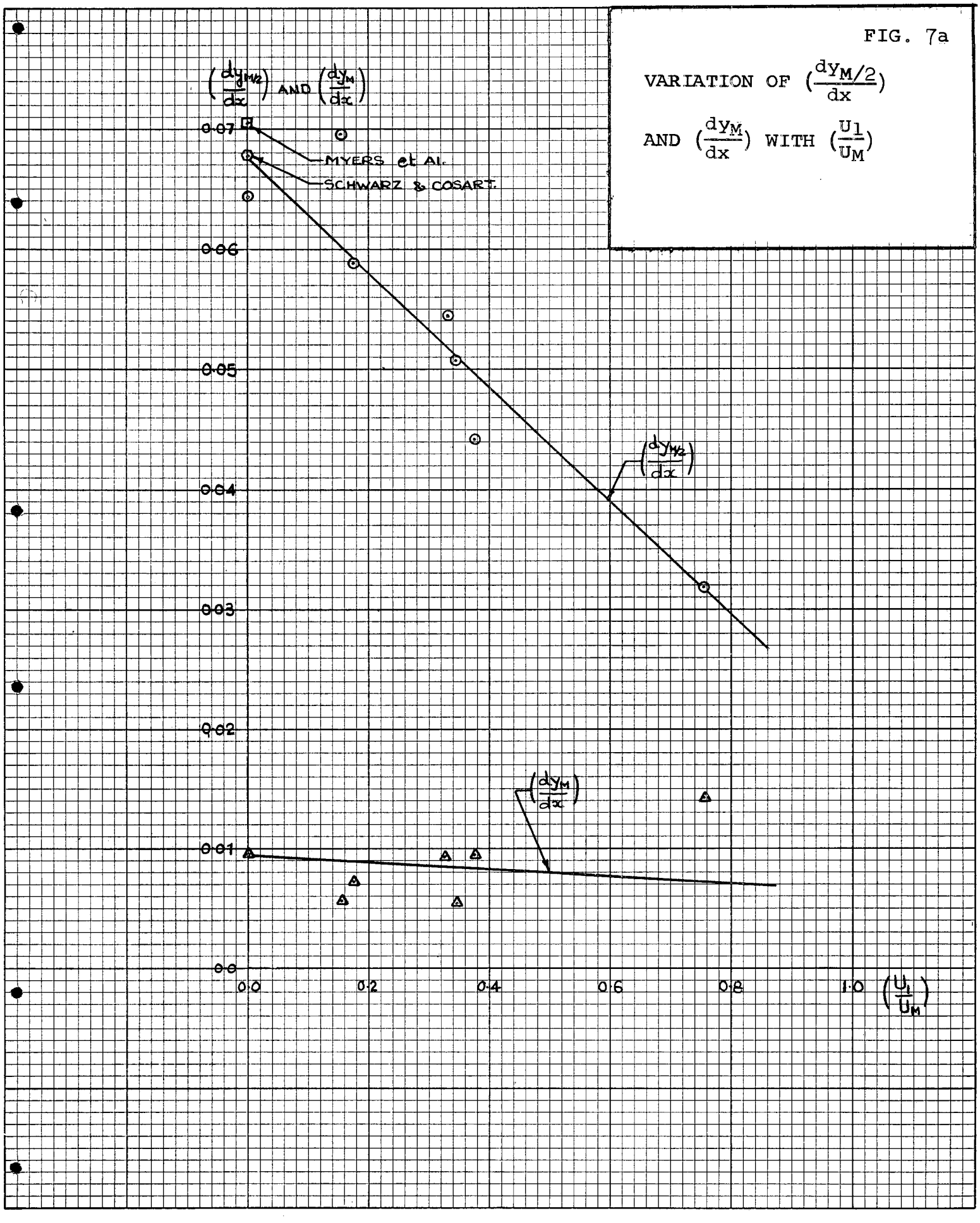

FIG. 31

VARIATION OF $\left(\frac{U_M}{U_j}\right)$ WITH $\left(\frac{x}{b}\right)$

$b = 0.375$ ins. $\left(\frac{U_j}{U_{is}}\right) = 4.45$

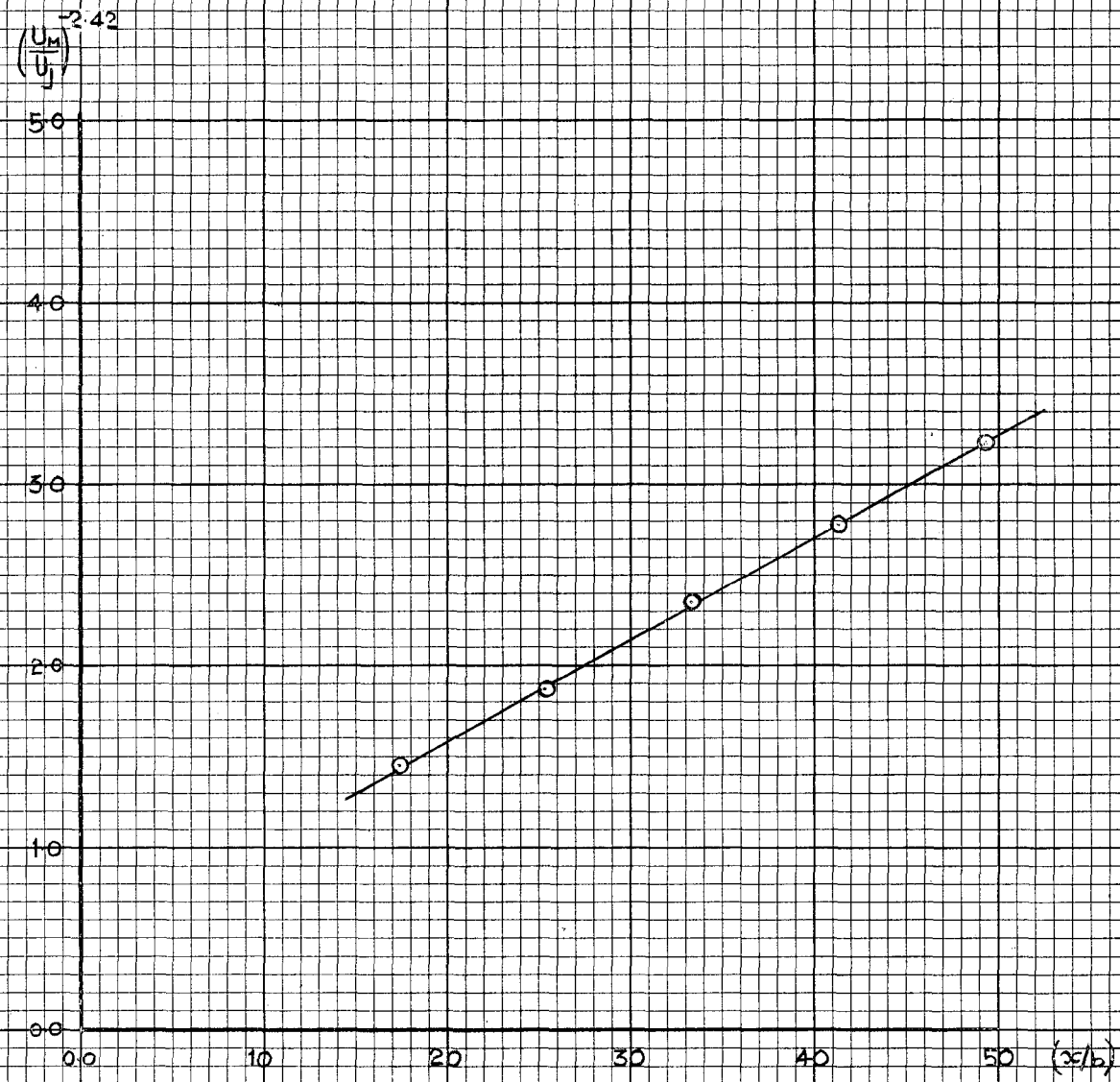

FIG. 8.2

VARIATION OF $\left(\frac{U_M}{U_j}\right)$

WITH $\left(\frac{x}{b}\right)$

b = 0.20ins. $\left(\frac{U_j}{U_{is}}\right)$ = 3.0

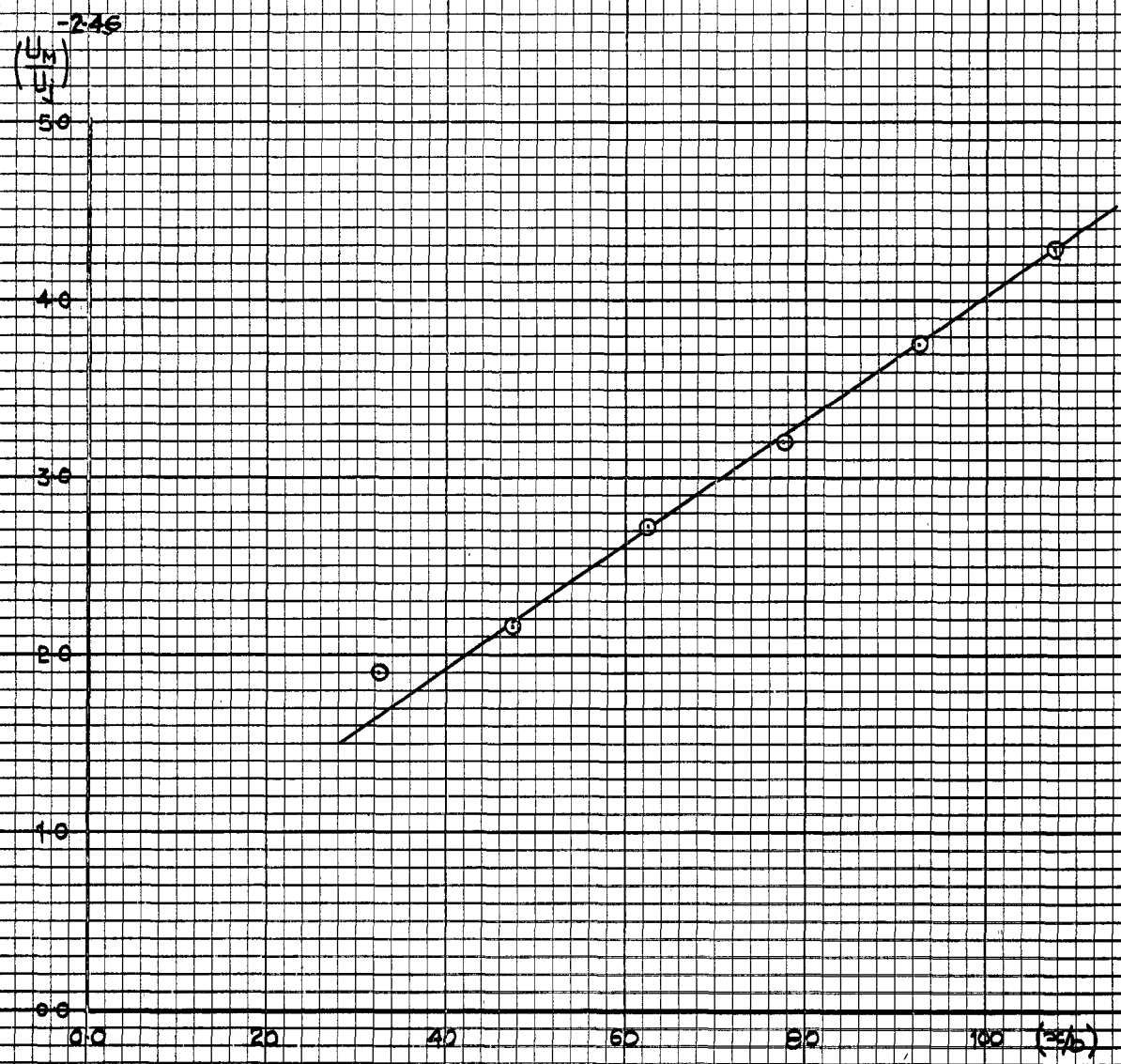

FIG. 8.3

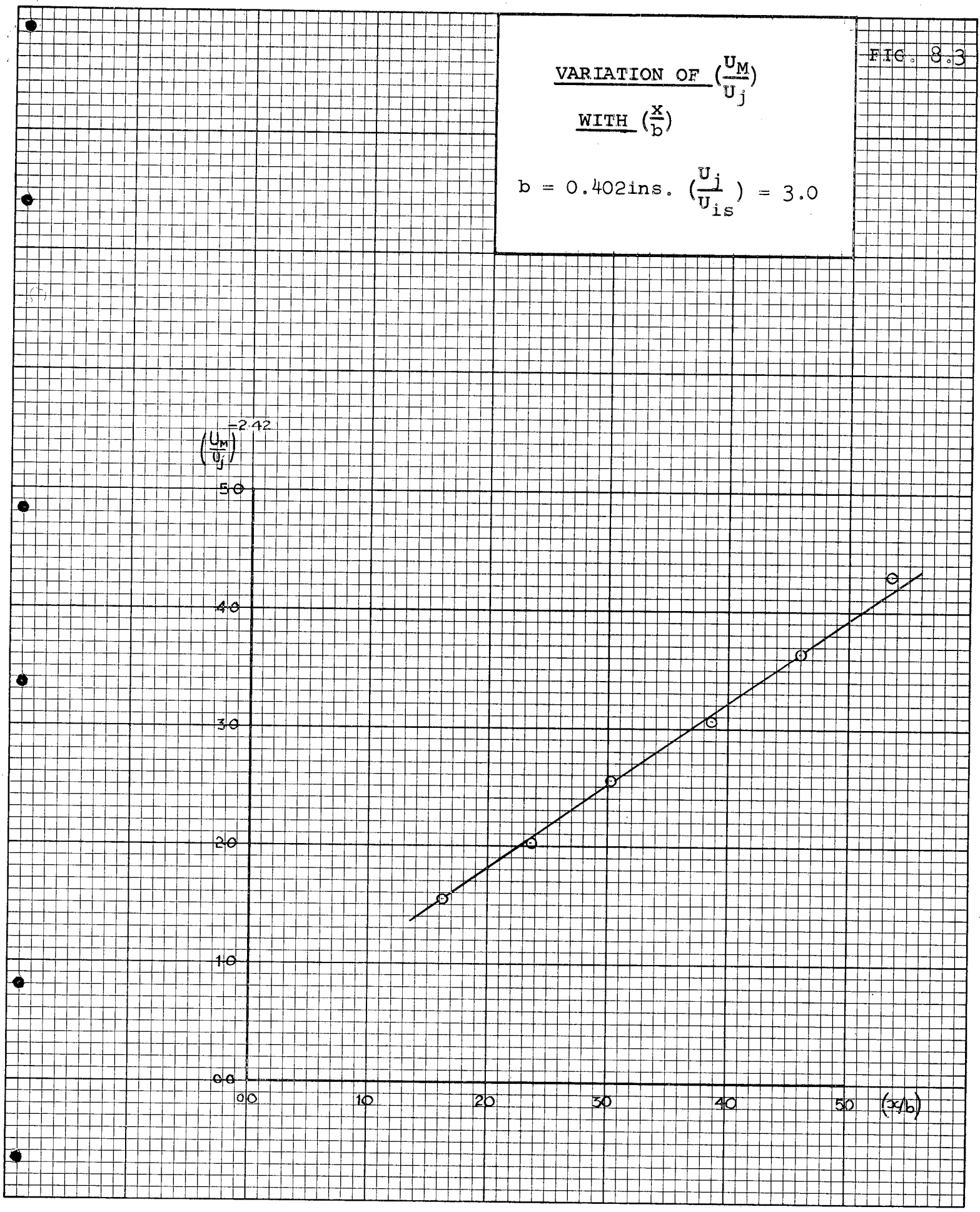
VARIATION OF $(\frac{U_M}{U_j})$
WITH $(\frac{x}{b})$
b = 0.402ins. $(\frac{U_j}{U_{is}})$ = 3.0
$(\frac{U_M}{U_j})$
-2.42
5·0
4·0
3·0
2·0
1·0
0·0
0·0
1·0
2·0
3·0
4·0
5·0
(x/b)

FIG. 8.1

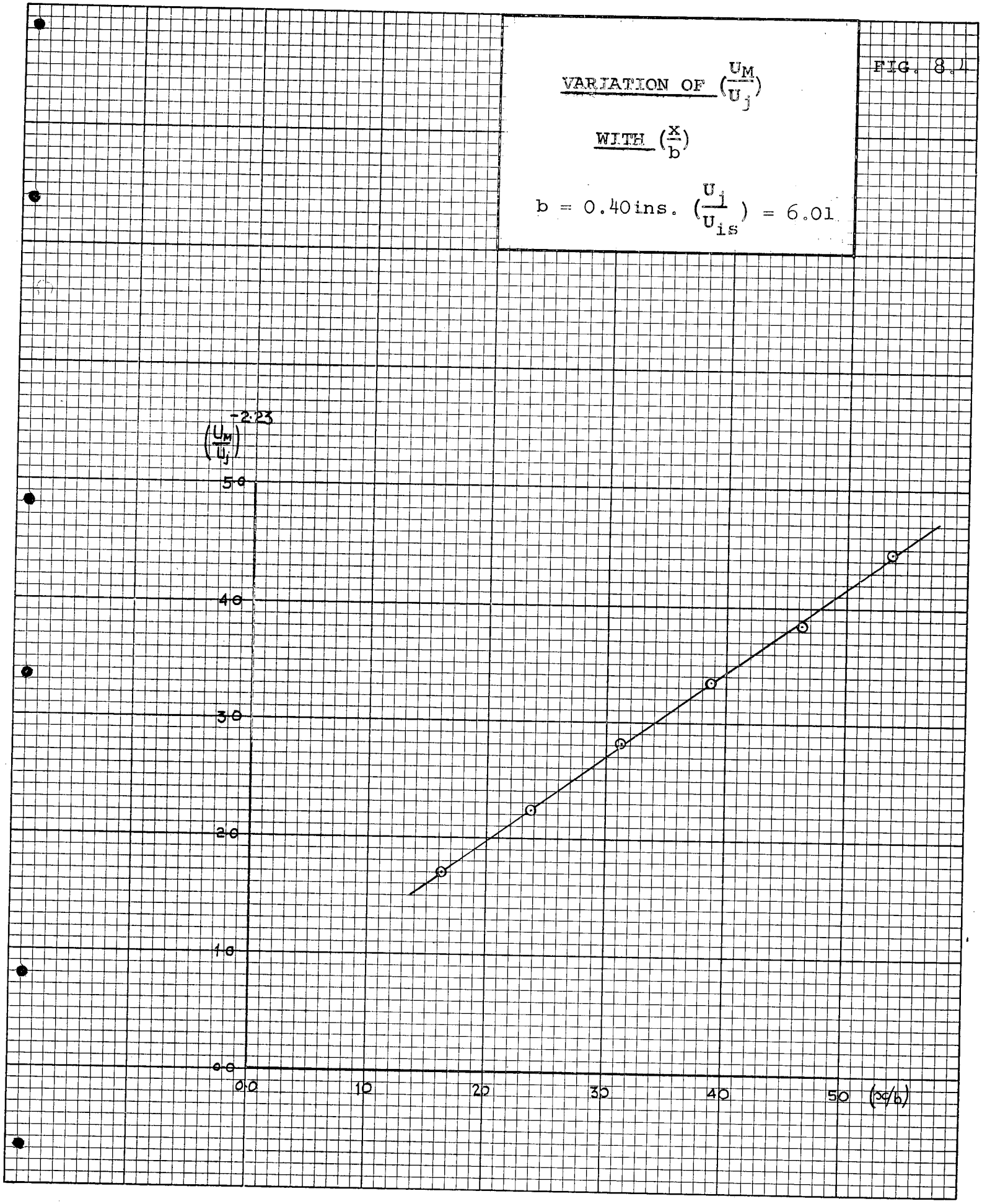
VARIATION OF $(\frac{U_M}{U_j})$
WITH $(\frac{x}{b})$
b = 0.40ins. $(\frac{U_j}{U_{is}})$ = 6.01
$(\frac{U_M}{U_j})^{-2.23}$
5·0
4·0
3·0
2·0
1·0
0·0
0·0
10
20
30
40
50
(x/b)

FIG. 8.5

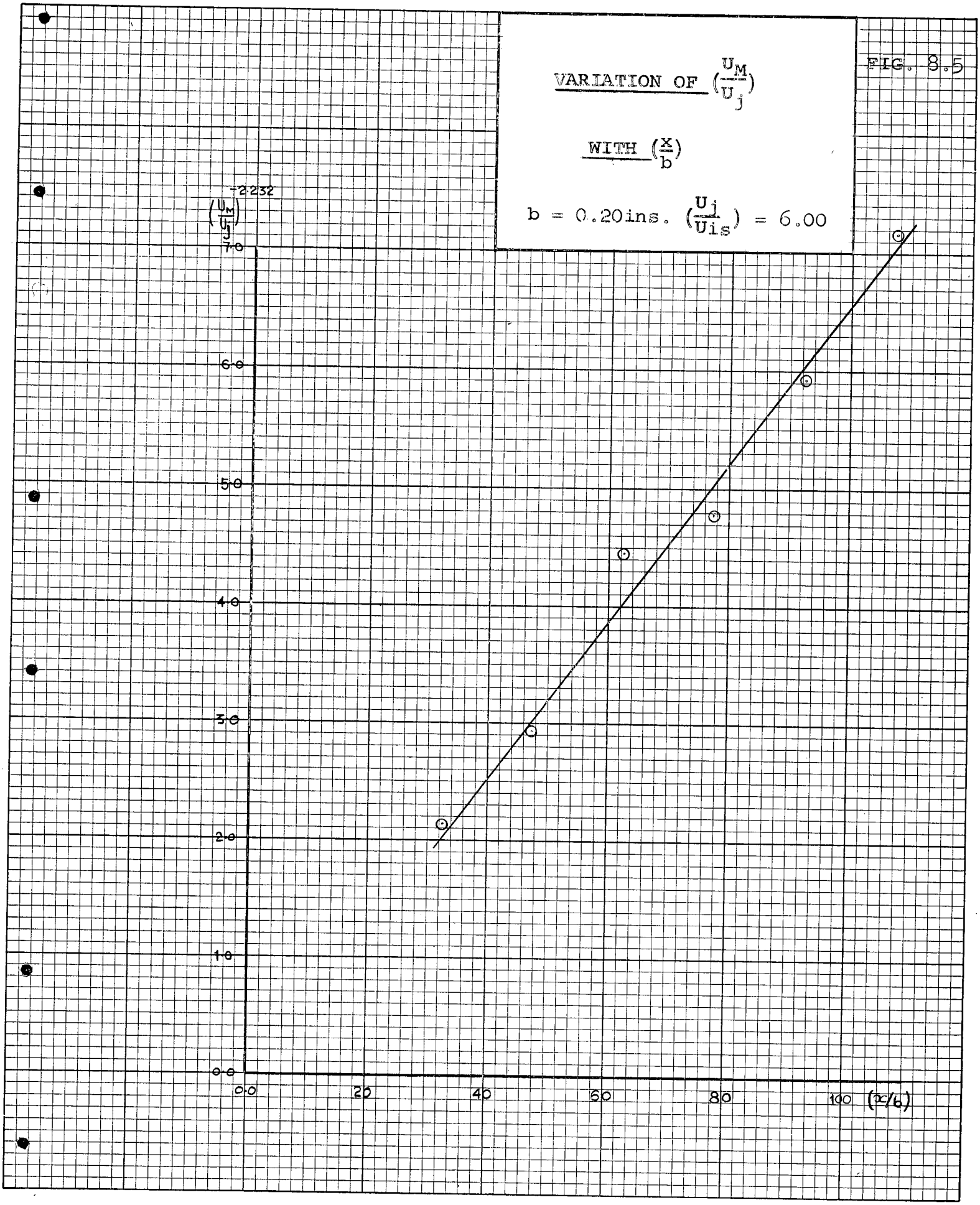
VARIATION OF $(\frac{U_M}{U_j})$
WITH $(\frac{x}{b})$
b = 0.20ins. $(\frac{U_j}{U_{is}})$ = 6.00
$(\frac{U_M}{U_j})$
7·0
6·0
5·0
4·0
3·0
2·0
1·0
0·0
0·0
20
40
60
80
100
(x/b)

FIG. 8.6

VARIATION OF $\left(\frac{U_M}{U_j}\right)$

WITH $\left(\frac{x}{b}\right)$

b = 0.20ins. $\left(\frac{U_j}{U_{is}}\right)$ = 1.501

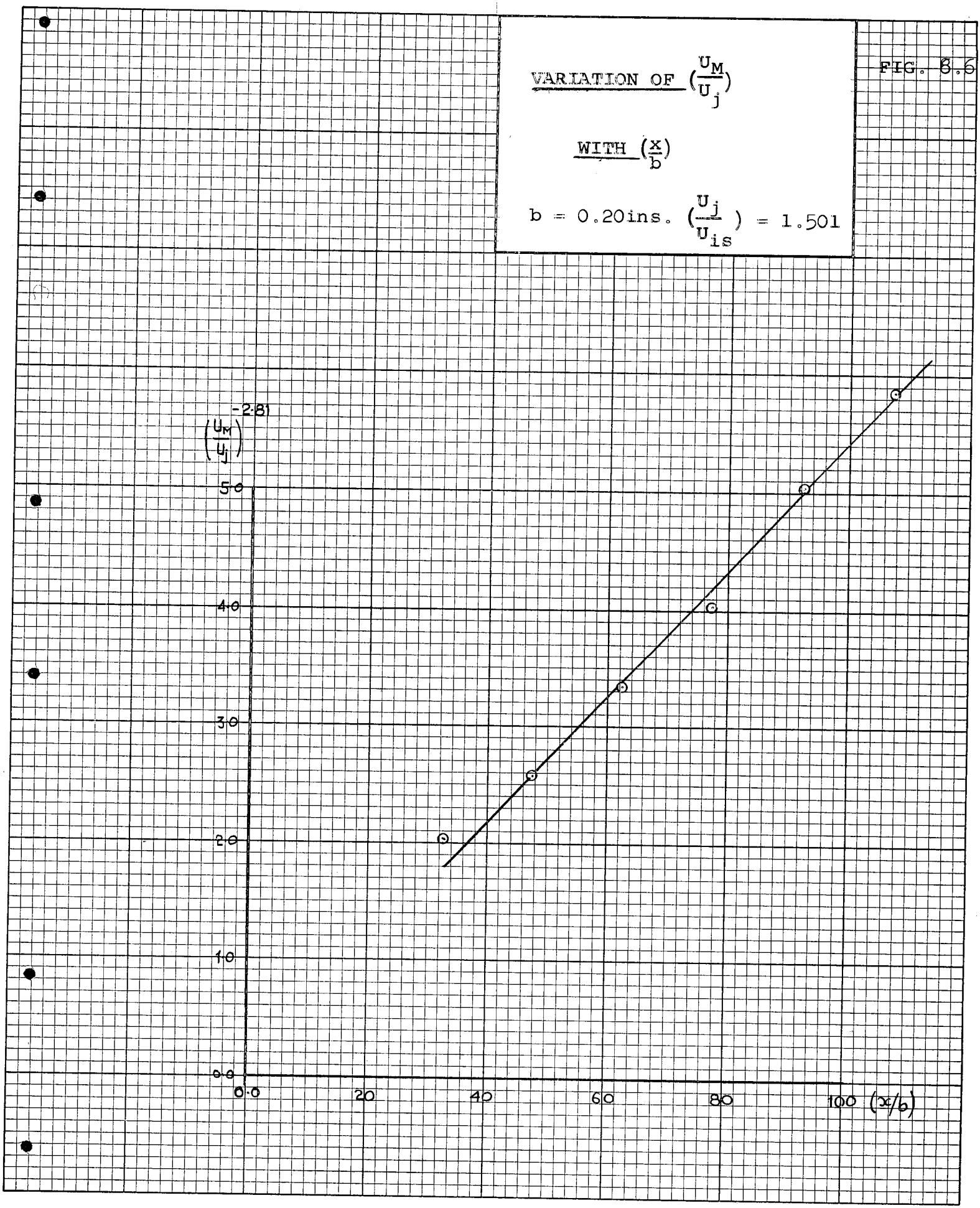

FIG. 9.2

MEAN VELOCITY PROFILES - INNER LAW PLOT
WALL JET IN TAILORED PRESSURE GRADIENT

$b = 0.20$ ins. $\left(\frac{U_j}{U_{is}}\right) = 3.00$

○ $x/b = 32.5$
□ $x/b = 62.5$
△ $x/b = 92.5$

$\frac{U}{U_\tau} = 3.81 \log\left(\frac{yU_\tau}{\nu}\right) + 10.2$

$\frac{U}{U_\tau} = 5.43 \log\left(\frac{yU_\tau}{\nu}\right) + 2.01 + \left(\frac{y}{\delta}\right)$

$\frac{U}{U_\tau} = \frac{yU_\tau}{\nu}$

$\left(\frac{U}{U_\tau}\right)$

$\left(\frac{yU_\tau}{\nu}\right)$

FIG. 9.5

MEAN VELOCITY PROFILES -
INNER LAW PLOT
WALL JET IN TAILORED PRES-
SURE GRADIENT

$b = 0.201\text{ms}$, $\left(\frac{U_1}{U_{1s}}\right) = 6.00$

- ⊙ $x/b = 32.5$
- ⊡ $x/b = 62.5$
- △ $x/b = 92.5$

$\frac{U}{U_\tau} = 4.81 \log\left(\frac{yU_\tau}{\nu}\right) + 6.9$

$\frac{U}{U_\tau} = 4.2 \log\left(\frac{yU_\tau}{\nu}\right) + 7.6$

$\frac{U}{U_\tau} = 3.81 \log\left(\frac{yU_\tau}{\nu}\right) + 9.6$

$\left(\frac{U}{U_\tau}\right)$

$\left(\frac{yU_\tau}{\nu}\right)$

FIG. 9.6

MEAN VELOCITY PROFILES - INNER LAW PLOT
WALL JET IN TAILORED PRESSURE GRADIENT

$b = 0.20$ ins. $\left(\frac{U_j}{U_{is}}\right) = 1.501$

⊙ x/b = 32.5
⊡ x/b = 62.5
△ x/b = 92.5

$\frac{U}{U_\tau} = 5.6 \log\left(\frac{yU_\tau}{\nu}\right) + 7.1$

$\frac{U}{U_\tau} = 5.5 \log\left(\frac{yU_\tau}{\nu}\right) + 6.2$

$\frac{U}{U_\tau} = 4.85 \log\left(\frac{yU_\tau}{\nu}\right) + 6.45$

$\frac{U}{U_\tau}$

$\frac{yU_\tau}{\nu}$

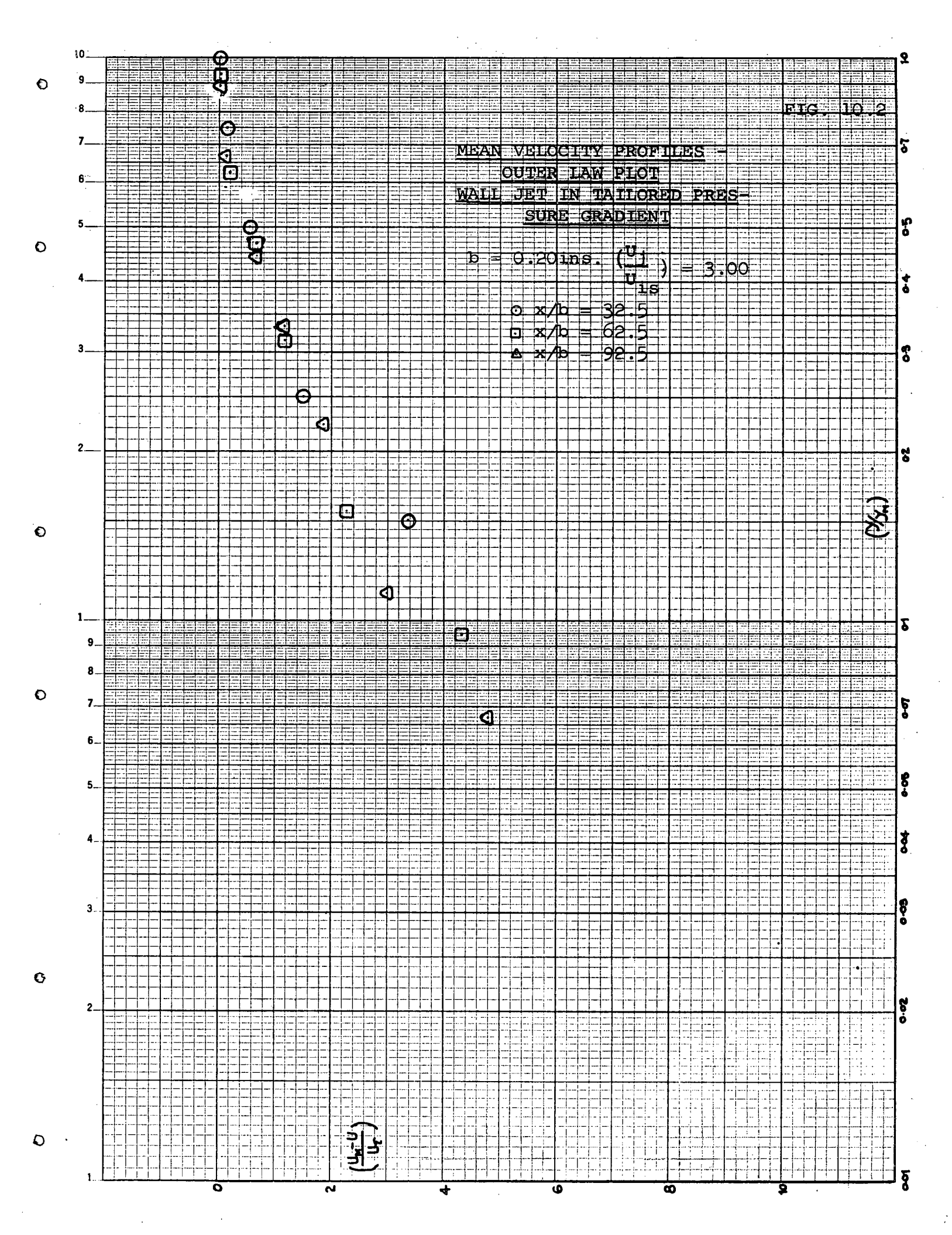
FIG. 10.2
MEAN VELOCITY PROFILES -
OUTER LAW PLOT
WALL JET IN TAILORED PRES-
SURE GRADIENT
b = 0.20 ins. $(\frac{U_1}{U_{1s}}) = 3.00$
○ x/b = 32.5
□ x/b = 62.5
△ x/b = 92.5
$\frac{U_{max}-U}{U_\tau}$
$\frac{y}{y_{0.5}}$

FIG. 10.5

MEAN VELOCITY PROFILES - OUTER LAW PLOT
WALL JET IN TAILORED PRESSURE GRADIENT

$b = 0.20$ ins. $\left(\frac{U_j}{U_{ls}}\right) = 6.00$

- ○ $x/b = 32.5$
- ⊡ $x/b = 62.5$
- △ $x/b = 92.5$

$\left(\frac{U_m - U}{U_m}\right)$

(y/y_m)

FIG. 10.6

MEAN VELOCITY PROFILES -
OUTER LAW PLOT
WALL JET IN TAILORED PRESSURE GRADIENT

$b = 0.20$ ins. $\left(\frac{U_1}{U_{is}}\right) = 1.501$

○ x/b = 32.5
□ x/b = 62.5
△ x/b = 92.5

$\frac{U_{max}-U}{U_{max}}$

$(y/y_{1/2})$

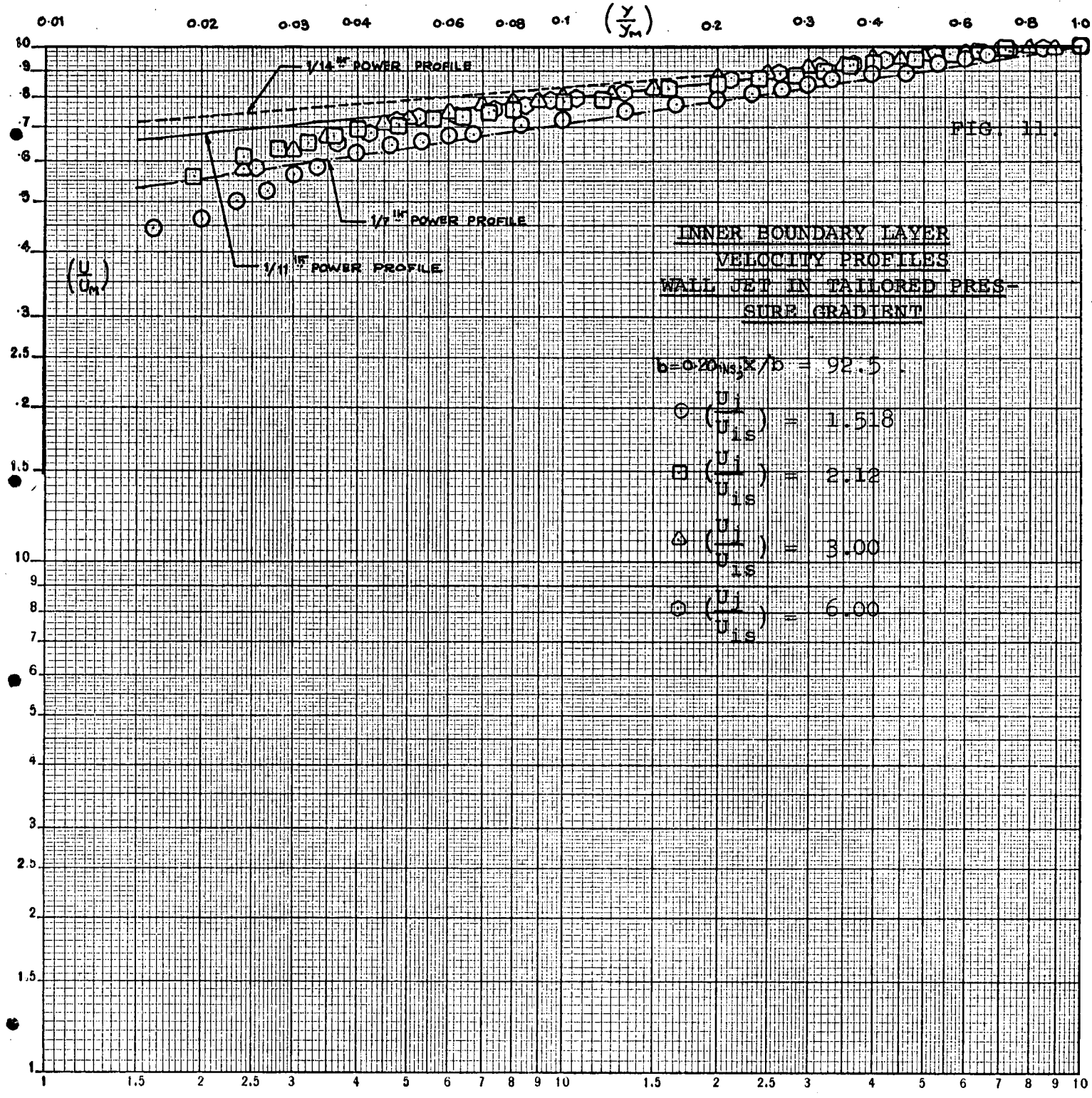
0·01
0·02
0·03
0·04
0·06
0·08
0·1
(y/y_M)
0·2
0·3
0·4
0·6
0·8
1·0
1/14th POWER PROFILE
1/11th POWER PROFILE
1/7th POWER PROFILE
(U/U_M)
INNER BOUNDARY LAYER
VELOCITY PROFILES
WALL JET IN TAILORED PRES-
SURE GRADIENT
b=0·20 IN.; x/b = 92.5
(U_i/U_is) = 1.518
(U_i/U_is) = 2.12
(U_i/U_is) = 3.00
(U_i/U_is) = 6.00

FIG. 11.

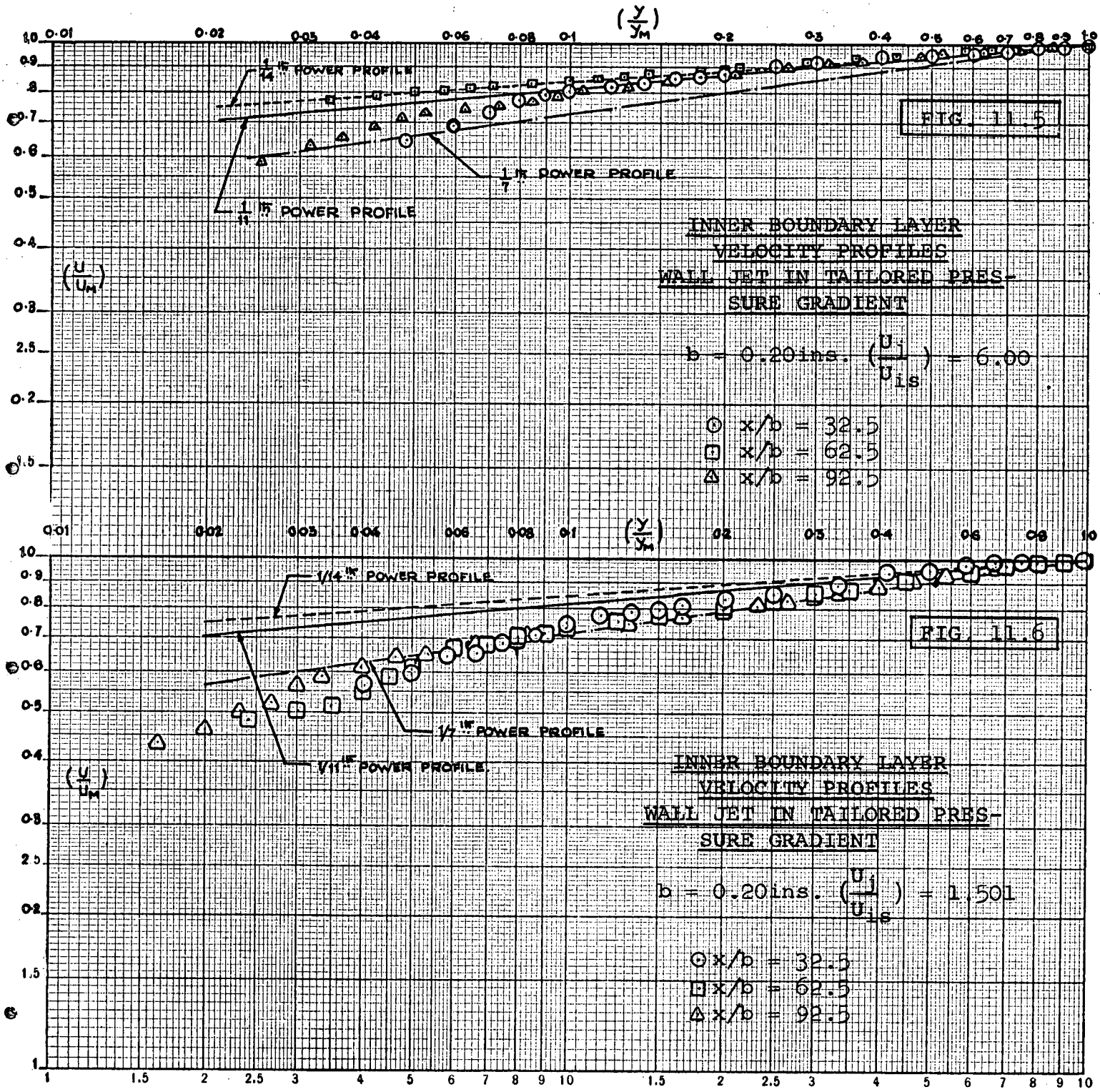
$\left(\frac{y}{y_M}\right)$
$\left(\frac{U}{U_M}\right)$
1/14 th POWER PROFILE
1/11 th POWER PROFILE
1/7 th POWER PROFILE
FIG. 11.5
INNER BOUNDARY LAYER
VELOCITY PROFILES
WALL JET IN TAILORED PRES-
SURE GRADIENT
b = 0.20ins. $\left(\frac{U_j}{U_{is}}\right)$ = 6.00
○ x/b = 32.5
□ x/b = 62.5
△ x/b = 92.5
1/14 th POWER PROFILE
1/11 th POWER PROFILE
1/7 th POWER PROFILE
FIG. 11.6
INNER BOUNDARY LAYER
VELOCITY PROFILES
WALL JET IN TAILORED PRES-
SURE GRADIENT
b = 0.20ins. $\left(\frac{U_j}{U_{is}}\right)$ = 1.501
○ x/b = 32.5
□ x/b = 62.5
△ x/b = 92.5

FIG. 12

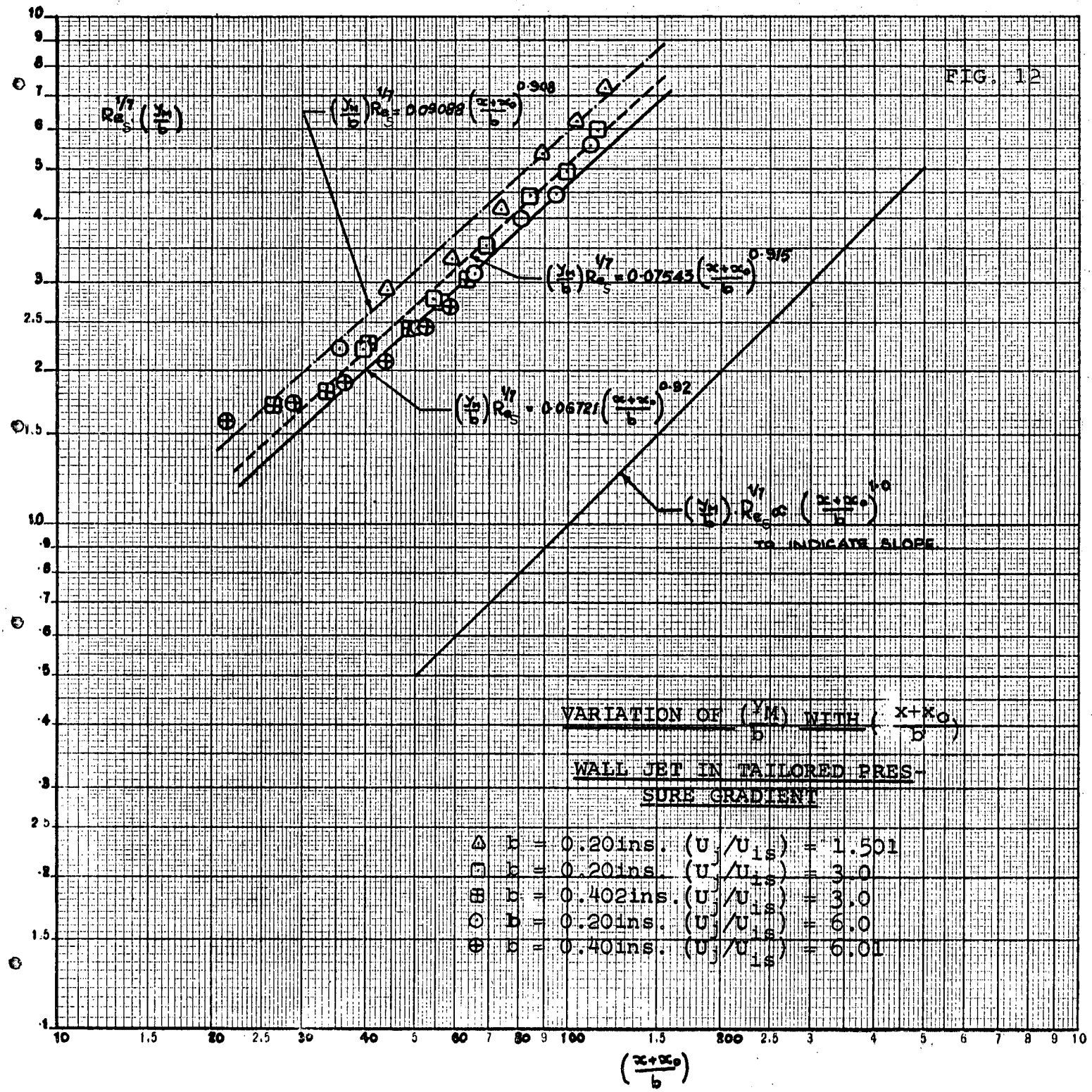

VARIATION OF $\left(\frac{y_M}{b}\right)$ WITH $\left(\frac{x+x_0}{b}\right)$

WALL JET IN TAILORED PRESSURE GRADIENT

△	b = 0.20ins.	(U_j/U_{is}) = 1.501
□	b = 0.20ins.	(U_j/U_{is}) = 3.0
⊞	b = 0.402ins.	(U_j/U_{is}) = 3.0
⊙	b = 0.20ins.	(U_j/U_{is}) = 6.0
⊕	b = 0.40ins.	(U_j/U_{is}) = 6.01

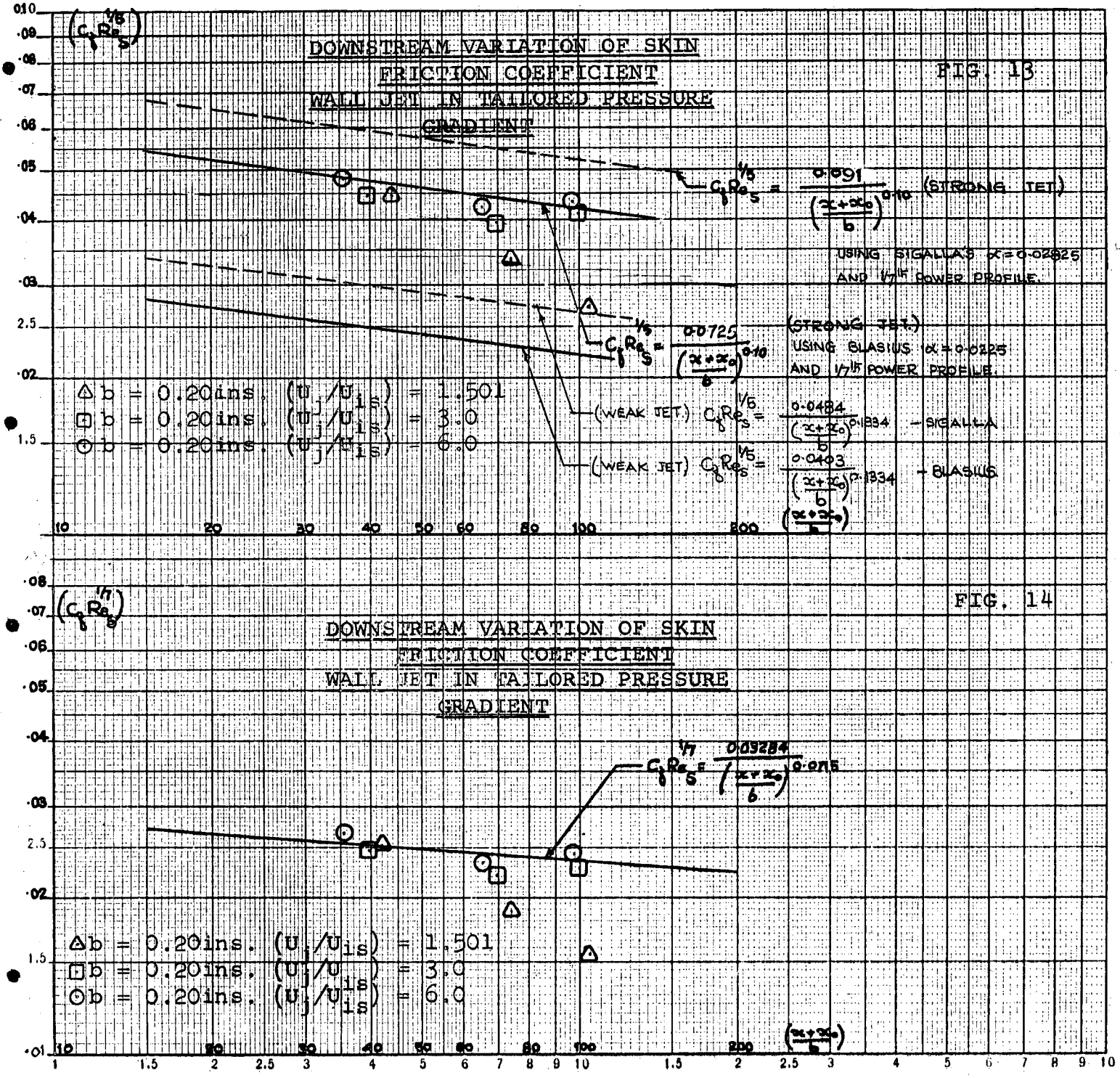

DOWNSTREAM VARIATION OF SKIN FRICTION COEFFICIENT WALL JET IN TAILORED PRESSURE GRADIENT

FIG. 13

DOWNSTREAM VARIATION OF SKIN FRICTION COEFFICIENT WALL JET IN TAILORED PRESSURE GRADIENT

FIG. 14

FIG. 15

COMPARISON OF TURBULENCE INTENSITY WALL JET IN TAILORED PRESSURE GRADIENT

⊡ Probe No.2
⊙ Probe No.3

b = 0.20ins. x = 19.2ins.

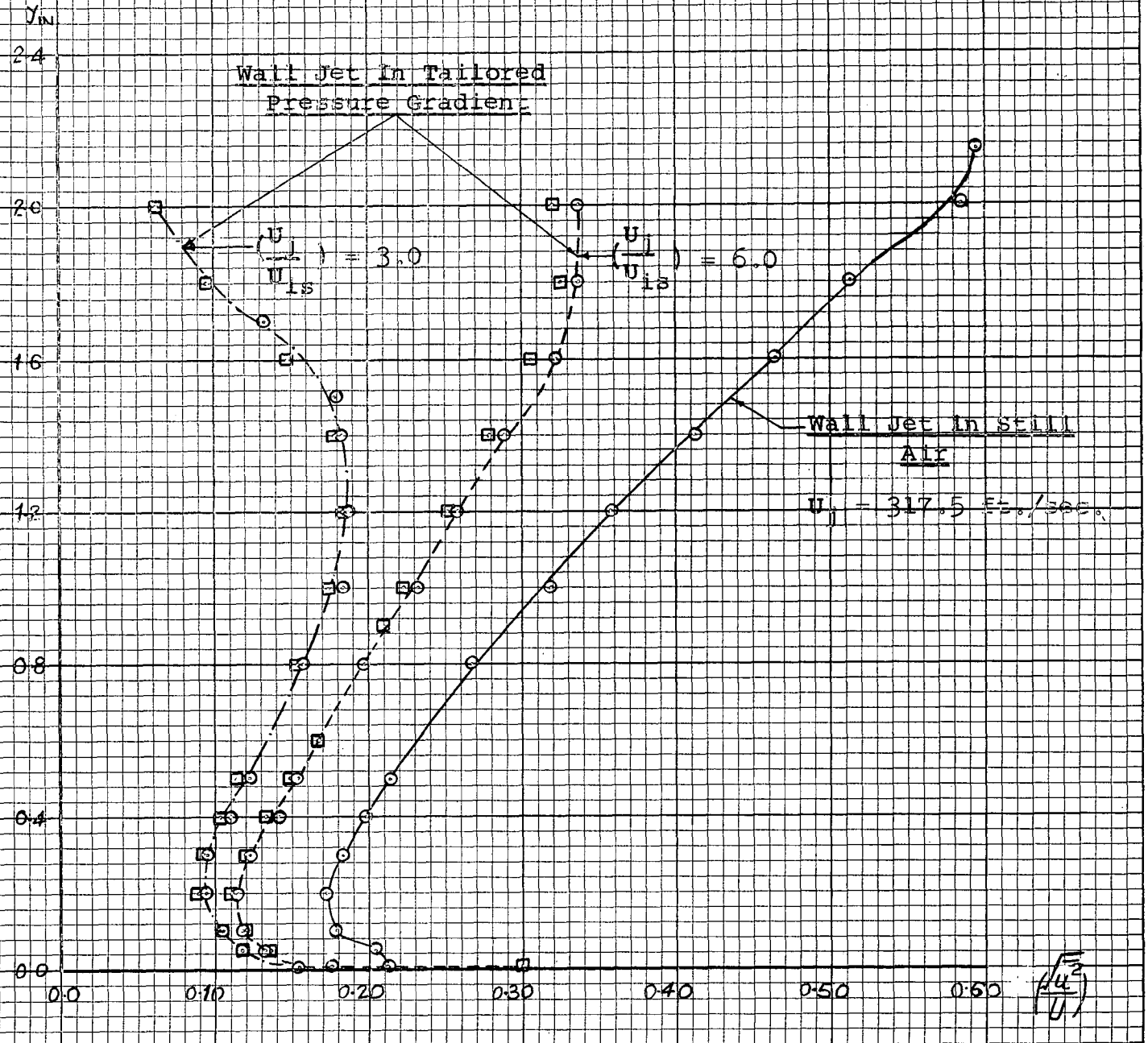

FIG. 16.2

TURBULENCE INTENSITY AND CORRESPONDING VELOCITY PROFILE.
WALL JET IN TAILORED PRESSURE GRADIENT.

$b = 0.20$ins. $\left(\frac{U_j}{U_{is}}\right) = 3.0$

$x = 19.2$ins.

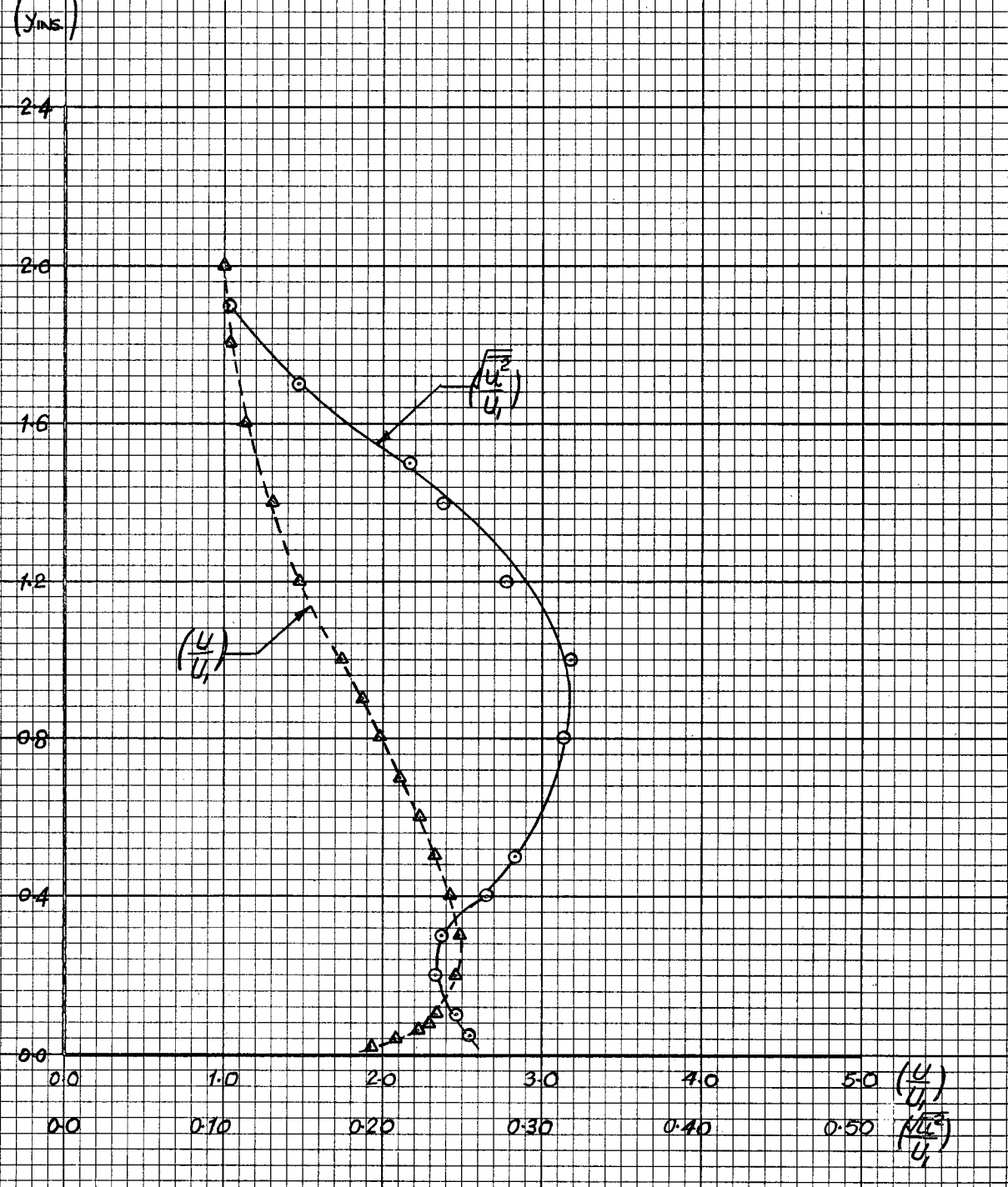

FIG. 16.5

TURBULENCE INTENSITY AND CORRESPONDING VELOCITY PROFILE.
WALL JET IN TAILORED PRESSURE GRADIENT.

$b = 0.20$ins. $\left(\frac{U_j}{U_{is}}\right) = 6.0$

$x = 19.2$ins.

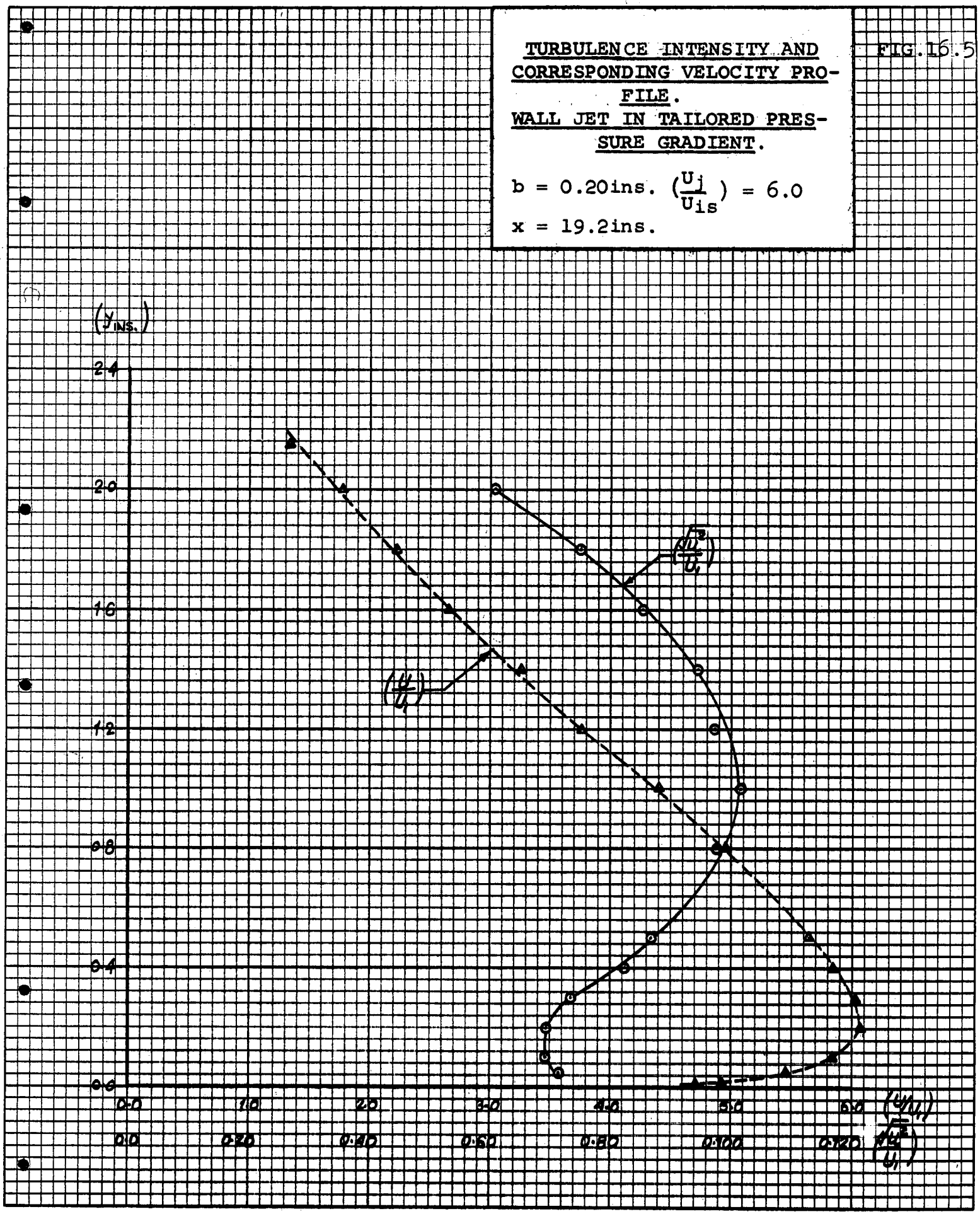

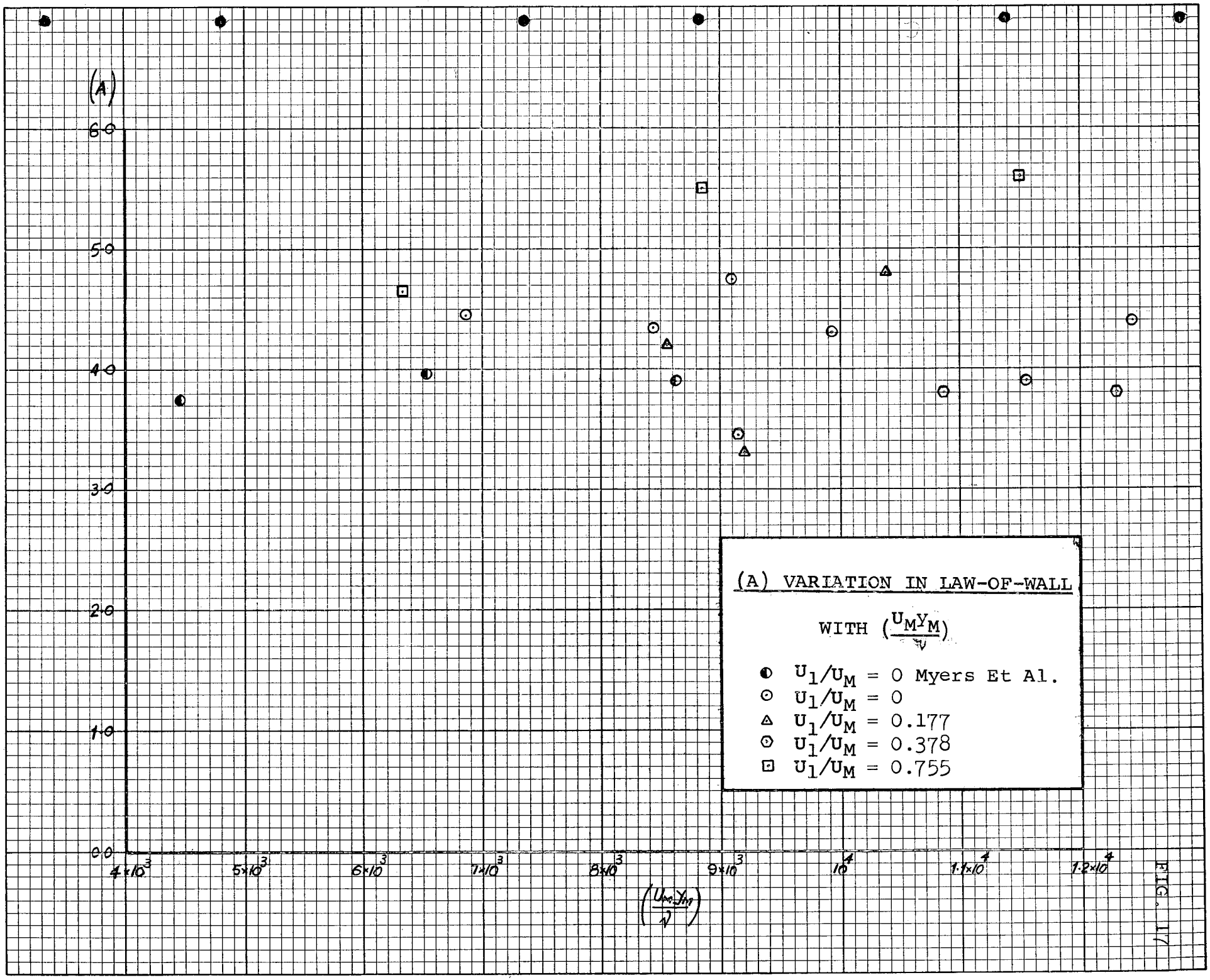
(A)
60
50
40
30
20
10
0.0
4×10³
5×10³
6×10³
7×10³
8×10³
9×10³
10⁴
1.1×10⁴
1.2×10⁴
$\left(\frac{U_M Y_M}{\nu}\right)$
(A) VARIATION IN LAW-OF-WALL
WITH $\left(\frac{U_M Y_M}{\nu}\right)$
U_1/U_M = 0 Myers Et Al.
U_1/U_M = 0
U_1/U_M = 0.177
U_1/U_M = 0.378
U_1/U_M = 0.755

FIG. 17

FIG. 18

(A) VARIATION IN LAW-OF-WALL

WITH $(\frac{U_1}{U_M})$

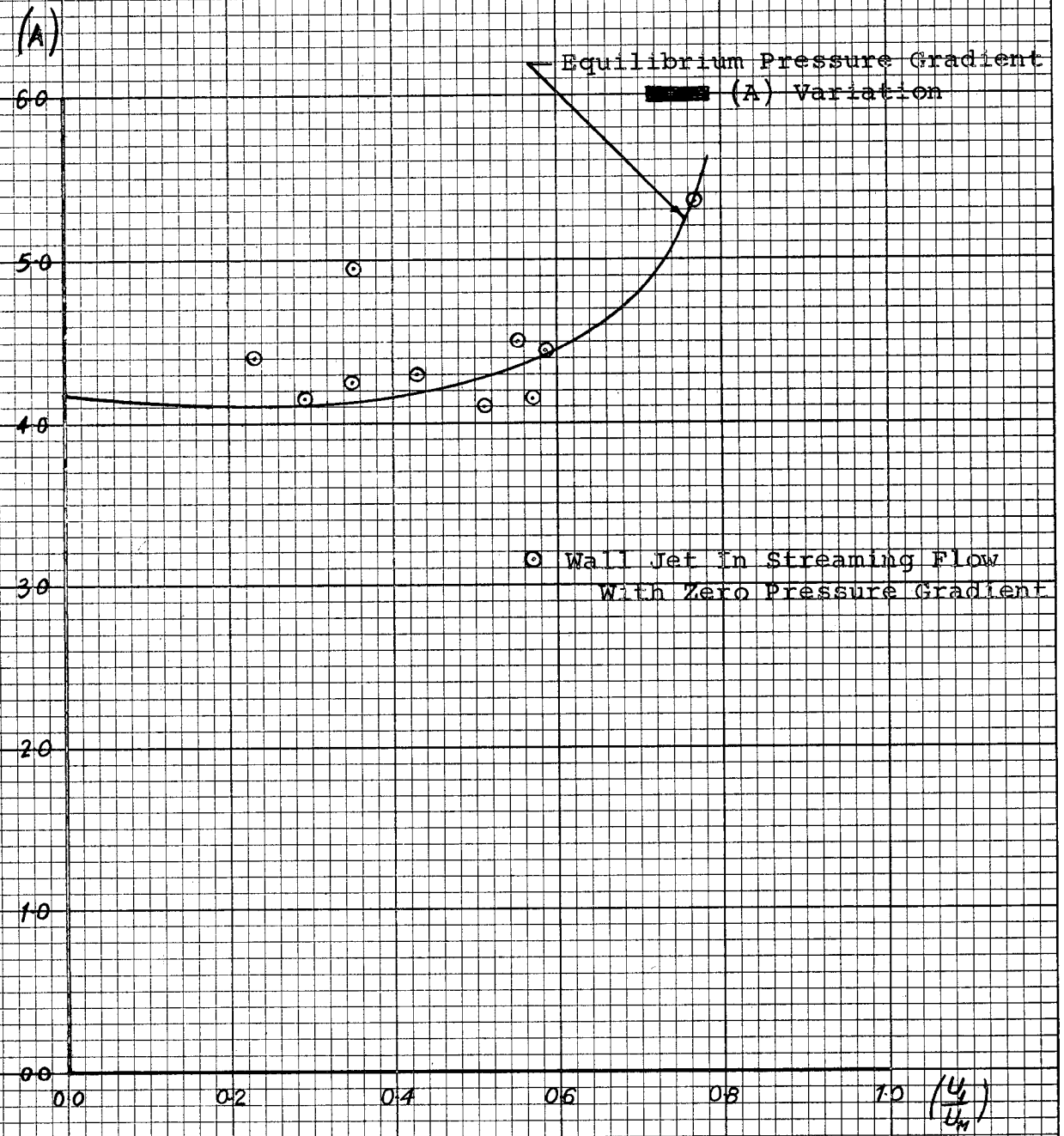

FIG. 19

VARIATION OF $\left(\frac{U_M}{U_1}\right)$ WITH $\left(\frac{x}{b}\right)$

WALL JET IN ZERO PRESSURE GRADIENT

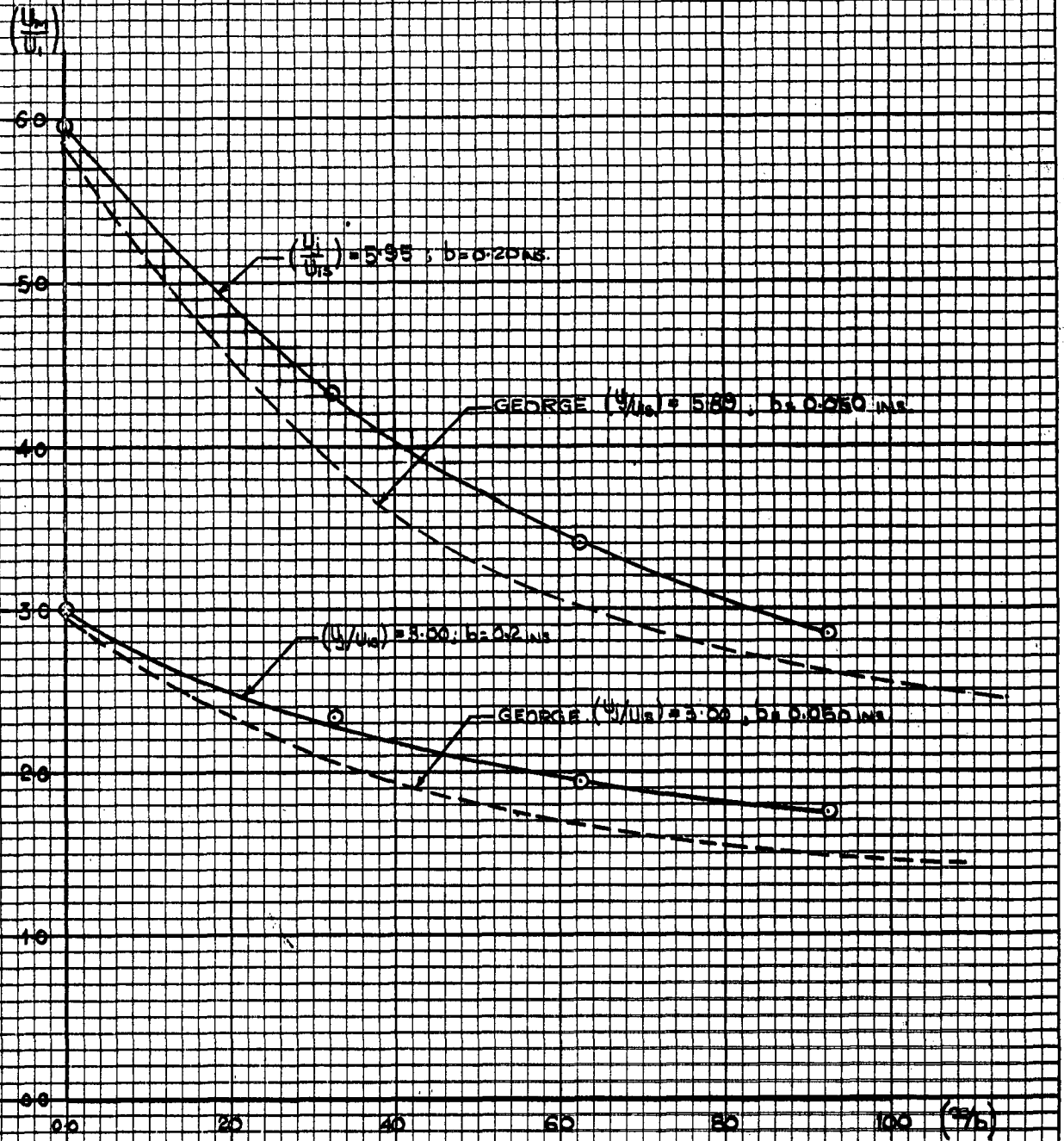

FIG. 20

VELOCITY PROFILES
WALL JET IN ZERO PRESSURE GRADIENT

$b = 0.375$ins. $\left(\frac{U_j}{U_{is}}\right) = 2.66$

- ⊙ x/b = 17.34
- ⊡ x/b = 33.34
- △ x/b = 49.34

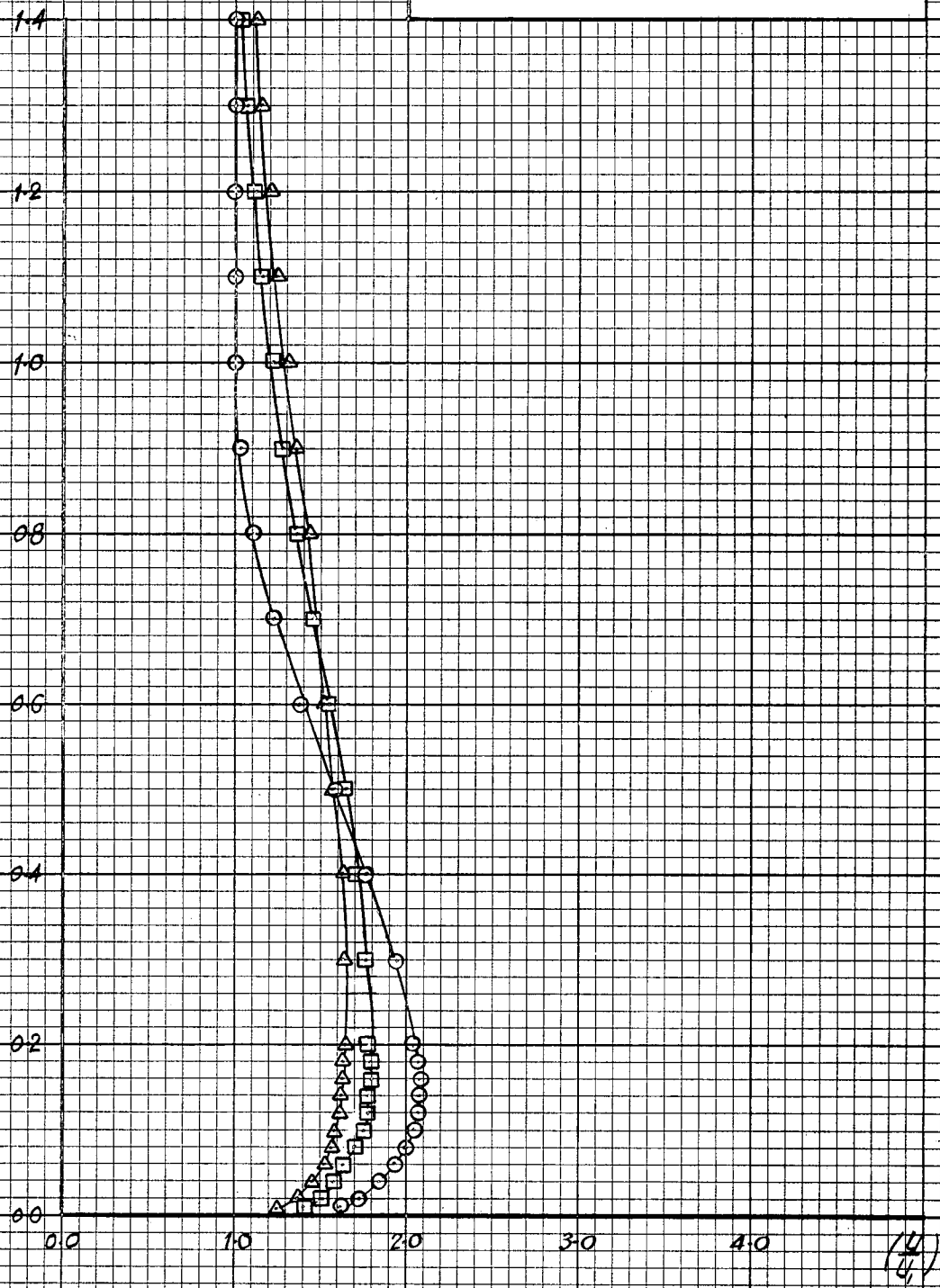

FIG. 21

VELOCITY PROFILES
WALL JET IN ZERO PRESSURE GRADIENT

$b = 0.20$ ins. $\left(\frac{U_j}{U_{is}}\right) = 3.0$

- ⊙ x/b = 32.5
- ⊡ x/b = 62.5
- △ x/b = 92.5

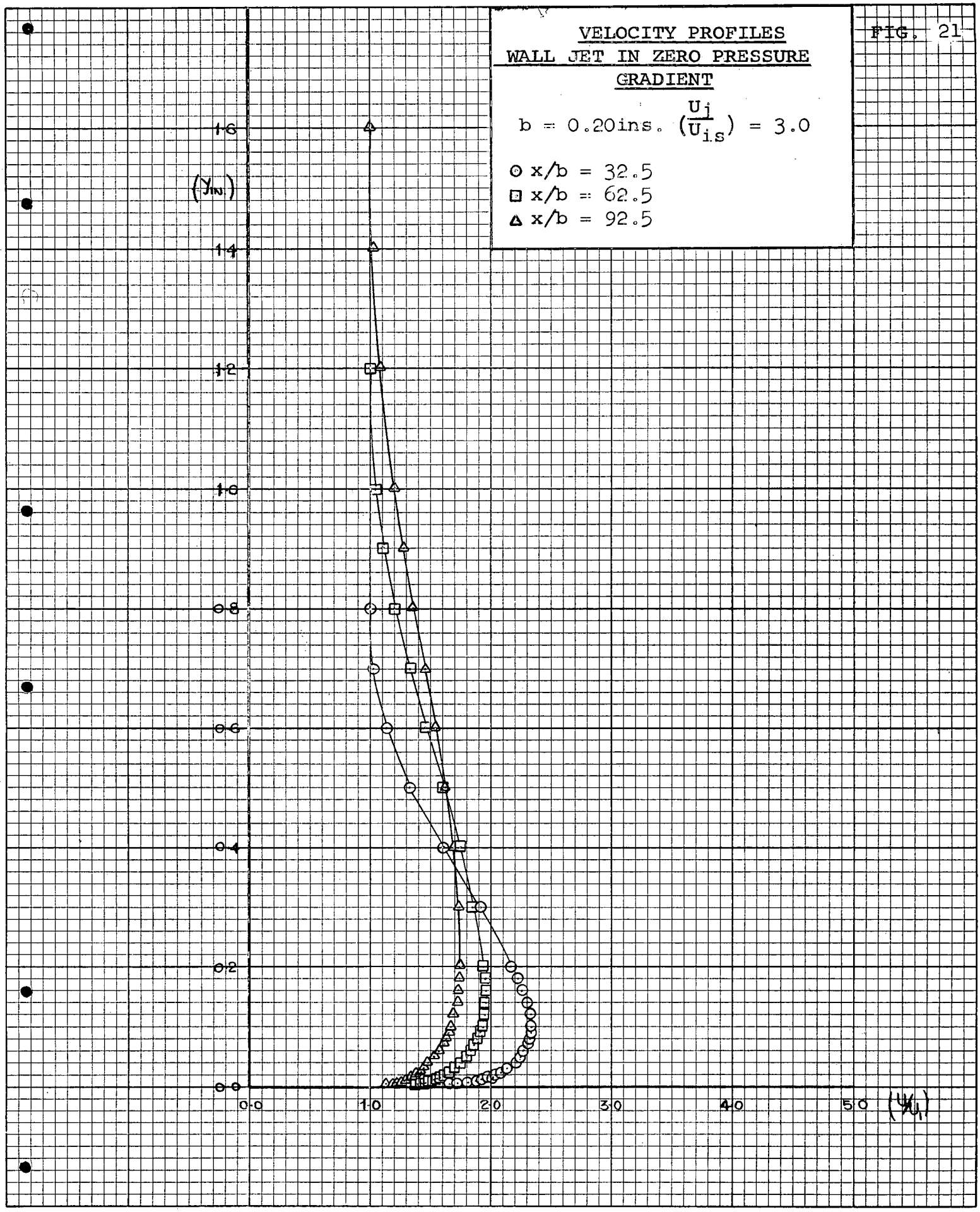

FIG. 22

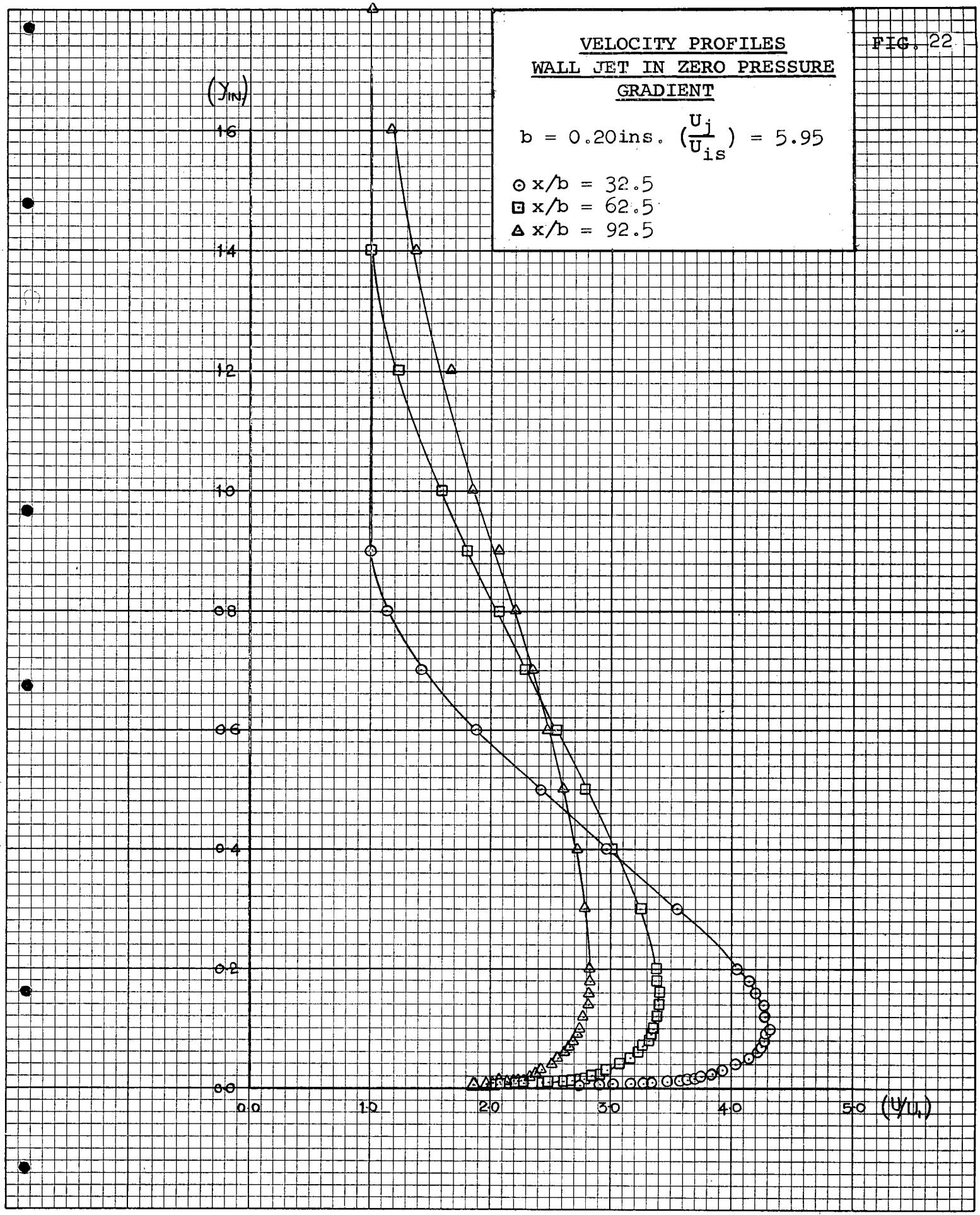
VELOCITY PROFILES
WALL JET IN ZERO PRESSURE GRADIENT
b = 0.20ins. $(\frac{U_j}{U_{is}}) = 5.95$
x/b = 32.5
x/b = 62.5
x/b = 92.5
(Y_{IN})
1.6
1.4
1.2
1.0
0.8
0.6
0.4
0.2
0.0
0.0
1.0
2.0
3.0
4.0
5.0
(U/U_1)

FIG. 23

NON-DIMENSIONAL MEAN VELOCITY PROFILES EXCLUDING INNER BOUNDARY LAYER IN ZERO PRESSURE GRADIENT.

$b = 0.375$ in. $\left(\frac{U_j}{U_{j_s}}\right) = 2.66$

- • $x/b = 17.34$
- ⊡ $x/b = 25.34$
- × $x/b = 33.34$
- ⊙ $x/b = 41.34$
- △ $x/b = 49.34$

$$\left(\frac{U_M y_{M/2}}{\nu}\right) = \begin{cases} 6.59\times10^4 \\ 7.53\times10^4 \\ 8.56\times10^4 \\ 8.89\times10^4 \\ 9.57\times10^4 \end{cases}$$

$$\left(\frac{y-y_M}{y_{M/2}-y_M}\right)$$

$$\left[\frac{U-U_j}{U_M-U_j}\right] = \text{Sech}^2\left[0.88\left(\frac{y-y_M}{y_{M/2}-y_M}\right)\right]$$

$$\left[\frac{U-U_j}{U_M-U_j}\right] = e^{-0.693\left(\frac{y-y_M}{y_{M/2}-y_M}\right)^2}$$

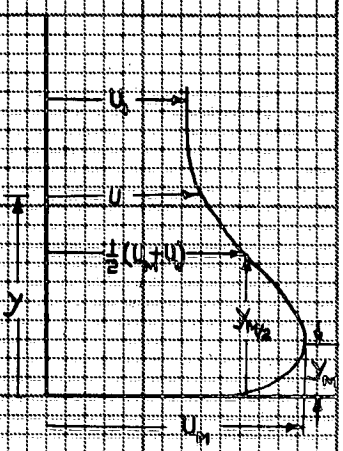

3·0 2·5 2·0 1·5 1·0 0·5 0 −0·5

0·2 0·4 0·6 0·8 1·0

$\left(\frac{U-U_j}{U_M-U_j}\right)$

NON-DIMENSIONAL MEAN VELOCITY PROFILES EXCLUDING INNER BOUNDARY LAYER IN ZERO PRESSURE GRADIENT

FIG. 24

b = 0.20ins.

x/b	$\left(\frac{U_j}{U_{is}}\right)$	$\left(\frac{U_M y_M/2}{\nu}\right)$
⊙ 32.5	3.00	3.44×10^4
▽ 62.5		4.35×10^4
⊗ 92.5		5.13×10^4
⊙ 32.5	5.95	4.08×10^4
⊡ 62.5		4.97×10^4
△ 92.5		5.66×10^4

$\left(\frac{y-y_M}{y_{M/2}-y_M}\right)$

$\left[\frac{U-U_1}{U_M-U_1}\right] = \text{SECH}^2\left[0.88\left(\frac{y-y_M}{y_{M/2}-y_M}\right)\right]$

$\left[\frac{U-U_1}{U_M-U_1}\right] = e^{-0.693\left(\frac{y-y_M}{y_{M/2}-y_M}\right)^2}$

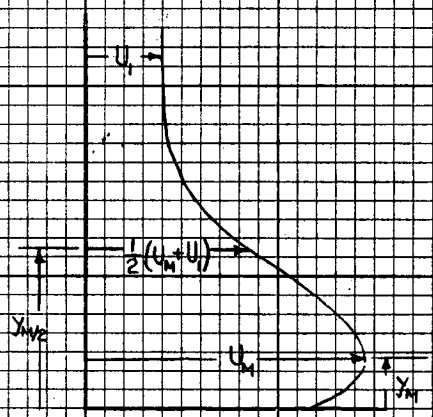

3.0
2.5
2.0
1.5
1.0
0.5
0.0
-0.5
0.2
0.4
0.6
0.8
1.0 $\left(\frac{U-U_1}{U_M-U_1}\right)$

NON-DIMENSIONAL MEAN VELOCITY PROFILES INCLUDING INNER BOUNDARY LAYER IN ZERO PRESSURE GRADIENT.

$b = 0.375\text{in.}$ $\left(\frac{U_j}{U_{is}}\right) = 2.66$

- ● $x/b = 17.34$
- ⊡ $x/b = 25.34$
- × $x/b = 33.34$
- ⊙ $x/b = 41.34$
- △ $x/b = 49.34$

$\left(\frac{U_M y_{M/2}}{\nu}\right) = \begin{cases} 6.59\times10^4 \\ 7.53\times10^4 \\ 8.56\times10^4 \\ 8.89\times10^4 \\ 9.57\times10^4 \end{cases}$

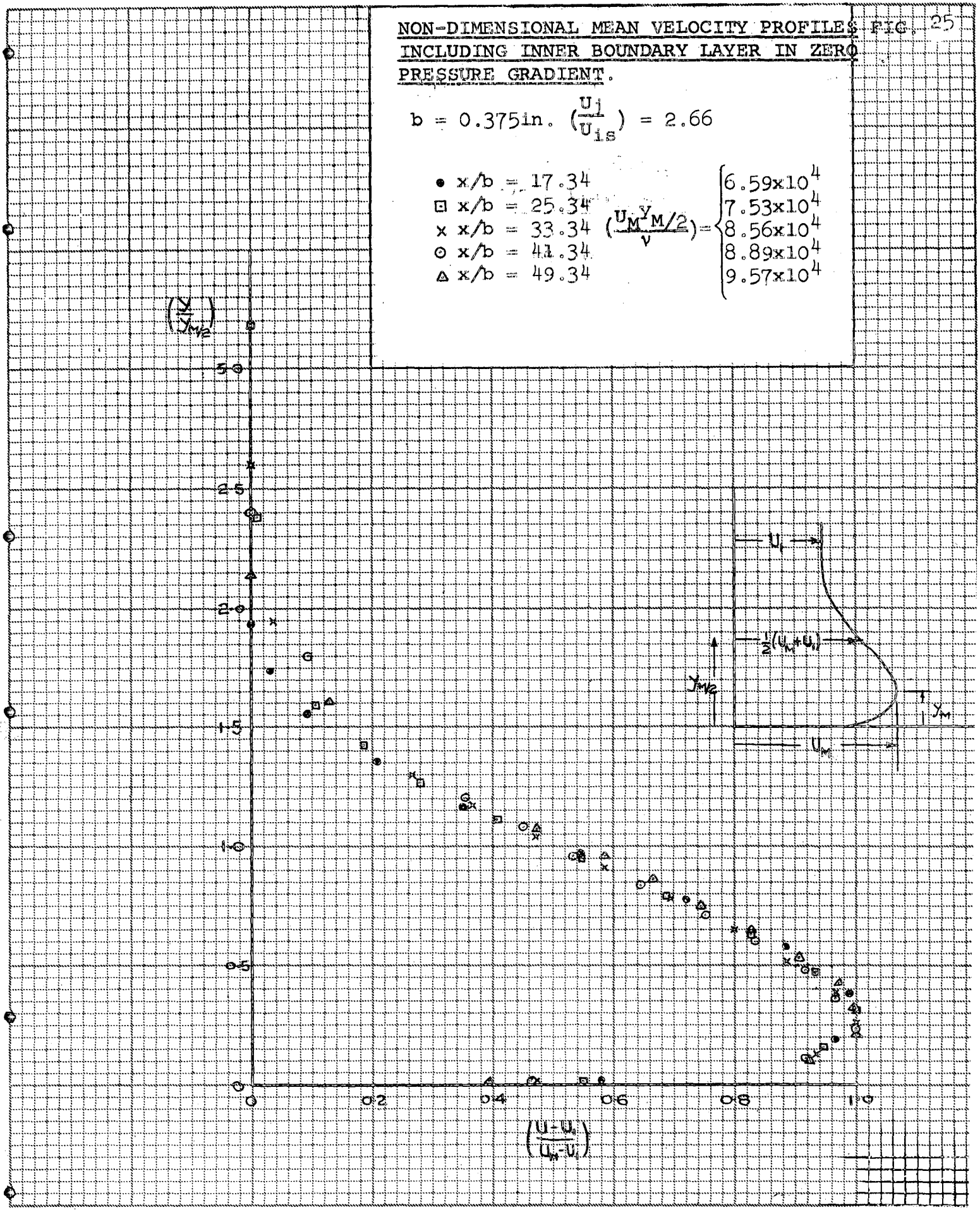

FIG. 26

NON-DIMENSIONAL MEAN VELOCITY PROFILES INCLUDING INNER BOUNDARY LAYER IN ZERO PRESSURE GRADIENT

b = 0.20ins.

x/b	$(\frac{U_i}{U_{is}})$	$(\frac{U_M Y_{M/2}}{\nu})$
⊙ 32.5		3.44×10^4
▽ 62.5	3.00	4.35×10^4
⊗ 92.5		5.13×10^4
⊙ 32.5		4.08×10^4
⊡ 62.5	5.95	4.97×10^4
△ 92.5		5.66×10^4

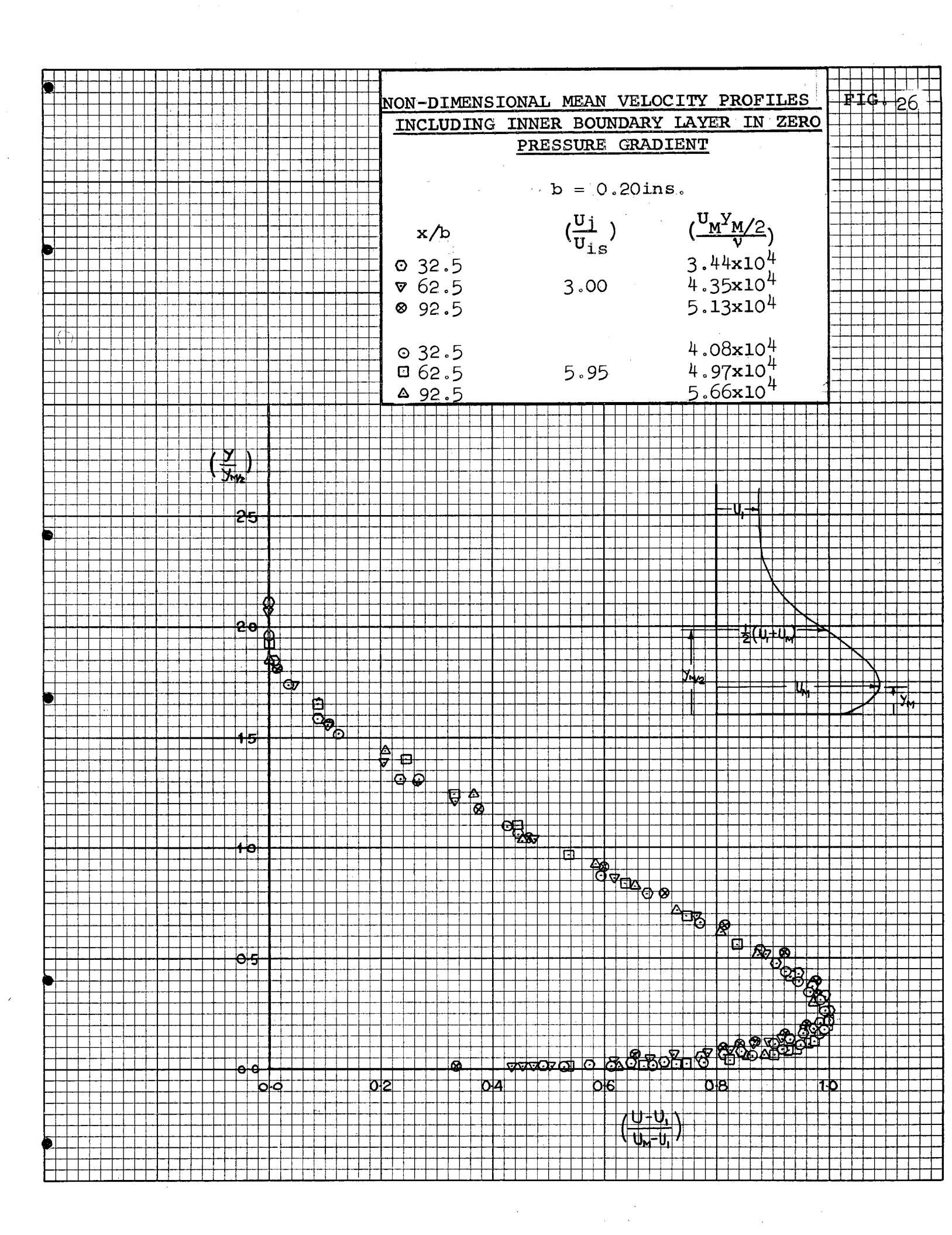

FIG. 27

DOWNSTREAM VARIATION OF $(\frac{Y_{M/2}}{b})$ AND $(\frac{Y_M}{b})$ WITH $(\frac{x}{b})$

WALL JET IN ZERO PRESSURE GRADIENT

$b = 0.375$ins. $(\frac{U_i}{U_{is}}) = 2.66$

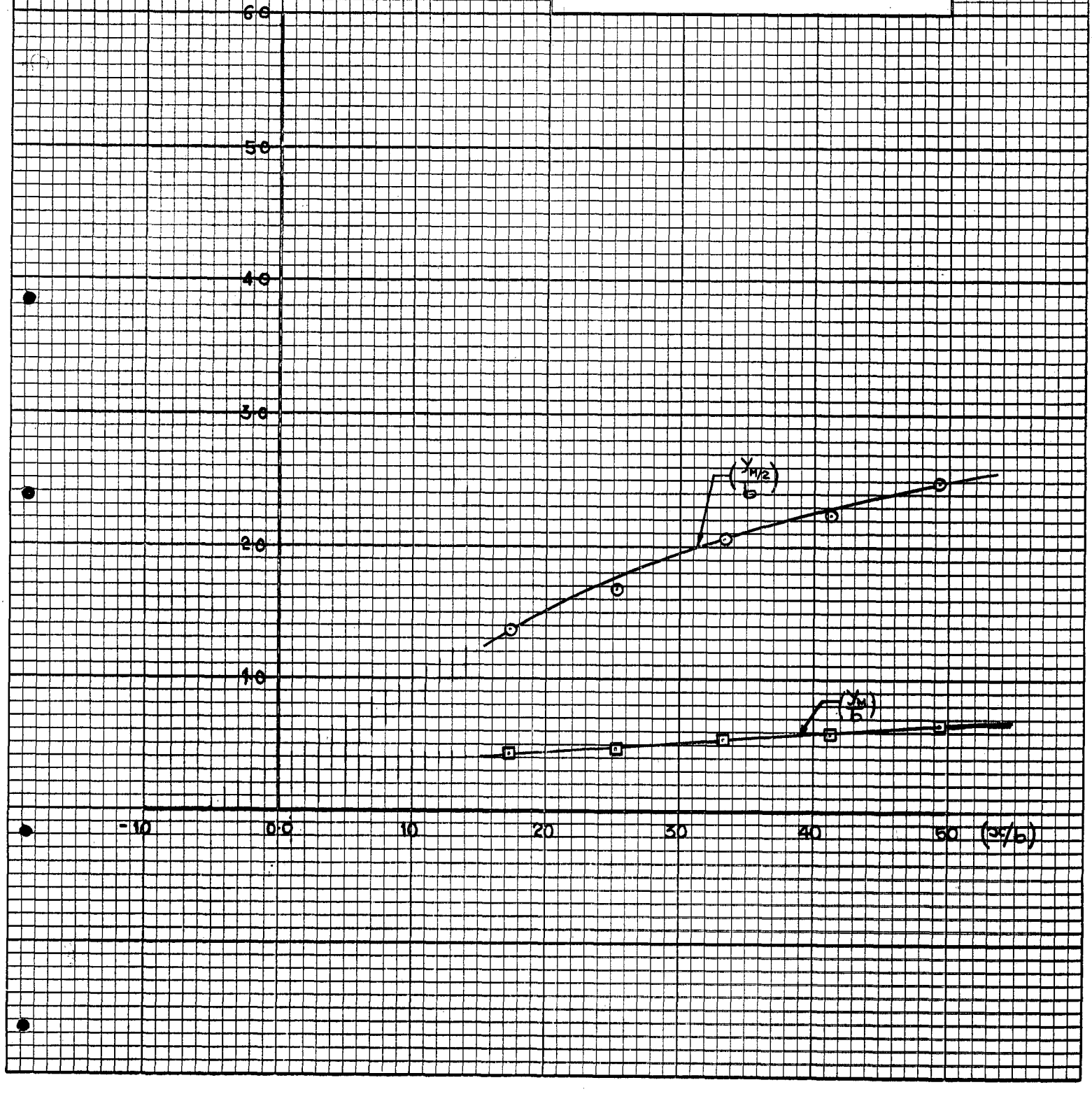

FIG. 28

DOWNSTREAM VARIATION OF $(\frac{Y_{M/2}}{b})$ AND $(\frac{Y_M}{b})$ WITH $(\frac{x}{b})$

WALL JET IN ZERO PRESSURE GRADIENT

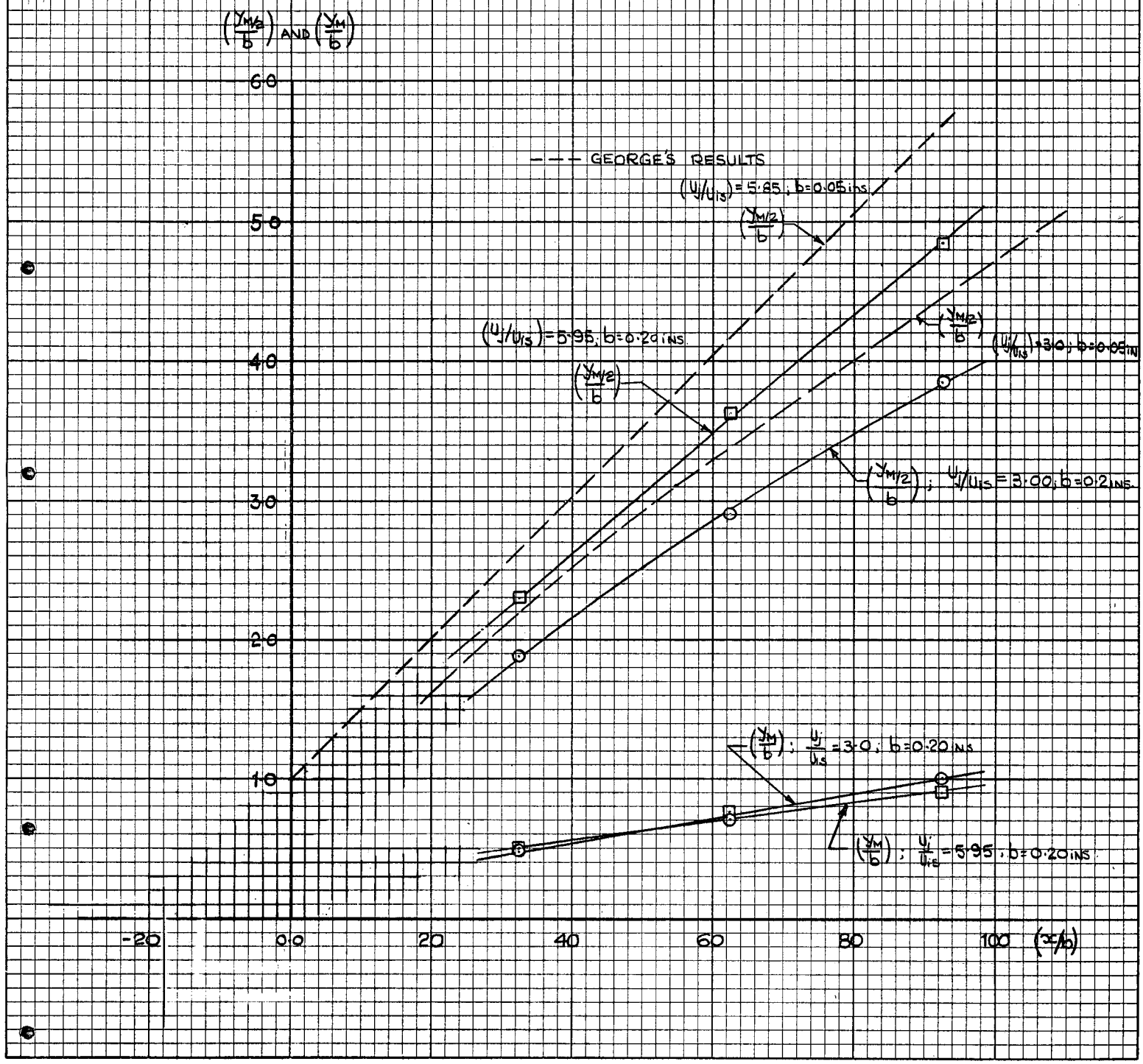

FIG. 29

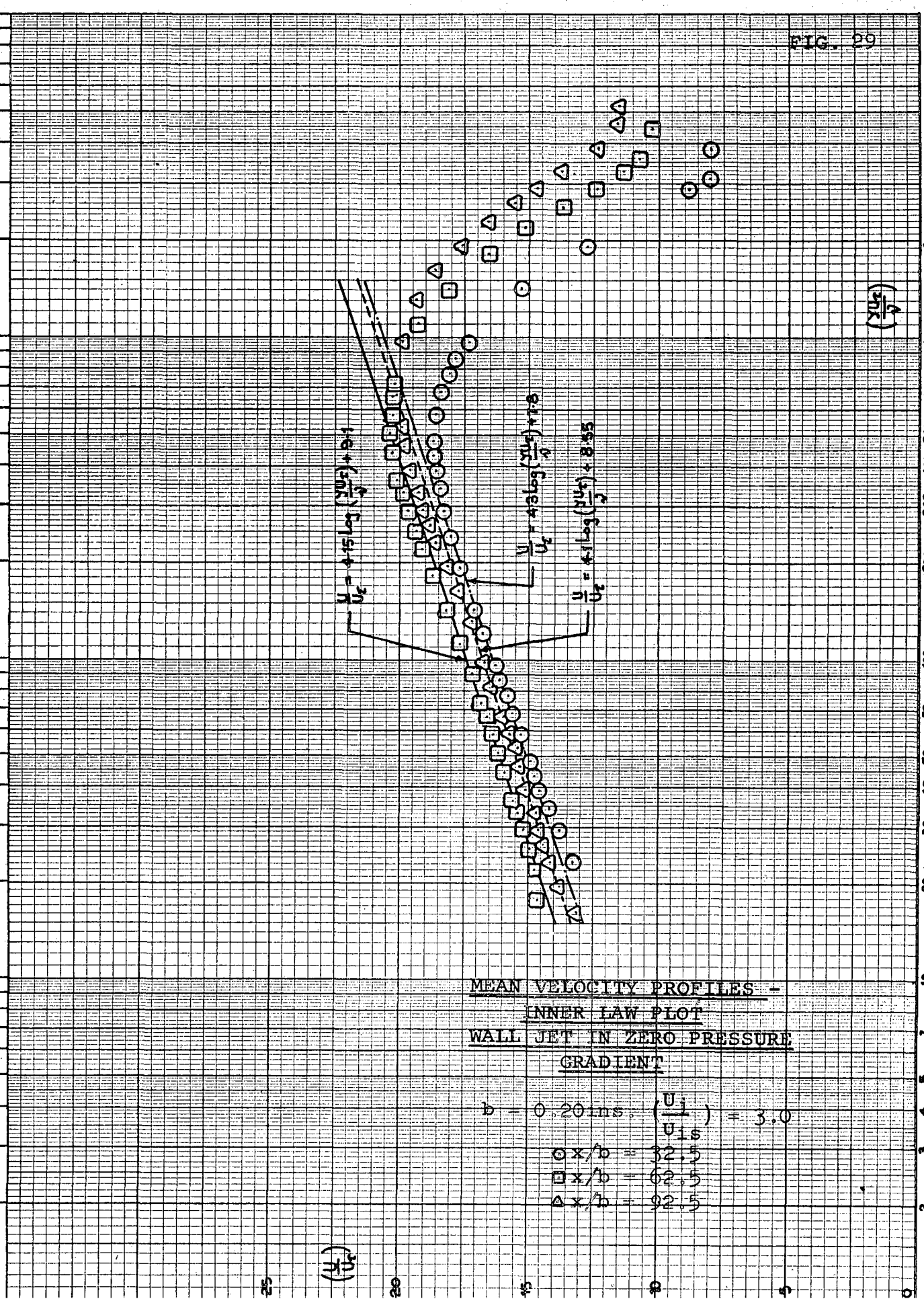

MEAN VELOCITY PROFILES - INNER LAW PLOT
WALL JET IN ZERO PRESSURE GRADIENT

$b = 0.20$ ins ; $\left(\frac{U_1}{U_{1s}}\right) = 3.0$

○ x/b = 32.5
□ x/b = 62.5
△ x/b = 92.5

FIG. 30

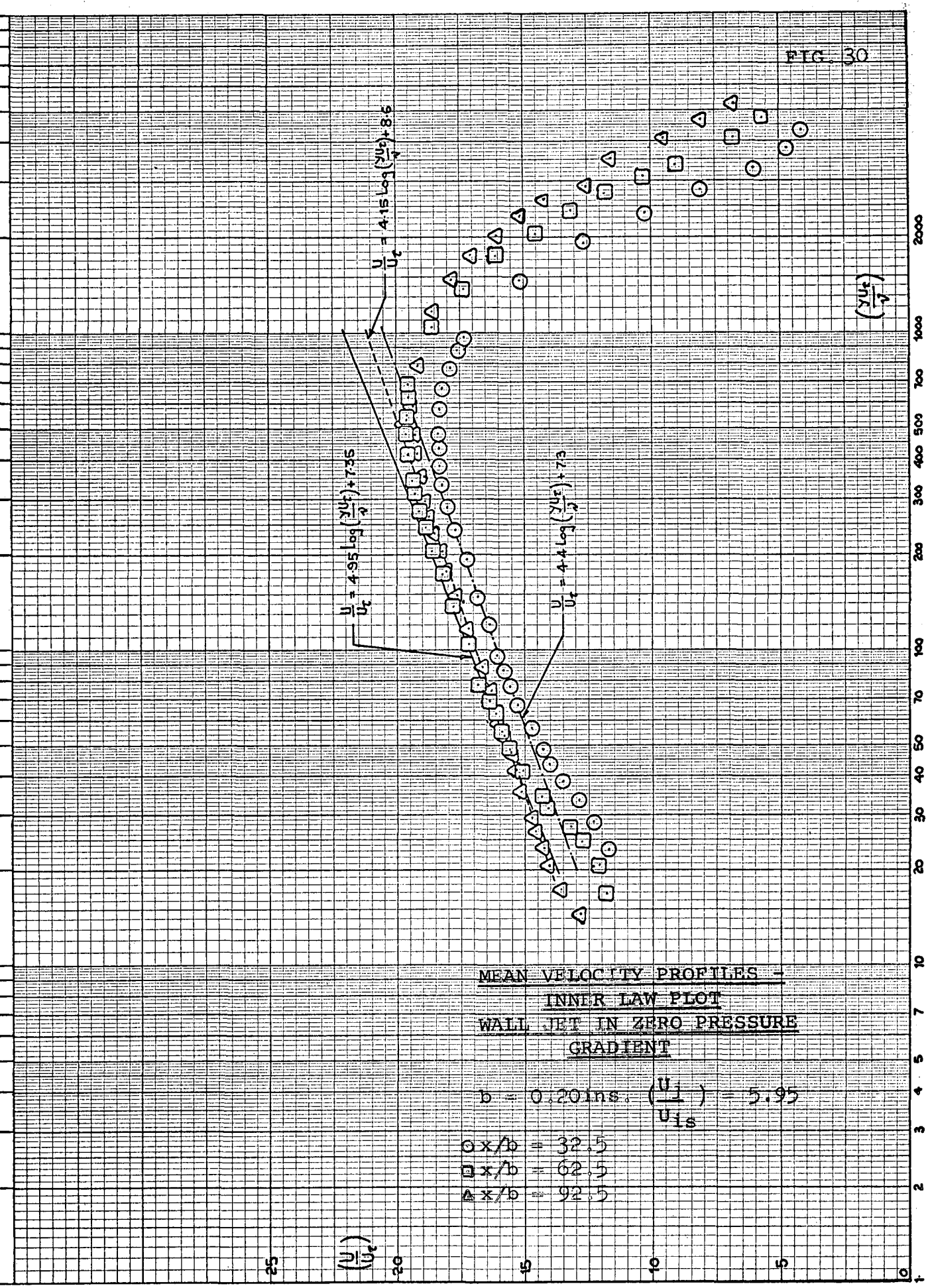

MEAN VELOCITY PROFILES - INNER LAW PLOT
WALL JET IN ZERO PRESSURE GRADIENT

$b = 0.201 ns.$ $\left(\frac{U_1}{U_{1s}}\right) = 5.95$

○ x/b = 32.5
□ x/b = 62.5
△ x/b = 92.5

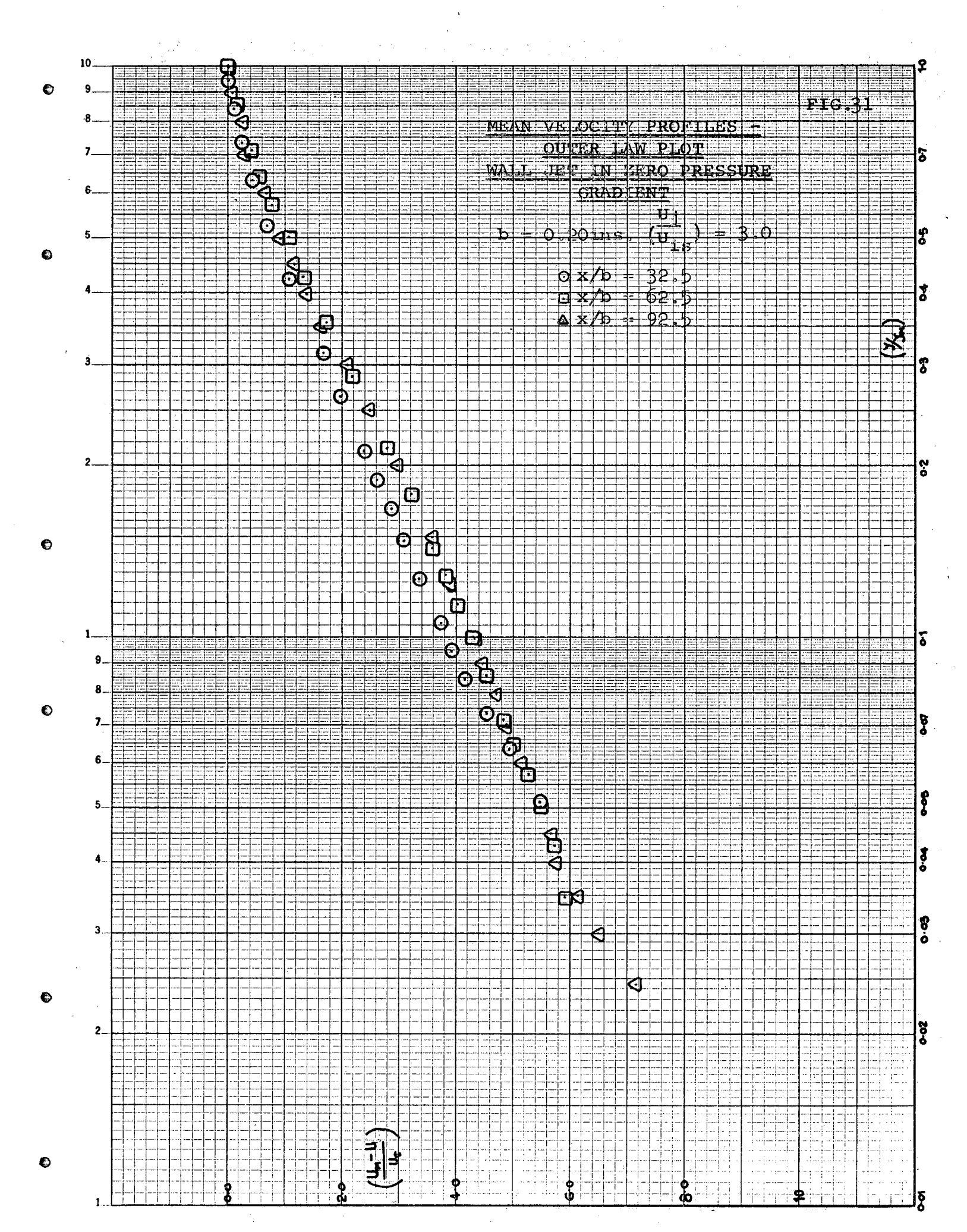
FIG.31
MEAN VELOCITY PROFILES –
OUTER LAW PLOT
WALL JET IN ZERO PRESSURE
GRADIENT
b = 0.20ms, $(U_1/U_{1/2}) = 3.0$
⊙ x/b = 32.5
□ x/b = 62.5
△ x/b = 92.5
(y/δ)
$(U_1 - U)/U_\tau$

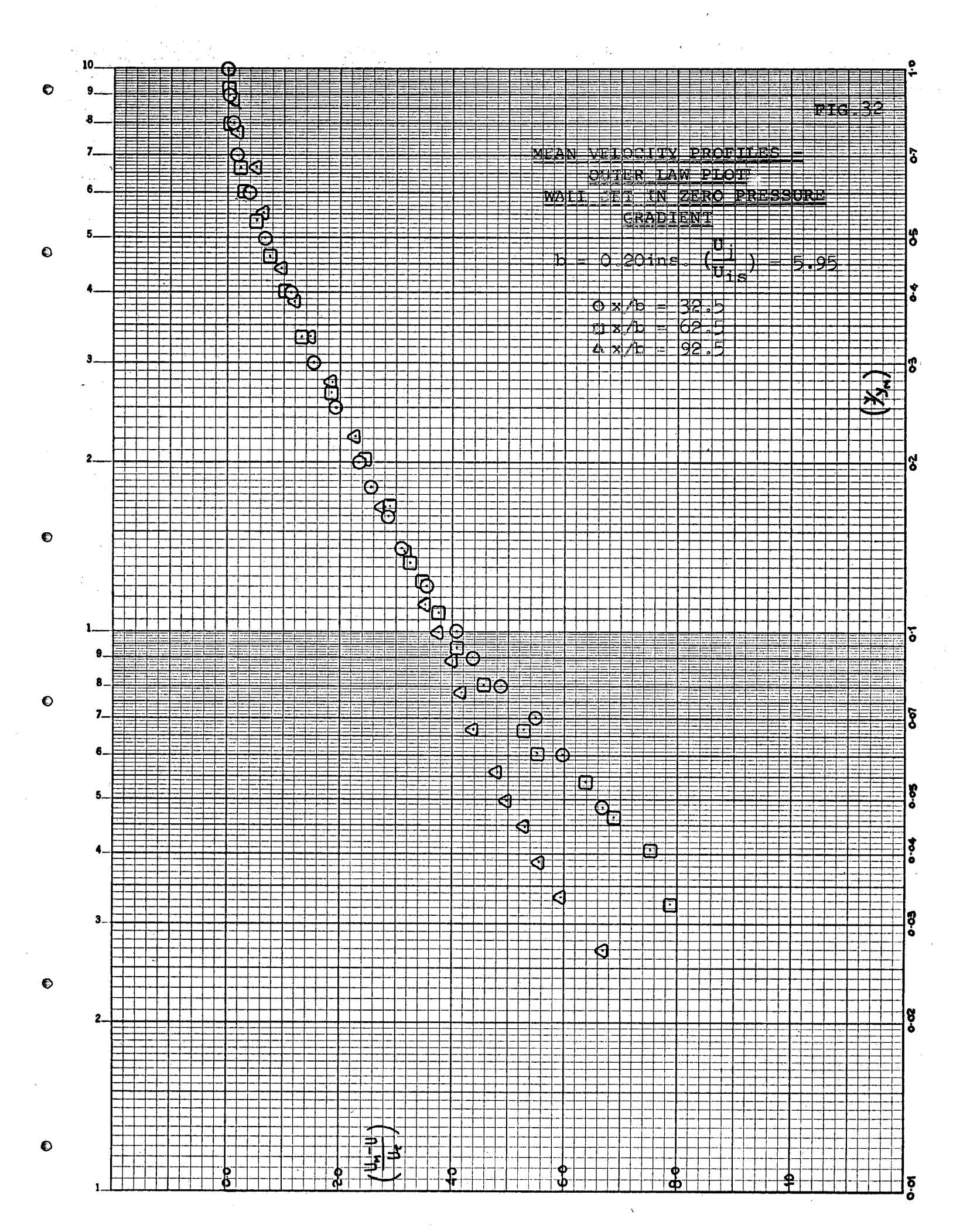
FIG. 32
MEAN VELOCITY PROFILES -
OUTER LAW PLOT
WALL JET IN ZERO PRESSURE
GRADIENT
b = 0.20ins. $(\frac{U_j}{U_{is}}) = 5.95$
○ x/b = 32.5
□ x/b = 62.5
△ x/b = 92.5
$(\frac{u_m - u}{u_{\tau}})$
$(\frac{y}{y_m})$

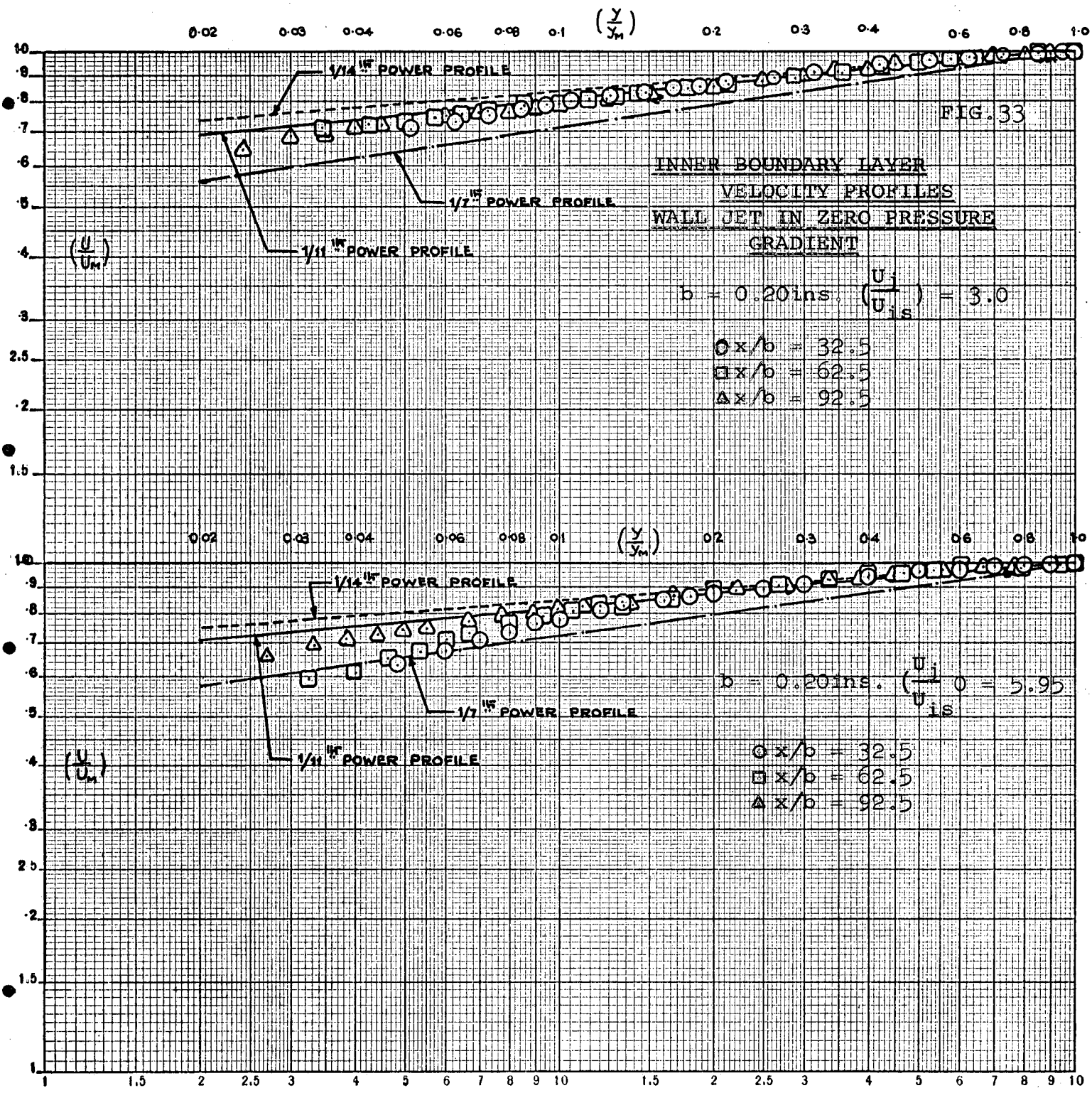
(y/y_m)
0·02 0·03 0·04 0·06 0·08 0·1 0·2 0·3 0·4 0·6 0·8 1·0
(U/U_m)
10 9 8 7 6 5 4 3 2.5 2 1.5 1
1/14th POWER PROFILE
1/7th POWER PROFILE
1/11th POWER PROFILE
INNER BOUNDARY LAYER
VELOCITY PROFILES
WALL JET IN ZERO PRESSURE
GRADIENT
b = 0.20ins. (U_j/U_is) = 3.0
○ x/b = 32.5
□ x/b = 62.5
△ x/b = 92.5
1 1.5 2 2.5 3 4 5 6 7 8 9 10

FIG. 33

(y/y_m)
0·02 0·03 0·04 0·06 0·08 0·1 0·2 0·3 0·4 0·6 0·8 1·0
(U/U_m)
10 9 8 7 6 5 4 3 2.5 2 1.5 1
1/14th POWER PROFILE
1/7th POWER PROFILE
1/11th POWER PROFILE
b = 0.20ins. (U_j/U_is) = 5.95
○ x/b = 32.5
□ x/b = 62.5
△ x/b = 92.5
1 1.5 2 2.5 3 4 5 6 7 8 9 10

FIG. 34

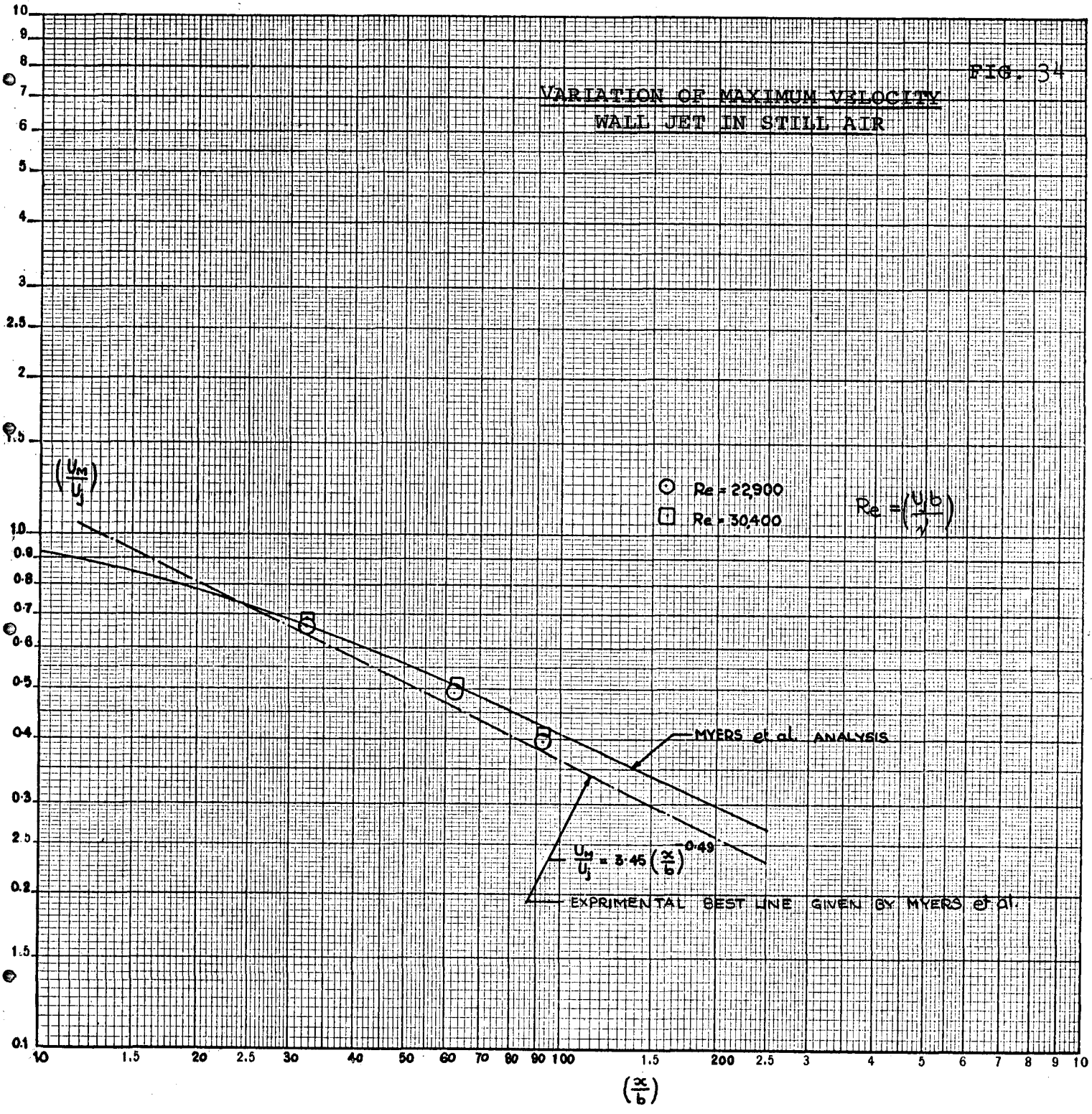
VARIATION OF MAXIMUM VELOCITY
WALL JET IN STILL AIR
$\left(\frac{U_M}{U_j}\right)$
$\left(\frac{x}{b}\right)$
Re = 22,900
Re = 30,400
$Re = \left(\frac{U_j b}{\nu}\right)$
MYERS et al. ANALYSIS
$\frac{U_M}{U_j} = 3.45\left(\frac{x}{b}\right)^{-0.49}$
EXPRIMENTAL BEST LINE GIVEN BY MYERS et al.

FIG. 35

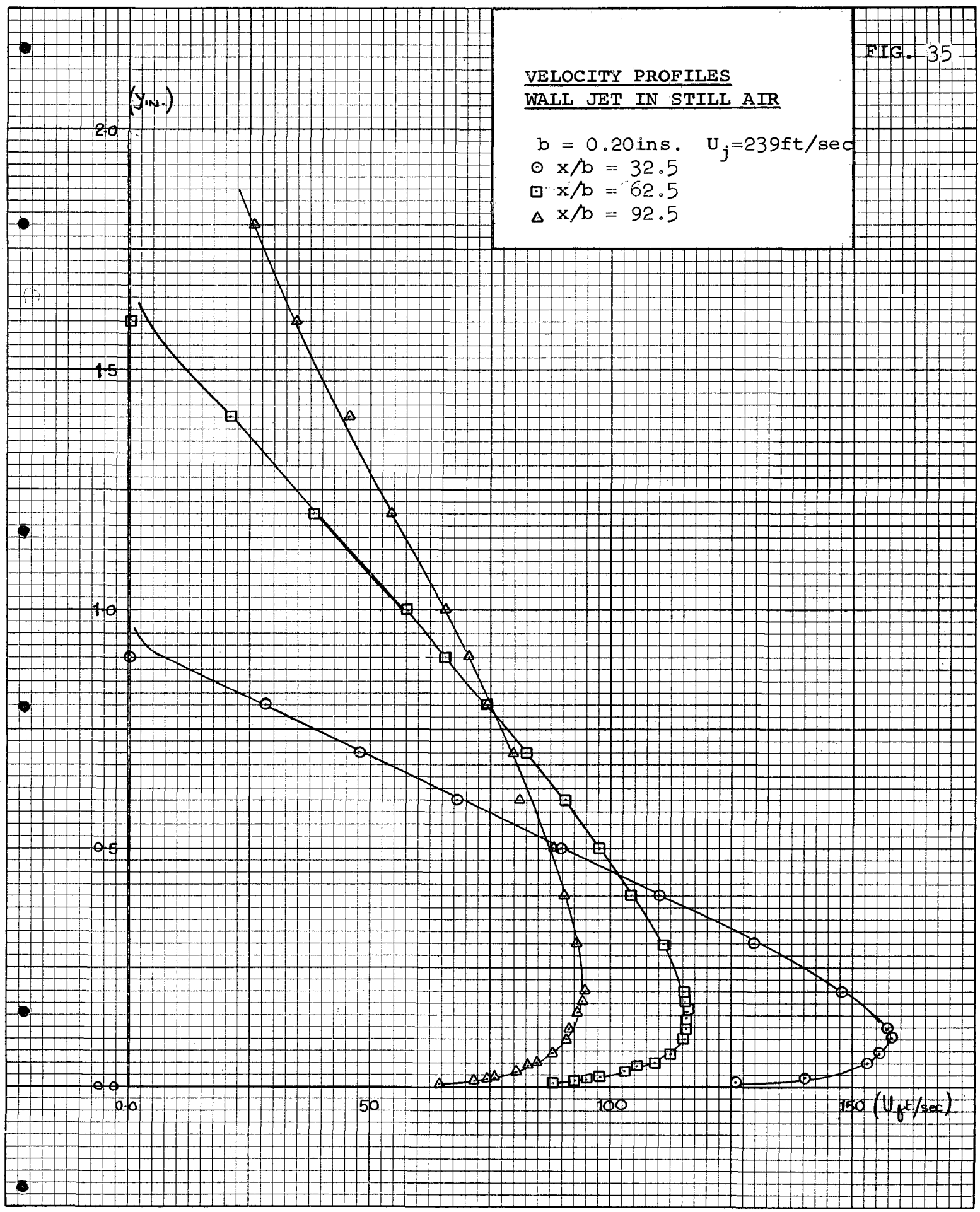
VELOCITY PROFILES
WALL JET IN STILL AIR
b = 0.20ins. U_j=239ft/sec
⊙ x/b = 32.5
⊡ x/b = 62.5
△ x/b = 92.5
(y ins.)
2.0
1.5
1.0
0.5
0.0
50
100
150 (U ft/sec)

FIG. 36

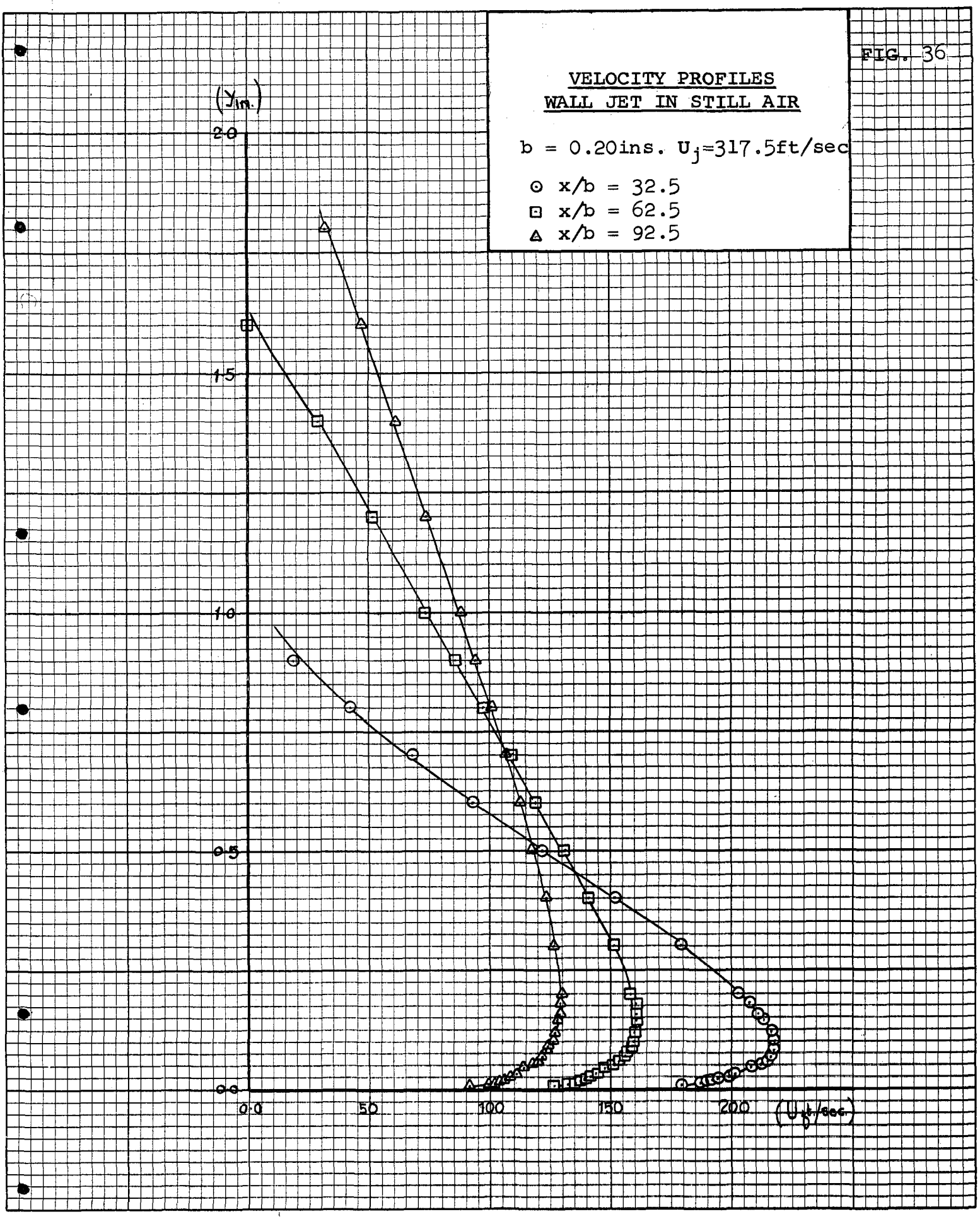
VELOCITY PROFILES
WALL JET IN STILL AIR
b = 0.20ins. U_j=317.5ft/sec
⊙ x/b = 32.5
⊡ x/b = 62.5
△ x/b = 92.5
(y in.)
2.0
1.5
1.0
0.5
0.0
0.0
50
100
150
200
(U ft/sec.)

FIG. 37

NON-DIMENSIONAL MEAN VELOCITY PROFILES INCLUDING INNER BOUNDARY LAYER

WALL JET IN STILL AIR

b = 0.20ins.

x/b	U_j ft/sec.	$\frac{U_M Y_{M/2}}{\nu}$
⊙ 32.5		4.27×10^4
□ 62.5	239	5.46×10^4
△ 92.5		5.68×10^4
⊙ 32.5		5.64×10^4
▽ 62.5	317.5	7.09×10^4
⊗ 92.5		8.34×10^4

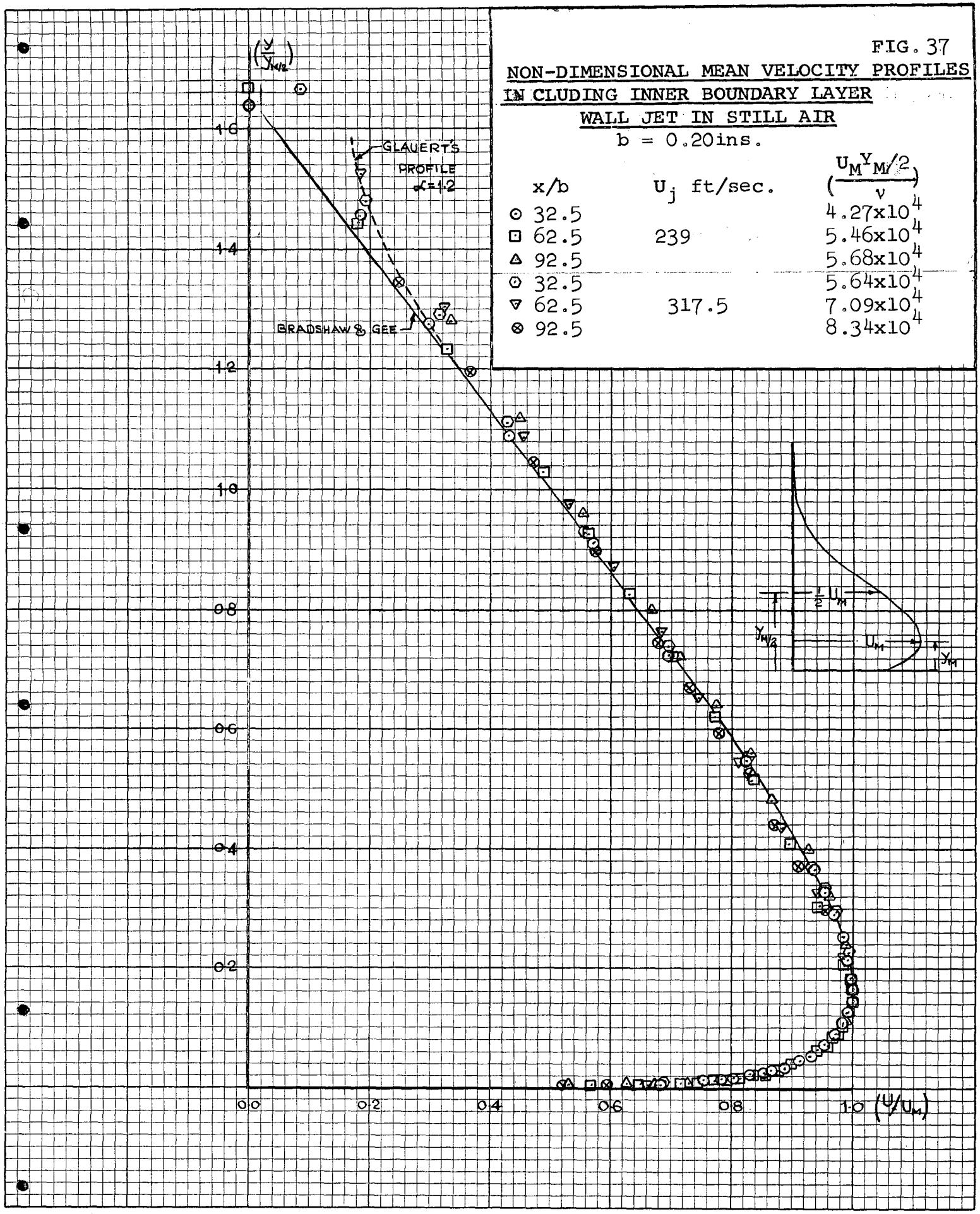

FIG. 38

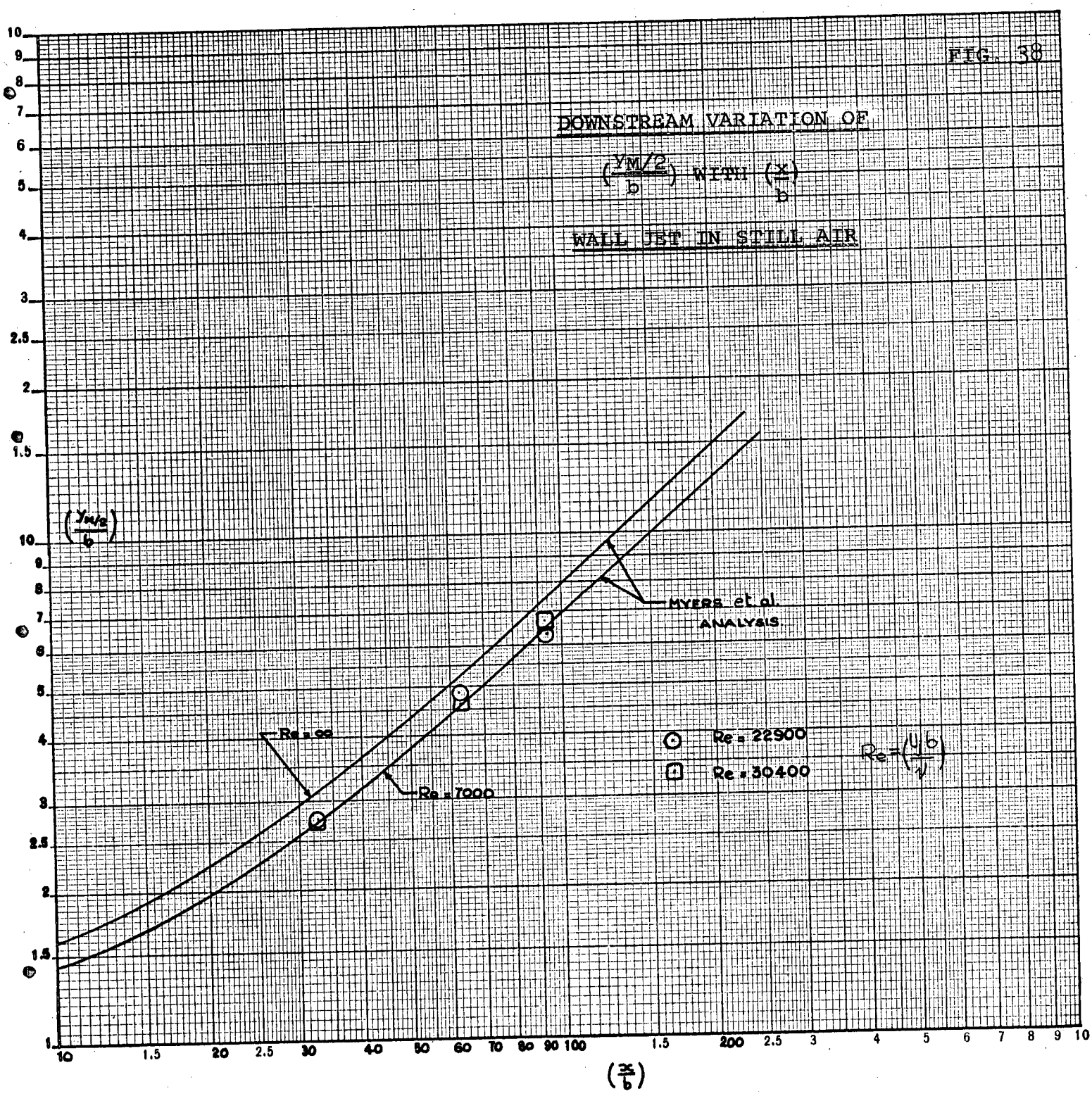
DOWNSTREAM VARIATION OF
$(\frac{y_{M/2}}{b})$ WITH $(\frac{x}{b})$
WALL JET IN STILL AIR
$(\frac{y_{M/2}}{b})$
$(\frac{x}{b})$
MYERS et al. ANALYSIS
Re = 22900
Re = 30400
Re = 7000
$Re = (\frac{U_0 b}{\nu})$

FIG. 39

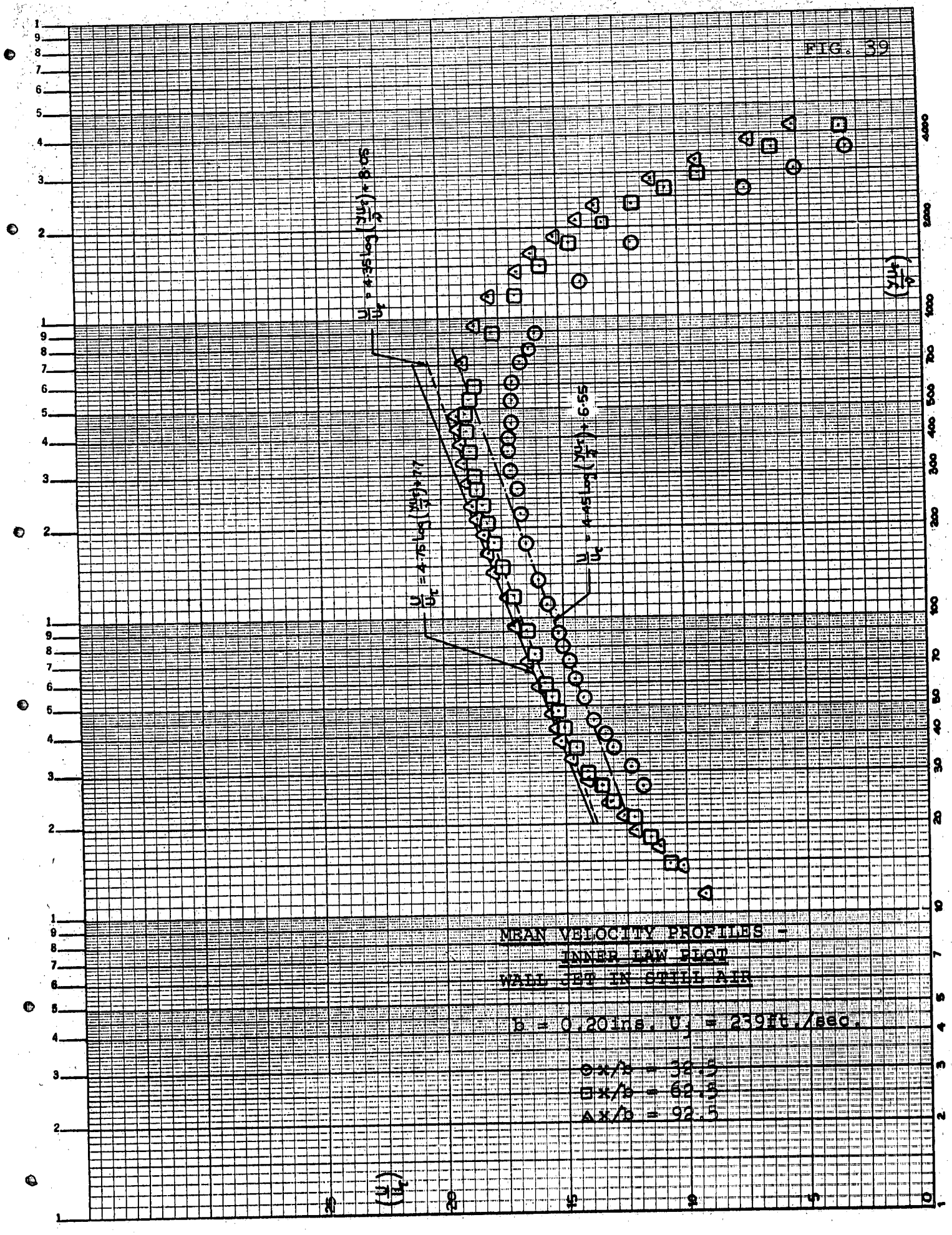

MEAN VELOCITY PROFILES -
INNER LAW PLOT
WALL JET IN STILL AIR

b = 0.20ins. U_j = 239ft./sec.

○ x/b = 32.5
□ x/b = 62.5
△ x/b = 92.5

FIG. 40

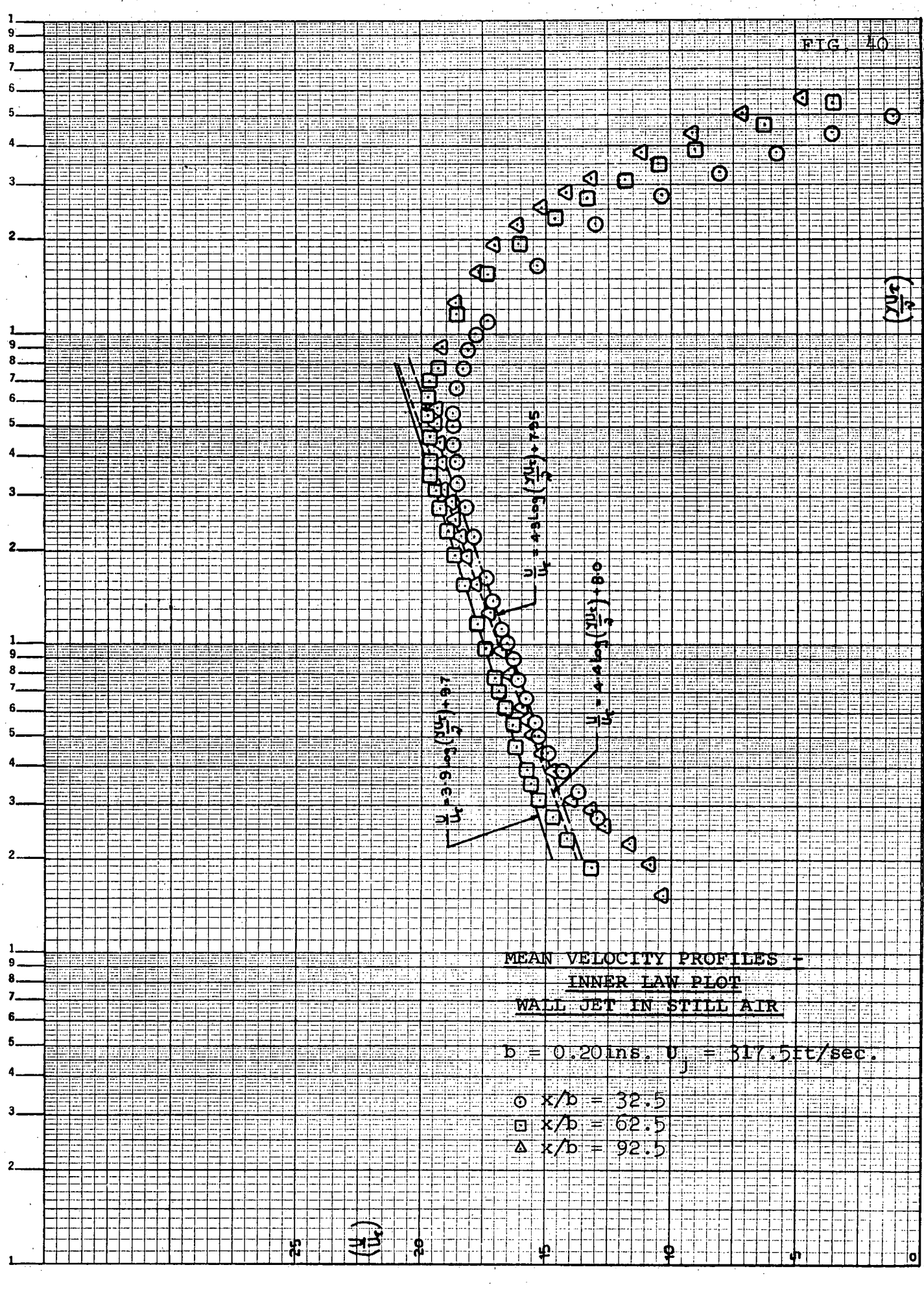

MEAN VELOCITY PROFILES –
INNER LAW PLOT
WALL JET IN STILL AIR

b = 0.201ns. U_j = 317.5ft/sec.

⊙ x/b = 32.5
⊡ x/b = 62.5
△ x/b = 92.5

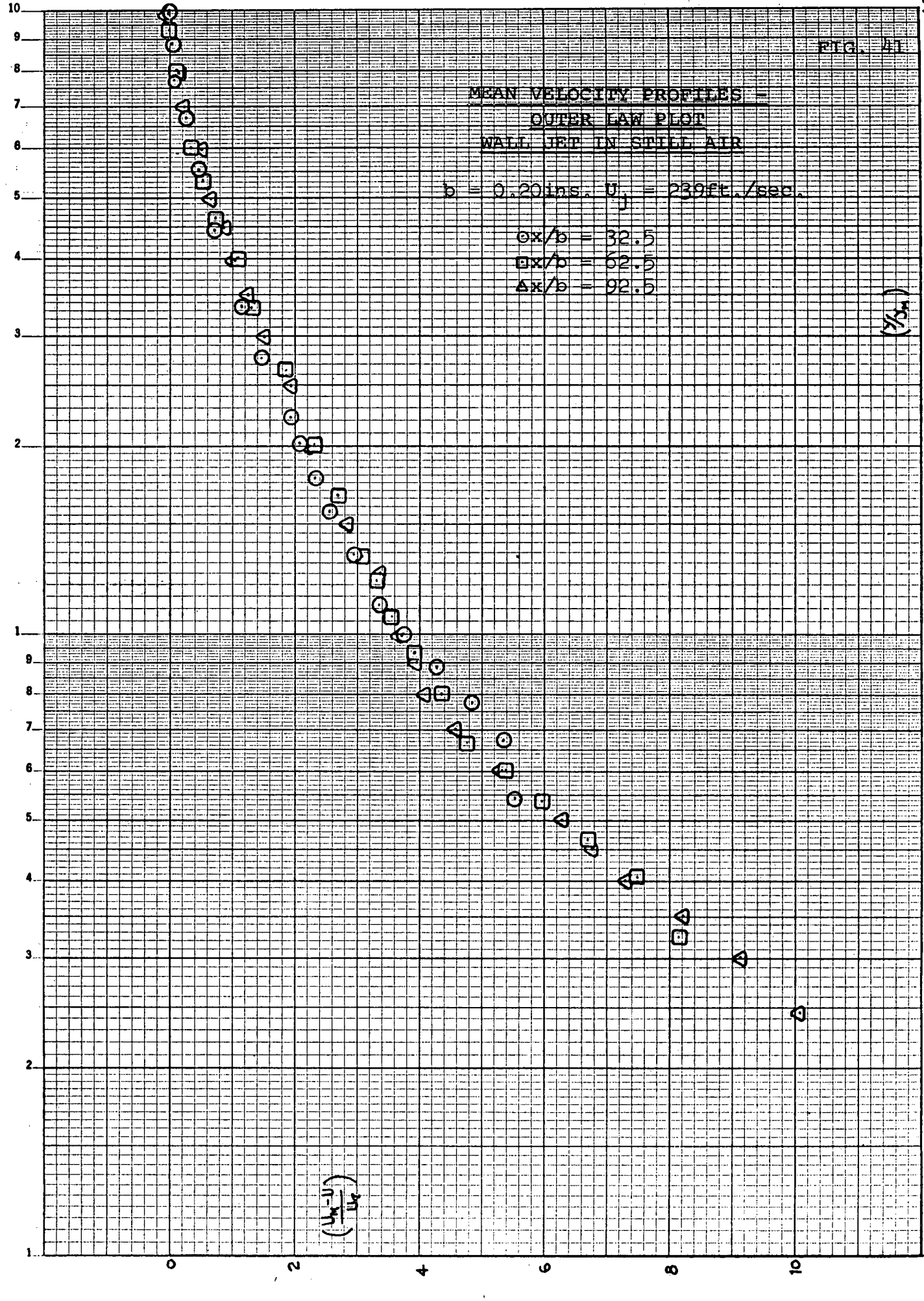
FIG. 41
MEAN VELOCITY PROFILES -
OUTER LAW PLOT
WALL JET IN STILL AIR
b = 0.20ins. U_j = 239ft./sec.
○x/b = 32.5
□x/b = 62.5
△x/b = 92.5
$(U_m-U)/U_m$
(y/y_m)
0
2
4
6
8
10

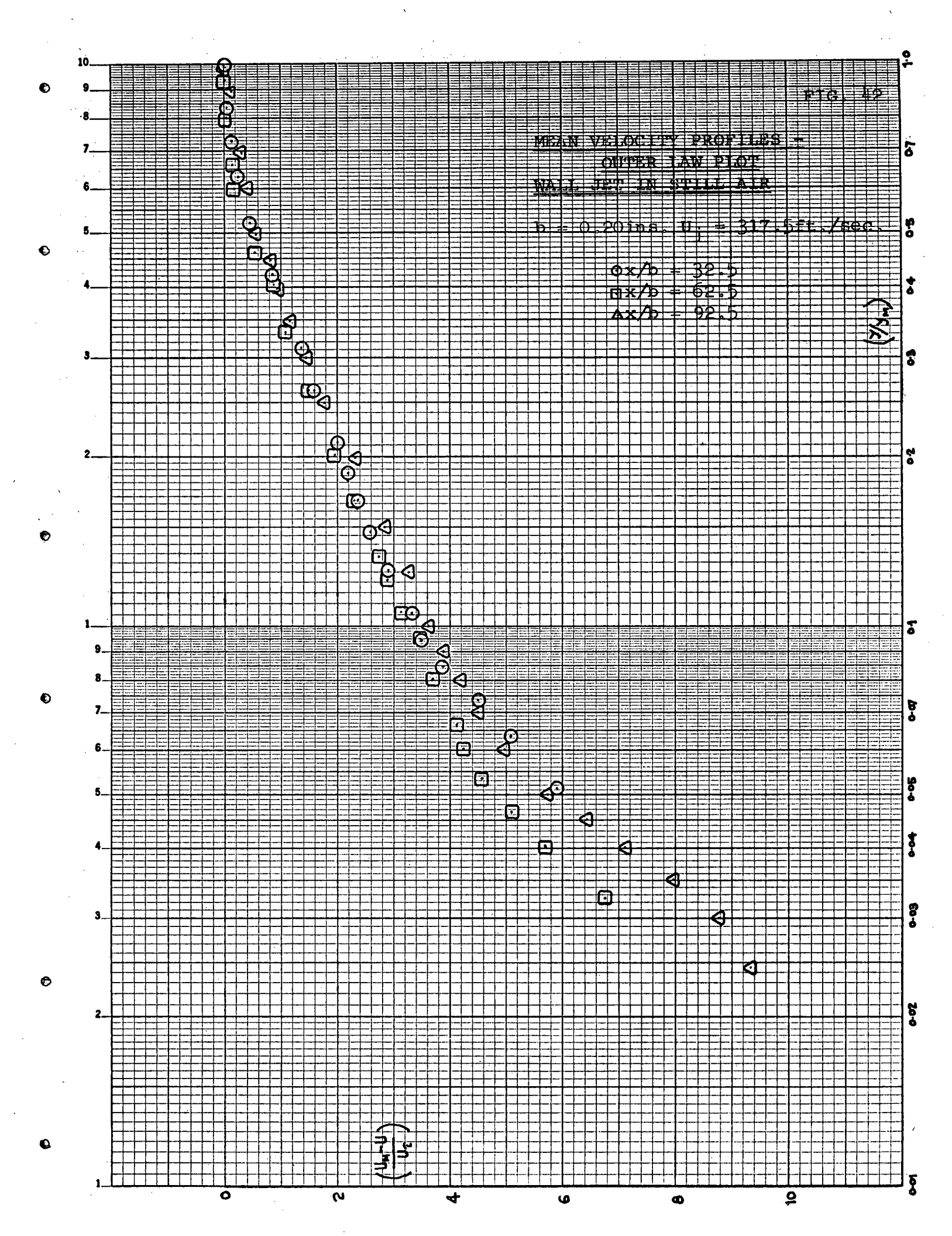
FIG. 12
MEAN VELOCITY PROFILES -
OUTER LAW PLOT
WALL JET IN STILL AIR
b = 0.20 ins. U_j = 317.5 ft./sec.
○ x/b = 32.5
□ x/b = 62.5
△ x/b = 92.5
$(y/y_{\frac{1}{2}})$
$\left(\frac{U_m - U}{U_m}\right)$
0
2
4
6
8
10

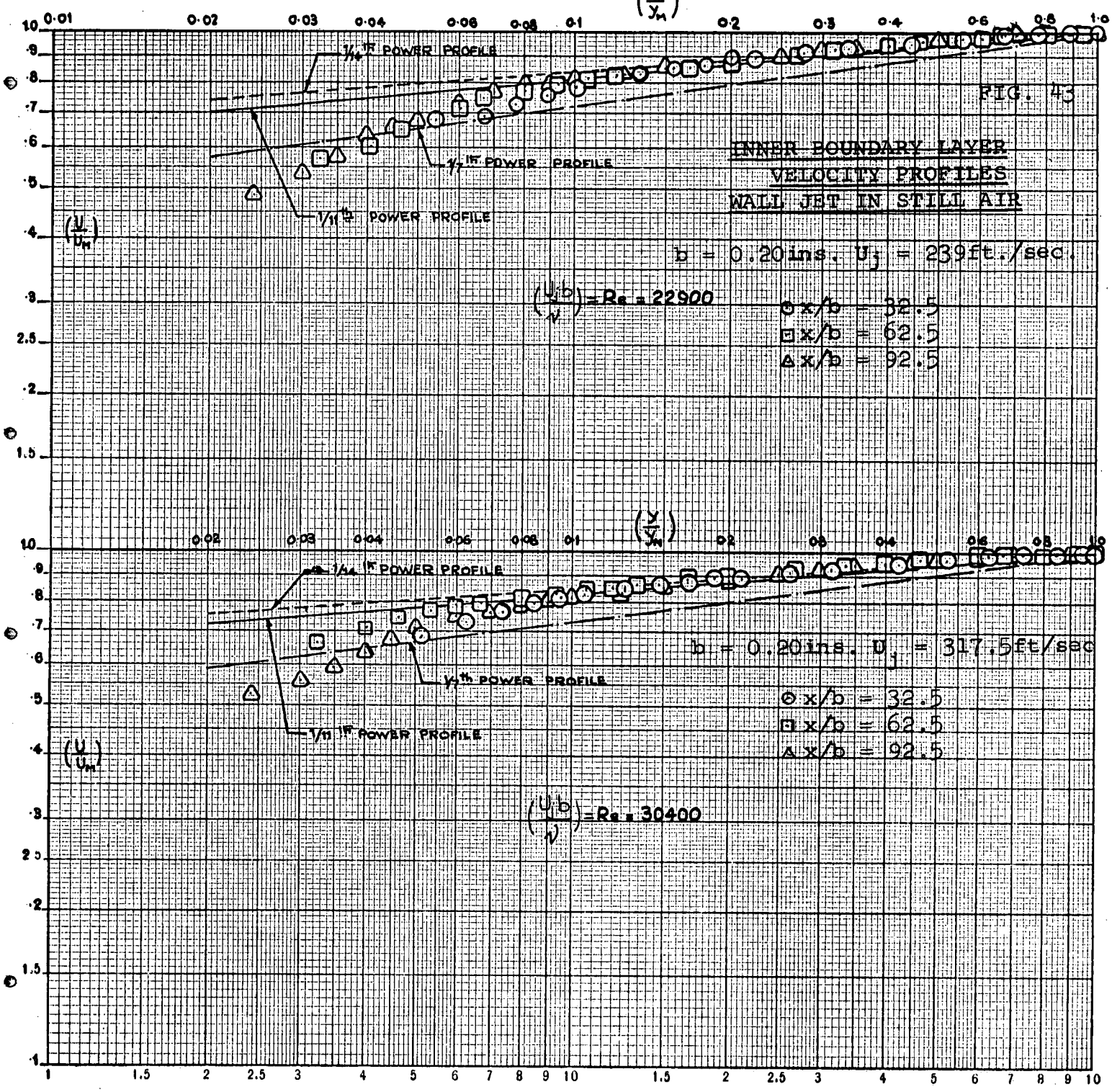
$\left(\frac{y}{y_m}\right)$
0·01
0·02
0·03
0·04
0·06
0·08
0·1
0·2
0·3
0·4
0·6
0·8
1·0
1/4th POWER PROFILE
1/7th POWER PROFILE
1/11th POWER PROFILE
$\left(\frac{U}{U_m}\right)$
FIG. 43
INNER BOUNDARY LAYER
VELOCITY PROFILES
WALL JET IN STILL AIR
b = 0.20ins. U_j = 239ft./sec.
$\left(\frac{U_j b}{\nu}\right)$ = Re = 22900
⊙ x/b = 32.5
⊡ x/b = 62.5
△ x/b = 92.5
b = 0.20ins. U_j = 317.5ft/sec
$\left(\frac{U_j b}{\nu}\right)$ = Re = 30400
10
9
8
7
6
5
4
3
2.5
2
1.5
1
1.5
2
2.5
3
4
5
6
7
8
9
10

FIG. 44

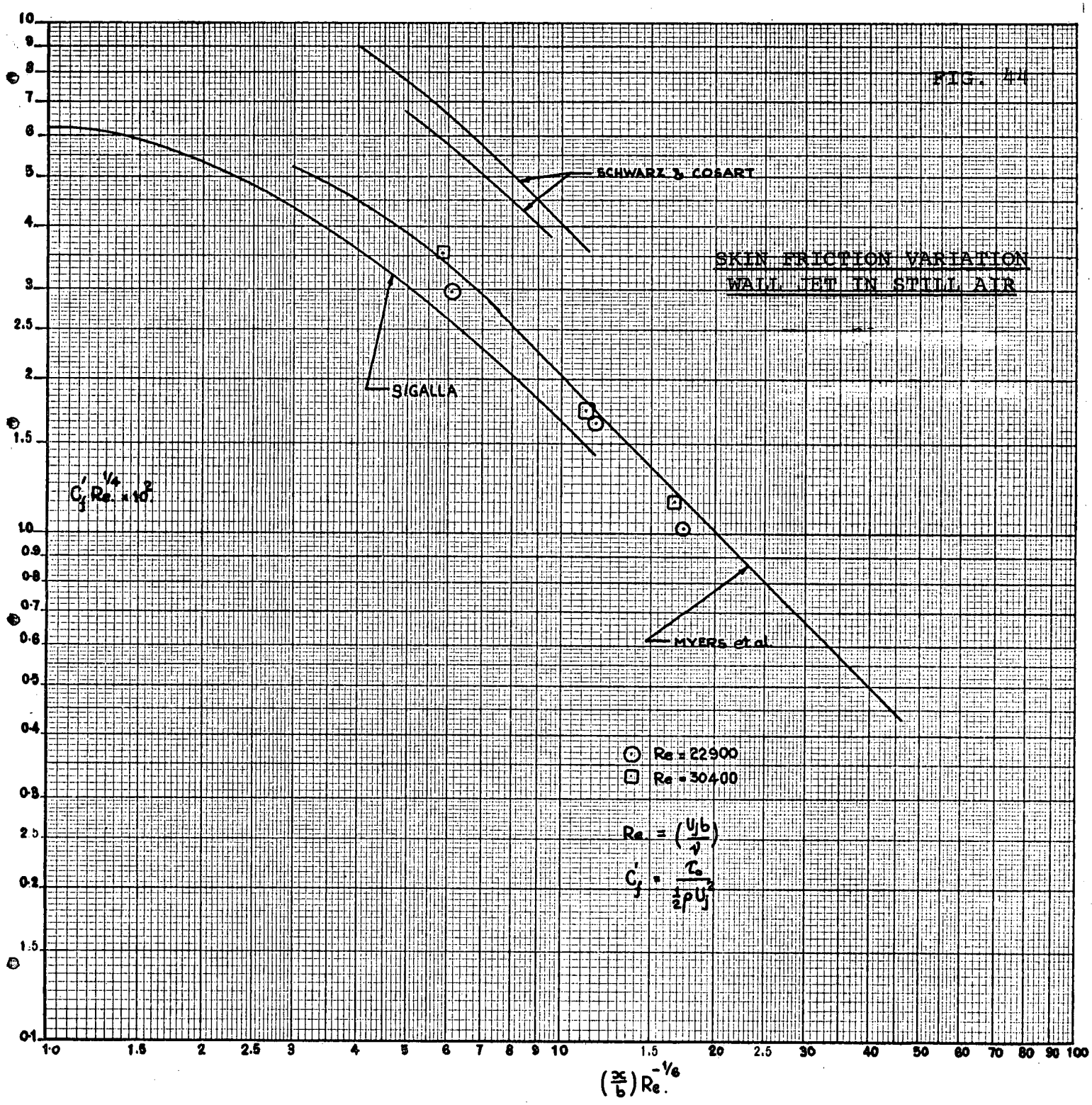
SKIN FRICTION VARIATION
WALL JET IN STILL AIR
SCHWARZ & COSART
SIGALLA
MYERS et al
$C_f' Re_b^{1/4} = 10^2$
Re = 22900
Re = 30400
$Re_b = \left(\frac{U_j b}{\nu}\right)$
$C_f' = \frac{\tau_o}{\frac{1}{2}\rho U_j^2}$
$\left(\frac{x}{b}\right) Re_b^{-1/6}$

FIG. 45

COMPARISON OF TURBULENCE INTENSITY AND CORRESPONDING VELOCITY PROFILES WALL JET IN STILL AIR

△ { b = 0.20ins. U_j = 317.5 ft/sec.
  { x = 92.2ins.

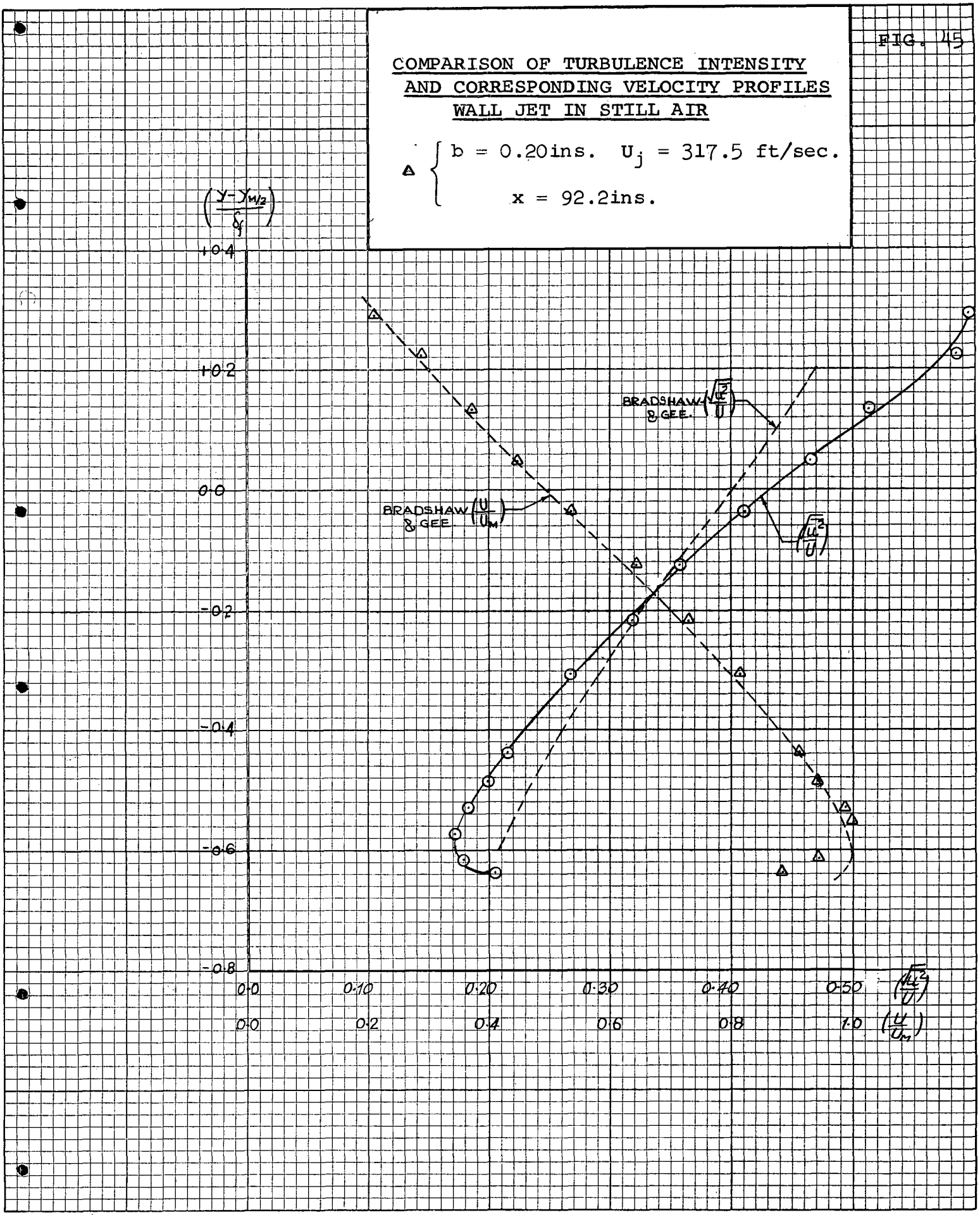

TWO-DIMENSIONALITY CHECK - WALL JET IN TAILORED PRESSURE GRADIENT.

$b = 0.375$ins. $\left(\frac{U_j}{U_{is}}\right) = 4.05$

△ a - 6ins. on Right
⊙ c - on Centre Line
⊡ d - 6ins. on Left.

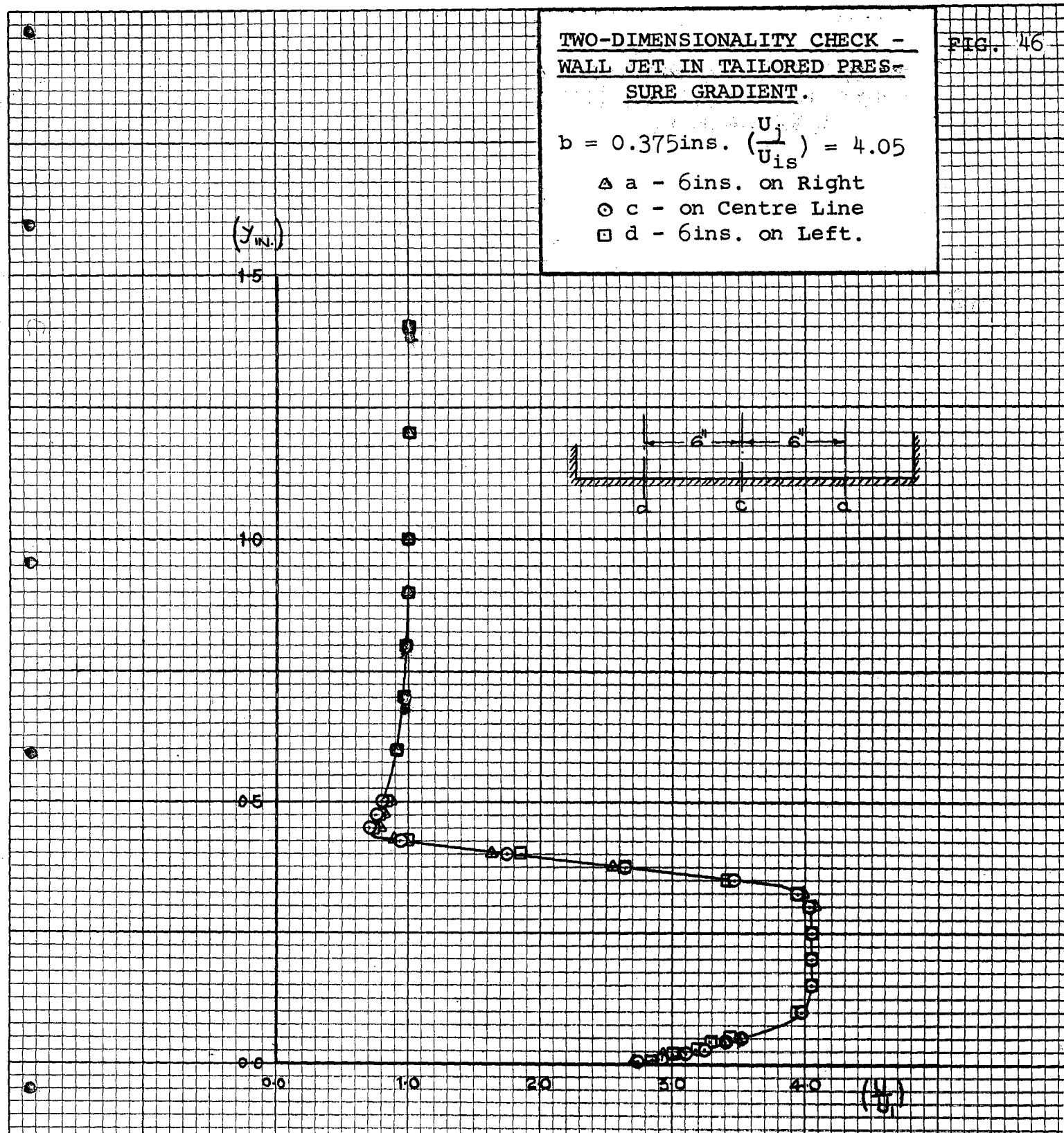

Velocity Profiles at x = 0.5ins. from the slot exit.

FIG. 47

TWO-DIMENSIONALITY CHECK - WALL JET IN TAILORED PRESSURE GRADIENT

$b = 0.375$ins. $\left(\frac{U_j}{U_{is}}\right) = 4.05$

- a - 6ins. on Right
- c - on Centre Line
- d - 6ins. on Left

$(Y_{ins.})$

2·0
1·5
1·0
0·5
0·0
0·0
1·0
2·0
3·0
$\left(\frac{U}{U_j}\right)$

Velocity Profiles at x = 15.5ins. from the slot exit.

FIG. 48

TWO-DIMENSIONALITY CHECK - BOUNDARY LAYER IN ZERO PRESSURE GRADIENT.

△ a - 6ins. on Right
⊙ c - on Centre Line
□ d - 6ins. on Left.

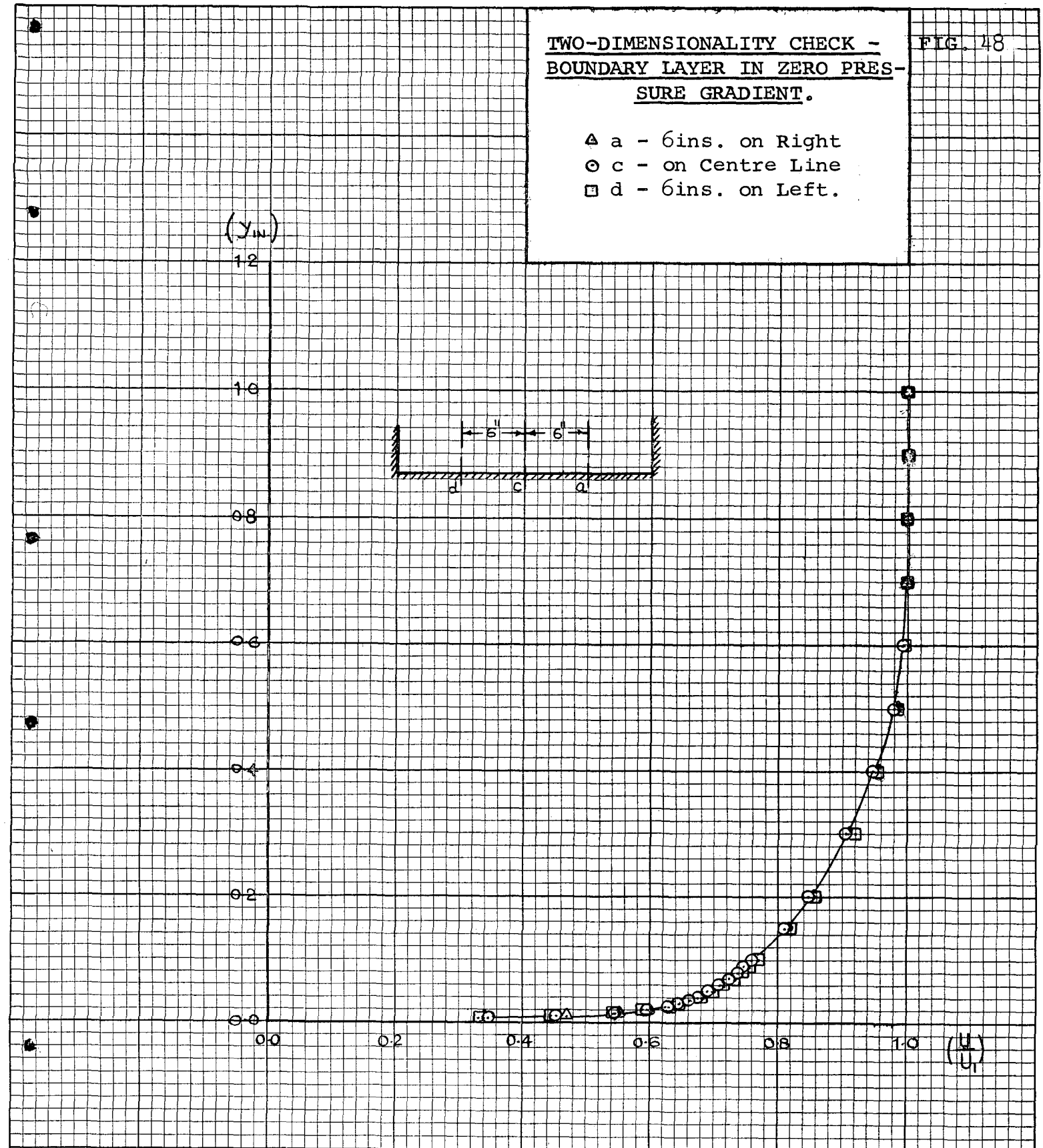

Velocity Profiles at x = 15.5ins. from the slot exit.

FIG. 49

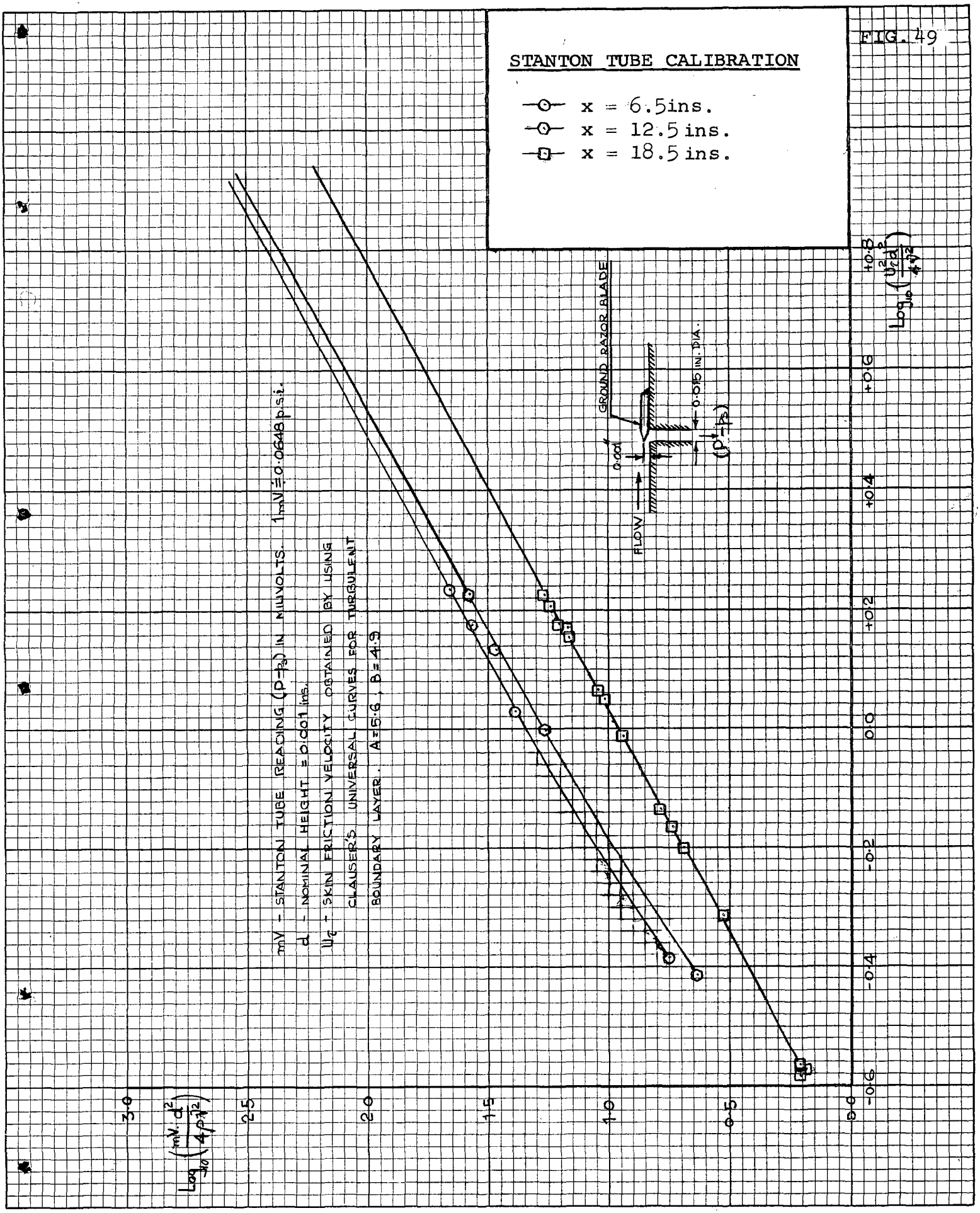
STANTON TUBE CALIBRATION
x = 6.5ins.
x = 12.5 ins.
x = 18.5 ins.
GROUND RAZOR BLADE
0.001
0.015 IN. DIA.
FLOW
$(p-p_s)$
$\log_{10}\left(\frac{u_2^2 d}{\nu x}\right)$
+0.8
+0.6
+0.4
+0.2
0.0
-0.2
-0.4
-0.6
3.0
2.5
2.0
1.5
1.0
0.5
0
$\log_{10}\left(\frac{mV \cdot d^2}{4\rho\nu^2}\right)$
mV = STANTON TUBE READING $(p-p_s)$ IN MILLIVOLTS. 1 mV = 0.0648 p.s.i.
d = NOMINAL HEIGHT = 0.001 ins.
u_2 = SKIN FRICTION VELOCITY OBTAINED BY USING CLAUSER'S UNIVERSAL CURVES FOR TURBULENT BOUNDARY LAYER. A = 5.6, B = 4.9

FIG. 50

PRESTON TUBE CALIBRATION

x = 18.5ins.

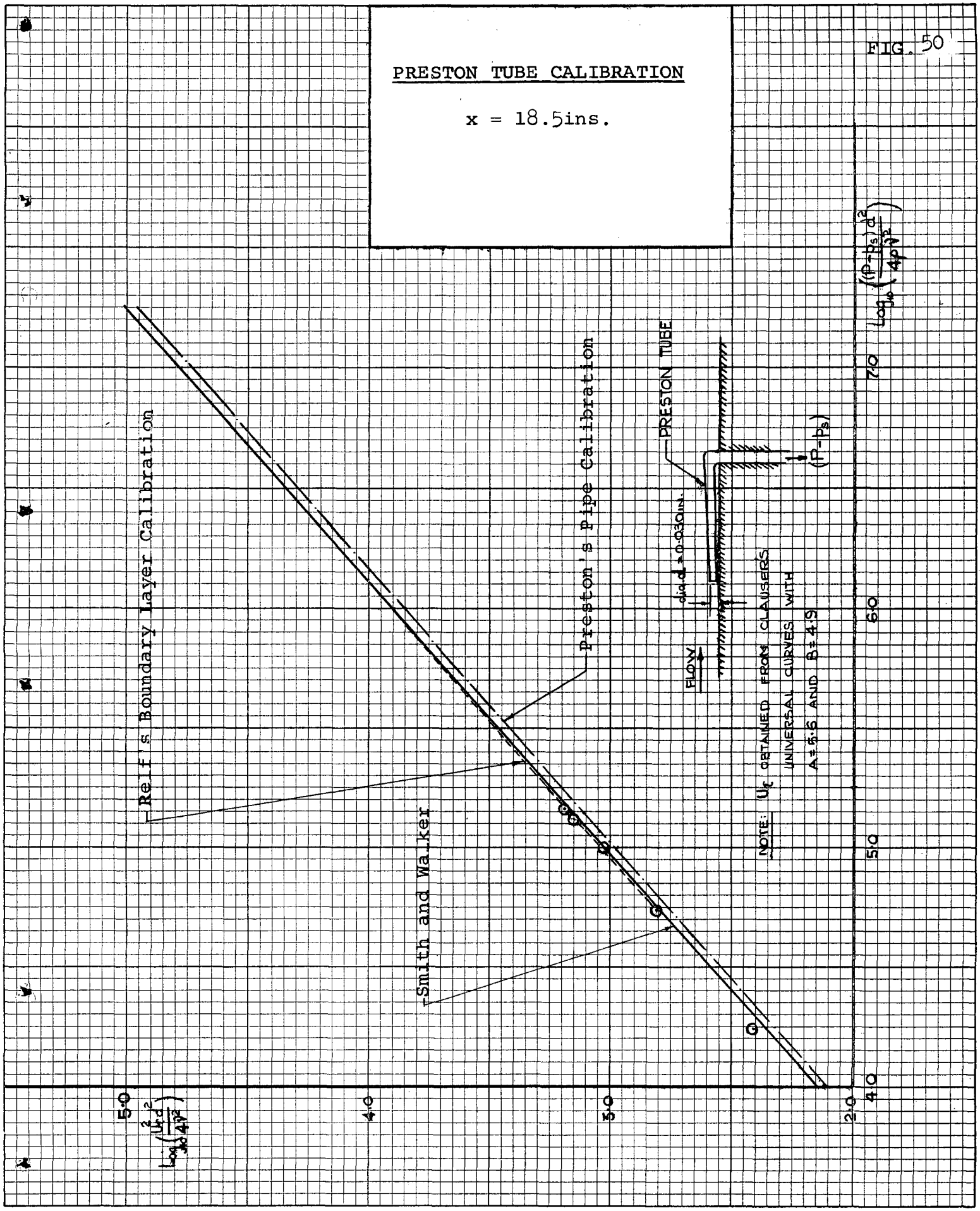

FIG. 51

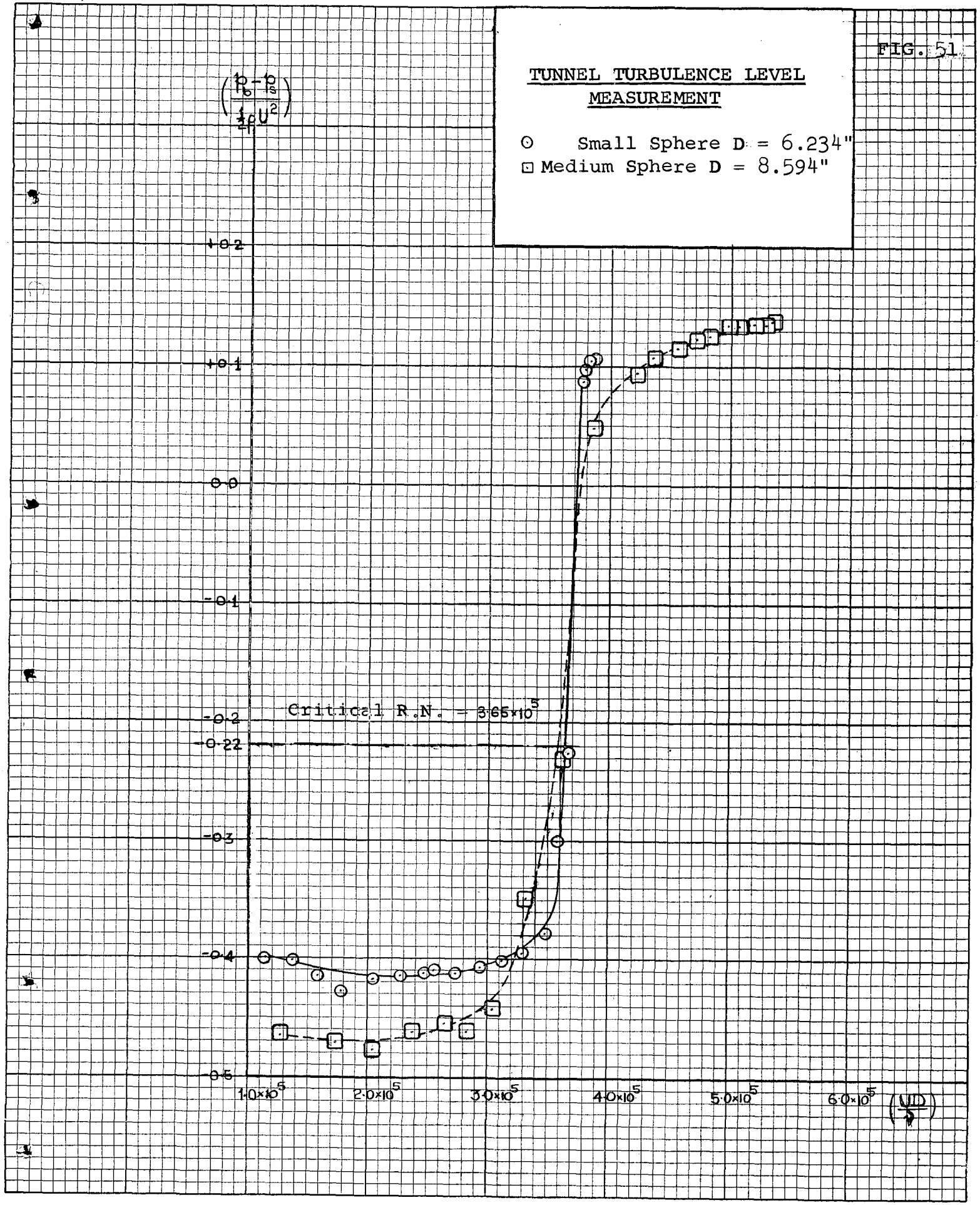
TUNNEL TURBULENCE LEVEL MEASUREMENT
⊙ Small Sphere D = 6.234"
⊡ Medium Sphere D = 8.594"
$\left(\frac{p_b - p_s}{\frac{1}{2}\rho U^2}\right)$
+0.2
+0.1
0.0
-0.1
-0.2
-0.22
-0.3
-0.4
-0.5
Critical R.N. = 3.65×10^5
1.0×10^5
2.0×10^5
3.0×10^5
4.0×10^5
5.0×10^5
6.0×10^5
$\left(\frac{UD}{\nu}\right)$